



The University of  
**Nottingham**

UNITED KINGDOM • CHINA • MALAYSIA

# **Innovative composite materials for heating, cooling and humidity control in buildings**

Mariana Velasco Carrasco

MSc

A thesis submitted to the University of Nottingham for the degree  
of Doctor of Philosophy

August 2021



*“Some are born great, some achieve greatness, and some have greatness thrust upon  
them.”*

William Shakespeare

# Acknowledgments

To Jorge love of my life, thanks for being part of this crazy adventure, every tear, every laugh. I guess we could never imagine what the PhD would look like, but we were young and unafraid. I could not find the words to express how much I love you.

To Prof. Saffa Riffat, I am eternally grateful for all the consistent support and guidance. I considered myself incredibly lucky to come across a supervisor so bright and kind.

To Dr. Su, for his invaluable support with insightful comments and suggestions.

To Dr. Siddig, thank you for your valuable contribution to enhance this research project.

To the technical staff, thank you for all your support throughout these years. You always managed to make the impossible possible.

To my friends and family, thank you for loving me unconditionally, even when I am a mess.

I would like to thank Innovate UK for sponsoring this research project.

Finally, I would like to thank all the people who directly or indirectly have made this work possible.



# Abstract

This research focuses on the integration of a tri-modular system that aims to achieve a complete thermal comfort approach in buildings. The system contemplates a passive PCM system that assists in the building cooling requirements, preventing overheating during summer days while maintaining a habitable temperature overnight. For the humidity control, a high performance water adsorbent, based on a solid desiccant is in charge of the air dehumidification, thereby maintaining relative humidity at a comfortable level. Finally, a high-performance solar-assisted heat pump (SAHP) to provide heating in winter, domestic hot water, and assisting in the regeneration of the humidity adsorbent.

Derived from the energy in building context, literature review, and research methodology, the system was experimentally tested. Based on simulation results, several PCM materials were evaluated, counteracting the material's low thermal conductivity with novel encapsulation methods. Furthermore, in some cases, the addition of highly conductive materials was analysed using DSC, SEM, and dynamic heat flow meter method (DHFM). For moisture control, the performance of a natural humidity adsorbent was evaluated. The project emphasised on the development of a novel natural composite materials for humidity control.

During the laboratory experimental work, the solar-assisted heat pump was tested with the aid of a solar simulator, investigating the performance of the solar thermal collector and heat pump system. The operation of the

fan coil unit was also assessed, showing the system's ability to provide indoor heating.

As part of the experimental procedure, the system was integrated into a dwelling, giving the opportunity for large scale testing. After intensive testing, the results demonstrated the effectiveness of the system to improve building energy performance. The PCM ceiling panels provided an alternative solution to address the cooling demands in the UK weather, several panels were developed, showing the positive effect as an enhancement mechanism. The experimental results show a temperature reduction between 3 °C to 5 °C helping maintain the building within the thermal comfort zone.

The solid desiccants experimentation demonstrates the effectiveness of different composite materials for humidity control.  $\text{MgSO}_4$ - $\text{CaCl}_2$ ,  $\text{CaCl}_2$ ,  $\text{KHCO}_2$ , and  $\text{LiCl}$  were compared to the raw vermiculite. Vermiculite- $\text{LiCl}$  and Vermiculite- $\text{MgSO}_4$ - $\text{CaCl}_2$  presented the highest adsorption performance. In terms of the regeneration performance, the vermiculite composites presented low-temperature requirements, being optimal for building applications.

The SAHP was able to provide a temperature range for space heating between 44 °C to 56 °C. During the house monitoring, the system worked in 12 hours cycles, demonstrating its effectiveness to maintain the heating demand at night-time, without solar radiation. Moreover, the desiccant regeneration was tested using the SAHP through a hot water

pipe system. The results confirm the system's efficacy to recharge the desiccant and cope with the space heating demand.

These results demonstrate the potential application of the tri-modular system for building application under the UK climate conditionings. The system shows endless possibilities, as each technology can work as a stand-alone system. The proposed research investigation provides an alternative solution to fossil fuel energy sources, assisting in the transition to a net-zero future.

# Table of contents

Chapter 1 Introduction .....	1
1.1 Background .....	1
1.2 Energy context .....	3
1.1.1 Energy figures.....	4
1.3 Building Context .....	6
1.3.1 Energy usage.....	7
1.1.2 Standards for thermal comfort and energy efficiency in buildings.....	9
1.4 Topic of study .....	10
1.5 Research scope and aims .....	14
1.6 Structure of the research .....	15
1.7 Summary.....	17
Chapter 2 Literature review: Phase Change Materials, solid desiccants for humidity control and solar assisted heat pumps.....	18
2.1 Introduction.....	18
2.2 Human thermal comfort .....	19
2.3 Phase change materials .....	21
2.3.1 Background.....	21
2.3.2 Classification and characteristics .....	25
2.3.3 PCM encapsulation.....	27
2.3.4 Integration of PCMs in the buildings .....	31
2.3.5 Enhancement methods .....	44
2.3.6 Main conclusions .....	56
2.4 Solid desiccants .....	58
2.4.1 Background.....	58
2.4.2 Materials classification .....	61
2.4.3 Review studies on composite desiccants.....	72
2.4.4 Main conclusions .....	75
2.5 Solar Assisted heat pump systems .....	76
2.5.1 Background.....	76
2.5.2 Classification and characteristics .....	78

2.5.3	Main conclusions .....	92
2.6	Summary .....	93
Chapter 3	System components.....	94
3.1	Introduction.....	94
3.2	Environmental control in a building.....	94
3.3	System description .....	96
3.4	System components.....	99
3.4.1	Phase Change Materials.....	99
3.4.2	Solid desiccant.....	105
3.4.3	Heat pump system .....	109
3.5	Summary .....	116
Chapter 4	Preliminary simulation on PCMs .....	119
4.1	Introduction.....	119
4.2	Modelling method .....	120
4.2.1	EnergyPlus modelling .....	121
4.2.2	SketchUp model .....	124
4.3	Simulation parameters .....	125
4.3.1	Heat balance algorithm .....	126
4.3.2	Project location and weather characteristics .....	128
4.3.3	Simulation settings.....	131
4.4	Results analysis and discussion.....	135
4.5	Summary.....	144
Chapter 5	PCM and solid desiccant preliminary experiments.....	147
5.1	Introduction.....	147
5.2	Phase Change Material selection.....	147
5.2.1	Encapsulation methods.....	149
5.2.2	Environmental chamber testing setup.....	150
5.2.3	Water tank experimental rig .....	152
5.2.4	Environmental chamber results .....	152
5.2.5	Water tank testing .....	169
5.2.6	PCM panel performance comparison.....	175
5.3	Solid desiccant selection .....	178

5.3.1	Environmental chamber testing setup.....	179
5.4	Summary .....	186
5.4.1	PCM panel testing.....	186
5.4.2	Solid desiccant testing .....	187
Chapter 6 Experimental results: heating, cooling, and humidity control in buildings		189
6.1	Introduction.....	189
6.2	Experimental results on PCM materials.....	190
6.2.1	Thermal conductive analysis.....	190
6.2.2	Blister panel INERTEK 23 and enhancement methods .	195
6.2.3	S27 .....	210
6.2.4	Capsule panel S27.....	219
6.3	Experimental results on vermiculites .....	222
6.3.1	Vermiculite preparation .....	224
6.3.2	Experimental setup: Method 1 .....	228
6.3.3	Experimental setup: Method 2 .....	235
6.3.4	Vermiculite regeneration in oven .....	238
6.4	Experimental results on solar assisted heat pump .....	240
6.4.1	Experimental setup .....	240
6.4.2	Solar simulator .....	244
6.4.3	Solar Assisted Heat Pump .....	245
6.4.4	Fan Coil Unit .....	249
6.5	Summary .....	253
Chapter 7 House monitoring of the system.....		255
7.1	Introduction.....	255
7.2	PCM house testing .....	256
7.2.1	S23 in Tarmac House .....	256
7.2.2	S23 in Z blockhouse .....	263
7.3	Solid desiccant and heat pump site testing .....	278
7.4	Vermiculite house testing .....	280
7.5	Solar assisted heat pump house testing.....	285
7.6	System integration.....	288
7.7	Summary .....	290

Chapter 8 Economic analysis and environmental impact.....	292
8.1 Introduction.....	292
8.2 Economic evaluation .....	293
8.2.1 Market environment .....	293
8.2.2 Estimation cost .....	296
8.3 Environmental analysis.....	302
8.3.1 Life Cycle Assessment.....	303
8.3.2 Modelling method.....	304
8.3.3 Environmental impact .....	304
8.4 Summary .....	309
Chapter 9 Conclusions and future work.....	311
9.1 Summary of the work .....	311
9.2 Major findings .....	312
9.3 Limitations and recommendations .....	313
9.3.1 Recommendations and future work .....	314
9.4 Concluding remarks .....	316
Appendix .....	318
References.....	320

# List of Figures

Figure 1.1 Analysis of the keywords from the urban, energy and climate context.....	2
Figure 1.2 Total final consumption by sector, 2018-2021 (Department for Business, 2013).....	4
Figure 1.4 Electricity generation from renewables since 2000 (Department of Energy and Climate Change (DECC) and National Statistics, 2014).....	5
Figure 1.5 Territorial greenhouse gas emissions by gas (Department of Energy and Climate Change (DECC) and National Statistics, 2014).....	6
Figure 1.6 Domestic consumption, temperature-corrected consumption, and average annual temperatures.....	7
Figure 1.7 Domestic energy consumption by end use in the UK (Department for Business, 2021).....	8
Figure 1.8 Electricity and gas consumptions (existing houses), (Dowds and You, 2019).....	8
Figure 1.9 Electricity and gas consumptions (new houses), (Dowds and You, 2019).....	9
Figure 1.10 Schematic representation of system components. ....	13
Figure 1.11 System description. ....	13
Figure 1.12 Schematic of the research work. ....	16
Figure 2.1 Energy storage methods (Yang, Huang and Zhou, 2020).	22
Figure 2.2 PCM thermal process.....	23
Figure 2.3 Phase change materials classification (Kylili & Fokaides, 2016). .....	26
Figure 2.4 Microencapsulated PCM. ....	28
Figure 2.5 Structure and working principle of the encapsulated PCM (Salunkhe and Shembekar, 2012).....	30
Figure 2.6 Schematic diagram of the experimental setup (Zhong <i>et al.</i> , 2015). ....	33
Figure 2.8 Schematic of single-tank HES system (Abdelsalam, et al., 2017). ....	39
Figure 2.8 Arrangement of PCM in the heat storage tank. (a) Sphere, (b) cylinder, (c) plate, and (d) tube (Wei <i>et al.</i> , 2005).....	41
Figure 2.10 Popular enhancement techniques (Yang, Huang and Zhou, 2020). ....	45



Figure 2.11 Summary of produced nanoparticles (Yang, Huang and Zhou, 2020). .....	45
Figure 2.12 Schematic diagram of the experimental procedure and setup for sample (Fan <i>et al.</i> , 2013). .....	48
Figure 2.13 Test wall with the PCM-enhanced wallboards (Biswas <i>et al.</i> , 2014). .....	52
Figure 2.14 Schematic description adsorption and absorption. ....	60
Figure 2.15 Common solid and liquid desiccant materials (Shehadi, 2018). .....	62
Figure 2.16 Comparison of dehumidification performance among silica gel, zeolite, and super absorbent polymer (White <i>et al.</i> , 2011; Chen <i>et al.</i> , 2018). .....	68
Figure 2.17 A typical scheme for preparing aerogels by sol-gel process and drying processes (Warwicker, 2010). .....	69
Figure 2.18 Water vapor adsorption isotherms for: (a) silica gel at 25 °C; (b) silica gel–LiCl at 25 °C; (c) sepiolite at 23 °C; (d) sepiolite–carbon by physical activation with steam at 23 °C; (e) sepiolite–carbon by chemical activation with KOH at 23 °C; (f) CaCl <sub>2</sub> –SiO <sub>2</sub> sol–gel at 25 °C; (g) CaCl <sub>2</sub> –MCM-41 at 20 °C; (h) silica gel–LiBr at 20 °C (La <i>et al.</i> , 2010). ....	71
Figure 2.19 Picture and outline of the adsorption heat exchanger (Pistocchini, Garone and Motta, 2016). .....	72
Figure 2.20 SEM (Secondary electron capture, accelerating voltage 15 kV) images of particles of vermiculite (a) and zeolitized vermiculite (b) (Verm/Zeo-72), (Johnson and Worrall, 2007b). .....	74
Figure 2.21 A generalised classification of the recent development in heat pump technologies (Chua, Chou and Yang, 2010). .....	78
Figure 2.22 Solar systems classification (Evangelisti, De Lieto Vollaro and Asdrubali, 2019). .....	79
Figure 2.23 Energy balance of a PVT collector or absorber (Hadorn, 2015). .....	79
Figure 2.24 The examined strip of the hybrid PV. ....	81
Figure 2.25 PV-T system for solar heating and cooling provision (Tripanagnostopoulos, et al., 2002). .....	82
Figure 2.26 PVT system and the control strategy and sensor locations. ....	83
Figure 2.27 Composition and working process of the PVT-VISHP system for water heating (Lu, et al., 2019). .....	85
Figure 3.1 System description for the thermal comfort model. ....	98
Figure 3.2 System description of the components. ....	98

Figure 3.3 PCMs in the melting temperature range of 0 °C to 35 °C (Whiffen and Riffat, 2013).....	100
Figure 3.4 Selection criteria for the successful PCM building integration. ....	101
Figure 3.5 Heat transfer enhancement techniques for PCMs (Elarem et al., 2020). ....	103
Figure 3.6 Selection criteria for the successful solid desiccant building integration.....	106
Figure 3.8 Selection criteria for the successful solar-assisted heat pump building system.....	110
Figure 3.9 Arkaya solar thermal collector. ....	111
Figure 3.10 Comparison of COPH for different refrigerants at 60 °C (Chata, Chaturvedi and Almogbel, 2005). ....	112
Figure 3.11 Schematic diagram of the solar-assisted heat pump.....	114
Figure 3.12 Solar-assisted heat pump workflow. ....	114
Figure 3.13 Impact of the single lifestyle key variables on the building energy use (Barthelmes et al., 2017).....	117
Figure 4.1 3D house model view. ....	121
Figure 4.2 Model house front (left), back façade (right). ....	122
Figure 4.3 Model house ground floor layout (left), first floor layout (right). ....	123
Figure 4.4 Schematic incorporation of the PCM panel in building section. ....	123
Figure 4.5. Front façade (left), south façade (right). ....	124
Figure 4.6 Birmingham temperature range extracted Climate Consultant. ....	129
Figure 4.7 Birmingham dry bulb x relative humidity, extracted from Climate Consultant. ....	130
Figure 4.8 Psychometric chart, extracted from Climate Consultant. ...	130
Figure 4.9. Material properties input in Energy Plus. ....	131
Figure 4.10. PCM enthalpy values example. ....	134
Figure 4.11 Building temperature comparison with and without PCM. ....	136
Figure 4.12 Heating loads without PCM in Birmingham. ....	137
Figure 4.13 Heating loads with PCM in Birmingham. ....	138
Figure 4.14 Heating loads comparison with and without PCM. ....	138

Figure 4.15 Cooling loads without PCM in Birmingham.....	139
Figure 4.16 Cooling loads with PCM in Birmingham.....	139
Figure 4.17 Cooling loads comparison with and without PCM.....	140
Figure 4.18 Thickness comparison INERTEK 23. ....	141
Figure 4.19 PCM material comparison. ....	142
Figure 4.20 Enthalpy distribution for 21 °C melting temperature between Rubitherm and Inertek. ....	142
Figure 4.21 Temperature comparison PCM Products Ltd products and INERTEK. ....	143
Figure 4.22 Heating loads comparison between PCM Products Ltd and INERTEK.....	144
Figure 4.23 Cooling loads comparison between PCM Products Ltd and INERTEK.....	144
Figure 5.1 Experimental setup for PCM panel testing. ....	151
Figure 5.2 Schematic diagram of the experimental apparatus with airflow pattern. ....	151
Figure 5.3 Water tank experimental setup. ....	152
Figure 5.4 Metal honeycomb structure with PCM. ....	153
Figure 5.5 INERTEK 23 small honeycomb panel. ....	153
Figure 5.6 A28 large honeycomb panel.....	154
Figure 5.7 INERTEK 23 small honeycomb panel, test 1.....	154
Figure 5.8 A28 honeycomb panel, test 1. ....	155
Figure 5.14 Metallic pots. ....	155
Figure 5.10 Metallic pot environmental chamber, test 1. ....	156
Figure 5.11 Metallic pot environmental chamber, test 2. ....	156
Figure 5.12 Aluminium pouch panel. ....	157
Figure 5.13 Aluminium pouch panel, test 1. ....	158
Figure 5.14 Plastic pouch with S27. ....	158
Figure 5.15 S27 plastic pouch, test 1. ....	159
Figure 5.16 S27 plastic pouch, test 2. ....	159
Figure 5.17 INERTEK 23 blister panel.....	160
Figure 5.18 INERTEK 23 blister panel, test 1.....	161
Figure 5.19 INERTEK 23 blister panel, test 2.....	161

Figure 5.20 INERTEK 23 blister panel with 2 hours temperature increments.....	162
Figure 5.21 S23 blister panel.....	163
Figure 5.22 S23 blister panel, test 1.....	164
Figure 5.23 A28 blister panel.....	164
Figure 5.24 A28 blister panels in the testing box.....	164
Figure 5.25 A28 blister panel, test 1.....	165
Figure 5.26 S27 capsule panel.....	165
Figure 5.27 S27 capsule panel, test 1.....	166
Figure 5.28 S27 capsule comparison by weight.....	167
Figure 5.29 S27 capsule temperature drop comparison.....	167
Figure 5.30 INERTEK 23 straw panel.....	168
Figure 5.31 Straight straws, test 1.....	169
Figure 5.32 Aluminium pouch panel in water tank testing.....	169
Figure 5.33 Aluminium pouch in water tank temperature, test 1.....	170
Figure 5.34 S27 pouch panel in the water tank.....	170
Figure 5.35 S27 pouch panel in the water tank, test 1.....	171
Figure 5.36 A28 blister panel in the water tank.....	171
Figure 5.37 A28 blister panel in the water tank, test 1.....	172
Figure 5.38 S27 capsule panel in the water tank.....	172
Figure 5.39 S27 capsule blister in the water tank, test 1.....	173
Figure 5.40 Corrugated straws with INERTEK 26 the water tank.....	173
Figure 5.41 Corrugated straws, testing results in water tank.....	174
Figure 5.42 Straws in water tank.....	174
Figure 5.43 Straws comparison in water tank.....	175
Figure 5.44 Results comparison by weight and temperature difference.....	177
Figure 5.45 Water adsorption quantity and regeneration ability of desiccant materials (Zheng, Ge and Wang, 2014).....	179
Figure 5.46 Schematic diagram of the experimental apparatus for solid desiccants.....	180
Figure 5.47 Experimental rig for solid desiccants.....	180
Figure 5.48 Silica gel testing panel.....	181

Figure 5.49 Silica gel humidity adsorption, panel A. ....	182
Figure 5.50 Silica gel panel humidity adsorption, panel B. ....	182
Figure 5.51 Moisture removal by Vermiculite $\text{CaCl}_2$ . ....	184
Figure 5.52 Moisture removal by Vermiculite $\text{MgSO}_4\text{-CaCl}_2$ . ....	184
Figure 5.53 Moisture removal by silica gel. ....	185
Figure 5.54 Moisture removal silica gel- $\text{CaCl}_2$ . ....	185
Figure 6.1 HFM-100 Heat Flow Meter. ....	192
Figure 6.2 PCM ceiling tile simulation zone. ....	194
Figure 6.3 PCM ceiling annual indoor room temperature comparison. .....	195
Figure 6.4 PCM ceiling indoor room temperature in July. ....	195
Figure 6.5 Schematic diagram of the experimental apparatus. ....	197
Figure 6.6 PCM blister panel schematic distribution. ....	199
Figure 6.7 Schematic diagram of blister panel. ....	200
Figure 6.8 Blister panel in HFM equipment. ....	201
Figure 6.9 INERTEK 23 enthalpy values, (MCI Technologies). ....	203
Figure 6.10 Scanning electron microscope 6490LV SEM (JEOL). ....	204
Figure 6.11 SEM Aluminium wool. ....	204
Figure 6.12 SEM INERTEK 23. ....	205
Figure 6.13 SEM Aluminium wool mixed with INERTEK 23. ....	205
Figure 6.14 SEM Aluminium wool with INERTEK 23 close-up. ....	206
Figure 6.15 Blister panels comparison at 28 °C, test 1. ....	207
Figure 6.16 Blister panels comparison with 2 °C increments, test 2. .	208
Figure 6.17 SRB laboratory test room. ....	210
Figure 6.18 Laboratory testing room. ....	211
Figure 6.19 Encapsulation container. ....	211
Figure 6.20 Panels mounted. ....	212
Figure 6.21 SRB testing room layout. ....	213
Figure 6.22 Thermal camera. ....	214
Figure 6.23 S27, heating without PCM. ....	216
Figure 6.24 S27, heating temperature comparison. ....	216
Figure 6.25 S27 representative cooling data. ....	217

Figure 6.26 Cooling temperature comparison (14 panels).....	218
Figure 6.27 Cooling temperature comparison (30 panels).....	218
Figure 6.28 Capsule panel (10 panels).....	219
Figure 6.29 Capsule panels mounted on the testing room. ....	219
Figure 6.30 Capsule panel, heating temperature comparison. ....	221
Figure 6.31 Capsule panel, cooling temperature comparison. ....	222
Figure 6.32 Magnetic stirrer schematic function. ....	225
Figure 6.33 Magnetic stirrer.....	225
Figure 6.34 Saturated $\text{MgSO}_4\text{-CaCl}_2$ . ....	226
Figure 6.35 Vermiculite experimental rig in the environmental chamber. .....	229
Figure 6.36 Raw vermiculite. ....	230
Figure 6.37 Vermiculite + Potassium Formate ( $\text{KHCO}_2$ ). ....	230
Figure 6.38 Calcium Chloride ( $\text{CaCl}_2$ ). ....	230
Figure 6.39 Vermiculite + Magnesium Chloride ( $\text{MgSO}_4\text{-CaCl}_2$ ). ....	231
Figure 6.40 Vermiculite + Lithium Chloride ( $\text{LiCl}$ ). ....	231
Figure 6.41 Vermiculite adsorption rate comparison. Method 1, test 1. .....	232
Figure 6.42 Raw Vermiculite at 1.5 kg. ....	233
Figure 6.43 Vermiculite + Potassium Formate ( $\text{KHCO}_2$ ) at 1.5kg. ....	233
Figure 6.44 Calcium Chloride ( $\text{CaCl}_2$ ) at 1.5kg. ....	234
Figure 6.45 Vermiculite + Magnesium Chloride ( $\text{MgSO}_4\text{-CaCl}_2$ ) at 1.5 kg. .....	234
Figure 6.46 Vermiculite + Lithium Chloride ( $\text{LiCl}$ ) at 1.5 kg.....	234
Figure 6.47 Humidity adsorption performance. Method 1, test 2. ....	235
Figure 6.48 Vermiculite, experimental setup. Method 2, test 1.....	236
Figure 6.49 Humidity adsorption results by percentage. Method 2, test 1. .....	237
Figure 6.50 Vermiculite, experimental setup. Method 2, test 2. ....	238
Figure 6.51 Humidity adsorption percentage. Method 2, test 2. ....	238
Figure 6.52 Solar-assisted heat pump experimental setup.....	241
Figure 6.53 Solar simulator front view (left), solar thermal collector schematic array (right).....	242

Figure 6.54 Solar simulator back view (left), solar thermal collector (right).	242
Figure 6.55 Distribution of the measurement reading points in the solar collector.	243
Figure 6.56 Schematic model of solar heating subsystem (a) solar thermal collector ; (b) water tank. Adapted from (Yin et al., 2017).	244
Figure 6.57 Solar radiation simulator.	245
Figure 6.58 SAHP refrigerant temperature inlet/outlet.	247
Figure 6.59 Model A: COP.	248
Figure 6.60 Model B: COP.	249
Figure 6.61 Model C: COP.	249
Figure 6.62 Model D: COP.	249
Figure 6.63 Model A: fan air.	250
Figure 6.64 Model B: fan air	251
Figure 6.65 Model C: fan air.	251
Figure 6.66 Model D: fan air	252
Figure 6.67 Model E: fan air.	252
Figure 7.1 Tarmac Masonry Houses, front and back facades.	257
Figure 7.2 First floor layout measurements, (The University of Nottingham).	257
Figure 7.4 PCM panels on a shelving system.	258
Figure 7.3 Shelving system in the testing room.	258
Figure 7.5 Room sensors location in Tarmac House.	259
Figure 7.6 Average room temperature heating comparison with S27.	260
Figure 7.7 Average temperature loss comparison with S27.	261
Figure 7.8 Average room temperature heating comparison with S23.	262
Figure 7.9 Average temperature loss comparison with S23.	262
Figure 7.10 House layout with testing room in yellow (The University of Nottingham, 2020a).	264
Figure 7.11 Testing room with PCM panels.	264
Figure 7.12 S23 panel (PCM Products Ltd, 2020).	265
Figure 7.13 Thermal conductivity S23 sample panel.	266
Figure 7.14 Testing room section with components.	267
Figure 7.15 Panels in shelving system.	268

Figure 7.16 Sensors temperature comparison. ....	269
Figure 7.17 DSC analysis for the S23. ....	270
Figure 7.18 S23, room temperature monitoring. ....	272
Figure 7.19 S23, room temperature monitoring heating and cooling. ....	273
Figure 7.20 Heating performance comparison. ....	274
Figure 7.21 Cooling performance comparison. ....	276
Figure 7.22 House testing site. ....	279
Figure 7.23 Installation of the thermal collector panels. ....	279
Figure 7.24 Desiccant box in room testing. ....	280
Figure 7.25 Solid desiccant array inside testing the box. ....	281
Figure 7.26 Desiccant box control temperature. ....	282
Figure 7.27 Desiccant adsorption and regeneration cycle. ....	283
Figure 7.28 Regeneration process with hot water pipe. ....	284
Figure 7.29 Adsorption and regeneration cycle. ....	284
Figure 7.30 Tri-modular system integration in a residential dwelling. ....	289
Figure 8.1 Roadmap to future homes standard. ....	293
Figure 8.2 Prefabricated panel with copper pipes. ....	299
Figure 8.2 LCA chain. ....	303
Figure 8.3 Environmental impact of total CO <sub>2</sub> emissions Carbon Equivalent mass. ....	305
Figure 8.4 Electricity consumption comparison with and without PCM. ....	306
Figure 8.5 Carbon emissions. ....	307
Figure 8.6 Carbon Equivalent CE. ....	308



# List of Tables

Table 2.1 Desirable characteristics of Phase Change Materials. ....	25
Table 2.2 PCM advantages and disadvantages (Pons, et al., 2014)... ..	26
Table 2.3 Potential of shell materials in various situations (Jacob & Bruno, 2015). ....	31
Table 2.4 Review PCM studies.....	42
Table 2.5 Comparison of reduction of solidification time for the PCMs in pure form and with dispersed nanoparticles (Kalaiselvam, Parameshwaran and Harikrishnan, 2012). ....	53
Table 2.6 Synthesis table of PCM enhancement methods. ....	55
Table 2.6 Synthesis table of the solid desiccant studies.....	75
Table 2.7 Summary of solar thermal studies. ....	90
Table 3.1 Commercial PCMs with low melting temperature. ....	101
Table 4.1 Zone area measurements.....	123
Table 4.2 Weather file input data.....	128
Table 4.3 Example of PCM input data on software.....	132
Table 4.4 PCM simulation properties.....	133
Table 4.5 PCM material input. ....	136
Table 5.1 PCM thermal properties.....	148
Table 5.2 PCM panels by encapsulation method. ....	149
Table 5.1 Model comparison by PCM panels. ....	166
Table 5.4 Testing record of encapsulation methods. ....	176
Table 5.5 Silica gel regeneration in the oven.....	183
Table 6.1 Thermal conductivity analysis by panel. ....	192
Table 6.2 Simulation parameters based on thermal conductivity. ....	193
Table 6.3 Blister panel enhancement method. ....	196
Table 6.4 PCM blister panel composition. ....	199
Table 6.5 Aluminium wool composition. ....	202
Table 6.6 PCM thermal characteristics.....	203
Table 6.7 Thermal performance analysis. ....	209
Table 6.8 Thermal camera comparison analysis of S27.....	214
Table 6.9 Capsule panel thermal images. ....	220

Table 6.10 Example procedure of $\text{CaCl}_2$ .....	227
Table 6.11 Vermiculite samples for testing.....	227
Table 6.12 Vermiculite testing procedure. ....	228
Table 6.13. Humidity adsorption capacity $\pm 2\text{kg}$ . Method 1, test 1.....	232
Table 6.14 Humidity adsorbed capacity 1.5 kg. Method 1, test 2. ....	235
Table 6.15 Vermiculite experimental results. Method 2, test 1. ....	237
Table 6.16 Vermiculite experimental results. Method 2, test 2. ....	238
Table 6.17 Vermiculite oven regeneration at 0.6 kg. ....	239
Table 6.18 Solar radiation simulation data ( $\text{W/m}^2$ ). ....	245
Table 7.1 Temperature comparison between S23 and S27. ....	263
Table 7.2 S23 panel (PCM Products Ltd, 2020). ....	265
Table 7.3 S23 thermal conductive results.....	271
Table 7.4 PCM thermal conductivity comparison.....	271
Table 7.5 Average temperature comparison results. ....	275
Table 7.6 Room temperature cooling comparison. ....	276
Table 7.7 SAHP COP. ....	287
Table 8.1 Cooling control system cost.....	297
Table 8.2 Humidity control system components. ....	298
Table 8.3 Energy loads comparison of the desiccant composite vs a commercial dehumidification system.....	299
Table 8.4 Humidity control system cost. ....	299
Table 8.5 Commercial humidity control systems. ....	300
Table 8.6 Default collector parameters (BRE, 2014). ....	301
Table 8.7 Overshading factor (BRE, 2014).....	302
Table 8.4 Heating and cooling calculations per month. ....	308
Table 8.5 $\text{CO}_2$ emissions over a 20 year period. ....	308

# Nomenclature

Symbol	Term	Unit
AC	Air Conditioning	
AHS	Adsorption heat storage	
CNF	Carbon nanofiber	
CNT	Carbon nanotube	
COP	Coefficient of Performance	
DI	De-ionized	
DHW	Domestic hot water	
DSC	Differential scanning calorimeter	
DX-SAHP	Dual photovoltaic thermal heat pump system	
E	Electrical energy	kWh
FTIR	Infrared spectrometer	
GF	Graphite foam	
GNPs	Graphene nanoplatelets	
GSHP	Ground Source Heat Pump	
h	Enthalpy	J/kg
HE	Heat exchanger	
HPS	Heat pipe solar	
HTHS	High-temperature heat-collecting system	
HyNPCM	Silver-titania hybrid nanocomposite	
i	Node being modelled	
i + 1	Adjacent node to the interior of construction	
i – 1	Adjacent node to exterior of construction	
i-SAHP	Indirect solar-assisted heat pump	
j	Previous time step	
LHP	Loop heat pipe	
LHS	Latent heat storage	
LTHS	Low-temperature heat-collecting system	
m	Mass	kg
MIPs	Molecular printed polymers	
MOF	Metal organic frameworks	
MTHS	Medium-temperature heat-collecting system	
Mtoe	Million tonnes of oil equivalent	
MWNTs	Multi-walled carbon nanotubes	
n	Number of cycles during the day	
NEPMs	Nanocomposite-enhanced Phase Change Materials	
nZEB	Nearly-zero energy building	
PCC	Phase change composite	
PCMs	Phase Change Materials	
PET	Polyethylene terephthalate	
PV	Photovoltaic	

PVT	Photovoltaic thermal	
PVT-GSHP	Solar Photovoltaic/Thermal-Ground Source Heat Pump	
PV-LHP/SAHP	Photovoltaic Loop Heat Pipe/Solar Assisted Heat Pump	
RB	Reference building	
RH	Relative Humidity	
S	Total solar radiation shining on the collector	kWh/m <sup>2</sup> /year
SAHPD	Solar-Assisted Heat Pump Drying	
SAPs	Super-absorbent polymers	
SDHW	Solar domestic hot water	
SEM	Scanning Electron Microscope	
SNOE	Silver nano-based organic ester	
STCHPS-PCES	Solar-Assisted Phase Change Energy Storage	
T	Temperature	°C
TES	Thermal energy storage	
UF	Utilisation factor	
VI	Vapor injected	
WB	Wallboard	
xGnP	Exfoliated graphite nanoplates	

## Subscripts

$A_{ap}$	Aperture area of collector	m <sup>2</sup>
$C_{eff}$	Effective thermal capacity	
$C_s$	Solution concentration	
$C_{composite}$	Specific heat capacity of the composite	J/kgK
$C_{matrix}$	Specific heat capacity of the matrix material	J/kgK
$C_{PCM}$	Specific heat capacity of the PCM	J/kgK
$C_p$	Specific heat capacity	J/kgK
$E_{latent}$	Heat storage capacity of the PCM	
$f_1$	Collector performance factor	
$f_2$	Solar storage volume factor	
$h_0$	Zero-loss collector efficiency	
$h_e$	Evaporator inlet specific enthalpy	
$h_{e+SH}$	Evaporator outlet specific enthalpy	
$k_0$	Value of thermal conductivity	
$k_1$	Change in conductivity per degree temperature difference	
$k_i$	Change in conductivity per degree temperature	
$m$	Mass	kg
$m_d$	Dry mass	
$m_r$	Refrigerant mass flow rate	kg/s

$M_s$	Mass of dry solid particles	
$m_{salt}$	Mass sample	
$m_{SIM}$	Mass of anhydrous sim composite	
$m_v$	Raw vermiculite	
$M_w$	Total mass of the water in the hot water tank	
$m_w$	Mass of water vapor in the given air volume	kg
$m_{ws}$	Mass of water vapor required to saturate at this volume	kg
$n$	Number of cycles during the day	
$T_{w.c.i}$	Water cold inlet	
$T_{w.c.o}$	Water cold outlet	
$T_{w,i}$	Refrigerant inlet	
$T_{w,o}$	Refrigerant outlet	
$T_{w.h.i}$	Water hot inlet	
$T_{w.h.o}$	Water hot outlet	
$q_{use}$	Power output of the collector	
$Q_{evaporator}$	Refrigerant mass flow rate	
$Q_s$	Solar input	kWh/year
$q_{rad,S}$	Shortwave solar radiation	
$q_{amb,sens}$	Longwave radiation exchange	
$q_{amb,lat,}$	Latent heat exchange	
$q_k$	Heat conduction	
$q_{rain}$	Energy gains from the rain	
$p_{el,pv}$	Electric power	
$V_{PCM}$	Volume of PCM	
$v_{suc}$	Specific volume of the refrigerant	
$V_{th}$	Theoretical displacement volume of the compressor	
$X_{PCM}$	Weight ratio of the pcm to the composite	
$Z_{panel}$	Shading factor for the solar panel	

## Greek letters

$\delta\tau$	Derived temperature	
$\delta T_{coll}$	Derived temperature of the collector	
$\lambda$	Thermal conductivity	W/mK
$\phi$	Relative humidity	%
$\rho$	Density	kg/m <sup>3</sup>

# Chapter 1 Introduction

## 1.1 Background

Worldwide, the rapid economic growth has led to an increase in energy demand. Nowadays the energy sector has been dominated by fossil fuels. However, conventional fossil energy sources are depleting, and their application creates harmful gases, endangering the environment and creating health concerns for people (Memon, 2014). The building sector has been considered a key part of global energy consumption. Buildings account for 40% of global energy use and contribute towards 30% of the total CO<sub>2</sub> emissions (Xie et al., 2017). According to Duarte et al., the energy usage in buildings is projected to increase by 32% between 2015 and 2040 worldwide (Duarte, Raftery and Schiavon, 2018). Globally, urbanized areas are expected to increase by over 70% and it is estimated that the world population will be located in urban centres by 2050 (Rupp, Giraldo Vásquez and Lamberts, 2015). Cities are ecosystems where a set of interconnected people interact not only with each other but also with their infrastructure and the environment. Figure 1.1 presents the correlation between the urban, energy in the climate context. To cope with the environmental by-products of social change through population

growth, awareness of the urban environment has increased, and the interaction of the environment with its inhabitants has been enhanced through Smart City projects (Mauree et al., 2019).

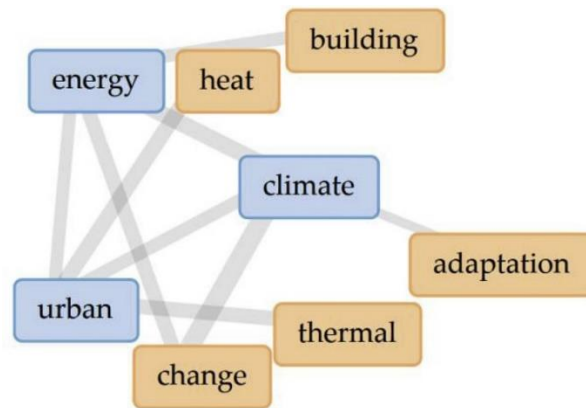


Figure 1.1 Analysis of the keywords from the urban, energy and climate context  
(Mauree et al., 2019).

For tackling the ongoing environmental issues, energy efficiency has become a major concern in the context of sustainable development over the world (Tran, Gao and Ge, 2021). Consequently, the international community has been facing the endeavour of creating a sustainable development that encompasses a system that satisfies “the needs of the present without compromising the ability of future generations to meet their own needs” (Doughty and Hammond, 2004). For this particular reason, energy efficiency in buildings is crucial to reduce energy usage and improve the local environmental sustainability (Ahmad *et al.*, 2016; Chwieduk, 2017; Xie *et al.*, 2017).

As consequence, technology-based strategies aim to develop effective and cost-efficient energy saving solutions for building applications.

## 1.2 Energy context

Energy saving is pivotal to accelerate decarbonization at a global level. Recent research suggests that energy policies are key in order to reduce energy consumption and climate mitigation costs (Labandeira *et al.*, 2020). Energy efficiency has an essential role in accelerating clean energy transitions and achieving global climate and sustainability goals. The relation between energy consumption, CO<sub>2</sub> emissions, and economic development has received significant attention in recent years by both policymakers and researchers, whereas the achievement of sustainable economic growth has gradually become a major global concern (Adedoyin and Zakari, 2020). The problem of these emissions is more critical in resource-rich countries that also experience high levels of economic uncertainty and geopolitical risk (Adams *et al.*, 2020). In general, energy generation from renewable sources is related to electricity as it is one of the most consumable forms of energy (Stolarski *et al.*, 2020).

Many countries have committed to reducing greenhouse gas emissions. According to the US Energy Information Administration and the European OECD countries have pledged to a 20% reduction in greenhouse gases by 2020 and between 80% and 95% by 2050 (Energy Information Administration, 2013; Pérez de Arce, Sauma and Contreras, 2016). In order to effectively address the climate change impact, a legally and politically binding long-term policy in construction is required (Contreras and Platania, 2019).



### 1.1.1 Energy figures

The UK energy consumption in 2021 was 173.1 million tonnes of oil equivalent, as illustrated in Figure 1.2 (Department for Business, 2013).

Domestic consumption rose by 19 percent, as people continued to work at home (due to COVID-19) in average temperatures that were 2.0 degrees Celsius colder than a year earlier, with April being noticeably colder, and colder than March for the first time since 2012.

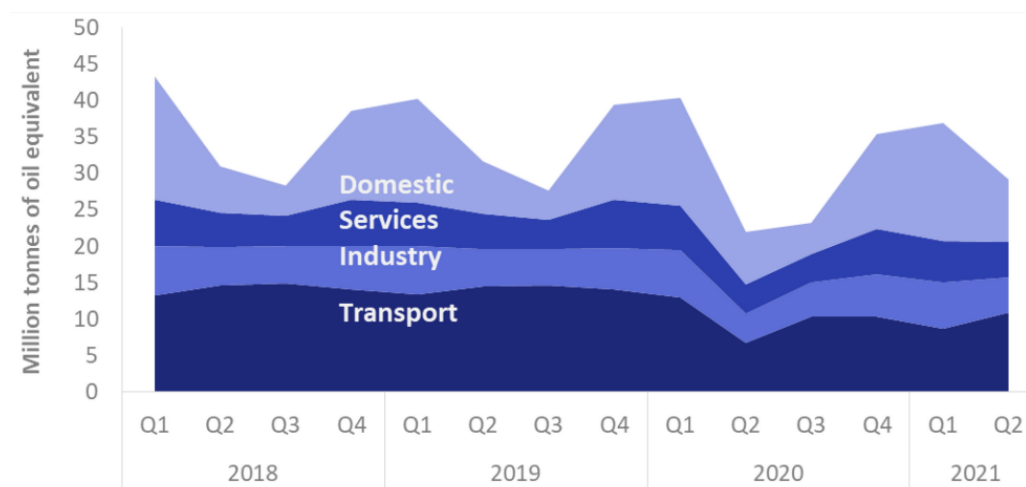


Figure 1.2 Total final consumption by sector, 2018-2021 (Department for Business, 2013).

Residential and commercial energy consumption consists mainly of energy use in building governmental measurements. The UK residential sector accounts for more than one-quarter of CO<sub>2</sub> emissions. Enacted in 2008, the Climate Change Act establishes a reduction in emissions from all six “Kyoto” greenhouse gases (GHG) in the UK by 2050. This means the UK will need to decarbonise across all sectors of the economy, and central to this will be cutting emissions further in the power sector (Department for Business, 2020a). Decarbonising heat is an important challenge for the future; where electricity is the second most widely used

fuel, accounting for just 13% of the energy consumption (Broad, Hawker and Dodds, 2020).

The UK's energy system is predominantly centralised with a major reliance on fossil fuels (Mirzania et al., 2019). The UK's Renewable Obligation establishes that a percentage of the electricity sold in the UK should be generated from renewable resources, thereby promoting the increased portion of renewable electricity generation (Anandarajah and Strachan, 2010), Figure 1.3 presents the electricity generation from renewables in the UK.

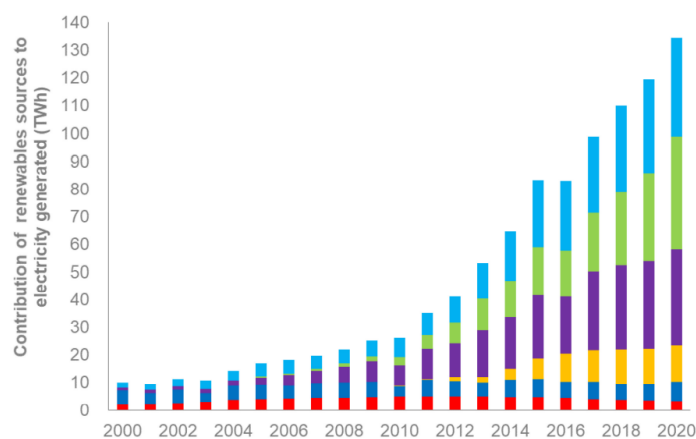


Figure 1.3 Electricity generation from renewables since 2000 (Department of Energy and Climate Change (DECC) and National Statistics, 2014).

While national and international policies will have a role to play in addressing greenhouse gas emissions, cities provide the infrastructure to apply the sustainable policies measures for immediate implementation and have a strategical position to curb local emissions and energy consumption. Figure 1.4 presents the greenhouse gases from 1990 to 2020 (Department of Energy and Climate Change (DECC) and National Statistics, 2014), where a significant reduction has been made in the past decade.

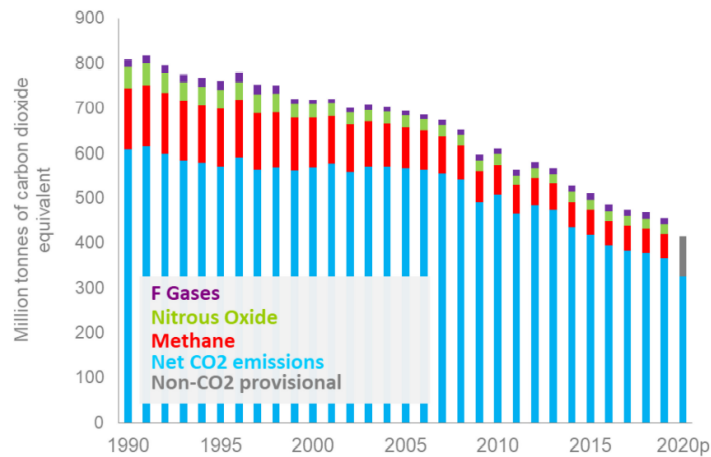


Figure 1.4 Territorial greenhouse gas emissions by gas (Department of Energy and Climate Change (DECC) and National Statistics, 2014).

Moving forward, to accomplish a meaningful reduction in energy consumption, actionable data is required, detailing the energy usage of buildings models that can help forecast the energy saving infrastructure (Streltsov *et al.*, 2020).

### 1.3 Building Context

In terms of the household energy demand and consequently the CO<sub>2</sub> emissions many conditions come into factor, for example, the type of dwelling, construction area, the insulation levels, the heating mechanism, water usage, electric appliances, as well as the lifestyle choices, income, among others. The average heat losses of different types of dwellings range from 365 W/°C for a detached house down to 182 W/°C for a flat (Druckman and Jackson, 2008). Generally, the heating, ventilation, and air conditioning (HVAC) systems account for approximately 40% of the total energy consumption of a building and contribute a considerable amount of peak demand (Ren *et al.*, 2021).

### 1.3.1 Energy usage

The domestic sector is accountable for temperature changes due to the high energy demand generated by space heating (Department for Business, 2020b). Efficient planning to meet building energy needs while increasing operational, economic, and environmental efficiency requires accurate, high spatial resolution information on energy consumption (Streltsov *et al.*, 2020). Figure 1.5 presents the energy intensity since 1990, the Electricity generation in 2020 was 1.4% higher than in 2019, while heat generation increased by 0.7%

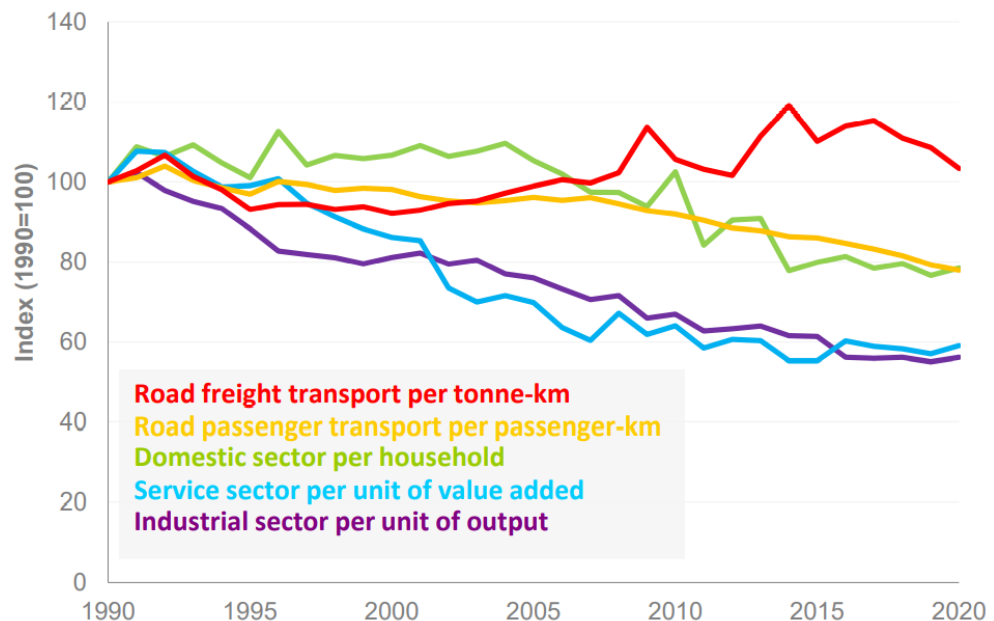


Figure 1.5 Domestic consumption, temperature-corrected consumption, and average annual temperatures.

Energy consumption per person fell from 0.8 ktoe in 2000 to 0.6 ktoe in 2020 with consumption per household following a very similar trajectory. Disposable income has increased more quickly than population and so the consumption per unit of disposable income has decreased even more rapidly. The improvements to energy intensity in this sector are likely related to higher energy efficiency of homes resulting from improvements

to insulation measures, boiler, and other appliance efficiencies (Department for Business, 2021).

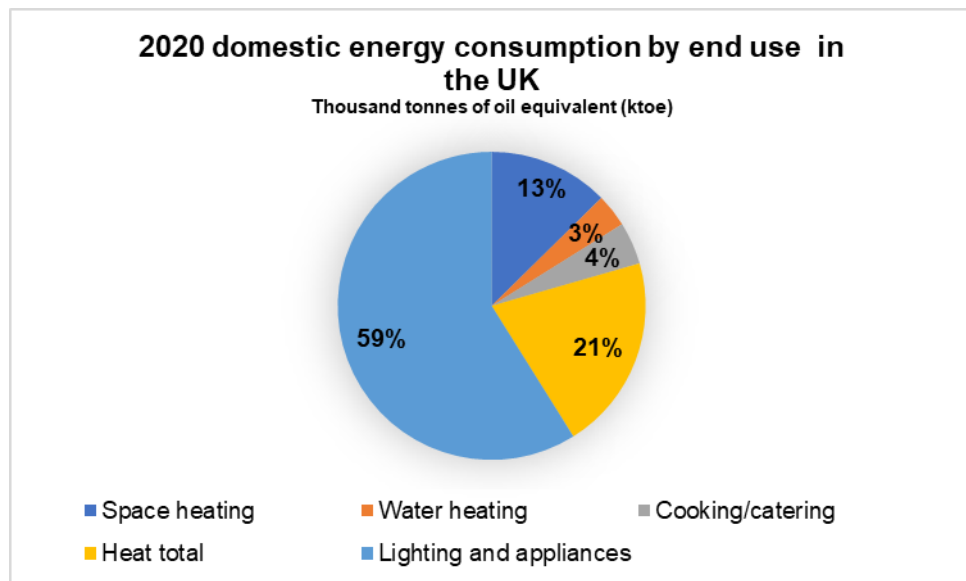


Figure 1.6 Domestic energy consumption by end use in the UK (Department for Business, 2021).

Dowds and You investigated the electricity and heat consumption data of existing dwellings in the UK, comparing the energy supply with the combination of renewable energy as shown in Figure 1.7 and Figure 1.8.

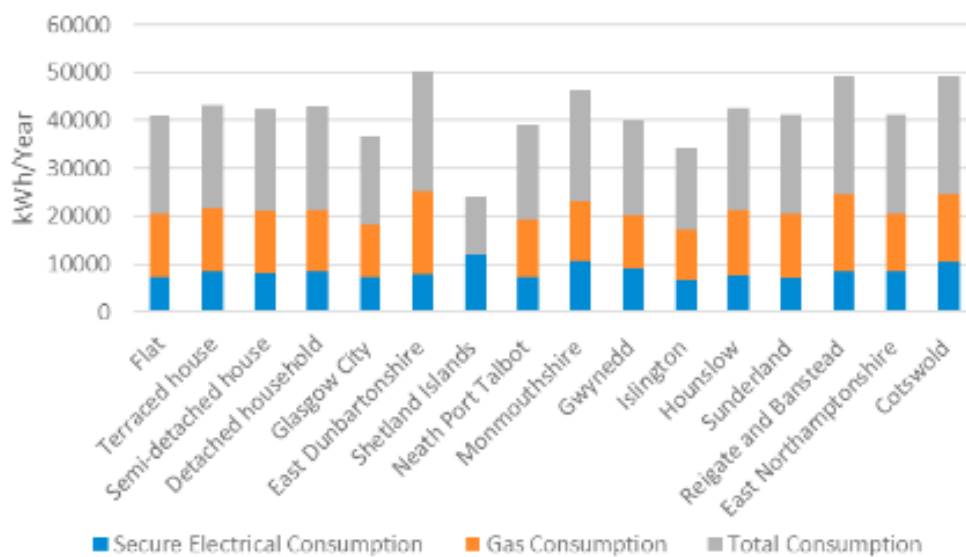


Figure 1.7 Electricity and gas consumptions (existing houses), (Dowds and You, 2019).

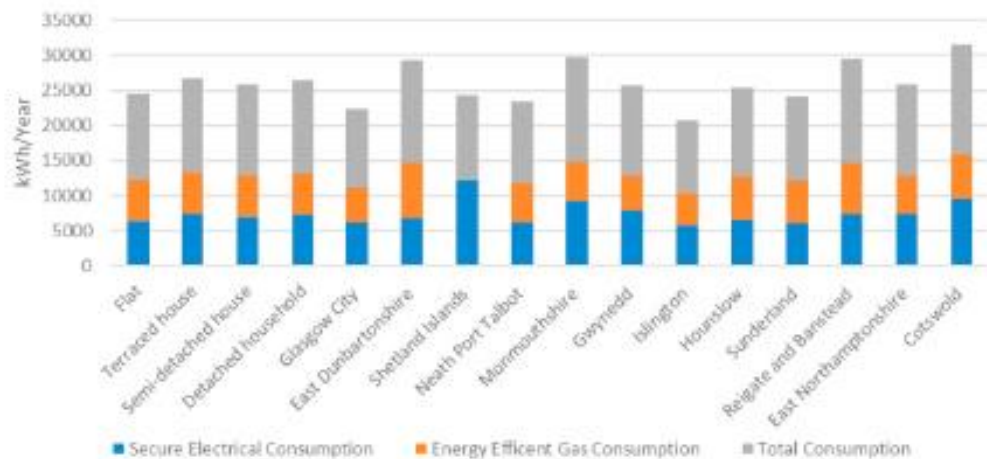


Figure 1.8 Electricity and gas consumptions (new houses), (Dowds and You, 2019).

### 1.1.2 Standards for thermal comfort and energy efficiency in buildings

Nowadays the popularity of building performance standards has increased through the advancement of building codes. These codes are used to enforce a minimum set of requirements in terms of energy performance and occupant's behaviour (O'Brien *et al.*, 2020).

A review of existing building codes is presented by (Papineau, 2017; Lu and Lai, 2019; Norouzi and Soori, 2020; O'Brien *et al.*, 2020).

According to the World Green Building Council, there are more than 40 green building rating tools applied worldwide (Lu and Lai, 2019), the most popular certifications are described as follows:

- LEED (Leadership in Energy and Environmental Design), is issued by U.S. Green Buildings Council and it's based on a points system.
- Energy star has been developed by the Department of Energy and the Environmental Protection Agency. To obtain the certification, the building needs to be at least 15% more energy efficient than traditional properties.

- BREEAM (the Building Research Establishment Environmental Assessment Method), focuses on the assessment of environmental, social, and economic sustainability performance and comes with a star rating from one to six.
- The Green Globes certification program is offered through the Green Building Initiative. To qualify, the building should meet at least 35% of the program's 1,000 available points.
- The Living Building Challenge certification is based on the building's sustainability performance over a year. To qualify, the construction requires to achieve all seven "petals," which include materials, site, water, health, equity, beauty, and energy.

## **1.4 Topic of study**

This research focuses on the integration of a tri-modular system that aims to achieve a thermal comfort approach in buildings. The system contemplates a high-performance heat pump to provide heating in winter and domestic hot water. A high-performance water adsorbent, based on a solid desiccant that provides air dehumidification, thereby maintaining relative humidity at a comfortable level. Finally, a passive PCM ceiling system that assists in the building passive cooling requirements, preventing overheating during summer days while maintaining a habitable temperature overnight.

The heat pump is coupled with solar thermal panels that can be mounted on roofs or walls. They draw thermal energy from the environment, even in the absence of direct solar irradiance. This gives the overall system a

higher coefficient of performance (COP) than traditional systems, and it can reach temperatures of up to 68 °C all year round with little decrease in the efficiency. The system has two cycles: a water cycle and a refrigerant cycle with a heat exchanger in between coupled with a sensor that monitors and minimises the heat loss. The proposed heat pump system works at a higher pressure than most heat pumps, which improves COP and reduces heat losses in winter and overnight. The high temperatures allow the heat pump to supply energy directly to traditional radiators.

The Phase Change Materials function as a passive cooling technology. These materials are characterized by their capacity to absorb the available thermal energy, store it, and passively release it by utilising latent heat during phase change, thus reducing temperature peaks and improving thermal comfort. The process of absorbing and releasing the heat consist of both sensible and latent heat, the latent heat has the capacity to store up to 14 times more thermal energy in comparison to conventional materials such as masonry. The PCMs will be fitted in the building as a ceiling tile system that would be in contact with the indoor environment, allowing the system to work passively. For the proposed application, the melting temperature of the material should be within the human thermal comfort temperatures.

In this case, the PCM will be fitted in the ceiling cavity or above ceiling tiles, allowing it to remove excess heat from the air at the top of the room, keeping the air lower down at a comfortable level.



The high-performance water adsorbent will cover the requirements for humidity control. As the room humidity increases the desiccant adsorbent passively removes the excess moisture from the air. The adsorbent moisture can then be naturally released back into the room if the humidity drops below the thermal comfort levels. Solid desiccant materials are considered an effective and economical approach for dehumidification and are less subject to corrosion compared to liquid desiccants. The dehumidification and regeneration performance of a solid desiccant-based system is expected with high water adsorption capacity, good renewability at relatively low regeneration temperature, low desorption energy input, and high durability. To boost the performance of the material the impregnation of two or more hygroscopic salts into a porous desiccant (composite desiccant) is considered. Composite desiccants have attracted attention in the last few years, and this study considers the experimental evaluation of different enhancement materials. In order to integrate this system, the regeneration method should be addressed. For this reason, the utilization of the heat pump system is considered a suitable option to regenerate the solid desiccant when the material gets saturated. As consequence, the desiccant regeneration temperature should range within the temperatures provided for domestic hot water applications, a schematic representation is shown in Figure 1.9, where the PCM panels are placed in the ground floor living area, the solid desiccant is in the kitchen area to contrast the high humidity in this section. The heat pump is placed on the outside wall and the solar

collector panels can be mounted on the roof. As a result of the modular arrangement, each system could potentially perform as a stand-alone.

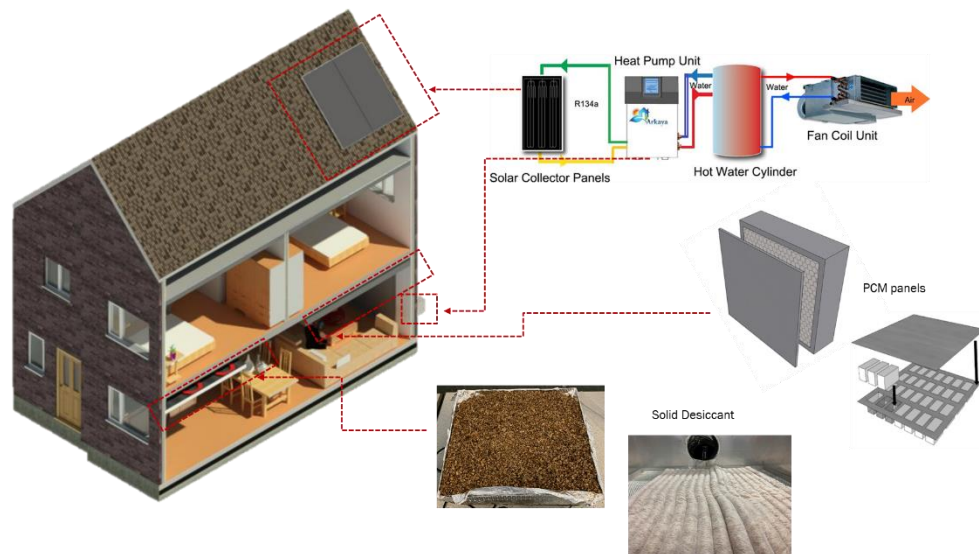


Figure 1.9 Schematic representation of system components.

Figure 1.10 presents the house section, where the PCM panels are absorbing the ambient heat, the air from the kitchen area is directed to the solid desiccant panel and the water tank is connected to the solar collectors and the desiccant panel. The integration of the system would depend on the specific characteristics of the building design, particularly for retrofit purposes.

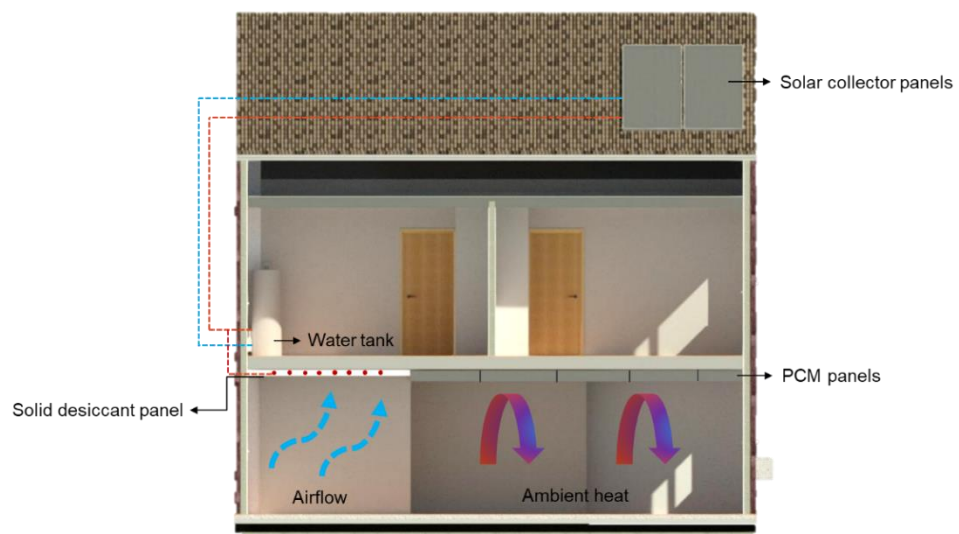


Figure 1.10 System description.

## 1.5 Research scope and aims

As an architect, the environmental motivation behind this research focuses on the constant need to innovate, adapt and change. It is important to embrace the current trends in the construction sector, taking the current energy policies as an opportunity to improve the building thermal comfort through environmentally friendly solutions.

Globally, the building sector comprised the largest energy end using sector and for this reason, the design and performance of buildings are pivotal to reduce energy consumption and CO<sub>2</sub> emissions. As the residential sector plays a crucial role, this research focuses on the design and development of novel solutions to address the major factors concerning energy performance and thermal comfort in buildings. However, most of the time, the energy conditions (energy demand, comfort, energy systems, building fabric, etc.) that affect the building performance are addressed individually even though they are highly interrelated and require an inclusive approach and understanding of both the environment and user occupancy.

The general aim of this study is to provide an opportunity to design a cost-effective and environmentally friendly system suitable to address the main parameters involved in human thermal comfort in buildings. More precisely, this project concentrates on the thermal characteristics of phase change materials for passive cooling, solid desiccants for humidity control, and solar-assisted heat pumps to cover the household heating

requirements. The detailed innovative features of the proposed research project focus on the following:

- The development of an innovative, energy-efficient system that controls the heating, cooling, and humidity in buildings. The system aims to minimise energy consumption through sustainable solutions, reducing CO<sub>2</sub> emissions.
- To promote indoor thermal comfort by controlling both temperature and humidity, through energy saving technologies.
- The selection and evaluation of a suitable PCM, including the analysis of the thermal properties and enhancement methods.
- Development and experimental assessment of novel encapsulation methods appropriate for PCM ceiling integration.
- To design a new composite desiccant adsorbent material, which can be regenerated by the domestic exhaust heat by using natural mesoporous material.
- To evaluate the performance of a solar-assisted heat pump for space heating and the regeneration of the desiccant composite.

## **1.6 Structure of the research**

Based on the theoretical and experimental methodologies this project is divided into four stages. The following nine chapters detail and illustrate the research process on the tri-modular system focusing on the PCMs, solid desiccants, and a solar-assisted heat pump unit. The overall structure of the thesis work is presented in Figure 1.11.

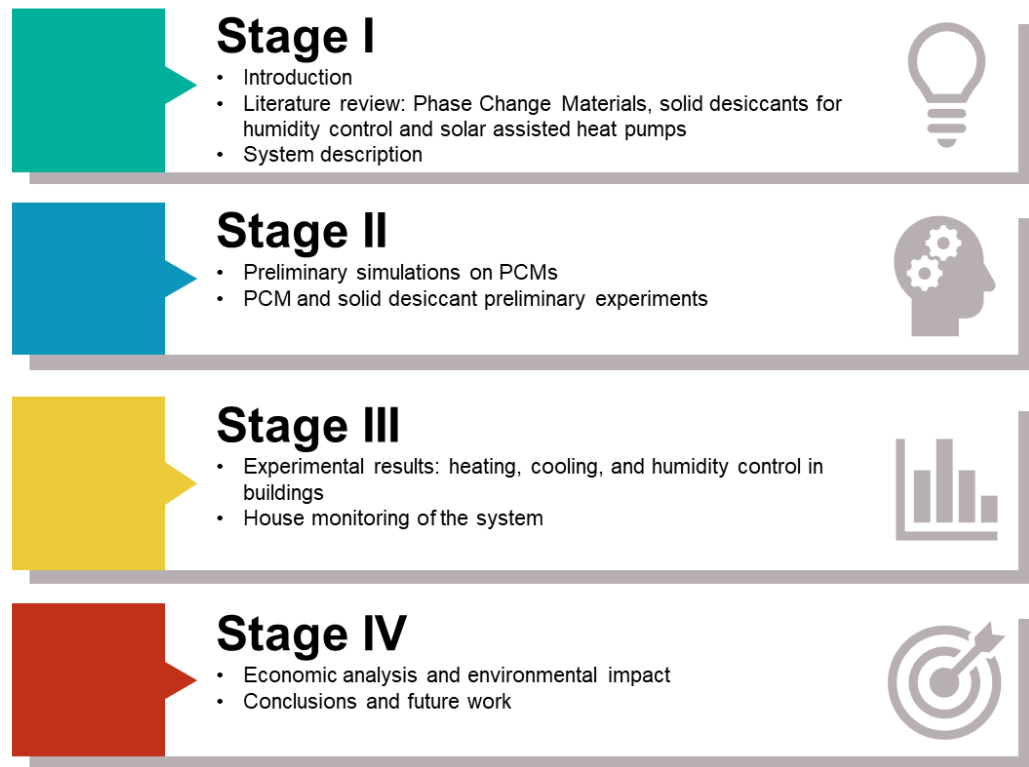


Figure 1.11 Schematic of the research work.

Stage I, provides the relevant information focusing on the state of the art of the proposed technologies and setting the bases for the system evaluation. In this case, the literature review of previously published theories of each system is detailed. The system design is introduced, detailing the proposed components derived from the literature, and the proposed design is refined at this stage.

Stage II, emphasizes in the theoretical analysis and preliminary assessment of the material components. The selection, development, synthesis, and optimization of the materials and enhancement methods are discussed.

During Stage III, the experimental evaluation is executed, in the first instance, the individual elements of the system are measured in the laboratory. Further experimentation of the large-scale system is

performed with the integration of the three system components in a residential dwelling.

Stage IV, concentrates on the economic and environmental analysis as well as recommendations. The life cycle assessment is included in this section. The conclusions and future work are discussed.

## **1.7 Summary**

The built environment, with its vast consumption of energy and natural resources, generates harmful emissions during the construction, operation, and at end of life.

In the current context of energy use reduction and the decarbonization of energy supply and demand, researchers have the opportunity to investigate and develop novel ideas to reduce greenhouse gases and meet sustainable development goals. Enquiring the factors involved in the energy consumption of buildings play an important role towards reducing the energy demand. Additional research development and large-scale projects are required to prove the viability of integral sustainable energy solutions such as the tri-modular system proposed.

# Chapter 2 Literature review: Phase Change Materials, solid desiccants for humidity control and solar assisted heat pumps

## 2.1 Introduction

This chapter introduces the main aspects involved in thermal comfort with relation to the built environment, focusing on the impact on the building energy performance. An overview of the PCMs is introduced, the building applications are investigated. Furthermore, the introduction to the enhancement methods has been analyzed and compared. In addition, this chapter explains the absorption and adsorption desiccant processes for humidity control. Reviewing popular solid and liquid desiccants, together with practical applications. Moreover, the review uptakes a sustainable approach with the application of natural composite materials.

Finally, the chapter discusses the heat pump applications and recent developments, emphasizing the different applications that these systems provide, exalting the advantages of each technology.

## 2.2 Human thermal comfort

The main function of buildings is to provide a comfortable and healthy environment for the occupants. The importance of achieving thermal comfort in buildings is essential as people spend most of their time in them. When the building does not provide the necessary thermal conditions; the user tries to regulate these factors with alternative means, creating an increase in the building energy demand.

The detriment of the natural resources and the awakening of environmental consciousness have generated an interest in energy conservation and the development of innovative energy efficient technologies that improve thermal comfort (Raish, 2019). Thermal comfort is defined by ASHRAE 55 as “that condition of mind that expresses satisfaction with the thermal environment and is assessed by subjective evaluation” (RAA-C.E, 2013). Thermal comfort are the environmental conditions perceived by the human body in relation to the environment (Rupp, Giraldo Vásquez and Lamberts, 2015), due to its subjectivity thermal comfort varies in every individual. The human body responds to the environmental variables, the thermal comfort is achieved when the heat generated by the human metabolism is dissipated at a rate that allows maintaining the thermal equilibrium of the body. The interaction of the human body with the environment is done by conduction, convection, and evaporation. The boundary conditionings for the heat exchange are favour through the ambient temperatures, air movement, and relative humidity and are called human comfort requirements



(Mehling, 2008). In addition, the human body physiological and psychological response to the environment affects the assessment of the environmental conditions (Parsons, 2000). Human comfort requirements depend on several conditions, such as clothing, activity, air temperature, radiant temperature, humidity, and air movement. According to Raish (Raish, 2019) there are six primary thermal comfort variables:

- Ambient temperature (air temperature).
- Radiant temperature (the temperature of the surfaces around us).
- Relative humidity (measurement of the water vapor in an air-water mixture).
- Air motion (the rate at which air moves around and touches the skin).
- Metabolic rate (amount of energy expended).
- Clothing insulation (materials used to retain or remove body heat).

In his book Çengel divides the comfort requirements based on the air motion and the humidity; considering an acceptable air temperature range between 22 °C and 26 °C as for the relative humidity he proposes a value between 30% to 70% (Çengel, 1998).

There is a common misconception when assessing the environmental conditions, as often designers focus on the air temperature disregarding the additional factors, the humidity in particular as increase moisture can cause mold or mildew, which is a health hazard and a detrimental of the building materials (Parsons, 2014; Raish, 2019). The importance of thermal comfort in the architectural environment is pivotal since it should

be considered for the building design, as it not only affects and therefore affecting the energy performance.

Controlling the thermal properties in buildings includes heating, cooling, and humidity. In addition, the air quality should also be considered. In the case of building application, the PCM technology requires special attention in the parameters affecting human thermal comfort, such as the air temperature and the surface's surroundings, as the PCM can only affect these elements. In addition, the relative humidity can be incidentally influenced as it is a part of the air temperature (Mehling, 2008). In terms of humidity, there are different methods to remove moisture from buildings such as cooling below the air dewpoint or the application of desiccants.

The idea of a building is to provide comfortable conditions in comparison to the external climate. The current construction practices aim to achieve thermal comfort while reducing the building energy consumption. Nowadays, international standards regulate the parameters to assess thermal comfort. Construction codes must comply with regulations and standards designed to archive the basic comfort requirement and at the same time minimize the energy demand of buildings (ISO, 2005; CEN, 2007; Marino *et al.*, 2018).

## **2.3 Phase change materials**

### **2.3.1 Background**

Thermal energy storage (TES) focuses on improving energy efficiency through energy saving (Jeon, et al., 2010). TES can be incorporated in

buildings by sensible or latent heat. Sensible heat considers for example increasing and decreasing the building envelope temperature, an example of the application of latent heat can be the inclusion of phase change material that would increase the thermal inertia (Cabeza *et al.*, 2011). The thermal energy storage is divided by its physical and chemical properties and is described in Figure 2.1.

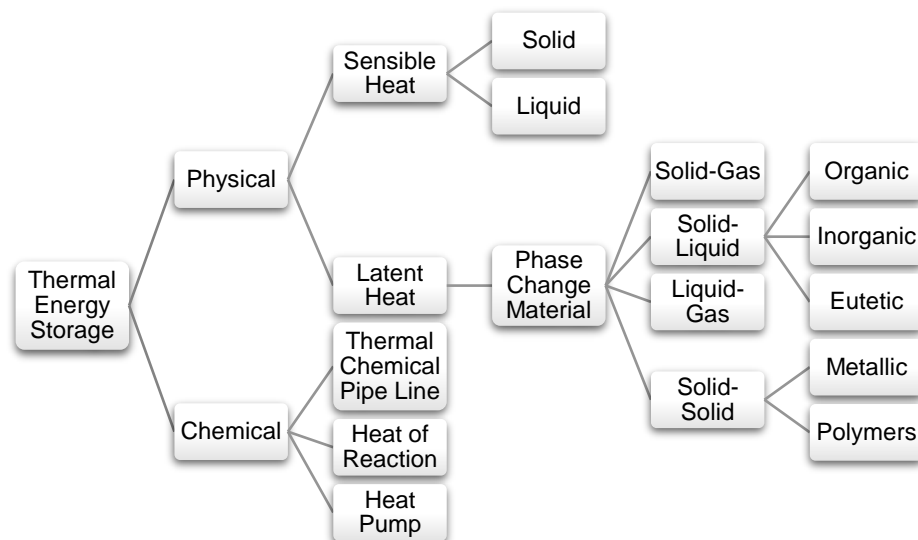


Figure 2.1 Energy storage methods (Yang, Huang and Zhou, 2020).

Phase Change Materials (PCMs) are characterised by their capacity to absorb available thermal energy, store it, and passively release it by utilizing latent heat during phase change as detailed in Figure 2.2, thus reducing temperature peaks and improving thermal comfort (Salunkhe and Shembekar, 2012), this are well suited for heat transfer and energy conversion applications where the state of the material normally varies from solid-liquid or vice versa.

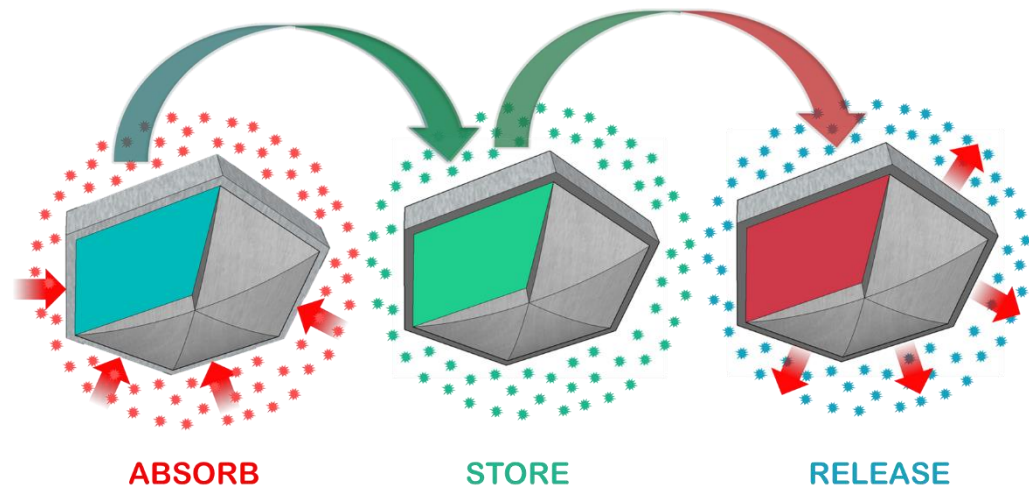


Figure 2.2 PCM thermal process.

For the PCM the process of absorbing and releasing the heat consist of both sensible and latent heat. In the sensible heat process, the thermal energy is absorbed and store at the start of the melting process, for the latent heat, the thermal energy is stored during the phase change process (Hamdan and Elwerr, 1996). The latent heat system is characterized by the isothermal discharge or gain of thermal energy. In contrast, sensible cooling and heating are done when the temperature increases or decreases. The latent heat has the capacity to store up to 14 times more thermal energy in comparison to conventional materials such as masonry (Salunkhe and Shembekar, 2012).

Latent heat storage (LHS) is considered as one of the most efficient methods to store thermal energy, having high storage density and at the same time, small temperature fluctuations while absorbing and releasing the heat (Khudhair and Farid, 2004; Ibáñez *et al.*, 2005). The thermal performance of PCMs depends on many characteristics; for building applications, the melting temperature, thermal conductivity, and energy storage density are key for the successful implementation. Ideally, the

PCMs would have a rapid melting and solidification response (Ji *et al.*, 2014; Ma, Lin and Sohel, 2016).

To boost the performance of the PCMs, several solutions have been proposed to enhance the thermal conductivity and promote energy exchange. Practical examples are the application of fins and heat pipes, different encapsulation methods and containers, micro and macro-encapsulation, or the addition of high thermal conductive materials into the PCM base fluid, among others (Khodadadi, Fan and Babaei, 2013; Ma, Lin and Sohel, 2016).

Mazzeo *et al.* identify the application of PCM in building envelopes to provide high thermal performance as a possible solution to archive net-zero energy buildings in the near future. For buildings applications the PCMs are used to control the ambient temperatures in order to archive thermal comfort, this can be applied to diverse components of a building, for example, floors, windows, ceilings, and walls (Mazzeo, Oliveti and Arcuri, 2017). Nevertheless, the success of the PCM would depend on several conditionings, the main elements that would determine the performance are: the PCM melting temperature, the quantity, the encapsulation method, the location within the building structure, building design and orientation, the building energy load, the climate conditions, the energy demand, the selection of the equipment, utility rate policy, occupancy schedule, system control, and operational algorithms, among others. The ideal requirements for PCMs are presented in Table 2.1, where an assessment of the properties should be considered for each application.

Table 2.1 Desirable characteristics of Phase Change Materials.

<b>Thermal properties</b>	<b>Physical properties</b>	<b>Kinetic properties</b>	<b>Chemical properties</b>	<b>Economics</b>
High latent heat of transmission	Small volume change	Sufficient crystallization rate	Long-term chemical stability	Abundant
High thermal conductivity	Low vapour pressure	No-supercooling	No toxicity	Cost-effective
Suitable melting/freezing temperature	High density	High nuclear rate	Non flammable	Available
			Noncorrosive	Commercially viable
			No phase separation	Aesthetic
			No degradation through repeated cycles	Easy installation
			Compatibility with container materials	

### 2.3.2 Classification and characteristics

The PCMs are commonly classified into organic, inorganic, and eutectic which is a combination of organic and inorganic materials (Quian, et al., 2015).

Organic PCMs: for building applications, there are three main categories, pure n-alkanes, fatty acids, and esters (Kenisarin, 2014). The organic PCMs are popular for their latent heat capacity, they cover a wide range of temperatures, and provide stability, nevertheless, their principal drawback is their high flammability as well as their low thermal conductivity. The most popular non-paraffin includes the alcohols, esters, glycols, and fatty acids being the last ones the more commercially used due to its advantages: high latent heat, no phase segregation, low super cooling although they tend to be highly flammable (Akeiber, et al., 2016).

Inorganic PCMs: the most popular inorganics PCMs are salt hydrates, salt solutions, and metals the advantages are their higher heat fusion, lower flammability, and cost, however, they present corrosion, low thermal stability, and phase segregation (Baetens, et al., 2010).

Eutectics: are a mixture of a minimum of two PCMs, this can be any combination of organic-organic, organic-inorganic, and inorganic-inorganic (Tyagi & Buddhi, 2007). Generally, due to the atomic ratio production, they have more desired characteristics such as a higher latent heat and a sharp melting point (Jaguemont *et al.*, 2018).

A broad classification of PCM used in buildings along with their thermo-physical properties is shown in Figure 2.3 and the thermal properties are detailed in Table 2.2.

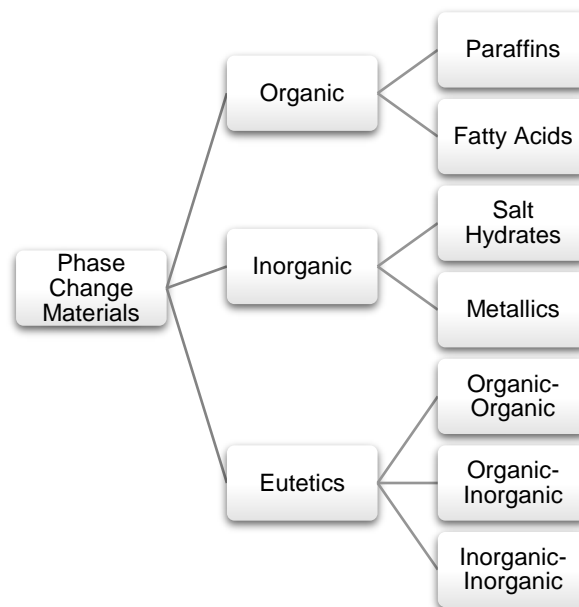


Figure 2.3 Phase change materials classification (Kylili & Fokaides, 2016).

Table 2.2 PCM advantages and disadvantages (Pons, et al., 2014).

PCMs	Advantages	Disadvantages
<b>Organic</b>	Physical and chemical stability Good thermal behaviour Little super cooling Noncorrosive Reliable Long freeze-melt cycle	Low thermal conductivity Low density Low melting point High volatile Flammable Volume change Higher price Non-compatible with plastic containers
<b>Inorganic</b>	Higher energy storage density Higher thermal conductivity Non-flammable Inexpensive Compatible with plastics	Subcooling Phase segregation Corrosive Smaller range of melting points Delay at start of solidification and segregation Efficiency decreases in each cycle
<b>Eutectics</b>	High thermal storage density	Strong odor

Wide range of phase change temperature	Phase segregation
Chemical stable	
No or little supercooling	

### 2.3.3 PCM encapsulation

Encapsulation is a process of covering the PCM (that forms the core part of the encapsulated PCM) with a suitable coating or shell material. A primary purpose of encapsulation is holding the liquid and/or solid phase of the PCM and keeping it isolated from the surrounding. This ensures the correct composition of the PCM that would have otherwise changed due to the mixing of the PCM with the surrounding fluid. Other advantages of encapsulation involve a reduction in the reaction of PCM with the surrounding, flexibility in frequent phase change processes, an increase in heat transfer rate, and enhancement in the thermal and mechanical stability of the PCM. It can also improve the compatibility of hazardous PCMs that cannot be directly used or immersed in certain applications such as blood transport, food storage, building cooling/heating, etc. (Salunke & Shembekar, 2012).

The encapsulation is based on the size which surrounds the PCM: the macro covers diameters of 1mm and more while the micro covers from 1 $\mu$ m to 1mm as depicted in Figure 2.4, while the nano is less than 1  $\mu$ m (Jacob & Bruno, 2015), being the macro encapsulation the most applied in the industry.



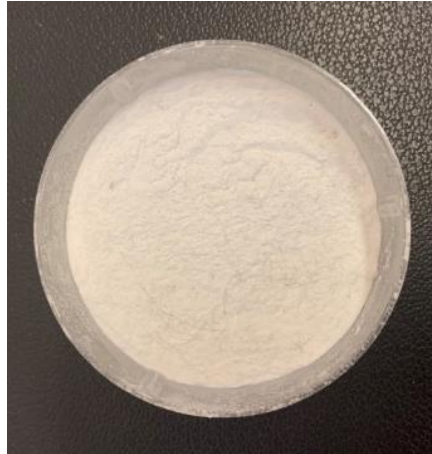


Figure 2.4 Microencapsulated PCM.

The manufacturing of microencapsulated PCM is more complex than macro encapsulated PCM as its size falls below 1 mm. However, microencapsulation results in higher heat transfer rates as compared to that of macro encapsulation (Hawladar, Uddin and Khin, 2003; Khudhair and Farid, 2004). Any container used for PCM encapsulation should meet the following requirements (Bland, et al., 2017):

- Be a barrier to the environment to protect from harmful interaction.
- Offer an adequate heat transfer surface.
- Ensure structural stability and offer easy handling.
- For its given application, it must offer corrosion resistance, thermal stability, required strength, and flexibility.

There are many methods for encapsulation of the PCM such as tubes, pouches, spheres. Another approach to incorporate PCM in building walls is its mixture with insulation materials, this is known as shape stabilized PCM (Silva, et al., 2016); nevertheless, the encapsulation is most common.

The advanced technological developments have made it possible to encapsulate the PCM at the nanoscale. Sukhorukov et al. applied the same force on 10 nm and 10  $\mu$ m size polyelectrolyte capsules and observed that deformation for the 10 nm capsule was substantially smaller as compared to that of 10  $\mu$ m capsule (Shkhorukov, et al., 2005). This shows that nano- capsules are structurally more stable as compared to macro and micro-capsules and there is a great potential in the use of nanocapsules for thermal energy storage applications.

#### **2.3.3.1 Effective volume**

For a given PCM, the storage capacity depends on the quantity of the PCM that is capable to change phases during a daily cycle (Alvarez, et al., 2013). This quantity is called the effective volume, and depends on:

- The amplitude of excitation for the PCM.
- Duration of this excitation.
- Convection heat transfer coefficient between the air and the PCM.

The encapsulation principle is detailed in Figure 2.5. In solid state, the supplied heat to the PCM increases its temperature until it reaches the melting point. The PCM temperature remains constant throughout the melting process. During this phase change process a substantial amount of heat is stored. The molten PCM transforms to solid when exposed to the surrounding with a temperature lower than its melting point. The phase transformation occurs through the release of thermal energy during sensible cooling and the phase change process from the liquid to solid state. The phase change of PCM from solid to liquid phase and from

liquid to solid phase are termed as charging and discharging processes, respectively (Salunke & Shembekar, 2012).

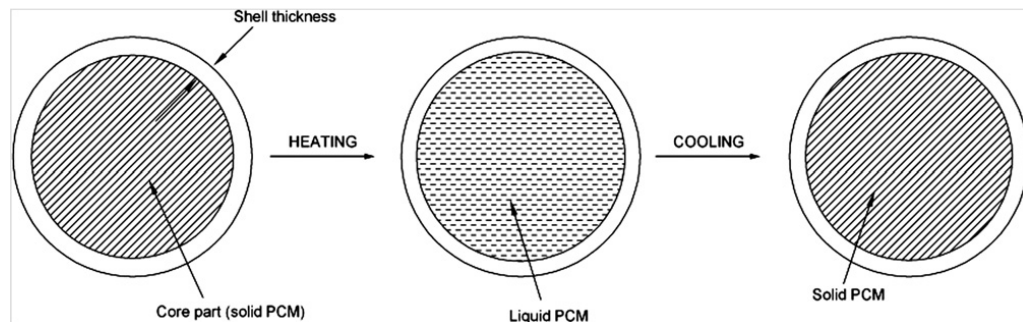


Figure 2.5 Structure and working principle of the encapsulated PCM (Salunkhe and Shembekar, 2012).

### 2.3.3.2 Capsule Material

Shell material plays an important role in deciding the heat transfer characteristics as well as mechanical strength of the encapsulated PCM. A high-strength shell material with good thermal characteristics not only improves the performance of a system but also increases the number of thermal cycles that the encapsulated PCM withstands.

Common materials that can be used for encapsulation are polypropylene, polyolefin, polyamide, silica, polyurea, urea-formaldehyde, copper, aluminium, etc.

### 2.3.3.3 Encapsulation geometry

The geometry has a substantial effect on the PCM system, the encapsulation serves as a way to enhance heat transfer (Amin & Belusko, 2014). In a study conducted by Wei et al. it was shown that between a sphere, cylinder, plate, and tube the sphere had the highest heat transfer rate, followed by the cylinder, plate, and tube at last (Wei, et al., 2005). Zhang et al. investigated a microencapsulated PCM based on a silica

shell. The study proves that the efficient heat transfer of the system (Zhang, et al., 2010). Another study presented by Darkwa et al. evaluated the thermal performance of a high composite microencapsulated PCM board with three configurations: rectangular, triangular, and pyramidal. The results showed that the thermal response time for the rectangular and triangular geometries was half that of pyramidal geometry. When compared with pure PCM the thermal conductivity increases over ten times, nevertheless a considerable reduction in the energy storage capacity was presented (Darkwa & Su, 2012). Table 2.3 presents potential materials for PCM encapsulation. One of the principal drawbacks of the salt hydrates is their corrosiveness with metal encapsulation, in contrast, the organic PCM are non-corrosive although their major disadvantage is their difficulty to mix with water.

Table 2.3 Potential of shell materials in various situations (Jacob &amp; Bruno, 2015).

Group	Proposed materials	Advantages	Disadvantages	Potential applications
Metals	Steel, aluminium, copper	High thermal conductivity Encapsulation by electroplating High thermal stability Strong structure	Potential corrosion Higher cost	High-temperature applications
Inorganic	Silicon, titanium dioxide, sodium silicate, silica, gelatin+acacia, melamine-resin	High thermal stability High thermal mechanical strength Inexpensive	Leakage risk	Industrial processes
Plastic	Polyolefine, propylene, polyester, polystyrene, polyethylene	Inexpensive Chemical and physical encapsulation methods	Relatively low thermal stability Low thermal conductivity	Building integration Food industry

#### 2.3.4 Integration of PCMs in the buildings

The integration of the PCM can occur using the building core, façades, ceiling ventilation systems, water tanks, etc. (Waqas & Din, 2013). The main barrier this technology faces is the difficulty of ensuring the full

solidification of the PCM in certain locations and under particular weather conditions where the temperature is not enough to allow the phase change. A solution to this problem is the enhancement of the thermal conductivity of the PCM (Garcia & Cabeza, 2015), commonly by adding alumina, graphite, and carbon materials.

The three most widely used techniques to integrate PCMs into building elements are immersion, direct incorporation, and encapsulation (Madessa, 2014).

Alawadhi conducted the technique of solar heat gain reduction in buildings through windows by using PCM. The experiment concluded that the PCM with the highest melting temperature (P116) showed the best thermal performance and that the heat gain could be reduced up to 23.29% (Alawadhi, 2012).

Zong et al. investigated the effects of the PCM-filled glass window (PCMW) during summer, the schematic diagram is shown in Figure 2.6. The outcomes showed that when applying paraffin MG29 in the window a reduction of 18.3% was archived on a typical summer day in China. The results concluded that the thermal insulation and shifting effects of the PCMW enhanced with the increasing fusion latent heat of the PCM and that the decrement of the temperature difference between liquid and solid phase provably improve the thermal performance of the system.

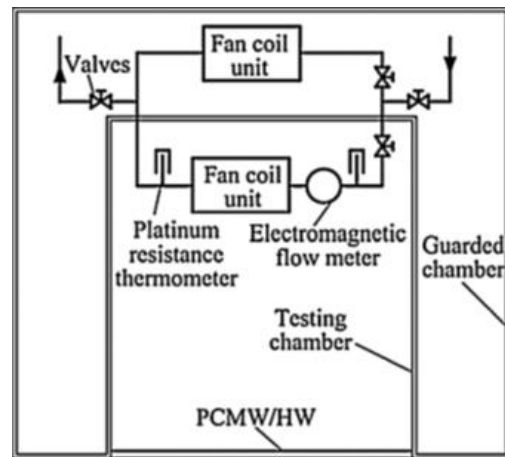


Figure 2.6 Schematic diagram of the experimental setup (Zhong *et al.*, 2015).

Furthermore, the minimal difference between liquid temperature and solid temperature and the appropriate melting temperature of PCM (about 25 °C to 31 °C in the hot summer and cold winter area of China) is essential to enhance the load shifting effect and thermal insulation effect of PCMW (Zhong *et al.*, 2015).

Voelker *et al.* studied the impact on the room temperature of gypsum plaster and a salt mixture. The study concluded that the utilization of phase change materials in buildings increases the thermal mass and contributes consequently to an improvement of the thermal protection during summer. A reduction of 4K could be ascertained. Moreover, it could be proven that the PCM forfeits their characteristic heat storage capacity after a few consecutive hot days if they cannot be discharged overnight; proposing night ventilation to counteract such effects (Voelker, Kornadt and Ostry, 2008).

Barrenceche studied the thermal and acoustic performance of a shape stabilized PCM layer for an intermediate wall of a building that was experimentally investigated in Spain. The new shape stabilized PCM was

composed of a polymeric matrix, 12% paraffin PCM, and electric arc furnace dust (EAFD) (waste from the steel recycling process). The thermal study involved in-situ measurements of ambient temperature, humidity, and wall temperatures for two identical cubicles with and without PCM dense sheets. The results of the thermal experiment demonstrated the potential of the PCM dense sheet to reduce the interior temperature up to 3 °C.

In a different study, Sayyar et al. used experimental and numerical approaches to evaluate the thermal performance of a nano-PCM integrated with gypsum wallboards. The nano-PCM consisted of fatty acid-based PCM and graphite joined nano sheets. The results showed a reduction of the interior temperature fluctuations and demonstrated the potential of the nano-PCM wall panels to maintain the internal temperature variations from 18.5 °C to 26.5 °C, in comparison to the control cell temperatures (13 °C to 32 °C). Furthermore, the peak load shifting of the test cell with nano-PCMs was 8 hours, which was significantly greater than that of the control cell. The new nano-PCMs also improved indoor thermal comfort by 79%. The findings highlight the benefits of nano-PCM in terms of thermal comfort, efficiency, and energy cost (Sayyar *et al.*, 2014).

Wu et al. investigated the efficiency of a thermal PCM wall layer into lightweight structures. The experimental results demonstrated that the temperature of the inner surface and indoor air was reduced, increasing the building efficiency (Wu, Wang and Meng, 2021).

Kuznik and Virgone experimented with the thermal performance of a PCM copolymer composite wallboard for three case scenarios: summer day, winter day, and mid-season day. The results show that for all cases a decrement factor between 0.73 and 0.78 was obtained. The air temperature with the PCM lowers up to 4.2 °C, also the PCM wallboards enhance the natural convection in the room, reducing the temperature fluctuations (Kuznik and Virgone, 2009).

Evola et al. evaluated the effectiveness of PCMs for the improvement of summer thermal comfort in lightweight buildings containing organic PCMs on the partition walls of an office building. The PCM was installed in honeycomb wallboards on the inner surface of the partition walls, a reduction in the peak operative temperature of about 1 °C was observed. Furthermore, a significant attenuation in the daily surface temperature swing was registered, reducing the temperature gap from 5.7 °C to 2.9 °C (Evola, Marletta, and Sicurella, 2013).

An investigation on wallboards integrating PCM to reduce the load of HVAC systems was reported by Shilei et al.; where a room was constructed containing 26% of PCM into gypsum wallboards. The transition temperature and latent heat of these PCM wallboards were tested by a differential scanning calorimeter (DSC). Compared with an ordinary room, the PCM wallboard room could significantly reduce the energy cost of HVAC systems (Shilei *et al.*, 2007)(Lu *et al.*, 2016).

Maleki et al. proposed the application of nanocapsules containing PCM to enhance thermal comfort. The PCM was placed in the walls and roof



plaster. The results indicate that the PCM system could reduce the indoor air temperature fluctuations and help maintain indoor thermal comfort for most of the time of the year (Maleki *et al.*, 2020).

Piselli *et al.* investigated the performance of PCM for passive cooling applications. In the simulation study, it was found that by integrating the Knauf PCM SmartBoard in the building envelope generated significant cooling savings, up to 300 kWh/year for mild climates in Italy (Piselli *et al.*, 2020). The PCM board was integrated into the innermost layer of the roof and the external walls, the study concluded that considerable building cooling energy reduction could be achieved through the optimum combination of PCMs and natural ventilation for mild climates.

Qunli *et al.* investigated a cooling ceiling embedded with capillary pipes and PCM to store and supply cool temperatures. The phase change energy storage radiant cooling system was composed of the insulation layer, the mortar screed-coat embedded with capillary pipes, and the PCM energy storage layer. The results analysed the heat flux and energy storage ratio and concluded that the energy storage ratio of the phase change energy storage system is higher in comparison to a concrete ceiling (Qunli *et al.*, 2017).

Yahaya and Ahmad conducted a comparison study on a single house that integrates PCM ceiling panels in order to evaluate the effectiveness of passive cooling to reduce the air temperature. The application of PCM gypsum board as ceiling panels with a higher melting temperature range and latent heat of fusion significantly improved the energy efficiency in

the buildings. The ceiling panels proved to be an effective solution to reduce the energy consumption by 2 °C through active cooling systems (Yahaya and Ahmad, 2011).

The thermal performance of lightweight aggregate concrete (LWAC) containing macro encapsulated paraffin in Hong Kong was reported by Memon et al. The results of the indoor test revealed that the macro encapsulated Paraffin– LWA panel was able to decrease the interior indoor temperature by 2.9 °C flattening the fluctuation of the temperature, as for the outdoor test it was found that the room temperature was optimized when there was an important temperature difference between day and night (Memon *et al.*, 2015).

Pasupathy and Velraj studied the thermal performance of an inorganic eutectic PCM-based thermal storage system for thermal management in a residential building. It was found that in order to maintain the temperature at 27 °C in the city of Chennai, India, a two-layer ceiling with different PCM melting temperatures was required. Additionally, the melting temperature of the PCM in the top panel needs to solidify during the night hours (Pasupathy and Velraj, 2008).

Saffari et al. assessed the effect of PCM with different layer thicknesses and melting points on the building HVAC operation based on the Fanger thermal comfort model. The results showed that the application of PCM over 24 hours HVAC systems produced energy savings in winter and summer. When the PCM had a melting point of 27 °C it achieved higher annual savings. In some cities, the 23 °C melting point was more effective

during winter. The payback period started from the second year for some case scenarios (Saffari *et al.*, 2016).

Ansuini *et al.* reported on the development of a lightweight piped radiant floor integrating a PCM layer, Rubitherm GR27. The aim was to buffer the internal gains at a constant temperature during summer without affecting the winter warming capacity. The internal structure of the radiant floor was optimized by inserting a custom-designed steel matrix acting as a thermal diffuser, leading to a reduction in the stratified melting behaviour of granular PCM. The system demonstrated that during summer a 25% of the water used for cooling could be saved and reduce the surface temperature by 4 °C (Ansuini *et al.*, 2011).

Royon *et al.* conducted an experimental investigation consisting of a new polymer composite containing 85% of paraffin, with a latent heat of melting of 110 kJ/kg and a melting point at about 27 °C, into a hollow concrete floor panel. The influence of PCM produced a reduction of the surface wall temperature by 2 °C and increased the thermal energy storage (Royon, Karim, and Bontemps, 2013). For the PCM application in floors the melting temperature of the material increases in comparison to walls, reducing 4 °C when combining the PCM with steel.

A heat pump water heater (HPWH) with a PCM for heat storage was developed by Zou *et al.* showing that the heat storage capacity of the system increased by 14%. The HPWH presented an optimal water temperature, additionally improving its coefficient of performance (Zou, *et al.*, 2017).

Moreno et al. experimented with a heat pump coupled to thermal energy storage comparing water and a PCM tank. The PCM tank was filled with a macro encapsulated salt hydrate. The PCM tank proved to be 14.5% colder; and maintaining the indoor temperature within comfort up to 20.65% more than the water tank (Moreno-Rodríguez *et al.*, 2012).

Abdelsalam et al. investigated the use of a thermal energy storage tank containing water with submerged PCMs, using a constant temperature coil heat exchanger, as referred to in Figure 2.7. The computational model reported an 85% surge in the charge rate for the PCM. The researchers proposed a future optimization of the encapsulation method to enhance the thermal conductivity to meet typical charging and discharging cycles (Abdelsalam *et al.*, 2017).

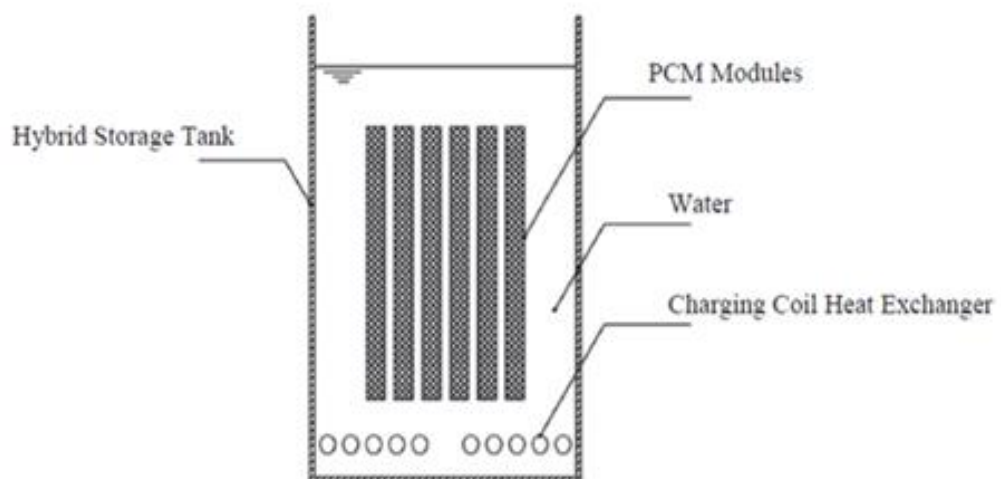


Figure 2.7 Schematic of single-tank HES system (Abdelsalam, et al., 2017).

Yanbing et al. proposed an innovative energy-efficient system Night Ventilation with PCM packed bed storage (NVP). The most important component is the Latent Heat Thermal Energy Storage (LHTES) system, which included a phase change material package bed and the air duct

among the PCM capsules. Experimental results show that the NVP system has great potential in the field of energy efficiency building (Yanbing, et al., 2003).

Similarly, Takeda et al. developed a ventilation system direct heat exchanger between ventilation air and granules containing PCM. In this case, the PCM stabilized the indoor temperature when applying different temperatures (simulating ambient air temperature fluctuations). The potential to reduce the ventilation load during summer was investigated for eight cities in Japan. Kyoto presented the best results with a reduction of ventilation load by 62.8%. Additionally, it was reported that the cooling load (defined differently to ventilation load) can also be reduced by the ventilation system (Takeda *et al.*, 2004).

Labat et al. proposed a heat exchanger containing 27 kg of PCM designed to provide a 1 kW heating power for 2 hours. The PCM was distributed into 34 plane-parallel aluminium containers. The exchanger was placed in an air-supply system used to produce a constant airflow rate. Nevertheless, the experiment reported that the system was insufficient to meet the 1 Kw heating power (Labat *et al.*, 2014).

Wei et al. tested the characteristics of different encapsulation methods: sphere, cylinder, plate, and tube in a thermal storage system containing paraffin wax FNP-0090. Figure 2.8 shows the PCM capsules inside a rectangular tank, using water as the working fluid and a plate heat exchanger was used as the storage tank. The spherical capsule had the best outcomes in terms of heat transfer performance (Wei *et al.*, 2005).

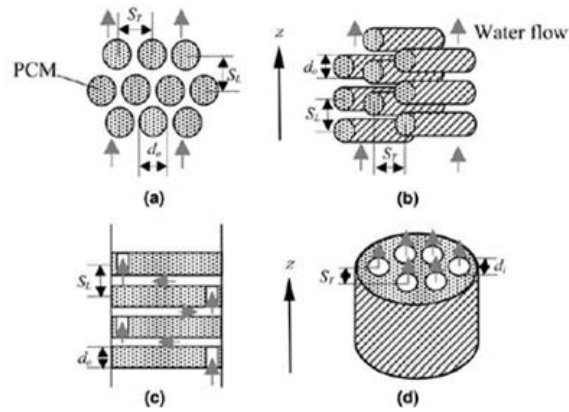


Figure 2.8 Arrangement of PCM in the heat storage tank. (a) Sphere, (b) cylinder, (c) plate, and (d) tube (Wei *et al.*, 2005).

Garg *et al.* investigated the thermal performance of a PCM-based heat exchanger in India. The encapsulated PCM with a melting range between 23 °C to 32 °C based heat exchanger was able to reduce the heat gain of the test chamber by 50%, dropping the mean air temperature by more than 6 °C (Garg *et al.*, 2018).

A different study was performed by Borden *et al.* analysing four ventilation modes of a double stream ventilation system in a retrofitted house for different cities in France. They used paraffin with a melting point of 23°C PCM for cooling forced airflow into a channel. The developed models were used to conduct simulations of day and night periods. The results revealed that for most of the PCM system configurations, the solidification of the PCM was partially achieved at night, due to the non-optimal performance of the system. Overall the overheating problems were reduced to 8% in Lyon and 2.6% in Trappes (Borden, Virgone and Cantin, 2015).

Wang and Niu design a new air conditioning system incorporating a cooling ceiling and a microencapsulated phase change material (MPCM)

slurry storage tank. The evaluation indicated that the MPCM slurry storage tank was able to shift part of the cooling load from daytime to night-time, the electricity demand was reduced by 33% in comparison to a cooling ceiling system (Wang and Niu, 2009). In a later study, Wang et al. developed a novel frost-free air-sourced heat pump (ASHP) system, integrating PCMs and dehumidification. The dehumidification efficiency performance increased from 31.8% to 34.7%. Concluding that the correlation between the desiccant and PCM mass must be carefully assessed. The coefficient of performance reached a maximum value of 2.99 when the weight of the desiccant and the volume of the PCM was 2.2 kg and 800 ml, respectively (Wang, Bu and Ma, 2012).

Table 2.4 presents the synthesis of the reviewed studies, with the PCM material and melting temperatures.

Table 2.4 Review PCM studies.

Building element	PCM Type	PCM name	Melting Point (°C)	Findings	Ref.
Window	Paraffin	n-Octadecane n-Eicosane	27 37	P116 presented the best thermal performance, the heat gain could be reduced up to 23.29%.	(Alawadhi, 2012)
Window	Paraffin	MG29	35-31	Evaluation of the heat transfer performance of a PCM-filled glass window, the results show a reduction of heat by 18.3%.	(Zhong, et al., 2015)
Wall	Paraffin Salt hydrates	- CaCl <sub>2</sub> ·6H <sub>2</sub> O	25-28 29.6	Two PCM were tested, reducing 3°C of the peak temperature in the testing chamber.	(Voelker, et al., 2008)
Wall	Paraffin	-	-	Indoor temperature reduction of 3°C.	(Barreneche et al., 2016)
Wall	Eutectic	Capric acid Palmitic acid	26.2	The nano-PCM reduced the energy demand up to 79%.	(Sayyar, et al., 2014)
Wall	Paraffin	-	20-30	Reduce the inner surface and air temperature.	(Wu, Wang and Meng, 2021)
WB	Paraffin	-	16.6	Reduced 3 °C of the peak temperature and the interior surface temperature by 2° C.	(Kuznik & Virgone, 2009)
WB	Paraffin	Micronal T23	19-25.5	Reduced the daily temperature swing of by 2.8 °C, from 5.7 °C to 2.9 °C.	(Evola, et al., 2013)

WB	Fatty Acids	Capric acid Lauric acid	20.4 and 19.1	Gypsum wallboards impregnated with PCM used in the building envelopes can shift heat and cold load to off-peak in electric power peak periods by thermal storage capacity.	(Shilei, et al., 2007)
Wall & Roof		n - dodecanol as poly methyl methacrylate (PMMA)	24	The nano-PCM reduce the indoor temperature fluctuations and help maintain thermal comfort.	(Maleki et al., 2020)
Wall & Roof	Organic	MICRONA L 23	23-26	The Knauf PCM SmartBoard generated cooling savings up to 300 kWh/year.	(Piselli et al., 2020)
Roof	-	-	16-20	The melting temperature mainly affects the energy storage ratio and the decrement time of average surface heat flux.	(Qunli, et al., 2017)
Roof	Eutectic mixture	Lauric acid stearic acid	28.9- 41.8	The application of PCM in gypsum board as a ceiling demonstrated a reduction of 2 °C in the indoor temperature.	(Yahaya & Ahmad, 2011)
Roof	Paraffin	LWAC	25-28	Decrement on the indoor air temperature by 2.9 °C.	(Memon, et al., 2015)
Roof	Salt hydrate mixture	48% CaCl <sub>2</sub> 4.3% NaCl 0.4% KCl 47.3% H <sub>2</sub> O	26 -28	Simulated a double layer PCM in a building roof, for space heating and cooling.	(Pasupathy & Velraj, 2008)
Roof	Paraffin	Rubitherm	23-27	Achieved annual energy savings, around 10–15%.	(Saffari, et al., 2016)
Floor	Paraffin	Rubitherm GR27	26-28	The PCM ensured savings of approx. 25% of the water used for cooling and the PCM-based floor surface temperature decreased by 4 °C.	(Ansuini, et al., 2011)
Floor	Paraffin	Rubitherm RT27 styrene–butadiene–styrene (SEBS)	27.5	The PCM increases the time lag and reduces the surface temperature by 2%.	(Royon, et al., 2013)
HP	Paraffin	RT44HC	41-44	The heat storage capacity increased by 14%.	(Zou, et al., 2017)
HP	Salt hydrate	-	10	PCM tank is able to store 35.5% more cold, the charging time is 4.55 times higher.	(Moreno, et al., 2014)
Storage tank	Fatty acid	Lauric acid	45	The energy density increased (two to five times).	(Abdelsalam, et al., 2017)
HE ventilation and heating system	Fatty acid	-	22-26	The thermal comfort can be improved when the night ventilation is used in combination with the PCM.	(Yanbing, et al., 2003)
HE	Paraffin	Rubitherm GmbH	23.5- 24.9	PCM reduced the use of ventilation by 62.8%.	(Takeda, et al., 2004)
HE	Paraffin	Microtek 37D	25-35	PCM in air heat exchanger storage ventilation, the PCM store 1kW for 2 hours.	(Labat, et al., 2014)
HE	Paraffin	FNP-0090	88	Four PCM capsules (sphere, cylinder, plate, and tube) were investigated. The sphere capsule had the best performance.	(Wei, et al., 2005)
HE	Inorganic	HS24	23-32	The system was able to reduce the heat gain by 50%.	(Garg et al., 2018)
AC system	Paraffin	-	23	Used PCM layers for cooling an airflow channel, the hours of overheating were reduced.	(Bordeon, et al., 2015)
AC system	Paraffin	Hexadecane C16H34	18	Decrease the daytime electricity demand by about 33% compared with CC system running with water.	(Wang & Niu, 2009)
ASHP	Salt hydrates	CaCl <sub>2</sub> -6H <sub>2</sub> O	29	The simulation results showed that the dehumidification efficiency was increased from 31.8% to 34.7%.	(Wang, et al., 2017)



---

2% SrCl<sub>2</sub>-  
6H<sub>2</sub>O

---

Building element; WB= wallboards, HE= heat exchanger, AC= air conditioning, ASHP= air source heat pump.

Walls and wallboards are the most common building envelope component selected for PCMs integration, correspondingly gypsum tends to be a suitable material for direct incorporation. Generally, PCM walls present a temperature reduction ranging from 1 °C to 3 °C and improve the thermal comfort up to 79%. It is important to highlight that some attempts to enhance the PMC material performance are presented, specifically the use of nano-PCMs, graphite, and the application of honeycomb structures as an attempt to increase thermal conductivity.

In the case of the PCM ceiling applications, improvements from 2 °C to 2.9 °C were observed, notably, gypsum continues to be a solution in this building component.

Heat exchangers are a promising solution to improve thermal comfort, the inclusion of PCM material in this system tends to increase the effectiveness of the performance, further reducing the ventilation loads and temperature. Similarly, to the heat exchanger, the air conditioning systems benefit from the inclusion of PCMs. The studies present efficiency increments up to 34% and electricity demand reductions for 33% with the application of PCMs, proving to be a positive solution to reduce energy consumption.

### 2.3.5 PCM Enhancement methods

One of the most common disadvantages in organic PCMs is the low thermal conductivity, this creates difficulties due to low heat flow in thermal charging and discharging processes (Wu *et al.*, 2011; Khodadadi,

Fan and Babaei, 2013). To enhance the thermal conductivity of the PCMs, different techniques have been investigated, Figure 2.9 shows a review of the most common enhancement materials. For example, the use of extended surfaces that provide more contact area for the material, the application of heat pipes and fins, the use of different encapsulation, and micro and nano encapsulation (Kasaeian *et al.*, 2017).

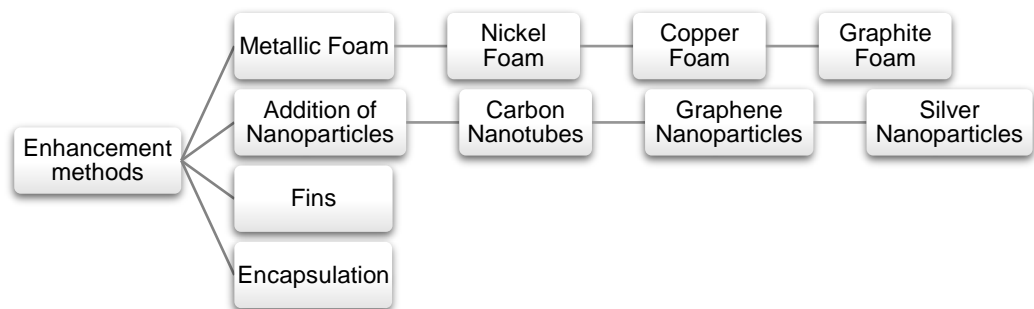


Figure 2.9 Popular enhancement techniques (Yang, Huang and Zhou, 2020).

According to Ji *et al.* and Wu *et al.* one commonly used technique is the addition of high thermal conductive materials, such materials come as nanoparticles, nanofibers, nanotubes, and nanosheets, and they are integrated into the PCM, other nanoparticles are included in Figure 2.10.

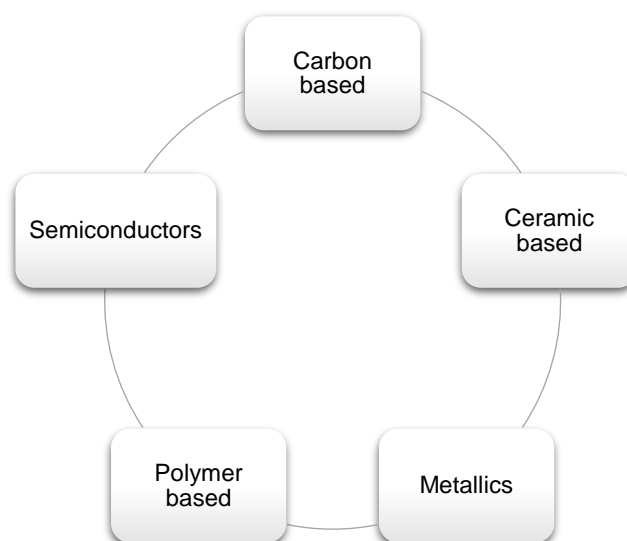


Figure 2.10 Summary of produced nanoparticles (Yang, Huang and Zhou, 2020).

Resulting in a significant increase in the thermal conductivity and at the same time improving the ability to promote the energy exchange (Fan *et al.*, 2013; Ji *et al.*, 2014).

#### **2.3.5.1 Applications of nano-enhanced PCM in buildings**

The nano-enhanced PCMs provide a wide range of applications, being suitable for heating, cooling, air-conditioning, ventilation among others. Some complications presented in the PCM application, such as the time-lapse for the phase transition, or the correct integration of nanometer-sized materials with the PCMs, or the highly nonlinear phase change characteristics. In consequence, it is difficult to estimate the energy flow during the phase change process (Ma, Lin and Sohel, 2016).

In 2005 Elgafy and Lafdi reported the use of nanometer-sized materials (i.e. nanofibers) in PCMs for improved thermal energy storage (Elgafy and Lafdi, 2005). From this point onwards, researchers have developed novel applications of nano-enhanced PCM suitable for various industrial and building applications, testing and characterization of their thermal energy storage performance, and investigation of their melting and solidification characteristics (Ma, Lin and Sohel, 2016).

#### **2.3.5.2 Nano-enhanced PCMs with paraffin as the base fluid**

Paraffin has proved a compelling storage performance for different applications and is one of the most popular organic PCMs (Ho and Gao, 2009; Memon, 2014). Several studies present nanometer-sized materials in order to enhance the thermal conductivity of these organic PCMs.

Colla et al. studied the feasibility of nano-enhanced PCM containing aluminium oxide ( $\text{Al}_2\text{O}_3$ ) and carbon black (CB). The evaluation focused on two paraffin waxes, Rubitherm RT20 with a melting temperature of 20 °C and Rubitherm RT25 with a melting temperature of 25 °C. The study evaluated the thermal properties such as the thermal conductivity, the latent heat, and the specific heat of the material. The results concluded that by adding carbon black nanoparticles an enhancement of 35% and 24% for the RT20/CB and RT25/CB, respectively (Colla *et al.*, 2017).

Wu et al. reported on copper nanoparticles using Hitenol BC-10 as the chemical agent. Using an infrared spectrometer (FTIR) the interaction of the copper particles, the paraffin, and the HitenolBC-10 was examined. Compared to pure paraffin, the nano-enhanced PCM showed a reduction of 33.3% in the melting time, as for the solidification time a 31.6% was obtained (Wu *et al.*, 2009). Teng and Yu investigated nanocomposite-enhanced phase change materials (NEPCMs). A differential scanning calorimeter (DSC) was used to evaluate the thermal performance of paraffin mixed with alumina, titania, silica, and zinc oxide particles. The results proved that out of the four particles the addition of the titania proved the highest heat conduction and thermal storage performance (Teng and Yu, 2012).

Ho and Gao investigated the thermo-physical properties of paraffin (n-octadecane) with the addition of alumina ( $\text{Al}_2\text{O}_3$ ) nanoparticles. The results showed that the PCM enhancement increased the thermal conductivity, furthermore the dynamic viscosity of the material rise

nonlinearly with the increase of the mass fraction of alumina nanoparticles (Ho and Gao, 2009). Paksoy and Sahan examined nano magnetite ( $\text{Fe}_2\text{O}_3$ ) particles added to paraffin PCM with a melting temperature range between  $56^\circ\text{C}$  to  $58^\circ\text{C}$ . The findings proved that the thermal storage capacity of paraffin could increase up to 20% by the addition of 10% nano magnetism (Paksoy and Sahan, 2012).

Fan et al. analysed the effect of adding paraffin wax with carbon nanofillers for thermal energy storage. The experiment contemplated the application of short and long carbon nanotubes, carbon nanofibers, and graphene nanoplatelets (GNPs), the experimental procedure is depicted in Figure 2.11.

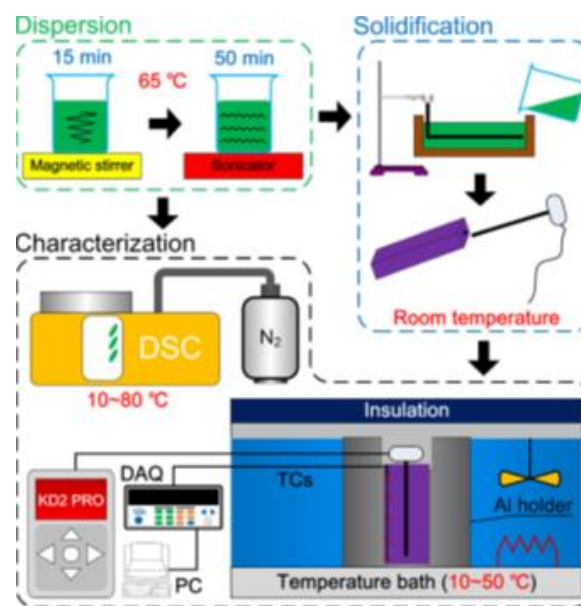


Figure 2.11 Schematic diagram of the experimental procedure and setup for sample (Fan *et al.*, 2013).

The study concluded that the integration of nanofillers slightly reduced the enthalpy and had a negligible influence on the phase change temperatures. The thermal conductivity increased proportionally to the amount of enhancement material; however, it was found that the

enhancement depended on the size and shape of the nanofillers. In comparison to the base fluid, the thermal conductivity of the GNPs mixture increased up to 164% with a 10% weight fraction, reducing the thermal interface resistance (Fan *et al.*, 2013).

Cui *et al.* studied the thermal properties of carbon nanofiber (CNF) and carbon nanotube (CNT) filled with paraffin wax in order to enhance thermal conductivity. The experimental results proved that both the CNF and CNT increased the thermal conductivity, although the CNF proved to have a higher performance. The experiment concluded that adding highly thermal conductive nanometer-sized materials in paraffin PCM could substantially improve the thermal conductivity, helping the application of these materials as a mass thermal energy storage medium (Cui *et al.*, 2011).

Zhong *et al.* investigated the enhancement of paraffin wax by adding graphite foam (Paraffin-GF). The thermal diffusivity of the material can increase 190, 270, 500, and 700 times in comparison to pure paraffin wax, moreover the study revealed that the smaller the pore size the higher thermal diffusivity, and the larger pore size resulted in larger latent heat (Zhong *et al.*, 2010)

### **2.3.5.3 Nano-enhanced PCMs with other PCMs as base fluids**

Aside from using paraffin as a based fluid, some studies have focused their attention to alternative PCMs. Oya *et al.* developed a novel phase change composite (PCC) by implementing erythritol as PCM and graphite nickel particles as a thermal conductivity enhancement. The results

demonstrated that the thermal conductivity increments were correlational to the enhancement material volume fraction and aspect ratio. In comparison to pure erythritol, the thermal conductivity increased up to 6.4 times (Oya *et al.*, 2013).

Zeng *et al.* reported on the thermal conductivity of Ag nanoparticles mixed with organic PCM (1-tetradecanol TD). The results showed an enhancement in the thermal conductivity, while the composite material thermal stability remained as close to that of pure PCM. Even though the Ag nanoparticles were dispersed uniformly into the base material, it was found that interaction between the Ag particles and the TD was considerably small (Zeng *et al.*, 2007).

Teng investigated the thermal conductivity of PCM with alumina ( $\text{Al}_2\text{O}_3$ )-water nanofluid and chitosan dispersant to improve the performance of ice storage air conditioning systems. It was concluded that by using the appropriate concentrations of the alumina water the system performance could be improved (Teng, 2013).

The application of a heat pipe coupled with nano-enhanced PCMs as energy storage for cooling applications was examined. The enhanced PCM was allocated in the adiabatic section of the heat pipe in which the heat is absorbed and released controlled by the power inputs at the evaporator and fan speeds at the condenser. The experiment consisted of the application of water, tricosane, and nano-enhanced tricosane as the energy storage material. For the nano-enhanced PCMs, three different volume percentages were used (0.5%, 1%, and 2%) of  $\text{Al}_2\text{O}_3$  nanoparticles with Tricosane. The study revealed that the nano-

enhanced PCM increased the thermal conductivity by 32%. It was found that the enhanced PCM could store up to 30% of the energy supplied at the evaporator, creating a reduction in the fan power electric consumption. Furthermore, the evaporator temperature of the heat pipe decreased 25.75% leading to energy savings of 53% of the fan power (Krishna, Kishore and Solomon, 2017).

He et al. experimentally investigated a nanofluid PCM containing  $\text{TiO}_2$  nanoparticles in  $\text{BaCl}_2$  aqueous solution. The results proved that the thermal conductivity increased by 12.76%, in addition, the supercooling degree decreased by 84.92%. Nevertheless, the study found that the nanoparticles created a slight reduction in the latent heat and the specific heat (He et al., 2012). In a different study, Cai et al. examined an innovative PCM by combining lauric acid (LA), polyethylene terephthalate (PET), and silica nanoparticles (nano- $\text{SiO}_2$ ). It was reported that the nano- $\text{SiO}_2$  in the fibers influenced the crystallization of the lauric acid and affected the heat enthalpy of the composite fibers, nevertheless, the phase change temperature remained unaltered (Cai et al., 2011).

Kurmaresan et al. focused their investigation on the thermal behaviour of de-ionized (DI) water and multi-wall carbon nanotubes (MWCNT) encapsulated in a spherical container. The time of solidification of the nano-enhanced PCM was reduced between 14% to 20.2% when the fraction of carbon nanotubes was 0.6%, additionally, the subcooling was also reduced. The report concluded that energy savings of 6 to 9% in the chiller could be achieved by integrating the nano-enhanced PCM (Kurmaresan et al., 2013).



Figure 2.12 presents the experimental procedure by Biwas et al., using a mixture of paraffin and alumina particles that were to be incorporated in a ceiling board.

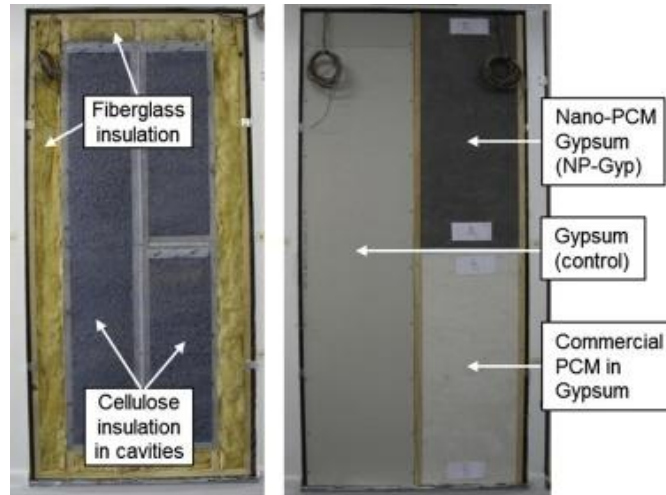


Figure 2.12 Test wall with the PCM-enhanced wallboards (Biswas *et al.*, 2014). The results concluded that the PCM ceiling board saves decreases the peak heat gains, although the exact percentage was not reported (Biswas *et al.*, 2014).

RT100 and water as the heat transfer fluid. The system was designed as a medium-scale unit for heating systems that would be utilized to transfer the heat from the district into the building heating network. The PCM was mixed with 15% graphite, the storage unit operated by charging at night-time and discharge at daytime during the peak demand, the results proved that this technology can provide higher energy storage densities (Colella, Sciacovelli and Verda, 2012).

The phase change heat transfer properties and thermal behaviour of nano-enhanced PCM spherically encapsulated was reported by Kalaiselvan et al. In the study various PCMs were embedded with aluminium and alumina nanoparticles, as shown in Table 2.5. The study

reported that the solidification process for the n-tetradecane and n-hexadecane could be reduced by 12.97% and 4.97% respectively (Kalaiselvam, Parameshwaran and Harikrishnan, 2012).

Table 2.5 Comparison of reduction of solidification time for the PCMs in pure form and with dispersed nanoparticles (Kalaiselvam, Parameshwaran and Harikrishnan, 2012).

PCM Description	Pure PCM	With aluminium nanoparticles ( $\phi = 0.07$ )		With alumina nanoparticles ( $\phi = 0.07$ )	
	Time (s)	Time (s)	Time Reduction (%)	Time (s)	Time Reduction (%)
60% n-tetradecane	15880	13820	12.97	15090	4.97
40% n-hexadecane					
Capric/Lauric Acid	10470	8760	16.33	9545	8.83
CaCl <sub>2</sub> ·6H <sub>2</sub> O	4480	3465	22.66	3690	17.63
n-Octadecane	10795	9195	14.82	10085	6.58
n-Hexadecane	13295	11470	13.73	12640	4.93
n-Eicosane	9105	7850	13.78	8640	5.11

Colella et al. reported the application of a paraffin composite based on Parameshwaran et al. analysed a silver nano-based organic ester (SNOE) phase change material thermal property. The experiment utilized a spherical-shaped surface-functionalized crystalline silver nanoparticles (AgNP) with different mass proportions. The experimental results revealed that dispersion of AgNP into PCM was efficient, presenting a reduction of the supercooling and the latent heat capacity for the freezing period declined by 7.88% and 8.9% for the melting. The study concluded that the SNOE PCMs could be considered as a suitable solution for cooling thermal energy storage (Parameshwaran, Jayavel and Kalaiselvam, 2013). In a separate study, Parmeshwaran et al. investigated the thermal properties of silver-titania hybrid nanocomposite (HyNPCM), a reduction in the supercooling degree by 1.82 °C was observed, while the freezing and melting times decreased by 23.9% and 8.5% respectively (Parameshwaran et al., 2014).

A study focused on Bio-based PCMs with exfoliated graphite nanoplatelets (xGnP), carbon nanotubes (CNT), and liquid Bio PCM was conducted by Yu et al. to improve thermal conductivity. The infrared spectroscopy shows a positive reaction between the PCM and the carbon materials. The thermal conductivity was augmented with the addition of carbon nanomaterials and was proportional to the enhancement quantity. The Bio-based PCM/xGnP composite had no change in its latent heat, having suitable phase change temperatures. It was concluded that the Bio PCM can be counted as the appropriate method for latent heat thermal energy storage (Yu *et al.*, 2014).

Ji et al. investigated the enhancement of palmitic acid (PA) into two forms of multi-walled carbon nanotubes (MWNTs). The results exposed that the enhancement materials improved the thermal conductivity and heat transfer of the PCM (Ji *et al.*, 2012).

Jiang et al. focused on the thermal dynamic mechanical properties of two organic PCMs, paraffin and stearic acid with porous aluminium (Al) foams. The addition of the enhancement material was achieved by constant-pressure/vacuum conditions. The study concludes that the PCMs composites can be eco-friendly manufactured with the constant-pressure impregnation method. The shape-stabilized PCMs/Al-foam show high thermal storage potential, the enhancement of the PCM proved to have a positive effect on the durability of the AL foams (Jiang *et al.*, 2012). Table 2.6 presents the range of PCM enhancement methods that are available, highlighting the major findings of each study.

Table 2.6 Synthesis table of PCM enhancement methods.

PCM Type	Enhancement material	Melting Point (°C)	Findings	Ref.
Rubitherm RT20 Rubitherm RT25	Aluminium oxide (Al <sub>2</sub> O <sub>3</sub> ) Carbon black (CB)	20-25	Thermal conductivity was improved by using the Al <sub>2</sub> O <sub>3</sub> and carbon black nanoparticles up to 35% for the RT20 and 24% for the RT25.	(Colla <i>et al.</i> , 2017)
Paraffin	Hitenol BC-10	58-60	Thermal conductivity was enhanced from 14.2%-18.1%.	(Wu <i>et al.</i> , 2009)
Paraffin n-octadecane	Alumina (Al <sub>2</sub> O <sub>3</sub> )	25.1-26.5	The thermophysical conductivity increases by 17% by adding the alumina.	(Ho and Gao, 2009)
Paraffin	Fe <sub>2</sub> O <sub>3</sub>	56-58	The thermal storage capacity of paraffin can increase up to 20% by the addition of 10% nano magnetism.	(Paksoy and Sahan, 2012)
Paraffin wax	Carbon nanofillers	59	The addition of the GNPs increased the thermal conductivity up to 164%.	(Fan <i>et al.</i> , 2013)
Paraffin wax	Carbon nanofiber (CNF)	52-54	The addition of highly conductive nanometer-sized increased the thermal conductivity of the paraffin, resulting in a 24%-40.6% increment.	(Cui <i>et al.</i> , 2011)
Paraffin	Graphite	57.85	The thermal diffusivity of graphite foams augmented, concluding that the smaller the pore size the higher thermal diffusivity.	(Zhong, et al., 2010)
Erythritol	Graphite/nickel particles	118	The thermal conductivity increased up to 6.4 times.	(Oya <i>et al.</i> , 2013)
1-tetradecanol	Nano-Ag	22	The Nano-Ag increased the thermal conductivity by 11%.	(Zeng <i>et al.</i> , 2007)
Paraffin	Alumina, titania, silica zincoxide	55-65	Out of all the materials tested, the titania had the best thermal conductivity.	(Teng and Yu, 2012)
Nano-tricosane	Al <sub>2</sub> O <sub>3</sub>	93.3	The nano-enhanced PCM increases the thermal conductivity by 32%.	(Krishna, et al., 2017)
Barium chloride	Titania particles	- 8	Thermal conductivity was enhanced by 12.76%, the supercooling degree was reduced by 84.92%.	(He <i>et al.</i> , 2012)
Lauric acid Polyethylene	nano-SiO <sub>2</sub>	38-38.8	The nano-SiO <sub>2</sub> in the fibers influenced the crystallization of the lauric acid and affected the heat enthalpy of the composite fibers.	(Cai <i>et al.</i> , 2011)
DI water	Carbon	-9 /-12	Energy savings of 6-9% in the chiller could be reached.	(Kumaresan <i>et al.</i> , 2013)
Paraffin, n-heptadecane	Graphite	19	Energy savings of 79% and maintained thermal comfort.	(Biswas <i>et al.</i> , 2014)
Paraffin RT100	Graphite	89.85-111.85	The PCM enhancement provided higher energy storage density.	(Colella, et al., 2012)
Organic ester	AgNP	6.8	Dispersion of AgNP into PCM was effective; the supercooling was reduced, and the latent heat capacity decreased by 7.88% in freezing and 8.9% in melting.	(Parameshwaran, et al., 2013)
Organic ester	Silver titania	6.8	A reduction in the supercooling degree by 1.82°C was obtained, the freezing and melting times decreased by 23.9 % and 8.5% respectively.	(Parameshwaran <i>et al.</i> , 2014)

Bio-based	Graphite and carbon	28.13	The thermal conductivity was augmented with the addition of carbon nanomaterials and was proportional to the enhancement quantity.	(Yu, et al., 2014)
Palmic acid	Carbon	62.7-67.3	The enhancement materials improved the thermal conductivity and heat transfer of the PCM.	(Ji, et al., 2012)
Stearic acids and paraffin	Aluminium	54.7-70.6	The shape-stabilized PCMs/Al-foam show high thermal storage potential, the durability, and resistance prove to be ideal for energy-saving material.	(Jiang, et al., 2012)

### 2.3.6 Main conclusions

The literature review suggests that the utilization of PCMs for building applications improves the overall energy performance at the same time reducing the temperature fluctuations. The studies suggest that walls are the most common building envelope component for PCM incorporation.

Generally, the inclusion of PCMs into roofs and walls provides a temperature drop of around 3 °C.

Paraffin stands out as the most common PCM utilized; nevertheless, this material faces low thermal conductivity. Consequently, the application of aluminium, steel, graphite, and even the encapsulation form tend to be a solution to enhance its performance.

A gap is observed regarding enhancement methods for inorganic PCMs, especially for the incorporation in building envelopes. Further research in this area will increase the commercial application that is most beneficial due to its low cost.

The future of PCM active storage systems is promising since they are a versatile solution to reduce energy consumption, having as an advantage the uncomplicated installation for new and retrofitted buildings. The performance of these systems varies depending on the application,

although generally heat pumps, heat exchangers, and air conditioning systems improve the building performance by 62%, 35% and 34%, respectively.

Enhancement methods:

For the organic PCMs, the paraffins stand out as the main material for the enhancement application. Paraffins have the advantage of non-corrosiveness that makes them suitable for mixing with alumina, titania, and carbon which have proven to be the most common boosting materials described in the literature.

There is limited research focused on enhancement methods for building applications. The majority of the enhancement methods present in the literature reviews focused on alternative applications, using high-temperature solutions, that go beyond the human comfort temperatures.

Incorporating nanoparticles with high thermal conductivity enhances the PCMs thermal response, resulting in additional energy saving. Nevertheless, there is still a research gap in the literature for three main areas:

- Novel enhancement methods, with for low melting temperatures that can interact within the human thermal comfort range.
- Investigate enhancement methods for other materials apart from paraffin, such as salt hydrates.
- Consider original encapsulation materials as PCM enhancement mechanisms.

## 2.4 Solid desiccants

### 2.4.1 Background

Moisture control has become a worldwide concern due to the current construction practices and building operational controls. Energy saving has been prioritized and for this reason, buildings are better insulated and airtightness has been reduced. This has increase moisture concerns in buildings that sometimes have been compensated by the incorporation of air-conditioning systems (Warwicker, 2010).

Similar to temperature, air humidity affects the thermal comfort perception (Kong *et al.*, 2019). Air humidity plays an important role in human health (Zhou, Shi and Chen, 2018). The maintenance of a comfortable and healthy indoor environment is one of the occupants and designer's main focus. In a temperate climate, the maintenance of a comfortable indoor environment is highly important, especially during the winter period. When a sub-temperature climate is in place, both winter and summer should be considered. In hot and humid climates, providing cool, low-humidity indoor air is particularly important (Enteria, Awbi and Yoshino, 2017). As the humidity levels do not create a considerable change in the air temperature, the occupant's perception is not as sensible. This has decreased the importance given to humidity controls. To achieve thermal comfort the relative humidity (RH) should range between 40 to 60%; below 40% increases the concentration of harmful chemicals in the air, which can cause respiratory infections and skin conditions. In contrast, having a relative humidity above 60% promotes the proliferation of viruses and mold spores (Cascione *et al.*, 2019).

The application of air conditioning systems or humidifiers has been used as a method to obtain an optimal humidity level. Nevertheless, the implementation of these mechanisms increases the building energy demand and has limited ability to control the humidity (Luo, Yang and Lu, 2014; Wen *et al.*, 2018; Lu, Kuok and Liu, 2020). In high-performance buildings, the percentage of dehumidification energy consumption in relation to the total energy consumption can increase from 1.5% to 22.4% if the relative humidity is dropped from the design value of 60–50% (Shehadi, 2018). Humidity-controlling materials can help stabilize indoor RH by absorbing or desorbing water molecules in the air. The term absorption is used when the molecules of the adsorbate penetrate the surface layer and enter the structure of the host matrix, changing the composition of the material (Yu, Wang and Wang, 2013). Desiccants are a group of hygroscopic substances that can attract water-vapor molecules via adsorption or absorption (Yang, Rana and Lan, 2015). Desiccants provide an alternative to traditional dehumidification processes of cooling air below the dew point (Longo and Gasparella, 2016), allowing independence to control the humidity notwithstanding the temperature based on the physical state.

Figure 2.13 presents the absorption process, where the material undergoes a physical change when it receives moisture. For the adsorption, the desiccant only changes in weight by the water it has retained. An example of an absorbent would be salt which changes from a solid to a liquid as it absorbs moisture, for the adsorption would be a



sponge. The majority of absorbents are liquid, while the adsorbents tend to be solid (Warwicker, 2010).



Figure 2.13 Schematic description adsorption and absorption.

In general liquid desiccants present more advantages over solid desiccants, as they have higher absorption capacity. Nevertheless, most of the liquid desiccants are unsuitable for building applications as they are considered toxic materials. Examples of liquid desiccants include concentrated aqueous solutions of hygroscopic salts such as calcium chloride or lithium chloride, lithium bromide, triethylene glycols. In contrast, solid desiccants not only can adsorb water vapor but also can effectively remove several contaminants providing air cleanness (Ge *et al.*, 2018). Furthermore, solid-desiccant dehumidification is suitable for low-grade thermal energy and can significantly reduce electricity consumption (Amani and Bahrami, 2021).

#### 2.4.2 Materials classification

In general, there are several approaches to classify desiccant materials, for instance, solid and liquid desiccants (i.e. depending on the physical state), other classifications are physisorption and chemisorption desiccants (i.e. depending on the strength of the bond between the

adsorbate and adsorbent), natural and artificial desiccants (i.e. depending on the material), bio and rock-based desiccants, composite and polymer-based desiccant (Chen *et al.*, 2018).

Shehadi summarizes the most common desiccant materials used for humidity control based on their physic state, as shown in Figure 2.14 (Shehadi, 2018). A suitable adsorbent is one that provides the following aspects: a reasonably large surface area or micropore volume and a relatively large pore network for the transport of molecules to the interior (Cevallos, 2012).

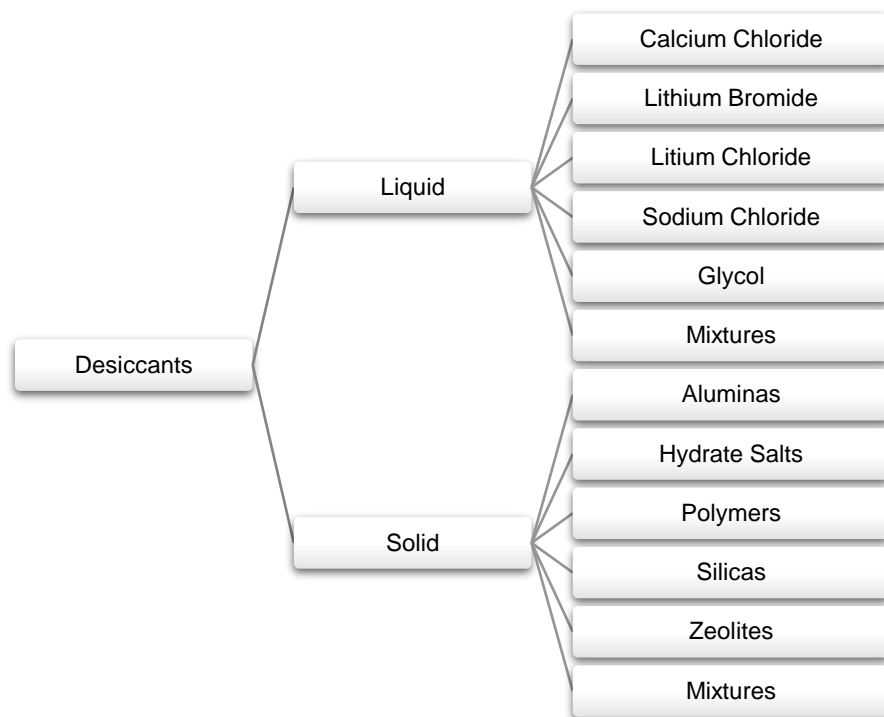


Figure 2.14 Common solid and liquid desiccant materials (Shehadi, 2018).

Solid desiccant materials are considered an effective and economical approach for dehumidification and are less subject to corrosion compared to liquid desiccants. In general, they are considered environmentally friendly. In some cases for desiccant cooling, solid

desiccant materials are more favourable for adsorption, due to their dryness, structure simplicity, chemical inertness, and ease of operation (Chua and Chou, 2003). On the other hand, the liquid desiccant materials require a complicated packing system for dehumidification and regeneration, while a simpler device like a rotary desiccant wheel can be used to accommodate solid desiccant materials, and without any carry-over problem of desiccant droplets, which may be harmful to building structure and human health (Huang and Zhang, 2013; Chen *et al.*, 2018). For this reason, the literature review focuses on solid desiccant as an environmentally friendly solution for building incorporation.

#### **2.4.2.1 Natural Materials**

Natural materials can be made from renewable sources such as agricultural waste, other materials consider wood, bamboo charcoal, activated carbon, clay, crop waste among others (Yu, Cui and Feng, 2016; Cascione *et al.*, 2019). These adsorbents are low-cost, easy to handle environmentally friendly, and often abundant materials. They are divided into two main categories of living organisms (including aquatic animals and agricultural residues, wastes, etc.), and elements and compounds from the earth's crust (including minerals, clay, sediment rocks, and soil), (Sadeghalvad *et al.*, 2021).

#### **2.4.2.2 Montmorillonite Clay**

Montmorillonite Clay is a natural porous adsorbent and is widely used as a desiccant. It is considered inexpensive and has an operational temperature and humidity are within a “low” range (Sultan *et al.*, 2015).

The primary chemical composition of clay includes silica and aluminium, magnesium oxide, calcium oxide, and ferric oxide (Chen, 2017). This material can be regenerated at low temperatures without substantial deterioration as it remains solid after adsorption, with no apparent change in texture. Clays are considered to have low environmental impact as they are composed of the disintegration of igneous rocks (Castrillo, Mercado and Volzone, 2018). The main concern when using clay as a dehumidifier is that it can release moisture very easily when the temperature rises.

#### **2.4.2.3 Carbon**

Carbon-based materials and their modifications have received significant attention over the last decades given the outstanding adsorption behaviour toward various dyes from aqueous solutions (Azari *et al.*, 2020). Carbon fiber presents low density and is widely used as an enhancement material. Activated carbon is often used as a desiccant and is one of the most popular and commonly used adsorbents for waste water treatment due to its versatility and high adsorption capacity, particularly when handling pollutants (Warwicker, 2010; Ianoş, Păcurariu and Mihoc, 2014). They present remarkable advantages, such as large specific surface area, abundant pore structure, high thermal stability, high mechanical strength, high adsorption capacity, and controllable morphology (Duan *et al.*, 2020). Nevertheless, these materials struggle with the management of saturated adsorbents. The regeneration process is usually at high temperatures (500 °C to 900 °C), (Munoz *et al.*, 2021).

#### 2.4.2.4 Vermiculite

Vermiculite is composed of a group of hydrated laminar minerals which are aluminium, iron, and magnesium silicates. The subtract of the vermiculite is produced by heating to 1000 °C, converting the water to vapour at high temperature creates a compact layer of the material. This process is referred as exfoliation and presents the expanded vermiculite that consists of granules of high porosity (Kipp, Wever and Kreji, 2000). These materials can present varying sizes, the most common being 0 to 2, 2 to 4, and 4 to 8 mm in diameter.

All grades are very light with a particle density of 0.9 g cm<sup>-3</sup> and a BD range of 0.07 to 0.1 g cm<sup>-3</sup>, for the coarse and fine grades, respectively. It is very porous, has strong capillary action, and can hold 3 to 4 times its weight in water (Papadopoulos *et al.*, 2008), the matrix is known for its ability to retain solution due to capillary forces. This effect may be used to extract more heat from the composite due to the absorption of water by the solution in pores (Shkatulov *et al.*, 2020).

#### 2.4.2.5 Zeolite

Zeolites are composed of crystalline aluminosilicates of alkali or alkali earth elements (potassium, calcium, etc.). They are divided into natural and synthetic. Natural zeolites are aluminosilicate minerals, while synthetic zeolites also called molecular sieves; are crystalline aluminosilicates thermally manufactured. Natural zeolites are more stable (Faghihian, Ghannadi Marageh and Kazemian, 1999). They have a mixture of a range of minerals with different friability, which can change

adsorption depending on post-mining treatment (Johnson and Worrall, 2007a).

#### **2.4.2.6 Molecular sieves/ synthetic zeolites**

Molecular sieves are formed by a uniform network of crystalline pores and empty adsorption cavities, these materials are commonly made of porous materials and molecularly imprinted polymers (MIPs), (Villa *et al.*, 2020). They have an open crystalline lattice that allows the water molecules to penetrate. Generally, zeolites are more hydrophilic compared to silica gels, leading to the fact that desorption temperatures above 150 °C or even 200 °C are required for extensive regeneration of the materials, which is a major drawback for many applications. The pore sizes of molecular sieves differ from silica gel, in that the pore size of a molecular sieve is small and precise, while that of silica gel is much larger with a broad distribution. Molecular sieves are available with different effective pore sizes, such as 3, 4, 5, and 10 Å. (Chen, 2017). They present a high performance for moisture adsorption, hence they are considered for different moisture removal and AC applications (Sultan *et al.*, 2015). At 25 °C with a 10% RH, molecular sieves can adsorb water to approximately 14% of their weight. This property makes it possible to create an extremely low humidity environment with a small amount of material. However, at any humidity greater than 50% RH at 25°C, the adsorption capacity of a molecular sieve is less than that of silica gel (Chen, 2017). Some composite materials containing synthetic zeolites and silica gel present favourable adsorption characteristics (La *et al.*,

2010). Nonetheless, the application of molecular sieves is low due to its high cost.

#### **2.4.2.7 Silica Gel**

Silica gel is silicon dioxide ( $\text{SiO}_2 \cdot x\text{H}_2\text{O}$ ), which is a natural mineral that is processed and purified into granular or beaded form with an amorphous microporous structure (Sultan *et al.*, 2015). Silica gel is one of the most popular desiccants due to its low cost (Yu, Wang and Wang, 2013). In addition, they are considered chemical inertness, toxic-free, and presents a long life. One major drawback for building application is the high regeneration temperature, ranging between 100 °C to 120 °C. Silica gels can perform in high humidity environments up to 90% RH and with an indoor temperature range between 21 °C to 32 °C. The characteristics of silica gel have been widely investigated; furthermore, experimental investigations have been conducted combining silica gel with other desiccants to improve their performance (Chen *et al.*, 2018).

#### **2.4.2.8 Activated alumina**

Activated alumina is an abundant and affordable adsorbent, it comes in granular form and ranges within 0.5 to 2 mm. They have high adsorption capacity and are considered thermally stable (Mohammad, Ghaemi and Tahvildari, 2019). Activated alumina is composed of aluminium hydroxide by dehydroxylation which enables higher surface area.

#### **2.4.2.9 Super absorbent polymer**

The history of superabsorbents goes back to the 1960s, where researchers developed cross-linked polyacrylamide. Super-absorbent

polymers (SAPs) are categorized as polymer materials and have a high-water absorption function. They can absorb water hundreds to thousands of times heavier than themselves and have an excellent water retention performance. A major drawback is that the water absorption expands into a hydrogel, making it difficult to separate the water even under pressure (Ai *et al.*, 2021). Figure 2.15 shows the performance comparison of silica gel, zeolite, and SAP. The comparison shows that the SAP performance was 10 to 15% higher than silica gel. Moreover, both the silica gel and the zeolite required higher regeneration temperatures (White *et al.*, 2011; Chen *et al.*, 2018).

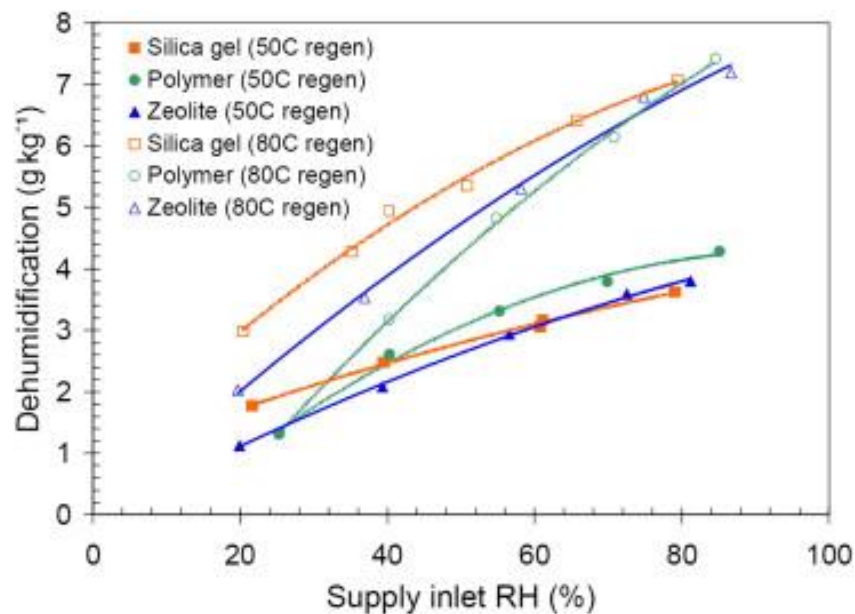


Figure 2.15 Comparison of dehumidification performance among silica gel, zeolite, and super absorbent polymer (White *et al.*, 2011; Chen *et al.*, 2018).

#### 2.4.2.10 Aerogels

An aerogel is a class of ceramic materials composed from a sol-gel procedure and a solvent evacuation as shown in Figure 2.16, they are a porous nanostructured material with approximately 90 to 99% air by volume (Gauthier *et al.*, 2004). They are considered to have good



adsorption performance for water vapour, due to their surface area, high porosity, and lightweight (Warwicker, 2010; Zheng, Ge and Wang, 2014). This material has a pore size range of 20 to 40 nm. They are resistant to moisture and mold, being a suitable option for wall incorporation. In addition to silica aerogels, carbon aerogels also show enhanced water adsorption capacities (Zheng, Ge and Wang, 2014).

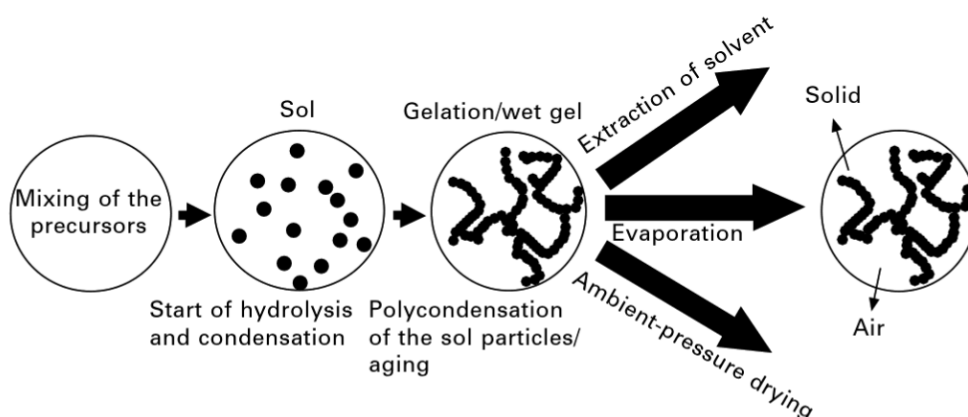


Figure 2.16 A typical scheme for preparing aerogels by sol-gel process and drying processes (Warwicker, 2010).

#### 2.4.2.11 Hygroscopic Salts

Hygroscopic salts have the capacity to absorb water vapor, they vary in size and concentration when exposed to humidity, directly impacting light absorption (Zhang *et al.*, 2021). These salts, present high absorption capacity, however, they are not stable under high humidity. Hygroscopic salts such as  $\text{MgCl}_2$ ,  $\text{LiCl}$ ,  $\text{Na}_2\text{S}$  and  $\text{MgSO}_4$  are considered a better solution compared to traditional liquid sorbents such as silica gel and zeolite due to high energy densities. Nevertheless, these salts suffer from a major drawback known as deliquescence, which refers to the saturation of the salts at certain relative humidity levels (Jarimi *et al.*, 2018). Hygroscopic particles can merge, reducing the specific surface

area and creating less resistance to the airflow (Pei, Ou and Pui, 2021), this can create complications for regeneration purposes.

#### **2.4.2.12 Metal Organic Frameworks (MOF)**

Metal Organic Frameworks is a coordination polymer (or coordination network) with an open framework containing potential voids. They are a relatively new absorbent material, based in a organic-inorganic hybrid solids with infinite and uniform crystalline coordination networks consisting of metal ions/clusters and organic linkers (Naeimi and Faghihian, 2017). This material resembles a sponge structure, composed of the transition metals coordinately linked or protected via ligands, and may be responsible for the active centres and large surface area (Ahmad *et al.*, 2020). Compared to other porous materials the MOFs present several advantages, such as high contact area, pore functionalization, and pore size tunability. A drawback presented for this material is the reduced stability presented in the aqueous medium (Ahmad *et al.*, 2020). Hydrothermal stability is fundamental for MOF performance, for this reason, metals such as aluminium, iron, vanadium, and zirconium are favoured over zinc and copper. The redox activity is another factor to take into account to maintain the material stability, making aluminium an optimal solution as it is inert towards the redox processes (Wu, Prasetya and Li, 2020). In addition, aluminium is cheap, lightweight, and available (Loiseau *et al.*, 2015).

### 2.4.2.13 Composite materials

The impregnation of two or more hygroscopic salts into a porous desiccant is called a composite desiccant and is a common method to enhance the moisture performance capacity. Natural rocks have brought attention as host materials, providing a wide range, having a low regeneration temperature (50 °C to 80 °C) and a considerable low price (Jarimi *et al.*, 2018). Composite desiccants have attracted attention in the last few years. Common host materials are silica gels, mesoporous silicate, active carbon, and natural rocks. They are characterized by their low cost; nevertheless, they present low adsorption capacity. Composite desiccants, create a balance between the stability of the porous desiccants and the high absorption capacity of the hygroscopic salts (Zheng, Ge and Wang, 2014). However, the dehumidification performance of composite desiccant materials varies significantly depending on the host and immersed salts, which implies the importance of an optimal selection of the component materials and optimization of material composition (Chen *et al.*, 2018).

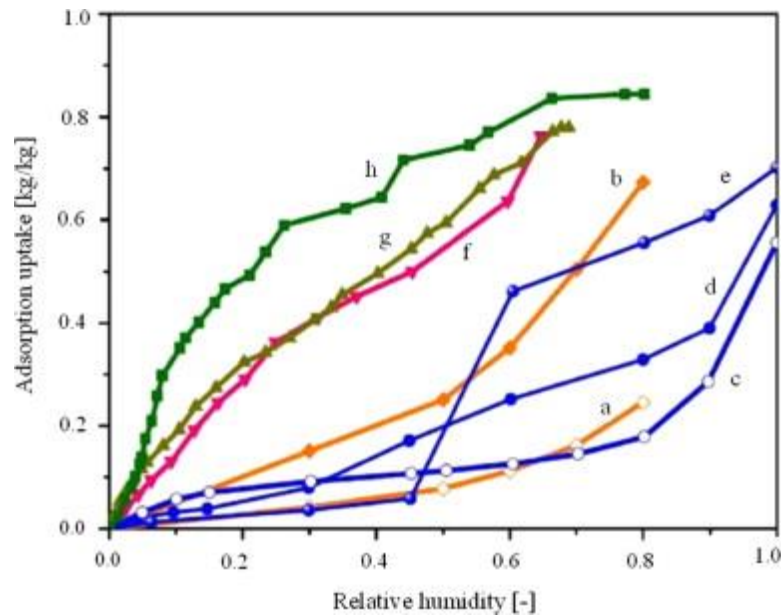


Figure 2.17 Water vapor adsorption isotherms for: (a) silica gel at 25 °C; (b) silica gel-LiCl at 25 °C; (c) sepiolite at 23 °C; (d) sepiolite-carbon by physical activation with steam at 23 °C; (e) sepiolite-carbon by chemical activation with KOH at 23 °C; (f)  $\text{CaCl}_2$ - $\text{SiO}_2$  sol-gel at 25 °C; (g)  $\text{CaCl}_2$ -MCM-41 at 20 °C; (h) silica gel-LiBr at 20 °C (La *et al.*, 2010).

Hygroscopic salts, natural materials, and activated carbon are commonly used as composite materials, having a large pore volume of the porous matrix allows the existence of some amount of salt solution in it. As a reference of the composite performance, Figure 2.17 compares different solid desiccants and enhancement methods.

### 2.4.3 Review studies on composite desiccants

Pistocchini *et al.* developed a prototype for a d-bed adsorption dehumidifier to control the latent load in an air conditioning system. They placed silica gel in a heat exchanger and had hot water running through the pipes, as displayed in Figure 2.18. The experimental results have shown the ability of the system to maintain the constant airflow during the adsorption and desorption process, without affecting the humidification rate performance (Pistocchini, Garone and Motta, 2016).

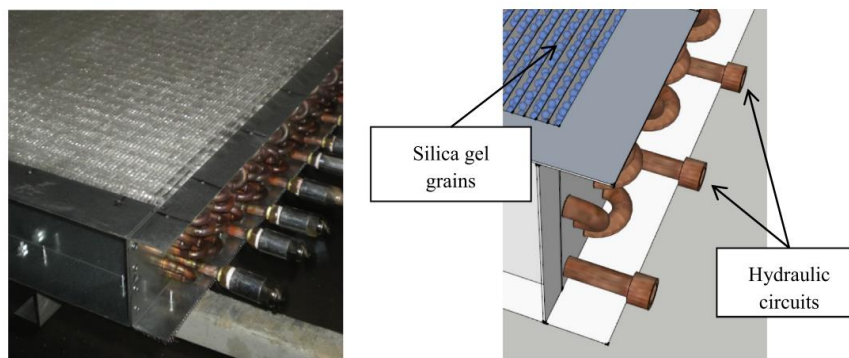


Figure 2.18 Picture and outline of the adsorption heat exchanger (Pistocchini, Garone and Motta, 2016).

Lui and Wang investigated a new type of composite based on  $\text{SiO}_2 \cdot x\text{H}_2\text{O} \cdot y\text{CaCl}_2$  which is composed of macro-porous silica gel and calcium chloride. The study revealed that the composite desiccant could absorb up to 0.4 g  $\text{H}_2\text{O}/\text{g}$  with a 40% RH, which in comparison is 5.7 times higher than macro-porous silica gel (Liu and Wang, 2003).

Wang et al. prepared a composite adsorbent with  $\text{CaCl}_2$  to enhance adsorption performance for an air-to-water system using activated carbon as the matrix. The results showed that the activated carbon fiber composite was a suitable option, up taking 1.7 g/g, which is three times more than silica gel- $\text{CaCl}_2$ .

Machado et al. investigated a new type of magnetic adsorbents based on vermiculite and iron materials to remove water contaminants. As vermiculite has the capacity to float on water, the researchers decided to incorporate iron. The study revealed that the composite material was able to remove spilled oil contaminants. After adsorption, the vermiculite/oil mixture can be separated by a magnetic process (Machado *et al.*, 2006).

Greko<sup>va</sup> et al. utilized vermiculite as an adsorption heat storage (AHS) system. The vermiculite heat storage allows low-temperature heat from renewable energy sources and various wastes to be utilized. In this study, the vermiculite was mixed with LiCl. The results show the viability to use the composite material as a heat storage system, proving to have a higher heat capacity in comparison to standard adsorbents. The heat storage capacity of LiCl/Vermiculite reached 1.5 kJ/g (Greko<sup>va</sup> *et al.*, 2019).

The properties of composite vermiculite were explored by Johnson and Worrall, reporting on an absorbent material based on a zeolite/vermiculite composite. The composite material presented a large particle size due to the adhesion of zeolite crystals within the protective lamellar matrix provided by the vermiculite. Results showed that the inclusion of zeolite particles within the structure of a supporting matrix could deliver the protection from abrasion required. Furthermore, it was found that the porosity of the host matrix increased, as shown in Figure 2.19. The material was shown to have a low bulk density ( $0.75 \text{ g cm}^{-3}$ ) adding the benefit that the majority of grains float on water for over 15 hours. The resulting material can be easily handled and separated from aqueous waste streams using either flotation or exploiting its granular nature (Johnson and Worrall, 2007b).

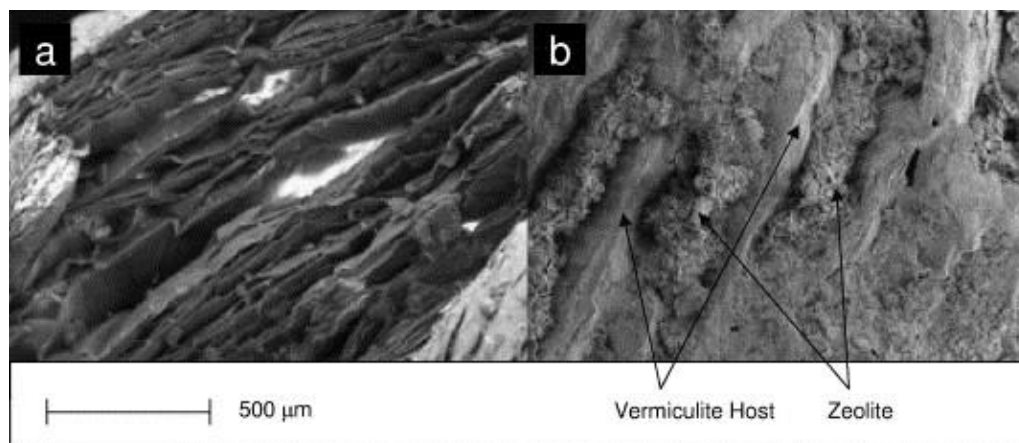


Figure 2.19 SEM (Secondary electron capture, accelerating voltage 15 kV) images of particles of vermiculite (a) and zeolitized vermiculite (b) (Verm/Zeo-72), (Johnson and Worrall, 2007b).

In a second study, the authors reported on the synthesis of a vermiculite/zeolite composite material to increase the control of a zeolite product for wastewater treatment. The results proved that the vermiculite-based composite presented the same hydraulic properties as a natural clinoptilolite with similar grain sizes (2–5 mm). In addition, the hydraulic conductivity was higher than synthetic power zeolite. The results demonstrate that the vermiculite-based composite shows the same hydraulic properties as a natural clinoptilolite with similar grain size (2–5mm), however, the rate of adsorption and maximum coverage were improved by a factor of 4. (Johnson and Worrall, 2007a).

Stawiński et al. investigate an acid bases vermiculite adsorbent, having NaOH as the enhancement material. The results show that NaOH of acid-activated vermiculite increased the adsorption capacity in comparison to samples modified only in acidic solution in respect to raw material. Nevertheless, a decrease in the adsorption performance was noted after 2 cycles (Stawiński *et al.*, 2017).

Table 2.7 Synthesis table of the solid desiccant studies.

System	Material	Main Findings	Reference
Dehumidifier (heat exchanger)	Silica gel	The system was able to keep a constant airflow and maintain the dehumidification.	(Piselli <i>et al.</i> , 2020)
Dehumidifier	$\text{SiO}_2 \bullet x\text{H}_2\text{O} \bullet y\text{CaCl}_2$	The composite presented an enhanced absorption performance in comparison to macro-porous silica gel.	(Liu and Wang, 2003)
Magnetic adsorbents for water spilled contaminants	Vermiculite/iron	The composite was able to adsorb water pollutants and was magnetically regenerated.	(Machado <i>et al.</i> , 2006)
Adsorption heat storage	Vermiculite/Li	The composite presented superior adsorption capacities, reaching 1.5 kJ/g.	(Grekova <i>et al.</i> , 2019)
Adsorbent	Zeolite/vermiculite	The zeolite increased the particle size and porosity.	(Johnson and Worrall, 2007b)
Wastewater treatment	Zeolite/vermiculite	Synthetic vermiculite-based composite shows improved the adsorption up to 4 times.	(Johnson and Worrall, 2007a)
Adsorbent	Vermiculite/NaOH	The adsorption capacity was enhanced by the addition of NaOH; however, this was reduced after 2 cycles.	(Stawiński <i>et al.</i> , 2017)

#### 2.4.4 Main conclusions

This review focuses on the available solid desiccant materials suitable for humidity control in buildings, focusing on the enhancement of the materials by creating composite desiccants. For the successful incorporation of the solid desiccant, it is important to develop an easy and cost-effective approach for humidity control (Lu, Kuok and Liu, 2020). According to Gordeeva *et al.*, the selection of the specific adsorbent is based on two main conditionings:

- Formulating the demands of particular application to the required adsorbent properties



- Synthesis of the adsorbent, which properties precisely or nearly fit these demands (Gordeeva *et al.*, 2009).

Solid desiccants have been extensively investigated for different applications, the optimization of composite materials has been analysed particularly for agricultural and pollutants removal. There are limited references for building applications, particularly in the case of natural materials.

## **2.5 Solar Assisted heat pump systems**

### **2.5.1 Background**

Domestic hot water accounts for the fourth largest energy user in the building sector. Domestic consumption of energy is mainly due to hot water production and space heating (Kara, et al., 2008). Energy supply systems are leaning towards renewable energy, supporting the transition from predominantly fossil fuels. The heat generation for domestic hot water and space heating are the main building's energy demands (Dott, Genkinger and Afjei, 2012).

A solar-assisted heat pump system (SAHP) is a technology that aims to reduce or eliminate the primary energy (coal, natural gas, etc.) consumption through the substitution of renewable-based energy sources (Sami & Saffa, 2016). In this scheme, a heat pump system is coupled with a solar thermal connector, in order to reduce the CO<sub>2</sub> emissions. The purpose of the thermal connector is to convert and transport thermal energy from the sun, to provide heating. In addition, the system allows transferring heat for storage purposes (Sami & Saffa,

2016). The heat pump (HP) function is to transport the heat from one source to another by a working fluid. Heat pump systems are heat-generating devices utilized to heat water either for hot water or space heating applications. Normally, the heat pumps are powered by electricity, running a mechanic compressor to operate the inverse Rankine cycle. Heat pumps take a significant role in efficiency (Del Almo, et al., 2019), and it is measured by the coefficient of performance (COP). The heat pumps COP depend on many factors such as the temperature of the evaporator, the temperature of the low-energy source, the delivered useful heat, the working medium used, among others (Hepbasli & Kalinci, 2009). The most efficient the heat pump, the less energy consumption it consumes.

There are two main classifications for the heat pumps systems: these are Direct Expansion Solar Assisted Heat Pumps (DX-SAHP) and Indirect-style Solar Assisted Heat Pumps (i-SAHP), (Sterling & Collins, 2012). DX-SAHP systems use the solar collector as the evaporator, or one of many potential evaporators, in a typical vapor-compression cycle (Chaturvedi & Chen, 1998). For i-SAHP systems, the solar collector the heat pump is integrated into the design as a closed unit (Sterling & Collins, 2012). The possibilities of SAHP systems are variated. One main advantage of the solar collector and the heat pump performance is to reduce the collector temperature and boost the heat pump evaporator temperature. Consequently, the performance of both systems could be enhanced (Kamel, et al., 2015). Heat pump systems have become an

indispensable technology that contributes towards a cleaner environment as shown in Figure 2.20.

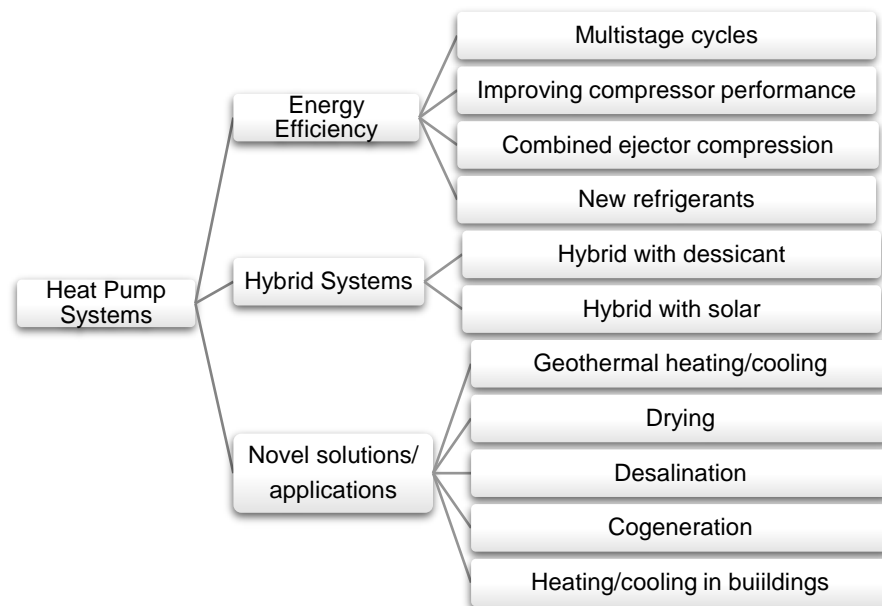


Figure 2.20 A generalised classification of the recent development in heat pump technologies (Chua, Chou and Yang, 2010).

## 2.5.2 Classification and characteristics

The integration of solar thermal collectors with heat pump systems contributes to increasing the system seasonal performance factor (SPF) and consequently reducing the final energy consumption, thereby reducing the CO<sub>2</sub> emissions.

### 2.5.2.1 Solar thermal collectors

Solar thermal collectors are devices applied to harvest solar radiation and convert it to thermal energy. They function by transporting the energy into a storage device for later use and this can be achieved by natural or forced circulation. They are commonly used to produce hot water for building applications. Figure 2.21 presents the solar thermal classification, where the non-concentrating collectors are generally used in residential

and commercial buildings for space heating (Evangelisti, De Lieto Vollaro and Asdrubali, 2019).

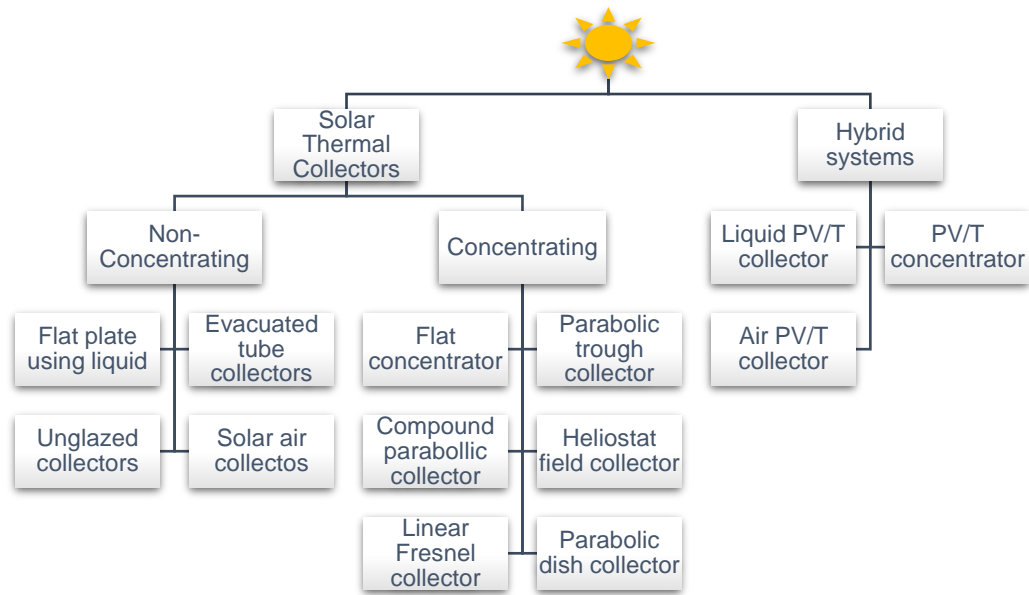


Figure 2.21 Solar systems classification (Evangelisti, De Lieto Vollaro and Asdrubali, 2019).

Utilizing a solar collector connected with a heat pump may be operated below the temperature of the ambient dew point. Classical collector energy balances do not account for this operation mode. Figure 2.22 presents different sources of heat gain for solar collectors. This can be shortwave solar radiation ( $q_{rad,s}$ ), long wave radiation exchange ( $q_{rad,L}$ ), convective heat exchange with the air ( $q_{amb,sens}$ ), and latent heat exchange ( $q_{amb,sens}$ ), and latent heat exchange ( $q_{amb,lat}$ ), heat conduction ( $q_k$ ), energy gains from rain ( $q_{rain}$ ), (Hadorn, 2015).

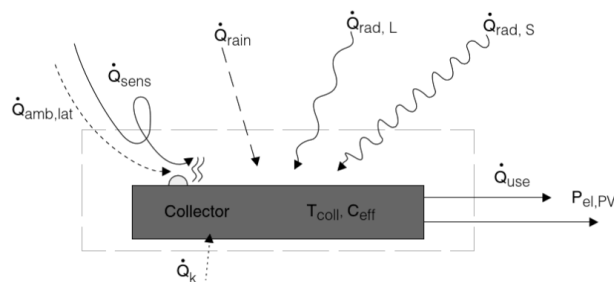


Figure 2.22 Energy balance of a PVT collector or absorber (Hadorn, 2015).

The useful power output of the collector consists of the practical heat gain ( $q_{gain}$ ) and in case of the PVT collectors, additionally of electric power ( $p_{el,pv}$ ). Moreover, it accounts for the internal energy change by the effective thermal capacity ( $c_{eff}$ ) of the collector as follows:

$$q_{use} = q_{gain} - p_{el,pv} - \frac{\delta T_{coll}}{\delta \tau} c_{eff}$$

Where  $\frac{\delta T_{coll}}{\delta \tau}$  is the time derivated of the average temperature of the thermal capacity of the collector.

Three elements affect the performance of solar thermal collectors and are condensation, freezing, and heat gains from the rain.

The potential for improvement has led to numerous research articles, particularly for domestic applications. Buker and Riffat (Sami & Saffa, 2016) carried out a complete and systematic review. In this literature the focus has been made to provide an update on the latest technology of solar-assisted heat pumps, considering PV, solar thermal, and alternative applications.

#### 2.5.2.2 Heat pumps and Photovoltaic (PV)

Photovoltaic thermal heat pump technology is characterized by its capacity to generate heating, cooling, and electricity. The electrical efficiency of the PV modules is highly dependent on the temperature of the cells. Bellos et al. combined a SAHP driven by a nanofluid-based hybrid PV collector for space heating and electricity production, as presented in Figure 2.23. The study found that in comparison to water, the nanofluids in the solar collector enhanced the thermal and electrical

performance, water/Cu and water/ $\text{Al}_2\text{O}_3$  are found to be the most efficient of the tested samples, improving the system efficiency by 4.8% and 4.34% respectively (Bellos, et al., 2019).

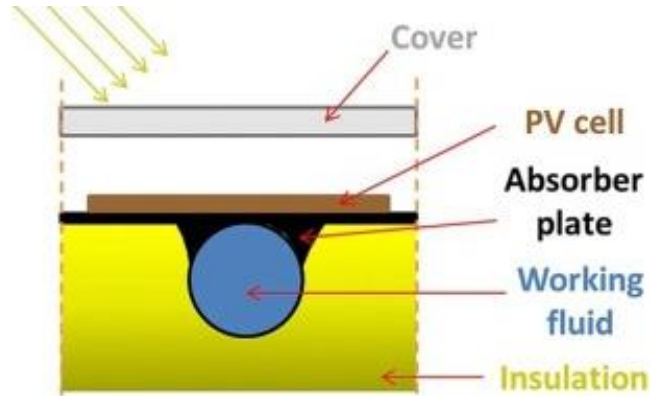


Figure 2.23 The examined strip of the hybrid PV.

Vallati et al. analysed the behaviour of a PV-assisted heat pump in three different European cities. The results showed that the system covers the demand up to 70% in Rome, 62% for Milan, and 47% in Cracow (Vallati, et al., 2019). Roselli et al. focused on the electricity production of a solar PV-based ground source heat pump for office applications. A simulation approach was considered using TRNSYS. The system included a battery to store the energy production from the PV. It was found that the percentage of on-site renewable electricity used decreases with photovoltaic capacity and increases with battery storage size (Roselli, et al., 2019).

Liu et al. investigated the optimal operation of a PV- battery system for heat pump units. Heat pumps generally increased the self-consumption ratio from the consumption of the midday surplus PV and decreased the optimal capacity of the battery storage. The commercial aspect of this technology depended on the battery price and capacity. (Liu *et al.*, 2019).

In a similar study, a PV-driven ground heat pump was used as a thermal battery. TRNSYS simulations were carried for small buildings, finding that for a single-family dwelling PV self-consumption could be increased significantly from 7% up to about 44% (Thür, et al., 2018).

Figure 2.24 shows a Photovoltaic/Thermal (PVT) heat pump as a hybrid solution with promising results for the simultaneous generation of electrical power and useful heat as total output energy. The hybrid PVT system reduced the PV modules temperature by circulating fluid, resulting in better electrical efficiency (Tripanagnostopoulos, et al., 2002).

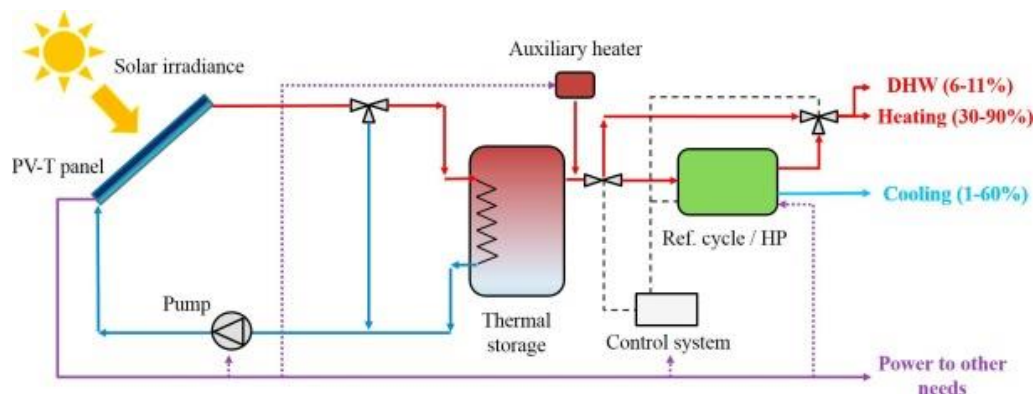


Figure 2.24 PV-T system for solar heating and cooling provision (Tripanagnostopoulos, et al., 2002).

Wang et al. combined a hybrid solar power system; integrating a photovoltaic direct steam generation solar collector with a chemical heat pump. The pump was used to upgrade the dissipated heat of the PV, this upgraded heat was then combined with the steam from the solar collector to drive the high-parameter steam Rankine cycle for efficient power generation. Results showed that the performance and energy storage improved, having an average electricity output of  $192.36 \text{ Wm}^{-2}$ , 170% higher than the  $70.41 \text{ Wm}^{-2}$  produced by the individual PV system (Wang, et al., 2019).

Figure 2.25 presents a solar PVT-assisted heat pump, with a cold storage tank to source the heat pump and a hot water domestic tank. The configuration allowed both heating and cooling, providing a hot water supply and covering part of the electricity demand. Results demonstrated that on average, the efficiency of PVT collector was more than 50% for PVT water heating mode when solar irradiance was sufficient, the COP also was enhanced (Wang, et al., 2018).

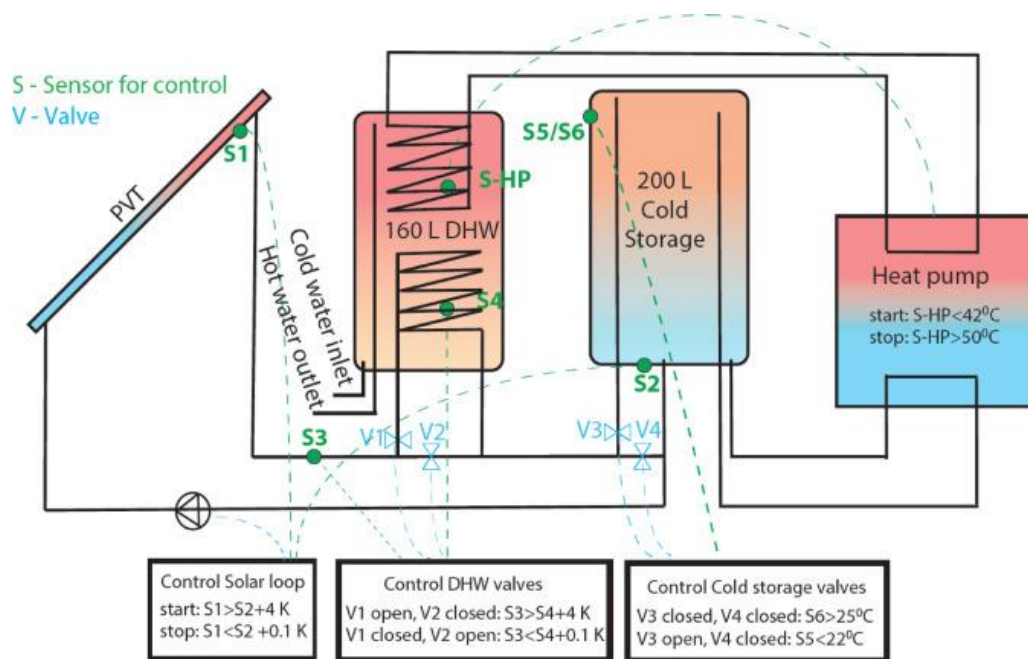


Figure 2.25 PVT system and the control strategy and sensor locations.

In a different study, Dabbemand et al. used a solar PVT assisted - heat pump system with a cold buffer storage tank. The results showed that the hot water demand was almost covered in full by the PVT during summer. Additionally, when the solar radiation is not high, the PVT added a significant amount of energy to the cold storage tank (Dannemand, Perers and Furbo, 2019).



A heat-pipe solar (HPS) photovoltaic/thermal heat pump system, combining HPS PVT collector with heat pump was introduced by Chen et al. When the solar radiation increased, the absorptivity of the PV decreased and it was reflected in the decrease of  $COP_{PVT}$  (Chen, et al., 2017).

Del Almo et al. focused on the optimum operating point of combining a PVT with a SAHP. The model was simulated on TRNSYS and validated with parametric results from a factory in Zaragoza, Spain. Overall, it was proved that when the temperature ranges from 10 °C to 20 °C the seasonal COP increased to 4.62, instead of 2.96 when working between 7 °C and 10 °C. Additionally, 67.6% of the electricity demanded by the heat pump could be supplied by photovoltaic production (Del Almo, et al., 2019). The operation performance of a solar photovoltaic/thermal-ground source heat pump (PVT-GSHP) was examined by Cai et al. Results demonstrated that the PVT-GSHP system can reduce the temperature of photovoltaic/thermal modules up to 10 °C, at the same time improving the efficiency of electricity production by 25% (Cai, et al., 2017).

A study containing a solar-driven direct-expansion heat pump system employing micro-channel PVT modules as the evaporator was performed. The system was designed to provide electrical power and thermal energy for space heating. It was found that the average COP was 4.7. Additionally, the heat pump was able to provide constant heating for a 150 m<sup>2</sup> room at 18.5 °C (Zhou, et al., 2020).

Besagni et al. experimentally tested a dual-source solar-assisted heat pump for heating and cooling. The system had hybrid photovoltaic and thermal panels and a reversible heat pump. The heat pump contained both, an air –source and a water source evaporator. The PVT panels produced the domestic hot water, at the same time providing water to the evaporator (Besagni, et al., 2019).

Zhou et al. investigated a dual-use roll-bond photovoltaic thermal heat pump system. The tri-generation performance was tested simultaneously, in terms of the heating, cooling, and power supply capacity. Results showed that the system was feasible having a COP between 3.9 to 2.5 (Zhou, et al., 2019).

Lu et al. utilized vapor injected (VI) into a DX-SAHP system with photovoltaic/thermal (PVT) modules used to harvest energy and electric power. The system is described in Figure 2.26, which showed the relationship between subcooling degree gain and injected vapour mass flow rate ratio was also found to be linearly dependent (Lu, et al., 2019).

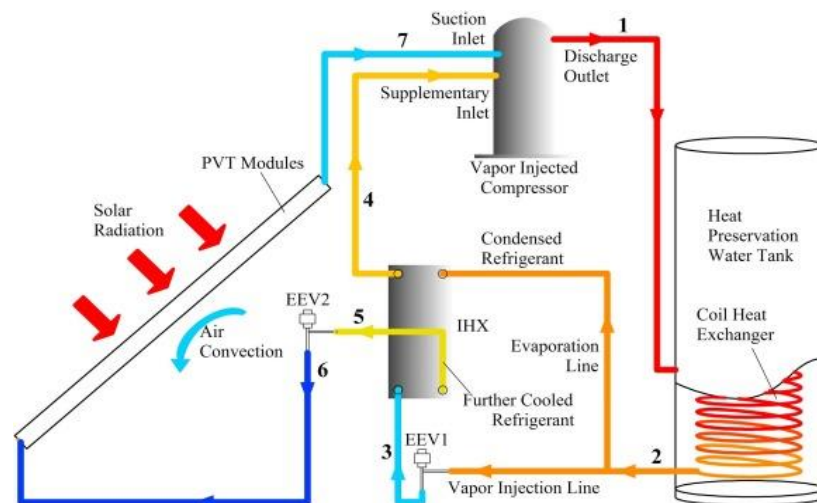


Figure 2.26 Composition and working process of the PVT-VISHP system for water heating (Lu, et al., 2019).

### 2.5.2.3 Solar thermal heat pumps

Han et al. developed a mathematical model for a solar-assisted transcritical CO<sub>2</sub> heat pump system with phase change energy storage (STCHPS-PCES) aimed at rural houses. For the PCES a spherical capsule was used filled with paraffin material. The COP during summer was 2.56, while the increased rates of solar and PCES for heat pump COP were 15.16% and 14.34%, respectively (Han, et al., 2018).

Moreno et al. developed a mathematical model to determine the operating characteristics of a DXSAHP for DHW production. The model can calculate external factors such as outdoor temperature, global radiation, and wind speed, and for a given cooling machine, the evaporation temperature and the power exchanged by the equipment. To validate the results, they installed a prototype in Madrid, the COP presented a range between 1.7 to 2.9 (Moreno-Rodriguez, et al., 2012).

Huang et al. investigated a direct-expansion solar-assisted heat pump for space heating under frosting conditionings. The model was numerical and experimentally tested and the frosting characteristics were investigated. The ambient temperature, solar radiation, and relative humidity were monitored. It was found that a solar irradiance of 100 W/m<sup>2</sup> could prevent frost formation. In addition, it was concluded that no frost occurs with the relative humidity is lower than 60% and when the ambient temperature and solar irradiance are 1 °C and 0 W/m<sup>2</sup> (Huang, et al., 2019). A similar study investigated a direct-expansion solar-assisted heat pump (DX-SAHP) system during the autumn and winter period.

Experimental results showed that under the sunny and overcast day conditions the system could reach an average COP of 4.0 and 3.0, respectively (Kong, et al., 2018).

A direct expansion solar-assisted heat pump system (DX-SAHP) for cold climate applications was evaluated by Mohamed et al. A COP between 3 to 4 was found, while the solar collector efficiency was found to vary between 40% and 75%. For water temperatures in the condenser tank varies between 43 °C and 50 °C (Mohamed, et al., 2017).

In a study for an Indirect-style Solar Assisted Heat Pump (i-SAHP) a comparison was made of traditional solar domestic hot water (SDHW) and an electric domestic hot water (DHW). All the systems had the same load profile and delivered domestic hot water at a constant temperature. The dual tank i-SAHP system proved to be the most energy efficient and had the lowest annual operating cost of the three models analysed (Sterling & Collins, 2012).

Safijahanshahi and Salmanzadeh focused on the improvement of the COP by increasing the evaporator fluid, reducing the work in the compressor. The system comprehends an unglazed transpired solar collector and an air-to-air heat pump; as part of the investigation, developing a mathematical model in Kerman, Iran. The results showed that compared to a conventional air-to-air heat pump the proposed system could decrease the electricity consumption by 10% (Safijahanshahi & Salmanzadeh, 2019).

The performance of the novel type solar assisted heat pump system using a low global warming potential refrigerant (R-1233zd(E)) with the flexible solar collector was investigated by Joo et al. It was observed that in relation to the R-134a (popular refrigerant) the COP was improved by reducing the power consumption (Joo-Lee, et al., 2018).

A comparison among three systems integrated of solar energy and air source heat pump was proposed. Qui et al. compared three models based on the temperature. The first model Medium-temperature heat-collecting system (MTHS), a high-temperature heat-collecting system (HTHS), and a low-temperature heat-collecting system (LTHS). The medium temperature proved to have 55% higher efficiency than the other models (Qui, et al., 2018).

In a different study, a novel solar-assisted heat pump was developed to dry radishes. The evaporator and condenser were integrated into a drying chamber and the water storage tank was set up to recover the heat, improving the solar utilization. When the solar radiation was optimal, the system ran at the solar-assisted heat pump drying (SAHPD) mode; when the solar gain was insufficient the heat pump drying (HPD) was applied. It was reported that the SAHPD could save energy consumption by 40.53% in terms of heat recovery and thermal storage (Qiu, et al., 2016).

#### **2.5.2.4 Alternative solar sources and heat pumps**

Apart from the PV and solar thermal collectors, there are alternative technologies that harvest the solar radiation and are coupled with a heat

pump system. This is the result of novel integration ideas and specific building requirements.

He et al. proposed an innovative solar loop-heat- pipe façade combined with a heat pump for water heating. A comparison between R13a, R2, R600, and water as the working fluids in the heat pipe loop was selected. It was concluded that water presented the highest heat transfer capacity; however, it required the lowest pressure to function, hampering the operation at a large scale. R600a was selected as the favoured working fluid, having the second-highest efficiency (He, et al., 2014).

Lin and Sun investigated a novel photovoltaic loop heat pipe/solar assisted heat pump (PV-LHP/SAHP) water heating system. The system had three operation modes: PV-LHP mode, solar/air source heat pump (SASHP), and air source heat pump (ASHP). A mathematical model was developed to simulate the system working conditions, validated with experimental testing in Qinhuangdao, China. They reported that in order to meet the water temperature required the PV-LHP/SAHP system should work both in the PV-LHP mode and in the SASHP mode in winter (Li & Sun, 2018).

Long et al. investigated a dual heat source integrated heat pump evaporator, which uses energy and air energy to collect heat. The evaporator contained a unique distribution of the refrigerant and water coils. Results proved that the evaporator hot water supply could increase the refrigerant evaporation temperature and heat pump COP (Long, et

al., 2019). The summary of the studies is presented in Table 2.7 and is divided by technology.

Table 2.8 Summary of solar thermal studies.

System	Main Findings	1*	Ref.
PV HP	Water/Cu was found the most efficient samples, improving the system efficiency by 4.8% in comparison to pure water.	M	(Bellos, et al., 2019)
PV HP	The heating demand covered for Rome was 70%, for Milan was 62%, while for Cracow was 47%.	M/T	(Vallati, et al., 2019)
PV GSHP	The percentage of on-site renewable electricity used decreases with photovoltaic capacity and increases with battery storage size.	T	(Roselli, et al., 2019)
PV HP	Heat pumps generally increased the self-consumption ratio from the consumption of the midday surplus PV and decreased the optimal capacity of the battery storage.	M	(Liu et al., 2019)
PV GSHP	Single-family dwelling PV self-consumption can be increased by 37%.	T	(Thür, et al., 2018)
PVT HP	The PVT reduced the module temperature, resulting in better electrical efficiency.	M	(Tripanagnostopoulos, et al., 2002)
PVT HP	The performance and energy storage was improved, having 170% more electric production than an individual PV system.	M	(Wang, et al., 2019)
PVT HP	Under certain conditions, the PVT efficiency was 50% higher for water heating.	E/M	(Wang, et al., 2018)
PVT HP	The hot water demand was almost covered in full by the PVT during summer.	E	(Dabbenabd, et al., 2019)
HPS- PVT	When the solar radiation increases the absorptivity of the PV the COP decreased.	E/ M	(Chen, et al., 2017)
PVT HP	The COP increase 1.66.	E	(Del Almo, et al., 2019)
PVT-GSHP	A reduction in the temperature of the photovoltaic/thermal modules up to 10 °C was obtained, improving the efficiency of electricity production by 25%.	T	(Cai, et al., 2017)
PVT HP	Average COP 4.7 and provide enough energy for room heating.	E	(Zhou, et al., 2020)
PVT HP	The use of the water-source evaporator allowed to significantly increase the performance of the system and to avoid the defrost cycles.	E	(Besagni, et al., 2019)
PVT HP roll	The COP was between 3.9-2.5.	E	(Zhou, et al., 2019)
PVT DXSAHP	The relationship between subcooling degree gain and injected vapor mass flow rate ratio was also found to be linearly dependent.	E	(Lu, et al., 2019)
STCHPS-PCES	The phase change energy storage technology improves the heating performance of the heat pump by 14.34%.	M	(Han, et al., 2018)

DXSAHP	Developed a mathematical model was validated against experimental testing for the course of one year.	M	(Moreno-Rodriguez, et al., 2012)
DXSAHP	No frost occurs with the relative humidity lower than 60% when the ambient temperature and solar irradiance are 1 °C and 0 W/m <sup>2</sup> .	M/E	(Huang, et al., 2019)
DXSAHP	Under the sunny and overcast day conditions, the system could reach an average COP higher than 4.0 and 3.0, respectively.	E	(Kong, et al., 2018)
DXSAHP	The COP is between 3-4, the solar collector efficiency was found to vary between 40% and 75%.	E	(Mohamed, et al., 2017)
i-SAHP	The dual tank i-SAHP system proved to be the most energy efficient and had the lowest annual operating cost.	T	(Sterling & Collins, 2012)
SAHP	An unglazed solar collector improved the efficiency by 10% in comparison to an air-to-air heat pump.	M	(Safijahanshahi & Salmanzadeh, 2019)
SAHP	Compared to the R-134a the COP was improved with the R-1233zd(E).	EE	(Joo-Lee, et al., 2018)
SAHP	The medium temperature proved to have 55% higher efficiency than the other models.	EE	(Qui, et al., 2018)
SAHPD	The SAHPD can save energy consumption by 40.53% in terms of heat recovery and thermal storage.	M/S	(Qiu, et al., 2016)
Heat-pipe	R600a was selected as the favourite working fluid, presenting the second-highest efficiency.	S	(He, et al., 2014)
Heat pipe SAHP	The life cycle cost of the PV-LHP/SAHP system could be reduced by 29.6%.	M/E	(Li & Sun, 2018)
SAHP	COP increased by 15%.	M/E	(Long, et al., 2019)

System; PV= Photovoltaic HP= Heat Pump, GSHP = Ground Source Heat Pump, PVT= Photovoltaic/Thermal, DXSAH= Direct Expansion Solar Assisted Heat Pumps, i-SAHP= Indirect-style Solar Assisted Heat Pumps, SAHP= Solar Assisted Heat Pump, SAHPD= Solar Assisted Heat Pump Drying. 1\* Method of analysis; M = mathematical model, T= TRNSYS, E= experimental, S= simulation.

### 2.5.3 Main conclusions

Heat pump systems aim to provide heating, cooling, and in some cases electricity, by harvesting solar energy and at the same time reducing the CO<sub>2</sub> emissions. For heating applications, it can be applied for domestic hot water and/or space heating. By using PV modules, the electricity input can be stored in a battery system. It was found in the literature that most of the studies focused on solar thermal applications, in comparison to PV and alternative sources. The combination of photovoltaic-thermal (PVT) systems is a popular solution that simultaneously produces electrical power and useful heat, in some cases improving the COP by 50%. Many



researchers have focused their investigation on developing mathematical models, however, each system has specific boundaries, making them difficult to compare or apply in different regions.

One major drawback of this technology is that is limited to solar availability, this means that in the case of heating, the peak values of solar radiation are contrary to the heating demand. For this reason, the implementation of thermal storage is a viable solution to maximize the application.

The reviewed studies demonstrate the positive effect of solar heat energy on performance, particularly when compared with conventional systems. Solar-assisted heat pumps can make a significant contribution towards increased renewable production for space heating and domestic hot water supply and additional alternatives.

## **2.6 Summary**

This chapter reviewed the PCMs for building applications, finding them as a compelling solution for passive cooling due to their latent heat storage capacity. Research has shown the energy saving potential resulting from its application. There is still a gap in terms of the enhancement methods, particularly for inorganic materials. From this point forward the challenge focuses on creating a ceiling panel, that is aesthetic, lightweight, and has a high thermal performance.

In the case of the solid desiccant materials, the defiance focuses on the selection of a suitable for low-temperature regeneration material. Furthermore, the enhancement methods should be evaluated to reduce

the quantity required. Similar to the PCM application, the selection of a breathable and aesthetic container, lightweight and with high moisture control should be addressed.

In terms of the solar-assisted heat pump, the evaluation of the COP performance must be considered, as well as the heat pump capacity to regenerate the solid desiccant material.

The tri-modular system must be experimentally investigated to address the performance for building integration. Moreover, the integration of the complete system will validate the adequate performance and capacity to provide total thermal comfort in buildings. Preliminary testing is presented in Chapter 5, focusing on the enhancement materials for PCMs and solid desiccants.

# Chapter 3 System components

## 3.1 Introduction

This chapter provides a detailed description of the system components. The tri-modular system aims to develop an innovative, energy efficient system to control the cooling, heating, and humidity in buildings. The system is coupled with a solar-assisted heat pump with a direct system expansion. A high-performance solid desiccant material to provide dehumidification, regulating the relative humidity. Additionally, the system contemplates the application of phase change materials to assist in the cooling demands, this will be integrated into the building in the form of ceiling panels, that will passively regulate the indoor room temperatures, regulating the peak temperatures.

## 3.2 Environmental control in a building

The idea of a building is to modify the external climate, providing higher comfort inside than outside, the principal factors involved are described as follows:

Heating: heat energy is required to maintain the thermal gradient between inside and outside. The rate of heat loss is related to the insulation in the building envelope and the volume of external air entering the building that requires heating.

Thermal storage: driving heat in and out of the building requires a swing at room temperature. Ideally, the thermal mass should be in direct contact with radiation and convection. The thermal mass of the material is governed by its thermal conductivity, mass, and specific heat capacity.

Cooling: insulation works preventing the heat from coming inside the building. Thermal mass can help by absorbing heat when the temperature increases and releasing it when the temperature drops.

Ventilation: CO<sub>2</sub> level in the buildings has a direct correlation with the occupancy, where 8 litres of fresh air per second per person (l/s/p) will equate to a CO<sub>2</sub> level of 1000 ppm.

Internal moisture and pollutant control: moisture levels depend on the number of occupants and other indoor activities (cooking, bathing, etc.), humidity levels should be lower than 70% to prevent mold growth. Absorbent materials will act as sponges to control the moisture, desiccants can absorb moisture at low temperatures and release them at high temperatures.

Energy usage: heating, cooling, lighting, hot water, and electrical appliances are the highest energy consumers in buildings. In cold climates, heating represents the highest energy demand, whereas in hot

climates cooling the opposite effect occurs. The amount of fan and pump power depends on the heating, cooling, and ventilation systems and the lighting load depends on the building usage.

### **3.3 System description**

The system will respond to varying occupancy and diurnal/seasonal fluctuations in weather conditions, minimising the energy consumption of the heat pump. The PCM panel will store the available heat/coolness by the melting/freezing of the material, in part driven by the difference between day and night-time temperatures and in part by the heat pump, providing heat in winter and cooling in summer. The PCM will act as thermal energy storage with enhanced transfer characteristics. The solar-assisted heat pump will obtain the heat from the outdoor ambient to warm the inside area during the winter. The system is set to achieve the human comfort requirements of a temperature range of 21 °C to 27 °C and relative humidity of 30 to 70%. The solid absorbent panel will control the air humidity level of the building when dehumidification is demanded, removing the excess moisture from the indoor room. Once the desiccant material is fully saturated, the heat pump is activated circulating hot water to the panel, heating the material, and recharging it. This can be controlled using a timer and a two-way zone valve that has been piped into the flow and return pipework. During this process, the air vents will be closed in order to contain the heat and help the system to run as efficiently as possible. The warm moist air is then expelled to the outside via ducting with the aid of a low voltage extractor fan. Once the cycle is complete the

zone valve will close preventing any circulation through the absorbent box and the heat pump can then operate under normal conditions.

Several innovative techniques will be implemented in this project including:

- Novel heat transfer PCM enhancement, increasing the thermal performance of the material.
- Novel PCM encapsulation method with enhanced thermal conductivity.
- Utilising of solid desiccant dehumidifier, capable of absorbing significant quantities of moisture to improve thermal comfort/air quality. To optimize the performance of the dehumidifier; an enhancement method of the solid desiccant is considered.
- PCMs testing using DSC, thermal conductivity analysis, and experimental evaluation of several organic and inorganic materials.
- Heat pump performance assessment, measuring the suitability to procure indoor space heating and solid desiccant regeneration.

Figure 3.1 shows a schematic house based on the Positive Homes layout, which is designed as a super low energy consumption home. In this section, the main system components are presented including two solar thermal collectors and the section for the PCM panels and solid desiccant panels.

Figure 3.2 presents the house model in detail, where the PCM panel was schematically placed in the living room, the solid desiccant is allocated in the kitchen to aid the dehumidification performance, the solar collectors, and hot water tank are represented in the roof and the first floor respectively.

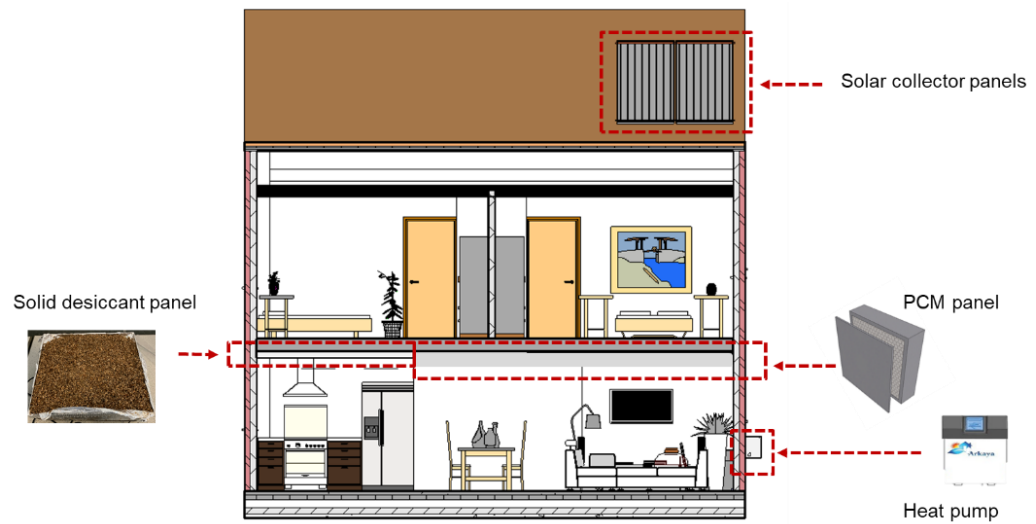


Figure 3.1 System description for the thermal comfort model.

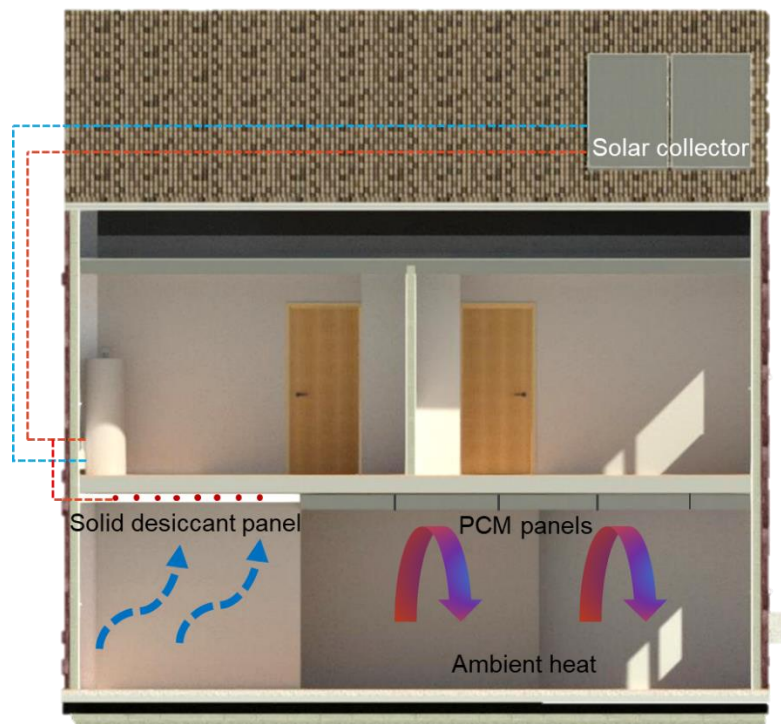


Figure 3.2 System description of the components.

The project aims to reduce the heating and cooling loads and at the same time improving the occupant's quality of life. The system is designed to offer a sustainable source of energy and heat supply as it serves to overcome a major shortcoming of current space heating and cooling systems in terms of CO<sub>2</sub> emissions.

### **3.4 System components**

The thermal comfort system is composed of three parts including PCMs, solid desiccant, and a solar collector. The system elements are envisaged for various combinations of hot/cold/humid/dry conditions. Coupling them with a solar/air heat pump is an especially attractive solution, by simultaneously aiding in temperature and humidity control. In contrast, sophisticated HVAC systems, small residential heat pumps typically only control temperature.

#### **3.4.1 Phase Change Materials**

For building applications, the PCM is required to undergo phase transition with a low operational temperature, normally within the thermal comfort range. In this case, the desirable indoor thermal comfort temperature ranges from 23.5 °C to 25.5 °C in summer and 21 °C to 23 °C in winter (Zhou, Zhao and Tian, 2012). As stated in the literature review (Peippo, Kauranen and Lund, 1991), the suggested melting temperature should be 1 °C to 3 °C higher than the average room temperature, in order to maximize the benefits of a diurnal PCM cycle. In this case, the selection of the PCMs should be in a temperature range between 18 °C to 29 °C



for indoor applications for the UK climate. Based on the review of the literature, Figure 3.3 displays the available PCMs with the melting temperature range of 0 °C to 35 °C (Whiffen and Riffat, 2013).

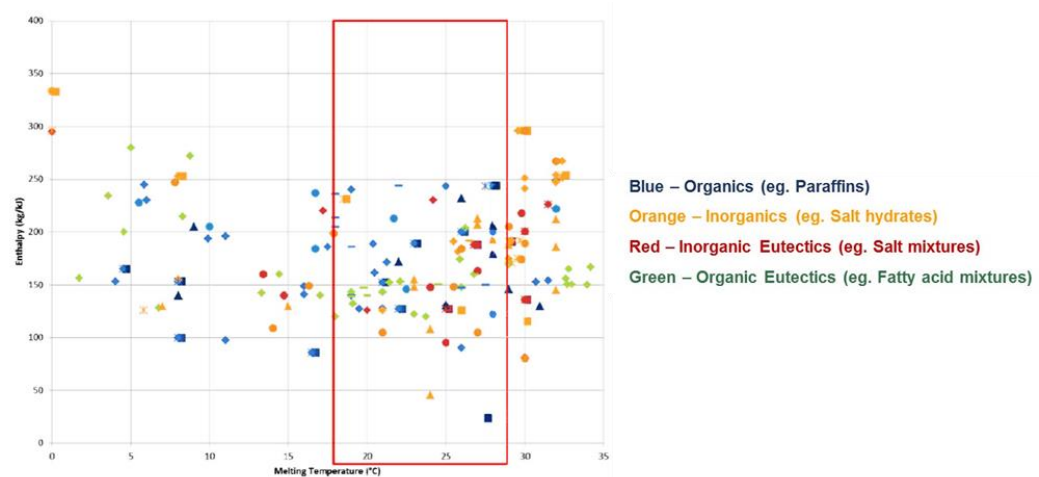


Figure 3.3 PCMs in the melting temperature range of 0 °C to 35 °C (Whiffen and Riffat, 2013).

Figure 3.4 presents the main parameters for successful PCM building integration, having the encapsulation method as the most common solution, especially for retrofit applications. When encasing the PCM it is highly important to consider the adequate heat transfer between the indoor environment and the material. In addition, the container material should avoid leakage, have no chemical interaction to maintain long-term stability and avoid corrosion. Furthermore, for the successful application of the PCM in buildings, the aesthetic factor is highly important to promote the application of this technology, structurally it is important to consider the weight of the ceiling tile as it may cause structural damage or require reinforcement. Finally, the CBA (cost-benefit analysis) should also be considered as the production and integration of the material should be accessible and have a sensible payback investment.

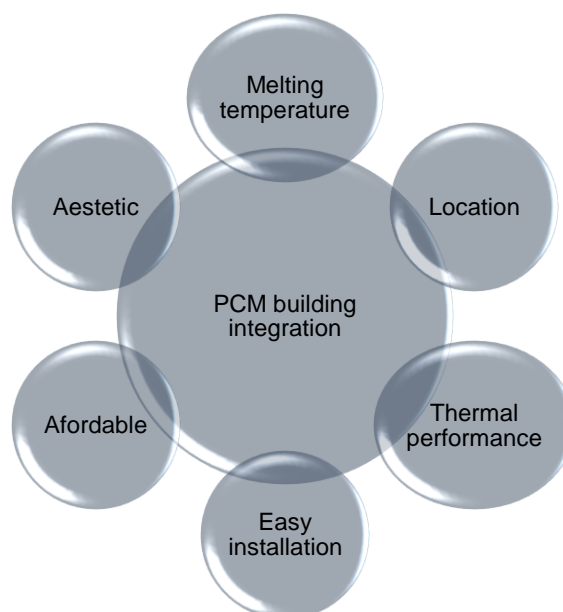


Figure 3.4 Selection criteria for the successful PCM building integration.

Commercial PCMs are available from different suppliers and have a wide range of materials, Table 3.1 presents a list of commercially available PCMs that possess suitable temperatures for building incorporation (Cabeza *et al.*, 2011; Whiffen and Riffat, 2013; Kalnæs and Jelle, 2015).

Table 3.1 Commercial PCMs with low melting temperature.

Material	Type	Melting point (°C)	Heat of fusion (kJ/kg)	$\lambda$ (W/m K)	Company source
RT 18HC	Organic	18	260	0.2	Rubitherm GmbH
S19	Inorganic	19	160	0.43	Phase Change Material Products Ltd.
RT 20	Organic	22	172	0.88	Rubitherm GmbH
RT 21	Organic	21	160		Rubitherm GmbH
S21	Inorganic	22	170	0.54	Phase Change Material Products Ltd.
INERTEK 21	Biobased	21	125	-	MCI Technologies
S23	Inorganic	23	175	0.54	Phase Change Material Products Ltd.
A22	Organic	22	145	0.18	Phase Change Material Products Ltd.
A23	Organic	23	145	0.18	Phase Change Material Products Ltd.
INERTEK 23	Biobased	23	180	-	MCI Technologies
Climsel C 23	Inorganic	15	130	0.6	Climator

Climsel C 23	Inorganic	23	148	0.6	Climator
E23	Inorganic	23	155	0.43	EPS Ltd.
Climsel C 24	Inorganic	24	108	0.6	Climator
TH 24	Inorganic	24	45.5	0.8	TEAP
RT24	Organic	24	148	-	Rubitherm GmbH
A24	Organic	24	145	0.18	Phase Change Material Products Ltd.
A25	Organic	25	150	0.18	Phase Change Material Products Ltd.
A26	Organic	26	150	0.21	Phase Change Material Products Ltd.
RT 25	Organic	26	232	-	Rubitherm GmbH
RT 26	Organic	25	131	0.88	Rubitherm GmbH
INERTEK 26	Biobased	26	200		MCI Technologies
STL 27	Inorganic	27	213	1.09	Mitsubishi Chemical
S27	Inorganic	27	207	0.54	Phase Change Material Products Ltd.
AC 27	Inorganic	27	207	1.47	Cristopia
RT 27	Organic	28	179	0.87	Rubitherm GmbH

Based on the materials presented in Table 3.1, Rubitherm GmbH and Phase Change Material Products Ltd. have the widest range of PCM suitable for the operational range desired. In Chapter 4 the simulation results would analyse and shortlist suitable candidates for the experimental process.

### 3.4.1.1 Heat transfer enhancement

To counteract the low thermal conductivity of PCMs some enhancement mechanisms are considered to maximize the performance. The integration of such methods is considered in two main categories: the encapsulation method and the dispersion of high thermal conductivity materials/nanoparticles and/or dispersion of low-density materials into the base PCM, examples of these materials are shown in Figure 3.5. Furthermore, combining the encapsulation method and the addition of high thermal materials are considered in order to achieve higher thermal performance.

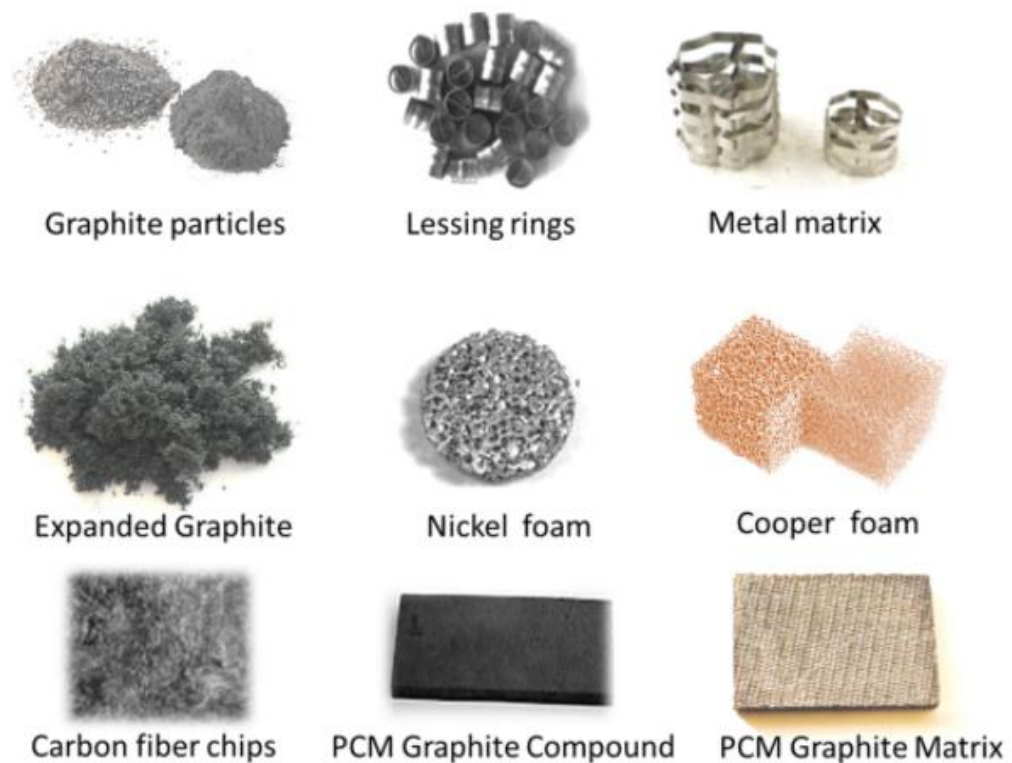


Figure 3.5 Heat transfer enhancement techniques for PCMs (Elarem et al., 2020).

The proposal of metal honeycomb structures, metal bars, and novel encapsulation methods is proposed for the integration of the material. In all cases, the objective of the encapsulation is the enhancement of the thermal performance between the ambient and the PCM. Some of the encapsulation materials found in the literature review focus on blister encapsulations, plastic containers, spheres. In this case, the proposal for the ceiling panel is to evaluate several encapsulation methods of plastic and metallic materials and analyse the response with different PCMs.

For the building integration, the PCM panels can be installed per m<sup>2</sup>. This can be achieved by installing the tiles in the open air or above a perforated ceiling for a more aesthetically pleasing finish. The calculation of the system load into the building structure should be considered,

particularly in the case of retrofits. Installing additional timber joists within the roof space can be a solution to support the PCM panels, working as a grid system was attached to this in order to avoid extra stress to the roof trusses and possibly damaging the roof. The quantity of PCM incorporated into building envelopes considerably affects the amount of thermal energy stored during phase transition. For example, when a small amount of PCM is included in building elements to decrease cooling loads during summer, the PCM stores limited heat in the charging phase and reaches the full liquid state in a short time. Thus, it cannot absorb more energy. By contrast, larger PCM amount stores more heat during the charging process and restricts the heat from passing through the element. The amount of PCM can be obtained as follows:

$$V_{PCM} = m_{PCM}/p_{PCM} \quad (3.1)$$

where:

$V_{PCM}$  = volume of PCM required.

$m$  =mass of the PCM (kg).

$p$  = density of the pcm (kg/m<sup>3</sup>).

The overall heat storage capacity of the PCM is determined as follows:

$$E_{latent} = n \times m \times H_f \quad (3.2)$$

where:

$H_f$  = the total energy exchange of PCM enthalpy content (kJ/kg).

$n$  = the number of cycles during the day.

### 3.4.2 Solid desiccant

The dehumidification demand for the building is addressed by adsorbents (solid desiccants), which are capable to adsorb air moisture. Desiccants are compounds or agents, such as montmorillonite clay or silica gel, used in facilitating low humidity environments by adsorbing moisture content from the air. All desiccants behave in a similar way, to select the adequate material it is important to determine the conditions of maximum product integrity, the size and type of container used, and the ambient conditions (temperature and relative humidity). Desiccants are proposed to be non-corrosive with high sorption capacity and low regeneration temperature. For this system, the integration of solid desiccant over liquid desiccants is considered due as they tend to be environmentally friendly, economic and in general they are easy to operate (Chua and Chou, 2003). The most common conventional solid desiccants are silica gel, activated alumina, molecular sieves, and activated carbon, however, as stated in the literature a new generation of composite materials provides alternative sustainable solutions for dehumidification. For building application, it is important to consider a wide range of conditionings that would satisfy in terms of performance, maintenance, and health concerns. As Figure 3.6 presents it is important to consider the thermos-physical properties, availability, economics, process, and operation condition.

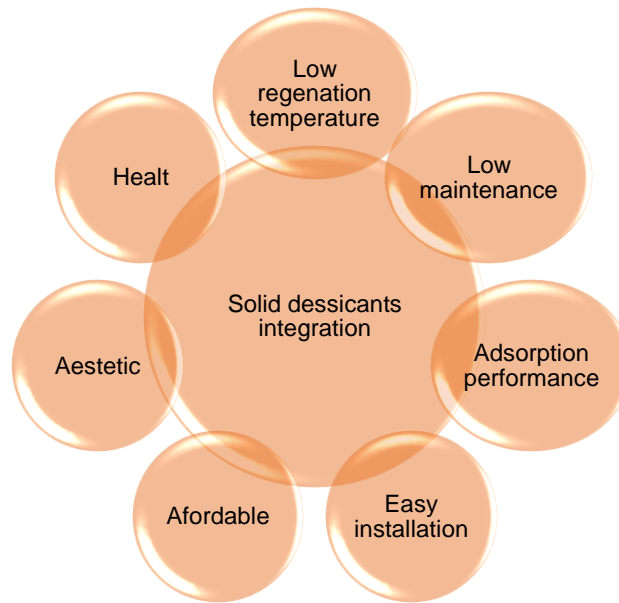


Figure 3.6 Selection criteria for the successful solid desiccant building integration.

The selection of the solid desiccant is based on the building requirements for dehumidification, which are in relation to the temperature and relative humidity. An effective desiccant will adsorb the water vapor in the air, lowering the relative humidity to the point where water cannot condense. For an improved dehumidification and regeneration performance of a solid desiccant-based system, the solid desiccant is expected to have high adsorption capacity, good regeneration performance at relatively low temperature, low desorption energy input, and high durability (Wang *et al.*, 2013).

A range of composite desiccants will be compared in terms of adsorption capacity and regeneration performance. To sustain the low maintenance of the dehumidification system, it is important to select a material suitable to regenerate by the solar-assisted heat pump system. Moisture may be removed from the desiccant material by heating and for this reason, the regeneration temperature for the material should be in a range between 50 °C to 70 °C (in reference to the HP output). In addition, the material should be able to dry and complete the cycle in a suitable range. This timing would depend on the building requirements, and at this stage, a

24-hour cycle is recommended for the adsorption and regeneration process.

High absorption desiccants such as MOFs, silica gels, and aerogels present a relatively high regeneration temperature (e.g., 70 °C to 100 °C). On the contrary, clay-based composite solid desiccant materials have relatively lower regeneration temperatures (e.g., 35 °C to 55 °C), which indicates that low-grade heat sources can be utilised for regeneration, this includes the vermiculite.

The integration of the solid desiccant aims to be available at room temperature to capture the moisture, still, it needs an escape route to remove the moisture outdoors. For this reason and considering the regeneration method a panel has been proposed to incorporate in the building structure. The optimal material quantity should be also predetermined as an insufficient quantity will not provide the required protection, while excessive use of desiccant may lead to over-drying and an unnecessary increase in product cost.

The proposal of natural materials such as vermiculites is considered for integration in this project. To validate the effectiveness of the material, the performance will be compared with silica gel during the preliminary testing. If the material is found suitable, the incorporation of hygroscopic salts as enhancement mechanisms will be evaluated.

In terms of encapsulation methods, desiccants are often incorporated into packaging for moisture-sensitive products. Similar to the challenges proposed by the PCM container, the vermiculite desiccant requires a lightweight structure that offers certain stability, made from a permeable



material that at the same time offers enough resistance to condensation. Additionally, it should be affordable and require low maintenance. In order to fulfill such characteristics, the packaging container is vital in determining how much of a particular desiccant material is required, the container should allow direct contact between the moisture and the absorbent, it should also be resistant and avoid leakage.

In this regard, the literature offers few solutions as such novel material has not been investigated for building applications. Some packaging examples may be found from the food and the pharmaceutical industries, where plastic sachets are commonly used. For this reason, different encapsulation methods would be revised for the suitable integration of the dehumidification system.

Fabric containers and permeable plastics are considered, as well several design concepts that provide an aesthetic solution. The incorporation of the desiccant system is proposed per m<sup>2</sup>, it should be installed close to an external wall to vent outside. The relative humidity can be expressed as the ratio at the actual mass of water vapor in a given air volume to the mass of water vapor required to saturate at this volume as is expressed as:

$$\varphi = m_w / m_{ws} \ 100\% \quad (3.3)$$

where:

$\varphi$  = relative humidity (%).

$m_w$  = mass of water vapor in the given air volume (kg).

$m_{ws}$  = mass of water vapor required to saturate at this volume (kg).

By knowing the total cubic capacity of the area to be dried, the moisture load by weight is calculated by:

Specific humidity (kg/kg) x total cubic capacity = total moisture load (kg)

The total moisture load can be divided by 24 to indicate the total airborne moisture available to be removed within an hour. The size of the room or the building is an indirect influence factor as the amount of water in the air determines the required dehumidification capacity. The air change is very important as outside air contributes to both the temperature and RH values inside the room.

### 3.4.3 Heat pump system

As the solar-assisted heat pump aims to utilize renewable sources to provide energy, in the proposed system the application of thermal panels is proposed. Residential applications of heat pump units have been available for more than 20 years; however, they have experienced limited success in the marketplace. The heat pump function is to transport the heat from one source to another by a working fluid. In principle, a refrigerant circulating through the evaporator of an air-to-air heat pump absorbs energy from ambient air, typically in the temperature range of 10 °C to 20 °C. The evaporated refrigerant is then compressed to a higher pressure and temperature by the heat pump compressor. The refrigerant is eventually condensed into a liquid state and the resultant heat released in the condenser is utilized for a designated thermal application. Heat pumps combined with solar thermal have a superior seasonal

performance factor for domestic applications. The solar thermal collector operates at a temperature low enough to boost the solar energy collection efficiency, yet it is high enough to enhance the heat pump performance compared to an air source heat pump. The general characteristics desirable for the solar-assisted heat pump are described in Figure 3.7

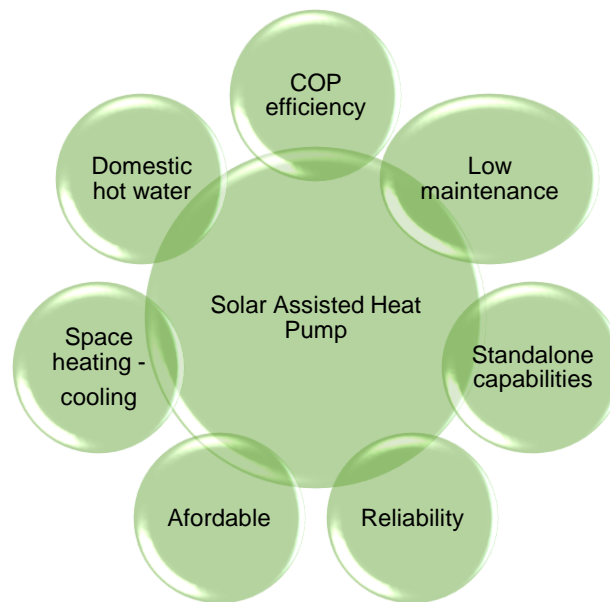


Figure 3.7 Selection criteria for the successful solar-assisted heat pump building system.

In general, the heat pump should provide a high coefficient of performance, providing hot water for domestic use. In addition, the system proposes the incorporation of space heating through a fan coil unit that could potentially be utilized for the regeneration of the solid desiccant. A basic factor of great importance for its successful application is the availability of a cheap, dependable heat source for the evaporator-preferably one at relatively high temperature. The coefficients of performance (COP) of the heat pump system would depend on several factors, such as the temperature of the low-energy source, the temperature of delivered useful heat, the working medium used, the

characteristics of components of HP systems, etc. Among the above-mentioned, the temperature of the evaporator is a key factor. The ideal requirements also contemplate an affordable cost of production and installation, low maintenance, reliability, stand-alone capabilities especially if boilers are to be phased out or in new builds.

#### 3.4.3.1 Solar Thermal collector

The importance of solar collectors as a sustainable alternative for energy generation has grown in the last decades (Evangelisti, De Lieto Vollaro and Asdrubali, 2019). Nowadays, solar thermal systems can generate heat for domestic hot water purposes, zone heating, cooking (solar ovens), water treatments (desalination), and some industrial processes (drying and maturation), (Maurer, Cappel and Kuhn, 2017). Figure 3.8 presents the solar collector panel proposal, where the solar radiation heats the dark surface, transferring the energy to the refrigerant for subsequent use.

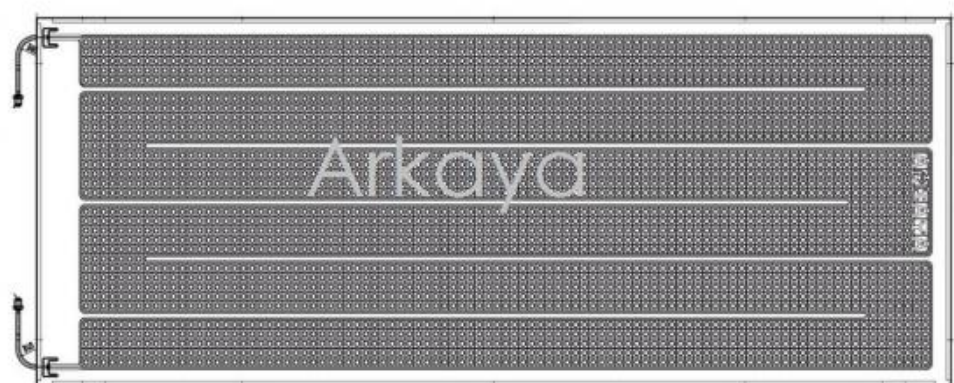


Figure 3.8 Arkaya solar thermal collector.

### 3.4.3.2 Working Fluid

In terms of refrigerants for solar-assisted heat pumps, halogenated refrigerants such as R22 and R134a are widely used due to their good thermodynamic and thermos-physical properties however they have high global warming potential. Figure 3.9 presents the variation of COP for a collector temperature ranging from 0 °C to 20 °C for various refrigerants at a condensing temperature of 60 °C (Chata, Chaturvedi and Almogbel, 2005). The results show the superior performance presented by the R12, R22, and R134A. A review presented by Chaturvedi et al. R134a was selected as an optimal solution, having performance comparable to R12 and R22 and is considered to be environmentally friendly (Chata, Chaturvedi and Almogbel, 2005; Vaishak and Bhale, 2019).

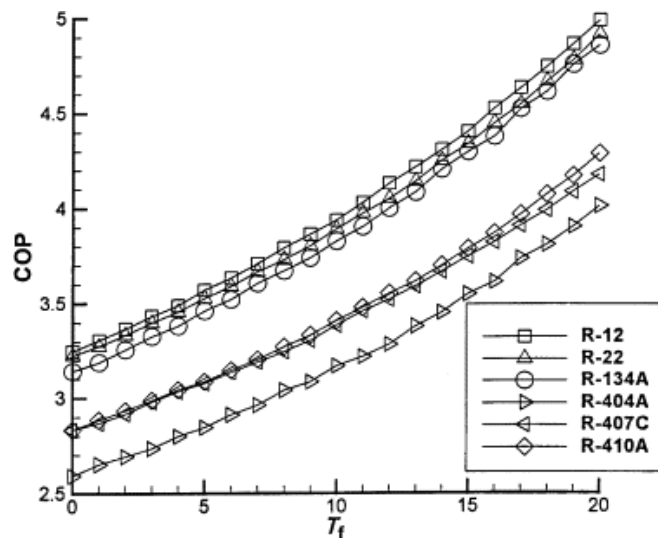


Figure 3.9 Comparison of COPH for different refrigerants at 60 °C (Chata, Chaturvedi and Almogbel, 2005).

As the SAHP system aims to have a high COP and manage the solid desiccant regeneration, the selection of the AKAYA heat pumps system is considered. This solar-assisted heat pump aims to provide hot water temperatures of  $\leq 60$  °C, covering desiccant dehumidification

requirements. It utilizes a vapour compression cycle like Air Source or Ground Source Heat Pump but offers the potential of significantly improving the performance without having a negative impact on the economic cost. The system achieves greater efficiency by achieving latent heat through all three modes of heat transfer namely conductive, convective and radiant through solar. The heat being gained from the environment thus reduces the strain on the compressor. The compressor then passes the heated refrigerant to the heat exchanger that is used to supply domestic hot water. This water can be stored in an unvented storage tank meaning it is ready on demand. The direct-expansion solar-assisted heat pump is a system combining both solar thermal collector and heat pump evaporator into one unit, where the refrigerant evaporates by the effect of both incident solar energy and ambient.

The mass flow rate of the refrigerant is calculated as follows:

$$m_r = \lambda \frac{V_{th}}{v_{suc}} \quad (3.4)$$

where:

$\lambda$ = volumetric coefficient.

$V_{th}$  = theoretical displacement volume of the compressor.

$v_{suc}$  = specific volume of the refrigerant at the inlet of the compressor.

For the integration of the system components, Figure 3.10 and Figure 3.11 present the schematic diagram of the system. The solar collector panels are connected to the heat pump (solar box), the heat pump directs

the water flow to the hot water cylinder and the fan coil unit. The fan coil unit will be utilized for space heating in this case.

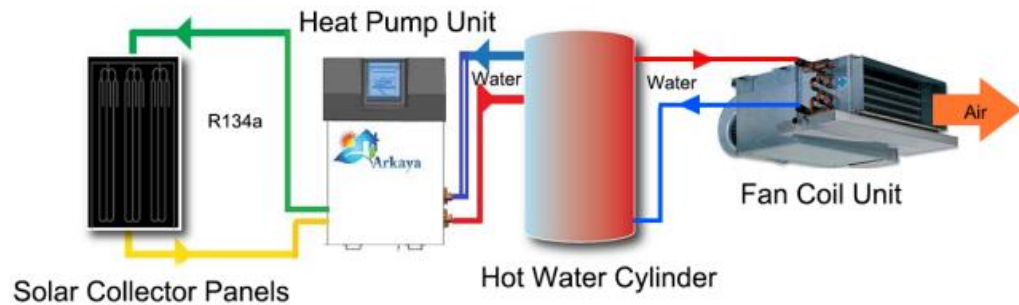


Figure 3.10 Schematic diagram of the solar-assisted heat pump.

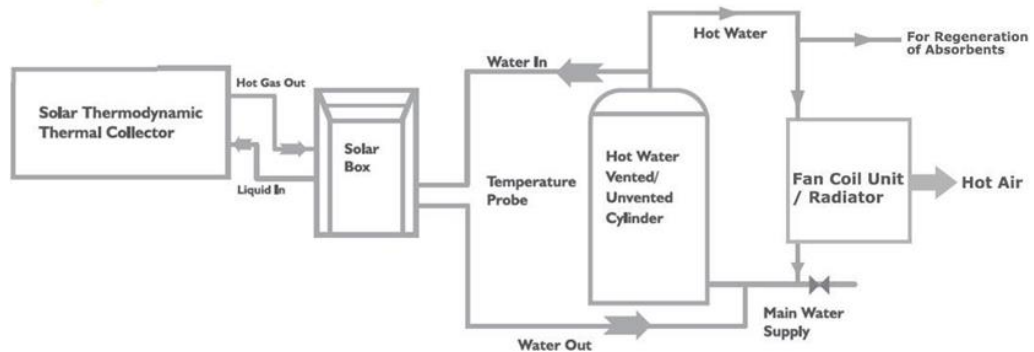


Figure 3.11 Solar-assisted heat pump workflow.

In this system, the refrigerant R134a liquid goes through the expansion valve inside the heat pump unit where the pressure on the refrigerant liquid is released and then the refrigerant goes into the solar thermal collector where it gains temperature depending on the ambient temperature. The refrigerant liquid is then heated to semi-gas semi-liquid form and enters the heat pump. This then will get compressed, turning the refrigerant into gas form and then this heat will get transformed into titanium coil in the coil heat exchanger. This cycle will keep on repeating until the whole cylinder has been heated up to 60 °C regulated by the electronic sensors in the solar box. The second cycle is the water cycle

in which the hot water cylinder first gets filled from the main supply. This water then leaves the cylinder and is circulated by the circulation pump into the heat exchanger inside the heat pump. Then the titanium coil in the coil heat exchanger transfers the heat of the refrigerant which is in gas form to the water and then this hot water leaves the solar box and is circulated back into the cylinder until the cylinder water reaches the optimum temperature of 60 °C. A pump would be utilized to utilize the hot water coming from the water cylinder to provide heat into the fan coil unit.

The four primary components of the solar thermal system include: the solar collectors, the storage tank, the solar loop, and the control system. There is a relationship between the hot water consumption and the collector area. The system requirements will depend on the climate conditions and the building occupancy requirements.

The UK uses the Standard Assessment Procedure (SAP), (BRE, 2014; O'Hegarty, Kinnane and McCormack, 2014); and the equation is described as follows:

$$Q_s = S \times Z_{panel} \times A_{ap} \times h_0 \times UF \times f_1 \times f_2 \quad (3.5)$$

where:

$Q_s$  = solar input (kWh/year).

$S$  = total solar radiation shining on the collector (kWh/m<sup>2</sup>/year).

$Z_{panel}$  = shading factor for the solar panel.

$A_{ap}$  = aperture area of collector (m<sup>2</sup>).



$h_0$  = zero-loss collector efficiency.

UF = utilisation factor.

$f_1$  = denotes the collector performance factor.

$f_2$  = is the solar storage volume factor.

### 3.5 Summary

The proposed system aims to achieve thermal comfort by controlling the heating, cooling, and humidity levels inside residential buildings. For this reason, a tri-modular system is introduced to target the specific building demands and provide an innovative and sustainable solution that counteracts the CO<sub>2</sub> emissions produced by commercial and residential buildings.

The building's main function is to provide to the users a comfortable and healthy environment and this is measured through the human thermal comfort perception. The main parameters that influence this perception in residential buildings are covered by the ambient and radiant temperature, which is covered by the heating and cooling demands. The second element which refers to the relative humidity is resolved with the application of the desiccant materials. In regards, to the rest of the parameters (air motion, metabolic rate, and clothing insulation) the occupiers have higher control in securing these levels within a building. Building occupants will try to reduce their thermal discomfort using different interventions such as window/door opening, fan use, change in clothing insulation, among others (Stopps and Touchie, 2020). The

occupant response to the thermal discomfort regarding the thermostat setpoints often has significant and unintended energy gains implications. Figure 3.12 presents the annual impact of the single variables on the total energy consumption, comparing the lifestyle of low and high consumer's energy behaviour patterns. This study by Barthelmes et al. compared the impact on the total energy use of a residential nearly-zero energy building (nZEB) and a Reference Building (RB). It is noticeable that the highest variation of the building energy use is due to the occupant's interaction and use of the equipment and lighting for both the low consumer and high consumer scenario (Barthelmes *et al.*, 2017).

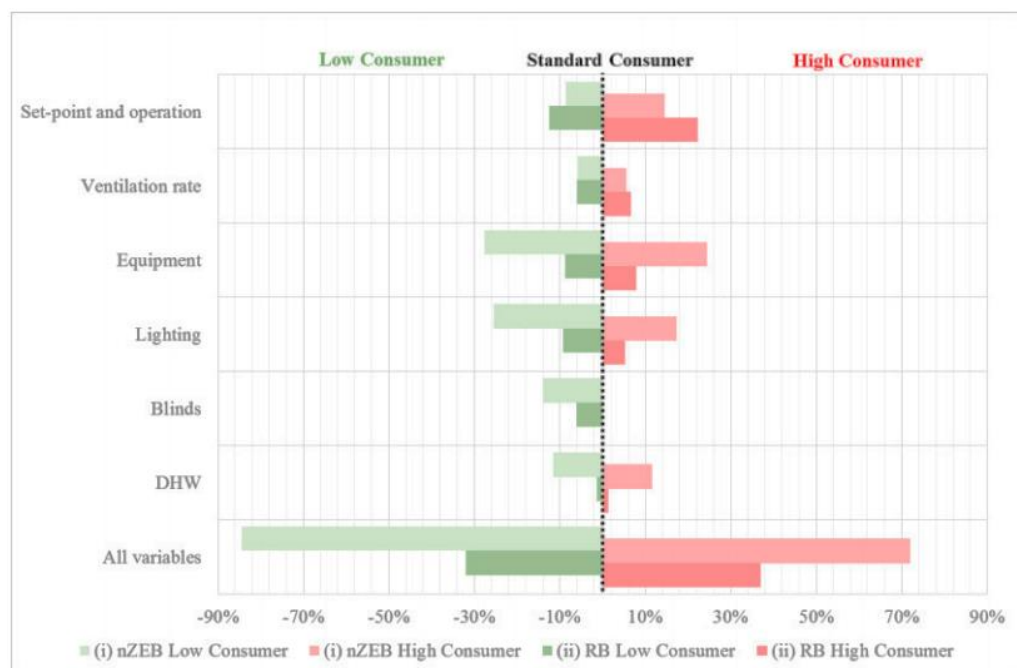


Figure 3.12 Impact of the single lifestyle key variables on the building energy use (Barthelmes *et al.*, 2017).

In consequence, having an optimal design of the temperature and humidity levels, not only will reduce the occupant's needs to regulate them but automatically reduce the building energy consumption.

The tri-modular system represents a high complexity, as each component is individually developed to satisfy a specific function. For the first stage of the project, the performance of each element will be individually assessed in the laboratory, this will ensure the successful application and will facilitate the assessment of the enhancement mechanisms developed; allowing for new solutions to be explored. Once the performance has been tested and the enhancement mechanisms have been selected; the integration of the system components in a large-scale scenario will be tested, showing the harmonious operation of the complete system. The testing of the different components would be detailed in Chapters 5, to 7 and will examine the individual performance of the PCM with the enhancement materials, the solid desiccant components as well as the boosting methods, and the efficacy of the heat pump unit.

# Chapter 4 Preliminary simulation on PCMs

## 4.1 Introduction

In this chapter, the computer simulation of the PCM system is assessed. As the properties of the PCMs are suitable for heating and cooling, both elements are reviewed. The application of this material in the proposed system focuses on the cooling properties. Nevertheless, the material properties for heating purposes provide additional energy savings, particularly during the winter period. This evaluation aims to develop an understanding of the function, capability, and operation of the material with the aid of simulation software.

The introduction of a house model for simulation purposes is detailed and the layout is based on an existing building. The house has standard spaces and regular construction materials, nevertheless, the selected model contemplates high thermal insulation materials to procure the reduction of the energy demand.

## 4.2 Modelling method

The practical integration of the thermal comfort system requires to be sized to the building, as the supplies are based depending on the space and the energy demand, additional considerations are associated with the economic cost and climatic conditions. For commercialization purposes, the climate conditions and energy requirements are the key factors to take into consideration. In general, the UK weather demand is considerably higher for heating rather than cooling loads. The temperature difference between inside and outside can result in large quantities of heat loss, for this reason, the selection of sustainable solutions would increase the efficiency performance.

As discussed in the literature, the incorporation of PCM in buildings has many applications, being a suitable option for heating and cooling. It can be concluded that the integration of this material into buildings helps maintain the overall thermal comfort, reducing the abrupt changes in the indoor temperature. Furthermore, these materials can be used as passive or active systems and many particular applications can be found. The great diversity of solutions has increased its interest in the last few years.

For the tri-modular system, the PCM will be applied to cover the cooling demands. The PCM panels are expected to decrease the indoor temperature fluctuations, working as a passive system. The ceiling panels are expected to work independently, and for this reason, it is

crucial to select a suitable PCM material able to perform unassisted from external equipment. Once installed the PCM panels would require low maintenance and for this reason, the adequate location of the material is highly important. Further applications could be reviewed, nevertheless, an analysis must be made for each application.

#### 4.2.1 EnergyPlus modelling

The model is based on a Positive Home layout, considering a total construction area of 99 m<sup>2</sup>, the 3D model and façades are displayed in Figure 4.1 and Figure 4.2 respectively.



Figure 4.1 3D house model view.

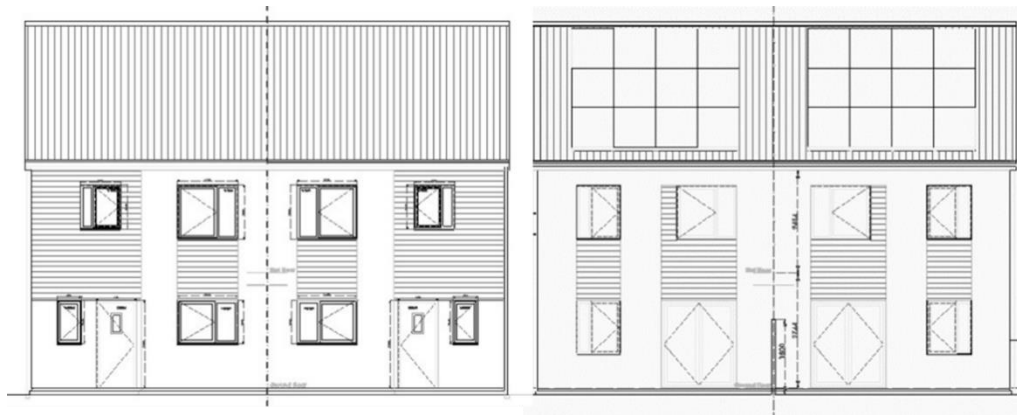


Figure 4.2 Model house front (left), back façade (right).

The selection of this house model for simulation analysis has been based on the following conditioning factors:

1. Positive home is a UK construction company focused on the development of energy-efficient homes. The house utilizes high insulation standards and is designed to reduce the number of CO<sub>2</sub> gases emitted.
2. The model house is a standard home in the UK, the house has the main characteristics particular of a newbuild and the analysis of such model should exemplify the system performance in terms of energy demands.

The house consists of main floors and the attic. The first floor contains the entrance lobby, toilet, kitchen, living area (dining room, living room, and study area), while the second floor has three bedrooms and a bathroom as shown in Figure 4.3. The specific zones are detailed in Table 4.1 and are divided by floor area.



Figure 4.3 Model house ground floor layout (left), first floor layout (right).

Table 4.1 Zone area measurements.

Zone	Area (m <sup>2</sup> )	Volume (m <sup>3</sup> )
Entrance lobby	3.19	Ground floor
Toilet	3.39	Ground floor
Kitchen	7.75	Ground floor
Living area	35.5	Ground floor
Room 1	13.6	First floor
Room 2	13.6	First floor
Room 3	7.3	First floor
Bathroom	5.8	First floor
Circulation space	8.6	First floor
Closet	1.0	First floor

For the simulation performance, the PCM material was considered in the ceiling as shown in Figure 4.4.

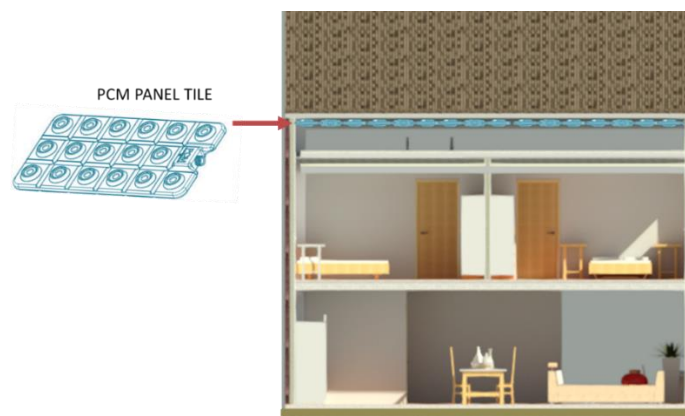


Figure 4.4 Schematic incorporation of the PCM panel in building section.



The schematic representation of the PCM in the building, and the amount and type of material vary in each simulation result. In this case, the PCM is considered without the encapsulation material, that as described in the literature could potentially boost the performance of the PCM.

#### 4.2.2 SketchUp model

Using the Legacy OpenStudio Plugin the house model can be drawn in the SketchUp model and imported to the EnergyPlus simulation software. By simulating the indoor air temperature, parameters of PCM such as the phase change temperature range, heat conduction coefficients, thickness, and the mass of PCMs, would be determined. The SketchUp model is divided into zones. In this section, the ground floor contemplates the entrance, living area, and stairs. The second floor considers stairs, landing, bedroom 1, bedroom 2, bedroom 3; while the roof is considered as another zone. Figure 4.5 presents the building model in SketchUp.

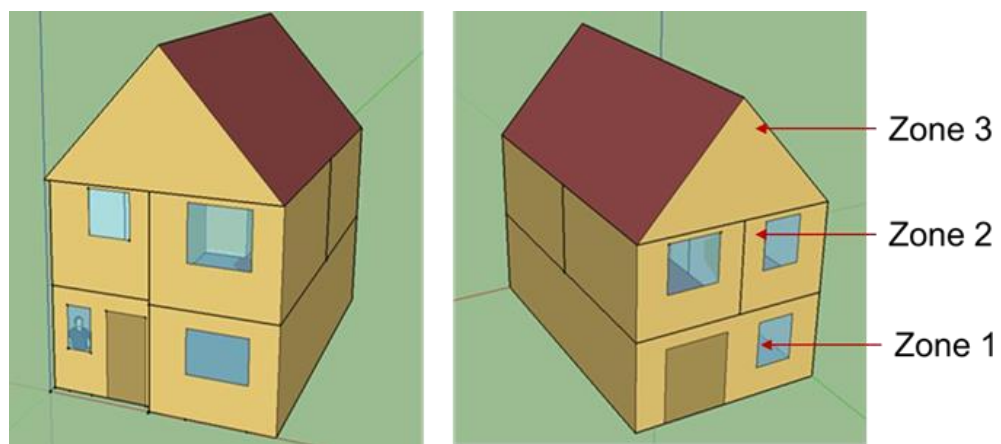


Figure 4.5. Front façade (left), south façade (right).

### 4.3 Simulation parameters

The environmental evaluation was performed using Energy-Plus v8.4, which is an energy building simulation software design to assess the building performance. EnergyPlus combines both BLAST and DOE-2 programs. It considered the building's characteristics such as heat balance load calculations, integrated loads, HVAC systems, and PCM among other variables. In addition, other calculations are: surface convection algorithms, advanced infiltration, environmental emissions, and economic evaluation. To assess the PCM performance in EnergyPlus, a conduction finite difference (CondFD) solution algorithm must be used. This algorithm discretizes the building envelope into various nodes which could be introduced optionally depending on the required accuracy and numerically solves the heat transfer equations by use of a finite difference method (FDM) which could be selected between Crank-Nicholson or fully implicit. To include the specific heat change due to the phase change process, the CondFD method is coupled with an enthalpy-temperature function, which reads the user inputs of enthalpies at different temperatures. Since an iterative implicit scheme is used for CondFD, the node enthalpies get renewed at each iteration, and then they are used to make a variable  $C_p$  (Crawley *et al.*, 2000; Saffari *et al.*, 2017; Energy, 2020).

The simulation-based model was carried out using EnergyPlus paired with the Legacy OpenStudio plugin, based on the prototype described in Figure 4.1. In terms of the electric loads calculated for the heating and

cooling demand, the following parameters are considered: heating, cooling, interior lighting, interior equipment, fans, pumps, humidification, water systems, refrigeration.

The PCM characteristic varies in some case scenarios and no enhancement methods of the PCM are presented in this report, the conditionings are detailed as follows:

#### 4.3.1 Heat balance algorithm

This field selects a type of moisture and heat transfer for the simulation of the building surfaces (ibid., p.48). The algorithm used is the Conduction Finite Difference for Phase Change Materials applications (Muruganantham, 2010).

##### 4.3.1.1 EnergyPlus Phase Change Material Model

CondFD discretizes walls, floors, and ceilings into several nodes and uses an implicit finite difference scheme to numerically solve the appropriate heat transfer equations. Equation 1 shows the calculation method for the fully implicit scheme for a homogeneous material with uniform node spacing (Crawley *et al.*, 2000; Tabares-Velasco, Christensen and Bianchi, 2012).

$$C_p \rho \Delta x \frac{T_i^{j+1} - T_i^j}{\Delta t} = k_W \frac{(T_{i+1}^{j+1} - T_i^{j+1})}{\Delta x} + k_E \frac{(T_i^{j+1} - T_i^{j+1})}{\Delta x} \quad (4.1)$$

where:

$$k_W = \frac{(k_{i+1}^{j+1} - k_i^{j+1})}{2} \quad (4.2)$$

$$k_E = \frac{(k_{i-1}^{j+1} + k_i^{j+1})}{2} \quad (4.3)$$

where:

T= temperature

i = node being modelled

i + 1 = adjacent node to the interior of construction

i – 1 = adjacent node to exterior of construction

j + 1 = new time step

j = previous time step

$\Delta t$  = time step

$\Delta x$  = finite difference layer thickness

$C_p$  = specific heat of material

P = density of the material

For the PCM algorithm, the CondFD method is coupled with an enthalpy-temperature function that the user inputs to account for enthalpy changes during phase change.

$h = h(T)$

$$C_p^*(T) = \frac{h_i^j - h_i^{j-1}}{T_i^j - T_i^{j-1}} \quad (4.4)$$

Where:

$h$  = enthalpy

#### 4.3.2 Project location and weather characteristics

The data simulated corresponds to the closest location available in the EnergyPlus database, in this case, Birmingham, UK. Table 4.2 presents the location characteristics from the EnergyPlus weather file. The weather data files for building simulations were mostly obtained from the EnergyPlus Weather (EPW) database which includes weather data provided in EnergyPlus format from 20 sources.

Table 4.2 Weather file input data.

Weather File	BIRMINGHAM
Latitude (deg)	52.45
Longitude (deg)	-1.7
Elevation (m)	99
Time Zone	0
North Axis Angle (deg)	0
Rotation for Appendix G (deg)	0
Hours Simulated (hrs)	8760

Further simulations were developed with the Climate Consultant 6.0 software in order to obtain the climate characteristics. The temperature range varies from -7 °C in winter up to 29 °C during summer, as shown in Figure 4.6. The grey area indicates the comfort zone, and it is appreciated that it is only archived for a limited time from May to August which means that alternative strategies must be implemented in order to achieve a comfortable indoor temperature.

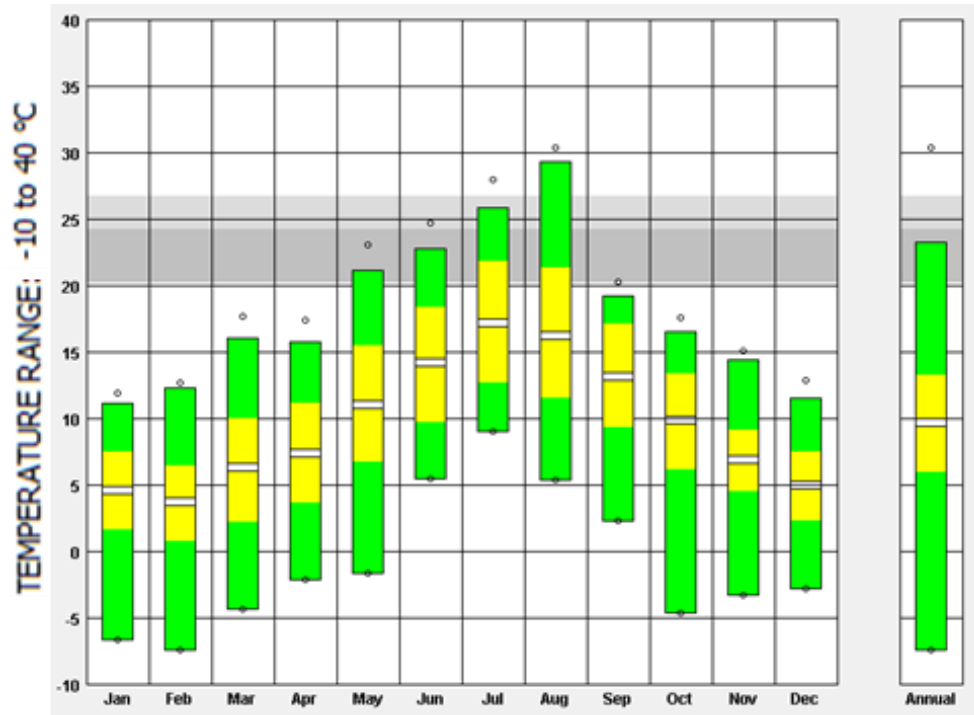


Figure 4.6 Birmingham temperature range extracted Climate Consultant.

Figure 4.7 displays the relationship between the dry bulb temperature and the relative humidity, the comfort zone is marked in the grey areas. The humidity level is represented by the green dots, having an annual range between 60 °C to 80 °C.

The psychometric chart displays can be seen in Figure 4.8. In this case, the dry bulb temperature ranges from 20 °C to 27 °C. It can be noticed that naturally, thermal comfort is achieved for 3.5% of the time during the year and is equivalent to 12.7 days. In order to reach thermal comfort during the rest of the year, alternative means must be implemented.

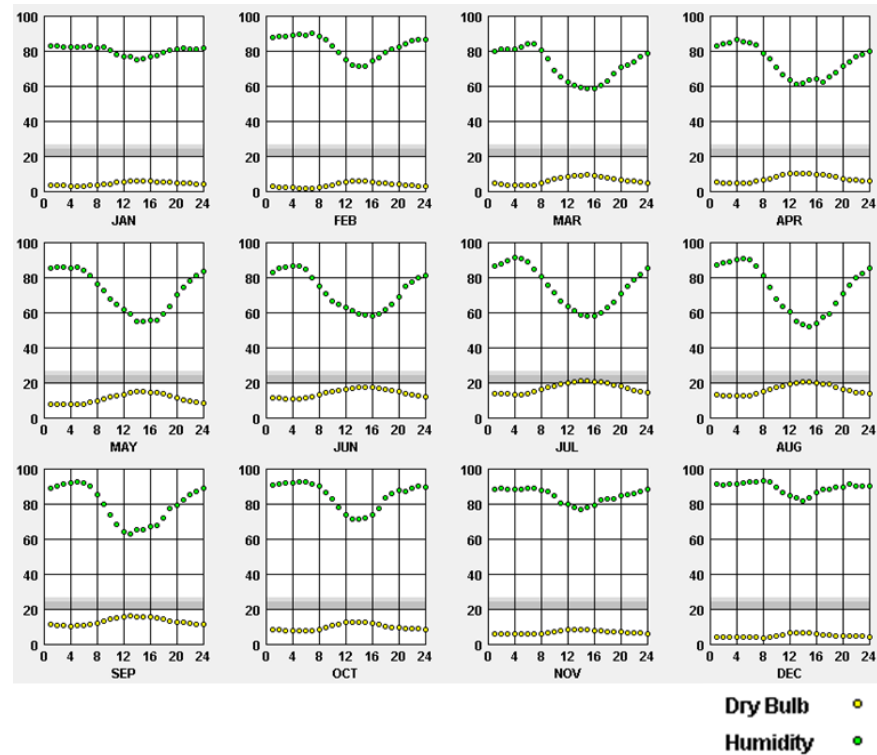


Figure 4.7 Birmingham dry bulb x relative humidity, extracted from Climate Consultant.

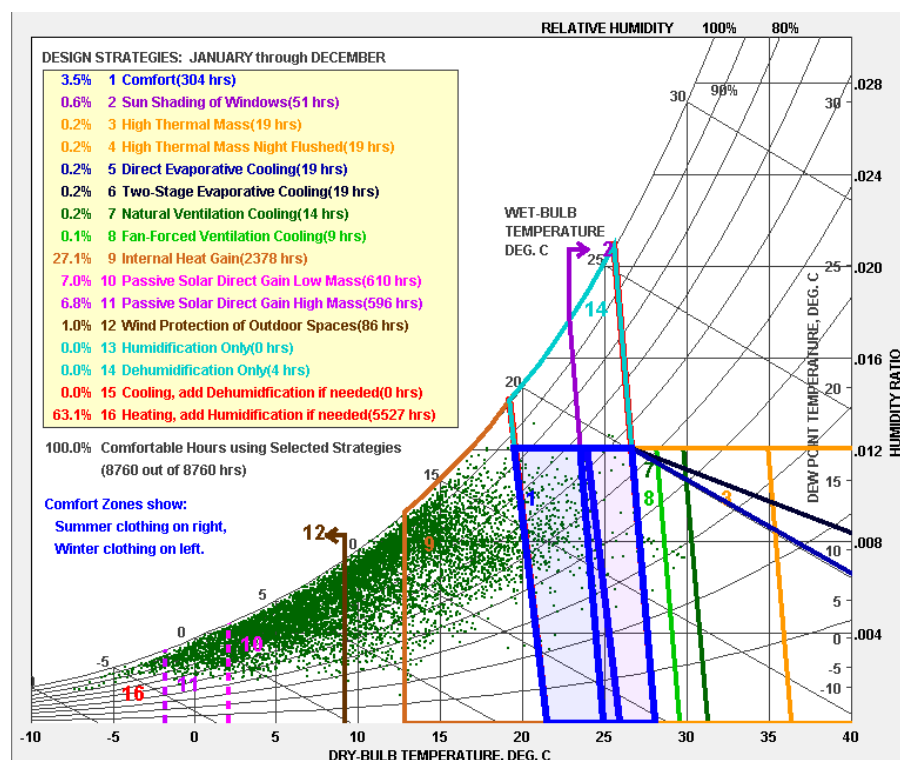


Figure 4.8 Psychrometric chart, extracted from Climate Consultant.

### 4.3.3 Simulation settings

Occupancy schedule: this focuses on the residential application. The selected operational parameters were used:

- Schedule: Compact, Multifamily SWH
- Schedule: Compact, Multifamily dwelling equipment
- Schedule: Multifamily dwelling unit lighting
- Schedule: Multifamily one zone dwelling unit occupancy
- Schedule: Multifamily dwelling unit bedrooms and bathrooms occupancy

The schedule week compact includes the domestic electric appliances found in a standard residential house (lighting, refrigeration, plugs, dishwasher, washing machine, clothes dryer, baths, shower, sinks, etc.).

Material: this section contains the physical properties of the building materials. The characteristics described are roughness, thickness (m), conductivity (W/mK), density (kg/m<sup>3</sup>), specific heat (J/kg-K), and absorptance. For this particular model, the materials were kept as the default configuration and the addition of the PCM layer was established as shown in Figure 4.9.

Field	Units	Obj1	Obj2	Obj3	Obj4	Obj5	Obj6	Obj7	Obj8	Obj9	Obj10
Name		I01 25mm insulation	I02 50mm insulation	G01a 19mm gypsum	M11 100mm lightweight	F15 Acoustic tile	M01 100mm brick	M15 200mm heavy	M05 200mm concrete	G05 25mm wood	PCM
Roughness		MediumRough	MediumRough	MediumSmooth	MediumRough	MediumSmooth	MediumRough	MediumRough	MediumRough	MediumSmooth	Smooth
Thickness	m	0.0254	0.0508	0.019	0.1016	0.0191	0.1016	0.2032	0.2032	0.0125	0.1
Conductivity	W/mK	0.03	0.03	0.16	0.53	0.06	0.69	1.35	1.11	0.15	0.2
Density	kg/m <sup>3</sup>	43	43	800	1200	369	1520	2240	800	595	880
Specific Heat	J/kgK	1210	1210	1090	840	590	790	900	920	1630	1800
Thermal Absorptance											0.9
Solar Absorptance											0.7
Visible Absorptance											0.7

Figure 4.9. Material properties input in Energy Plus.

Table 4.3 has the material properties used for the simulations; this section contains the physical properties of the building materials. The characteristics described are roughness, thickness (m), conductivity



(W/mK), density (kg/m<sup>3</sup>), specific heat (J/kg-K), and absorptance. For this particular model, the materials were kept as the default configuration, the PCM material was modified depending on the selected material and thermal characteristics.

Table 4.3 Example of PCM input data on software.

Name	Roughness	Thickness (m)	$\lambda$ (W/mK)	$\rho$ (kg/m <sup>3</sup> )	Cp (J/kg-K)	Thermal absorptance
PCM	Smooth	0.1	0.2	880	1800	0.9

#### 4.3.3.1 Phase Change Materials

This tool is used to describe the temperature dependent materials used in the Conduction Finite Different algorithm. This allows to calculate of the thermal conductivity of PCMs. The enthalpy values should cover the entire temperature spectrum of the material to analyse and should necessarily be increasing numbers (USDE, 2016). The specific heat is calculated from the tabulated input data of temperature/enthalpy pairs:

$$Cp = \frac{h_{i,new} - h_{i,old}}{T_{i,new} - T_{i,old}} \quad (4.5)$$

Following the PCMs available in Chapter 3, the computer simulation aims to provide a better understanding of the material performance and help the selection of a suitable candidate for the tri-modular system. In this case, the selection of INERTEK 21, INERTEK 23, INERTEK 28, Rubitherm 21, S23, and S27 have been selected based on their melting point suitable for building integration, as it fits the human thermal comfort temperatures. The specifications for these materials are presented in Table 4.4, where the enthalpy values are pivotal for the accurate simulation of the material. The specifications are stipulated by the

manufacturer and in the case of the S23 and S27 the enthalpy values were obtained by the DSC analysis provided directly from the manufacturer.

Table 4.4 PCM simulation properties.

Commercial name	Melting Point (°C)	Heat storage capacity (J/g)	Enthalpy range (J/g)
INERTEK 21	20-22	165	16-23
INERTEK 23	23-27	200	18-28
INERTEK 26	26-28	240	22-30
RT 21 (rubitherm)	18-23	200	13-28
S23	23	220	20-29
S27	27	220	23-32

#### 4.3.3.2 Temperature Coefficient for Thermal Conductivity

The temperature dependent coefficient for thermal conductivity of the material uses (W/(m-K<sup>2</sup>)). This is the thermal conductivity change per unit temperature excursion from 20 °C. The conductivity value at 20 °C is the one specified with the basic material properties of the regular material specified in the name field. The thermal conductivity is obtained from:

$$k = k_o + k_1 (T_i - 20) \quad (4.6)$$

where:

$k_o$  = is the 20 °C value of thermal conductivity (normal idf input)

$k_1$  = is the change in conductivity per degree temperature difference from 20 °C.

#### 4.3.3.3 Temperature - Enthalpy

The temperature enthalpy set allows the input of the temperature enthalpy for the material, up to sixteen values could be integrated. These temperature values should be strictly increasing. Enthalpy contributions of the phase change are always added to the enthalpy that would result

from a constant specific heat base material a minimum range of three values is required as presented in Figure 4.10.

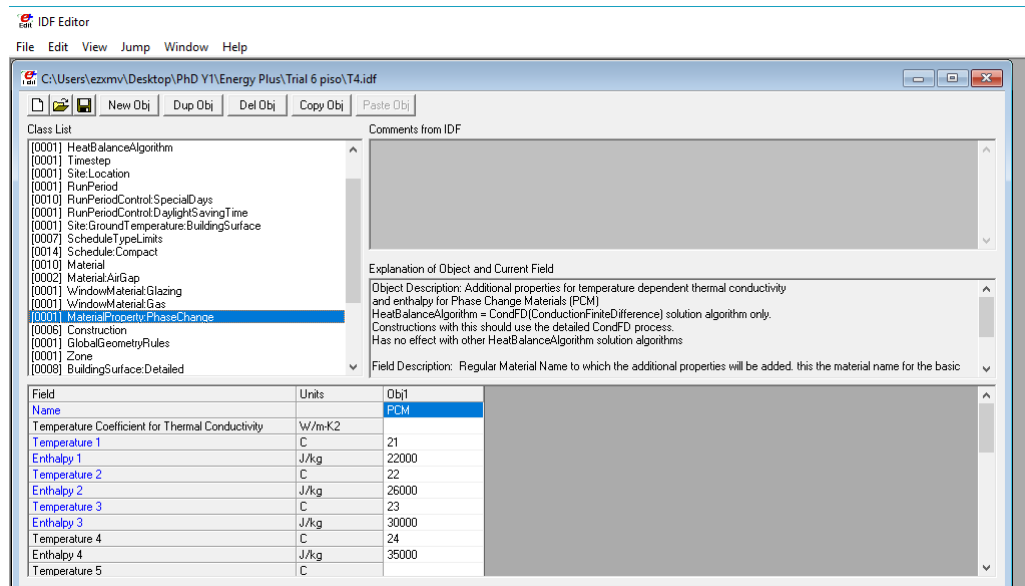


Figure 4.10. PCM enthalpy values example.

#### 4.3.3.4 Construction

Includes the floor, walls, roof, ceiling, windows, and doors and details the material layer of each element. Each layer of the construction is a material name listed in order from “outside” to “inside”. The addition of the PCM material is considered as exterior ceiling and/or interior ceiling.

#### 4.3.3.5 Building Surface, Detailed

Specifies the building elements of the model by surface type (floor, roof, walls), it also considers the boundary conditions and the exposition with the outdoor climate, referring to the wind and sun exposure or lack of it.

#### 4.3.3.6 HVAC, Unitary Heat Pump

The load side (air) of the unitary water-to-air heat pump consists of an on/off fan component, a water to air heat pump cooling coil component,

a water to air heat pump heating coil component, and an electric supplemental heating coil component. The source side (water) of the heat pump is connected to a condenser loop with a heat exchanger (ground heat exchanger or other types) or a plant loop with a heating source such as a boiler and a cooling source such as a chiller or cooling tower. This system aims to provide the heat pump reference for the system; however, it does not contemplate the simulation setting for the tri-modular system.

#### **4.3.3.7 Dehumidifier: Desiccant system**

Models the dehumidification of an air stream, normally called the process air stream. A second heated air stream, called the regeneration air stream, is used to remove the collected moisture from the desiccant heat exchanger, and this moisture-laden air is then usually exhausted from the building. This simulates a similar application to the one proposed in the tri-modular system. However, the exact conditionings are not possible to replicate in EnergyPlus.

## **4.4 Results analysis and discussion**

The simulation results focus on the indoor building temperature, having as a reference the building heating and cooling loads. Several conditionings are compared to further analysis of the performance of PCM materials within the building structure.

The building simulations results present the temperature variation of the building with and without PCM. In this evaluation, the PCM tested was

the INERTEK 21 and was located in the building ceiling with a 2 cm thickness. The PCM details are described in Table 4.5.

Table 4.5 PCM material input.

Simulation details	
PCM material	INERTEK 21
PCM weight	785 kg

Figure 4.11 presents the temperature comparison of the model house. In this case, the indoor building temperatures are higher without the addition of the PCM, proving the potential application of this material as a viable passive cooling source.

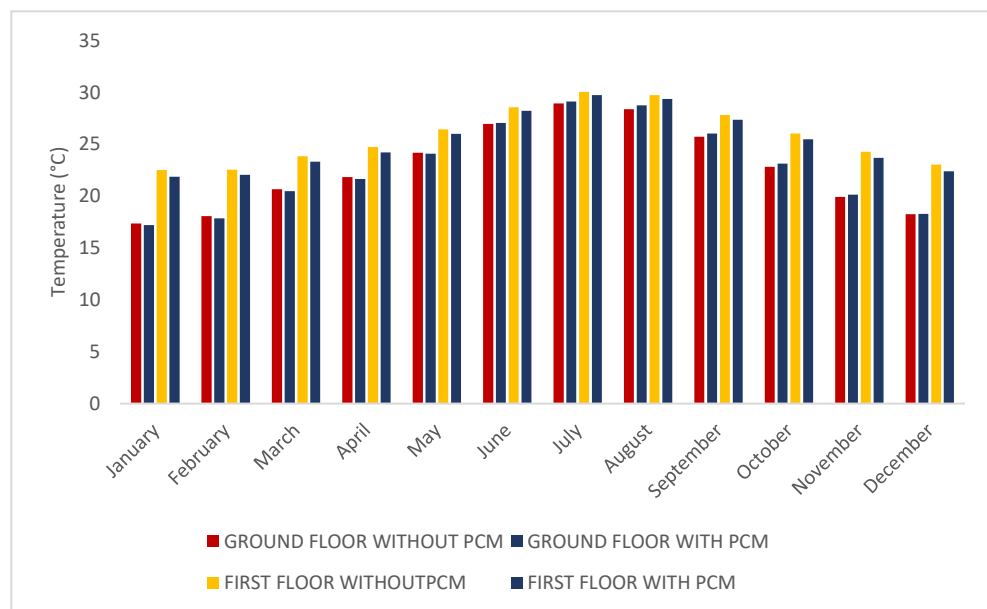


Figure 4.11 Building temperature comparison with and without PCM.

#### 4.4.1.1 Heating loads

Figure 4.12 presents the heating loads comparison. In case due to the site location, the heating requirement demand is higher during the winter period, approaching 180 kWh. The energy demand is proportional to the area, for this reason, the living area and ceiling required higher energy consumption.

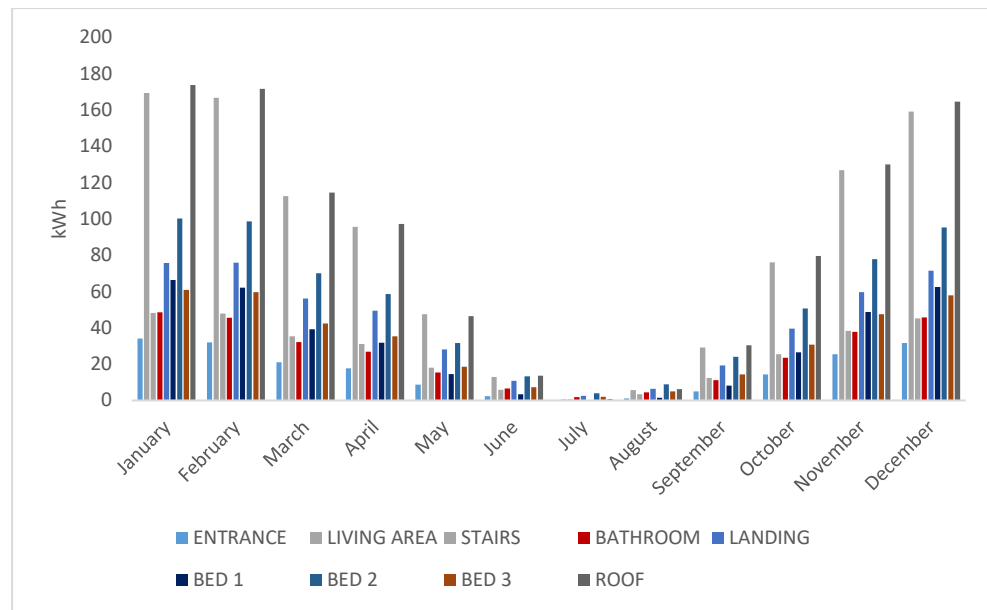


Figure 4.12 Heating loads without PCM in Birmingham.

Figure 4.13 presents the heating loads with the addition of the PCM in the ceiling tiles, reducing the heating loads under 160 kWh. It can be noticed that during the summer period, the heating loads are drastically reduced, having July with zero requirements.

Figure 4.14 shows the annual heating energy performance of the house model comparing the energy demand with and without PCM. It is important to highlight that no enhancement method has been considered for the PCM material. Even though the PCM is intended for passive cooling applications, a reduction in the heating demand could be observed. The results show that the ceiling PCM reduces annual the energy requirements, having a 13% reduction of the total heating demand.

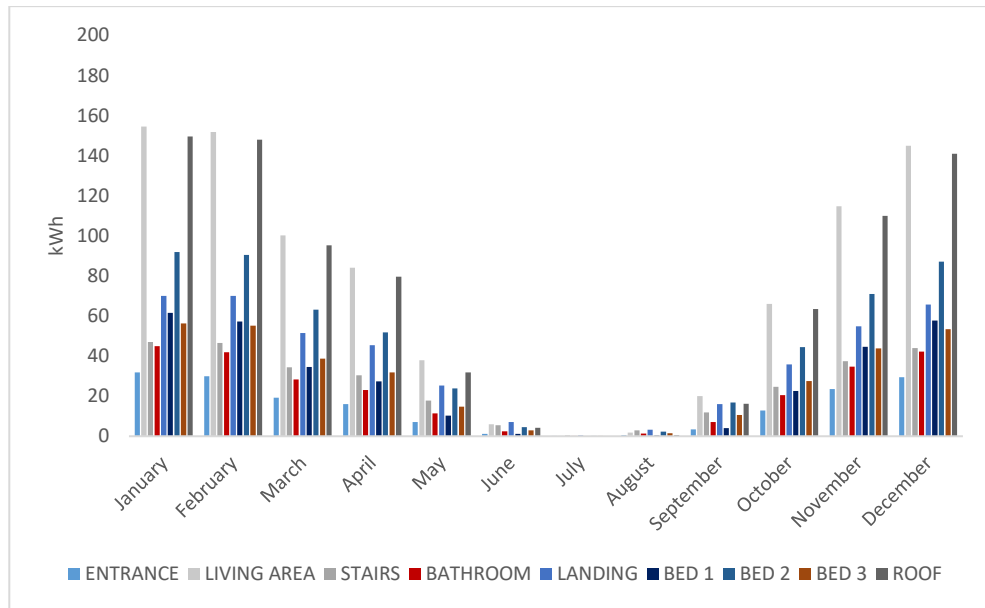


Figure 4.13 Heating loads with PCM in Birmingham.

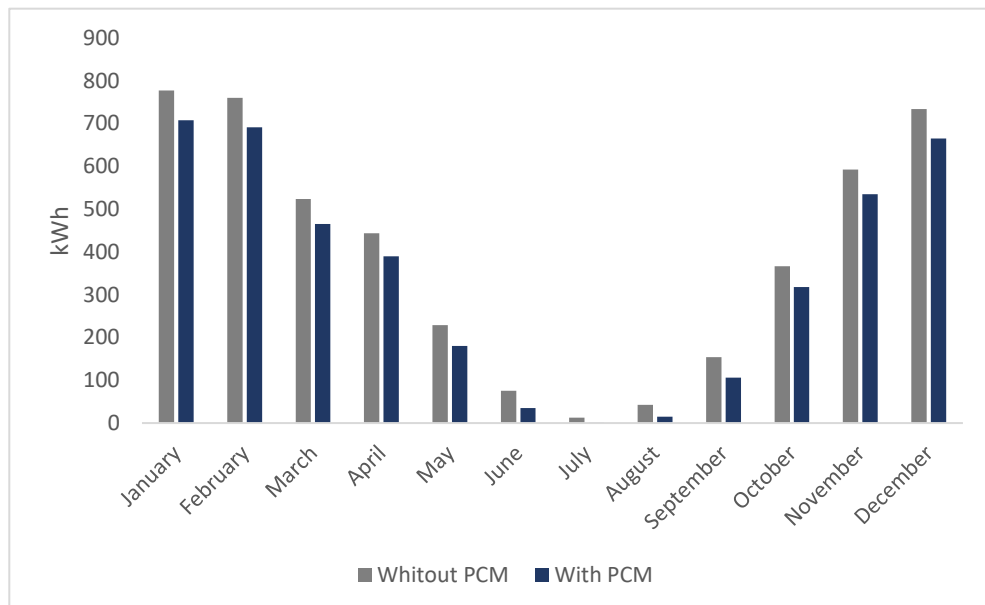


Figure 4.14 Heating loads comparison with and without PCM.

#### 4.4.1.2 Cooling loads

For UK weather the cooling demands are considerably lower in comparison to heating. Figure 4.15 shows the cooling requirements are between March and September, being July the month with the highest demand. Comparably to the heating loads, the ceiling and living area present higher cooling requirements due to the enlarged surface area.

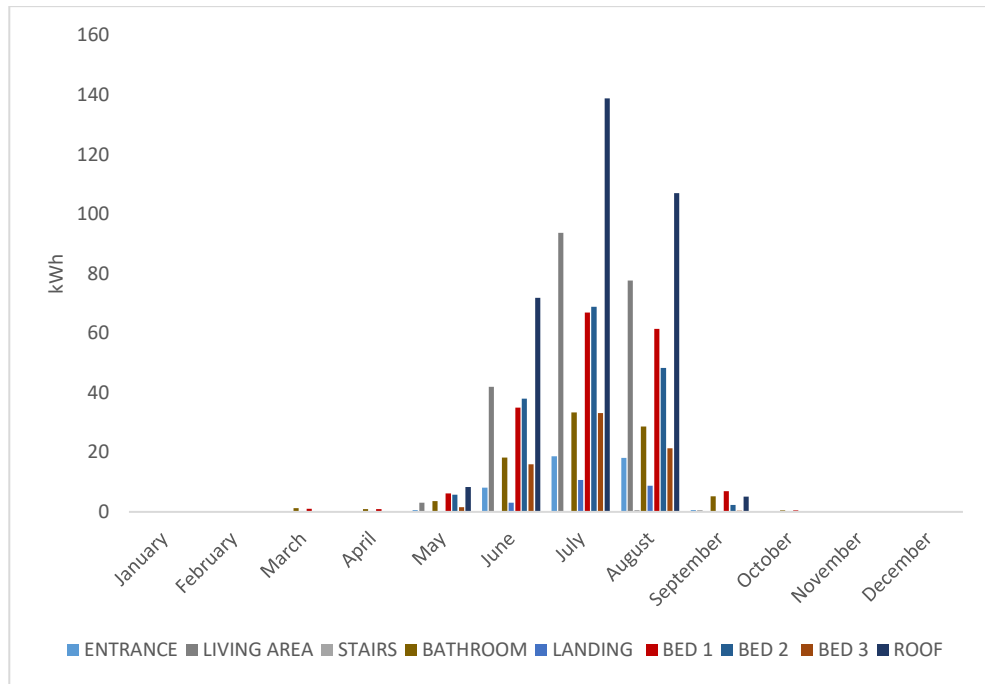


Figure 4.15 Cooling loads without PCM in Birmingham.

The incorporation of the PCM reduces drastically the cooling demands, eliminating the requirement from March to May as shown in Figure 4.16.

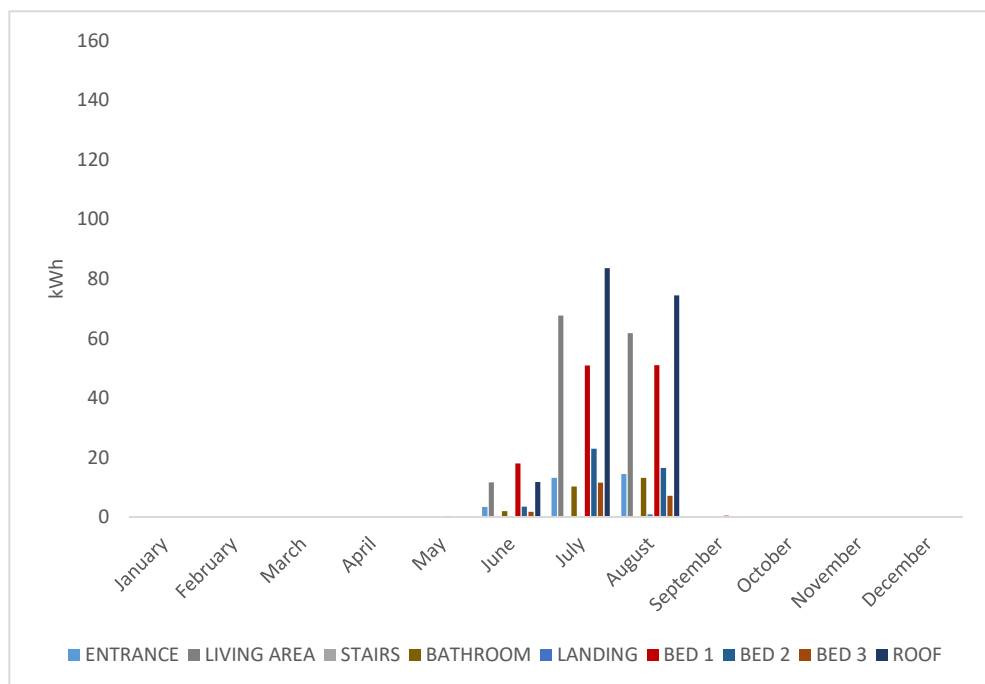


Figure 4.16 Cooling loads with PCM in Birmingham.

Figure 4.17 presents the cooling load comparison of the house model measuring the energy demand with and without PCM.



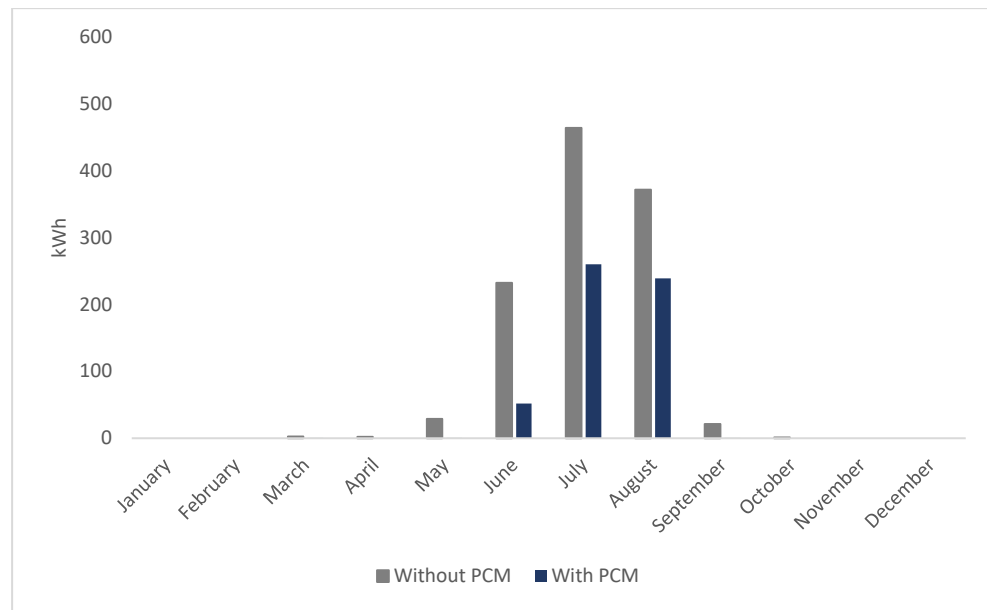


Figure 4.17 Cooling loads comparison with and without PCM.

It is important to highlight that no enhancement method has been considered for this simulation and a higher thermal performance is expected with the addition of highly conductive materials. It is apparent from the results that the PCM reduces the energy demand all year and a reduction of 51% of the total cooling demand is presented.

#### 4.4.1.3 Thickness comparison

The interest of determining the effect of the PCM in the ceiling a variation of the thickness layer is simulated. The same PCM INERTECK 23 was simulated with 0.02, 0.06, and 0.1 m layers for a week under Birmingham weather.

Figure 4.18 presents the thickness comparison of the same PCM (INERTEK 23). The results showed that the 0.1 m thickness has the highest temperature reduction, while the 0.02 m thickness is the lowest.

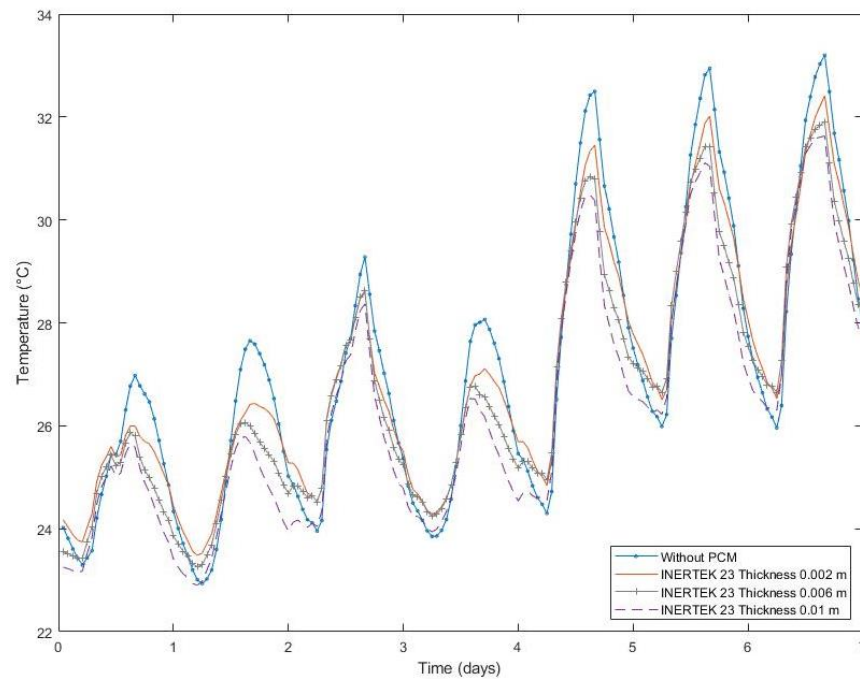


Figure 4.18 Thickness comparison INERTEK 23.

It can be concluded that larger quantities of embedded PCM have a higher impact in reducing average indoor temperatures for the model.

#### 4.4.1.4 Material comparison

Figure 4.19 describes two different PCMs with the same melting point against the building element without PCM. The simulation was run over 7 days and compares INERTEK 21 and RUBITHERM 21 (as both have the same melting temperature). Rubitherm presents slightly higher temperatures during the first days of testing.

The enthalpy values change are presented in Figure 4.20, where the solidification temperature of both materials is compared. It is noticeable that despite having differences in the enthalpy process the performance is relatively similar.

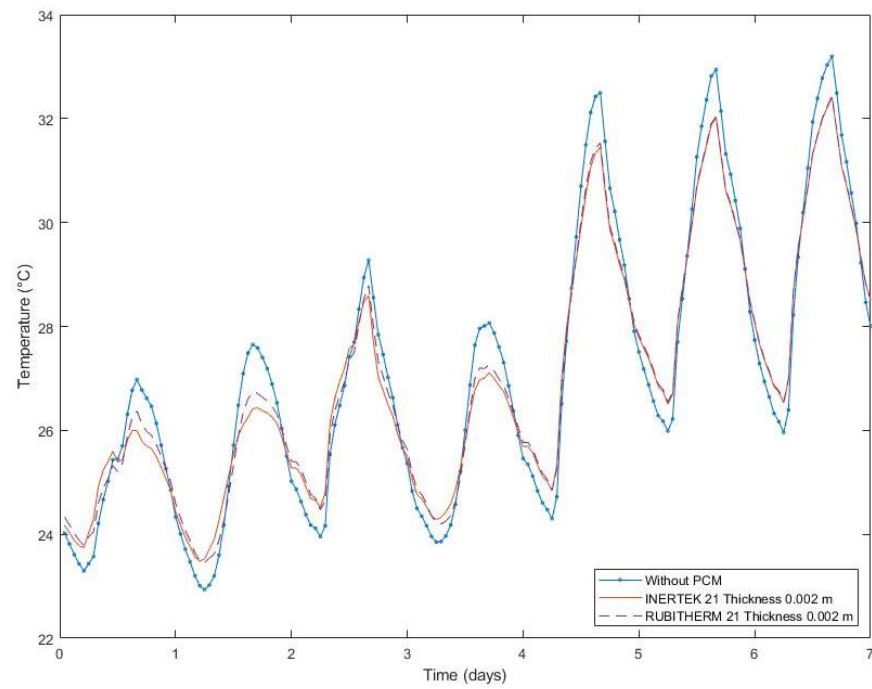


Figure 4.19 PCM material comparison.

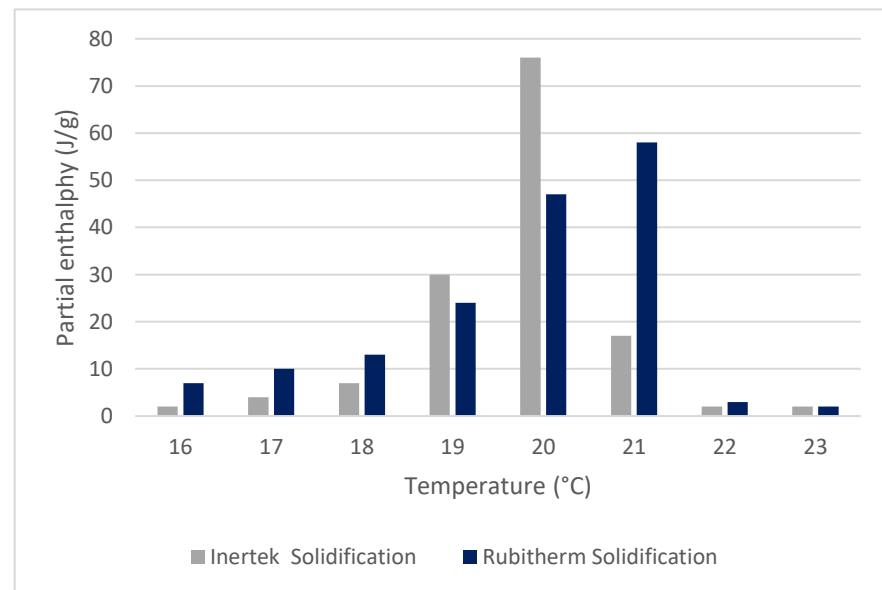


Figure 4.20 Enthalpy distribution for 21 °C melting temperature between Rubitherm and Inertek.

To select the PCM for experimental evaluation, different commercially available materials were simulated. Figure 4.21 presents different

commercially available PCMs with similar melting points, all within the human thermal comfort zone.

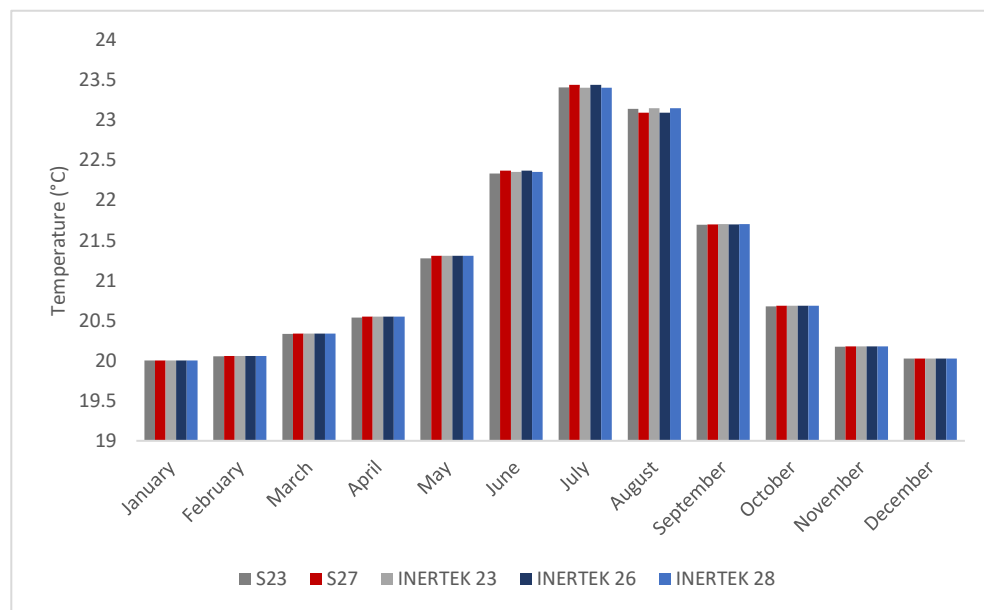


Figure 4.21 Temperature comparison of PCM Products Ltd products and INERTEK.

The enthalpy values were obtained from the manufacturer's datasheets. The results are present a minimal difference, for example, INERTEK 23 presents a slightly higher temperature in comparison to S23. The S27 and the INERTEK 28 present the same values; meanwhile the INERTEK 26 presents lower temperatures.

Figure 4.22 and Figure 4.23 present the heating and cooling loads respectively. The results exhibited that the R21 has higher temperatures in comparison to the INERTEK 21. When comparing the S23 and the INERTEK 23, the S23 presents lower temperatures. In the case of the S27 and the INERTEK 28; the S27 would be a more suitable option due to the lower melting point.

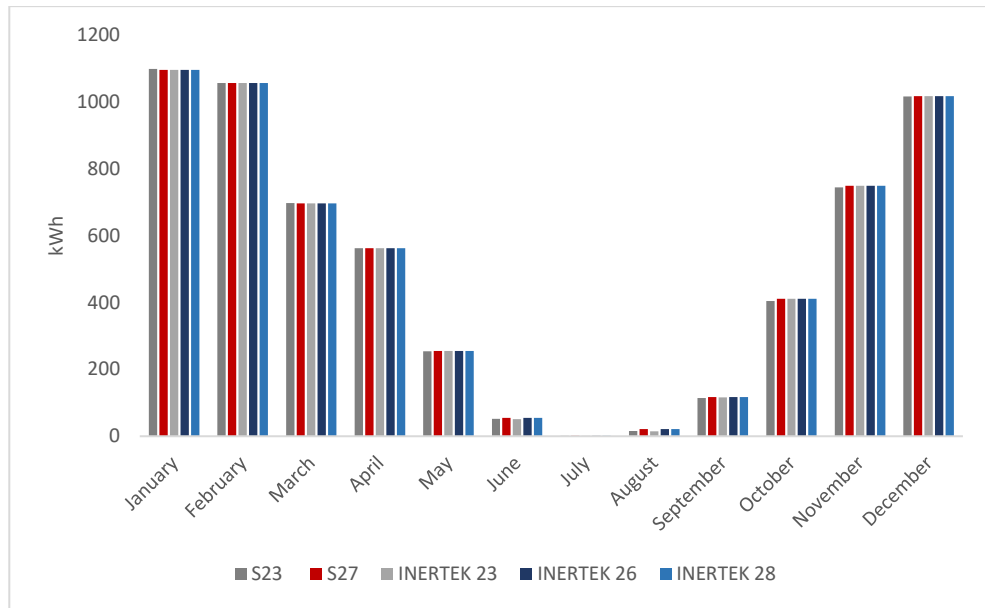


Figure 4.22 Heating loads comparison between PCM Products Ltd and INERTEK.

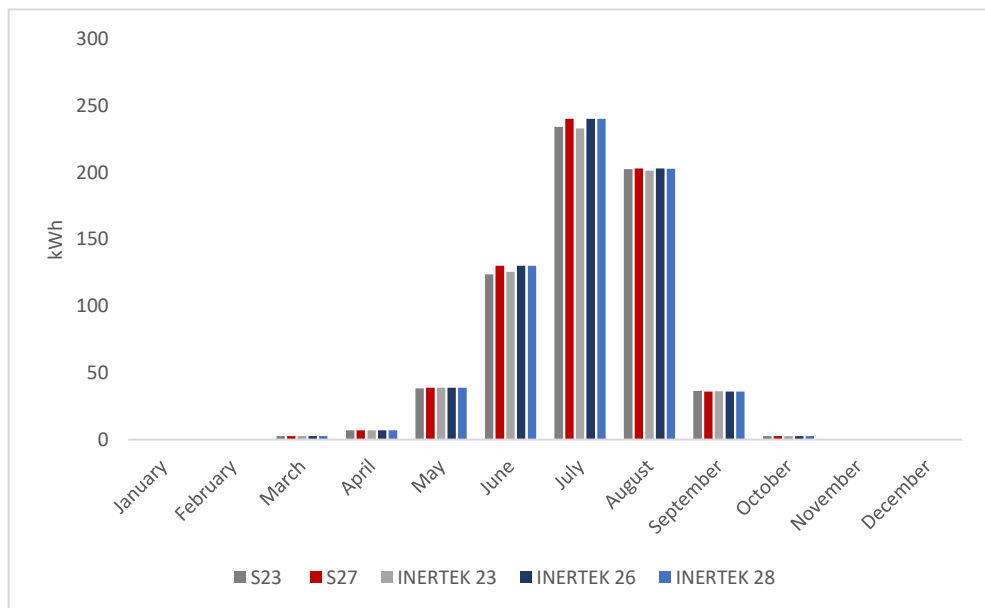


Figure 4.23 Cooling loads comparison between PCM Products Ltd and INERTEK.

## 4.5 Summary

The modelling evaluation presented throughout this chapter investigated the thermal performance of the PCM for indoor temperature control in

residential buildings. The aim of the study is to analyse the impact of the PCM on a residential house in Birmingham.

A series of simulations were carried out in the EnergyPlus software, it is important to highlight that no enhancement method of the PCM is taken into consideration. Enhancing the PCM would automatically provide higher thermal performance, reducing, even more, the temperature fluctuations and energy consumption.

PCMs are an attractive alternative to conventional cooling systems that focuses on thermal storage principles. The results showed that the PCMs helped the temperature fluctuations and reduce the indoor temperature all year. The cooling and heating loads were positively affected with the incorporation of the PCM in the ceiling, having energy savings of 13% and 51%, respectively.

The simulation results showed that the PCM with a melting temperature of 21 °C has a better performance for the Birmingham weather. In warmer climates, this particular PCM may increase the indoor temperature producing a negative impact on the building performance.

The thickness analysis exhibited that having a higher thickness resulted in higher thermal performance. In this case, three different thicknesses were simulated as follows: 0.02, 0.06, and 0.1m layer, where the 0.1m was found as the most efficient. Nevertheless, this conclusion may be counterproductive when the amount of PCM surpasses the building capacity to melt it. For this reason, it is pivotal to analyse each case

scenario to find the more suitable PCM according to the energy requirements.

The material comparison results are inconclusive; this could be because of the weather conditions, as detailed in section 4.1 Birmingham weather does not reach the melting points of the PCM. If the melting temperature is not reached, it can cause a reduction in the performance of the PCM due to the partial phase transition. Experimental validation may present different results. It is important to select a suitable PCM for the location or evaluate the performance of the dwelling to ensure the optimal performance of the PCM.

With increasing efforts to reduce the energy consumption associated with the operation of buildings, it is vital that these predictions be improved to represent the operation of buildings more realistically. For this reason, experimental analysis is vital to have a better understanding of the proposed systems, providing additional results that ultimately show the viability of the proposed application.

The environmental analysis presented will be detailed in Chapter 8, as the experimental results will provide further information on the optimal PCM candidate for the specific application.

# Chapter 5 PCM and solid desiccant preliminary experiments

## 5.1 Introduction

This chapter introduces the preliminary testing for the material selection, development and optimization of PCMs and solid desiccants. The evaluation of different materials is crucial for adequate thermal performance and enhancement mechanisms. In this chapter, properties and characteristics of different phase change materials and solid desiccants for building integration are investigated. In the case of the PCMs, the encapsulation method is discussed, having eight different ceiling panels. Based on the literature review, this chapter revises the performance of silica gels, being one of the most popular solid desiccants and compares them with vermiculite for building dehumidification purposes.

## 5.2 Phase Change Material selection

Considering the information presented in the literature review and the modelling analysis of PCMs, a shortlist of organic and inorganic materials have been selected for testing. The key parameter to select the PCM



focuses on the melting temperature, which in this case should range between 22 °C to 28 °C to satisfy the energy requirements for melting and freezing under the UK climate. In this case, a comprehensive review of the commercial PCMs is presented by Kalnæs and Jelle, where they classify the PCM by manufacturers and thermal properties (Jelle and Kalnæs, 2017).

Some of the most popular PCM companies are Phase Change Material Products Ltd, Microtek, Rubitherm and Entropy Solutions Inc, these companies present a wider range in comparison to other manufacturers and in some cases produce both organic and inorganic PCMs.

As compared during the modelling stage Rubitherm and Phase Change Material Products Ltd present similar performance due to the enthalpy value of the PCMs. For the experimental analysis S23, S27 and A28 have been selected from Phase Change Material Products Ltd due to their thermal properties and low cost. Furthermore, the investigation of microencapsulated PCM is considered, using INERTEK 23 and INERTEK 26. The PCM thermal characteristics are presented in Table 5.1. During the experimental procedure, a particular interest is made to compare the PCMs performance depending on the melting temperature.

Table 5.1 PCM thermal properties.

Commercial name	Melting Point (°C)	Heat storage capacity (J/g)	Thermal conductivity (W/Mk)
INERTEK 23	23-27	200	-
INERTEK 26	26-28	240	-
S23	23	220	0.31
S27	27	220	0.31
A28	28	220	0.21

5.2.1 Encapsulation methods

Organic PCMs can be mixed with high thermal conductive materials to boost the thermal performance, in which these materials are either added to the PCM base fluid or used as an encapsulation method. In contrast, for the inorganic PCMs, the enhancement methods are based on the encapsulation method (honeycomb structure, polyethylene) and the temperature distribution around them. In both cases, enhancement methods are proposed to counteract the phase segregation and at the same time, to promote the thermal performance. In the case of the organic PCM, aluminium seems to be a suitable option based on the literature review. This chapter focuses on the evaluation of different encapsulation methods for building integration, combining in some cases high thermal conductive materials and novel encapsulation methods for ceiling panel applications. The proposed solutions are presented in Table 5.2. During this preliminary evaluation, different panels were tested using novel applications, varying the materials, weight and enhancement mechanisms.

Table 5.2 PCM panels by encapsulation method.



Honeycomb panel



Metallic pots



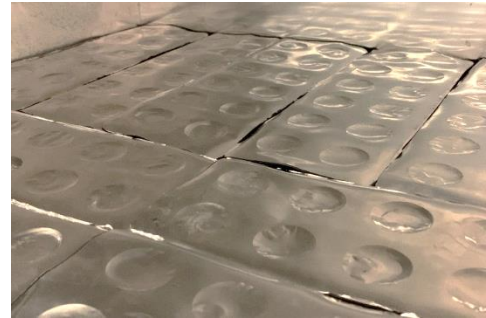
Aluminium pouch



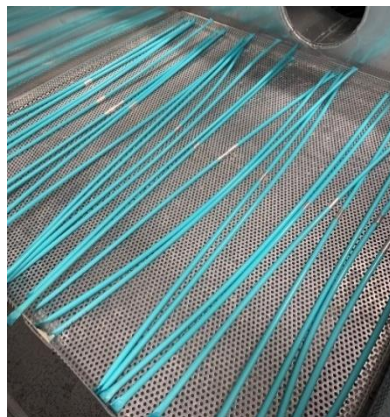
Plastic pouch



Blister panel



Capsule panel



Straws panel



Corrugated straws panel

### 5.2.2 Environmental chamber testing setup

An experimental setup was prepared to analyse the effect of the ceiling panels and enhancement methods. A set of experiments performed in the Environmental Climatic Chamber was developed by SJJ System Services Ltd. (Serial No. A2520). The experimental setup consisted of a control box of 70 x 67 x 73 cm, in which the PCM panels were allocated over a metallic mesh. The temperature measurements were made using

Type K thermocouples, and all readings were collected by the data logger (DT85), with a standard deviation of  $\pm 0.3^{\circ}\text{C}$ . Sensors were placed in the inlet, outlet, and inside the PCM panel, as shown in Figure 5.1. Both the inlet and outlet had openings of 18 cm diameter, with airflow coming from the Environmental Chamber blown through with the assistance of an electric fan. The experiments consisted of creating an airflow through the control box at the desired temperature, in order to analyse the thermal performance of the PCM panel as shown in Figure 5.2.



Figure 5.1 Experimental setup for PCM panel testing.

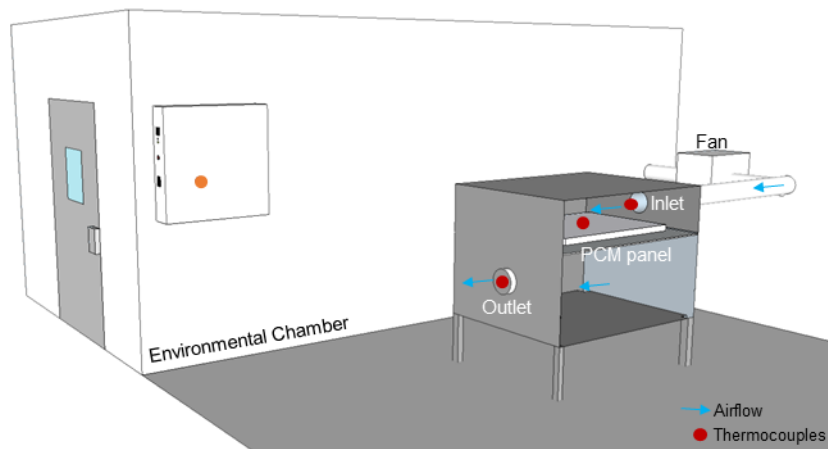


Figure 5.2 Schematic diagram of the experimental apparatus with airflow pattern.



### 5.2.3 Water tank experimental rig

Figure 5.3 presents the water tank experimental setup consisting of a plastic control box of 24.5 x 32.5 x 43 cm; cover by two insulation layers, the first layer was composed of fiberglass isolating material and the second layer consisting of duct slabs rockwool boards. The temperature measurements were made using Type K thermocouples, and all readings were collected by the data logger (DT85), with a standard deviation of  $\pm 0.3^{\circ}\text{C}$ . The sensors were placed inside the water tank and additional sensors monitored the ambient temperature. To establish a baseline, the experiments consisted of comparing the water heat lost and measuring the effect with the PCM panels, the water temperature exceeds the melting point of the PCMs, to ensure the phase change.



Figure 5.3 Water tank experimental setup.

### 5.2.4 Environmental chamber results

#### 5.2.4.1 Honeycomb Panel

The honeycomb panel consist of placing a metal honeycomb structure inside a Mylar bag. The honeycomb structure was sealed on the bottom part as well as the edges, after this, the INERTEK 23 was placed into

each honeycomb cavity. Once the honeycomb structure was filled, it was placed inside the Mylar bag, to reduce the air gap in the bag the panel was pressed before been thermally sealed with a heat gun. Figure 5.4 and Figure 5.5 shows the first honeycomb panel having a total weight of 1.178 kg, a second panel was created with a total weight of 5.672 kg as shown in Figure 5.6.



Figure 5.4 Metal honeycomb structure with PCM.



Figure 5.5 INERTEK 23 small honeycomb panel.



Figure 5.6 A28 large honeycomb panel.

Figure 5.7 presents the evaluation of the large honeycomb panel; the testing duration was of 4.3 hours and the temperature difference of 1.7 °C between inlet and outlet. The panel temperature was maintained at 26 °C during the testing period and corresponds to the panel presented in Figure 5.5.

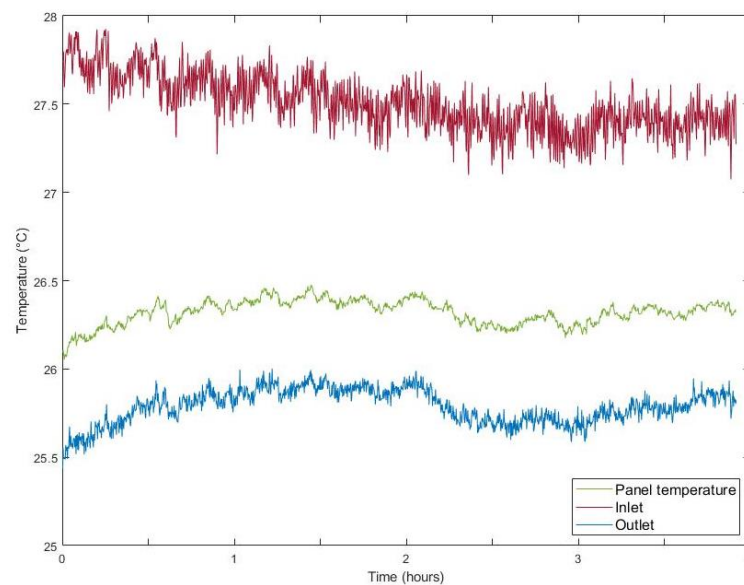


Figure 5.7 INERTEK 23 small honeycomb panel, test 1.

A28 was selected to test the honeycomb structure, using the panel presented in Figure 5.6. The panel weight was 4 kg and the testing results

are shown in Figure 5.8, having a temperature difference of inlet and outlet of 4.7 °C.

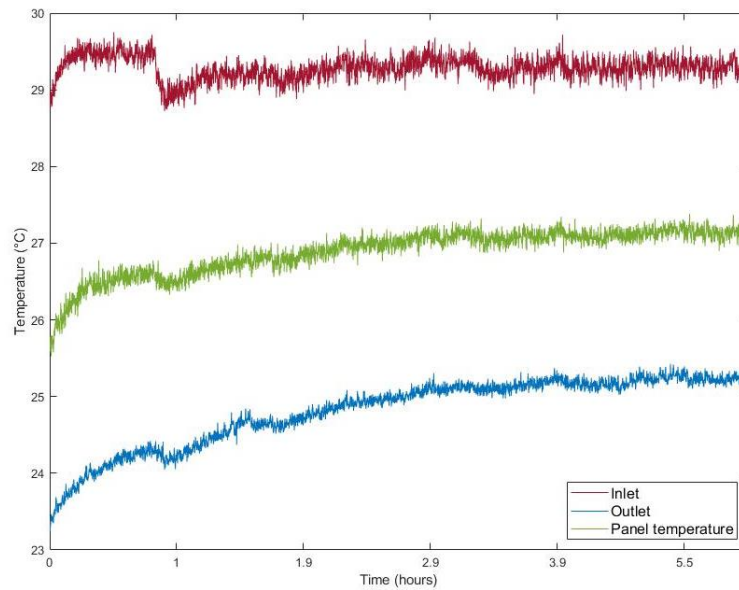


Figure 5.8 A28 honeycomb panel, test 1.

#### 5.2.4.2 Metallic pots

This panel consist of small metallic pots filled with INERTEK 26; the total weight was 3.1 kg out of which 2.074 kg correspond to the PCM. The number of panels utilized in the experiment was 57 and the pots were placed between two perforated metal covers to represent a ceiling tile, as presented in Figure 5.9.



Figure 5.9 Metallic pots.



Figure 5.10 displays the first test results from the metal pots, the chamber temperature was set at 30 °C, the panel temperature was lower than the inlet and outlet. The panel temperature increases constantly throughout the test, reaching a maximum temperature of 22.3 °C, which is below the PCM melting point.

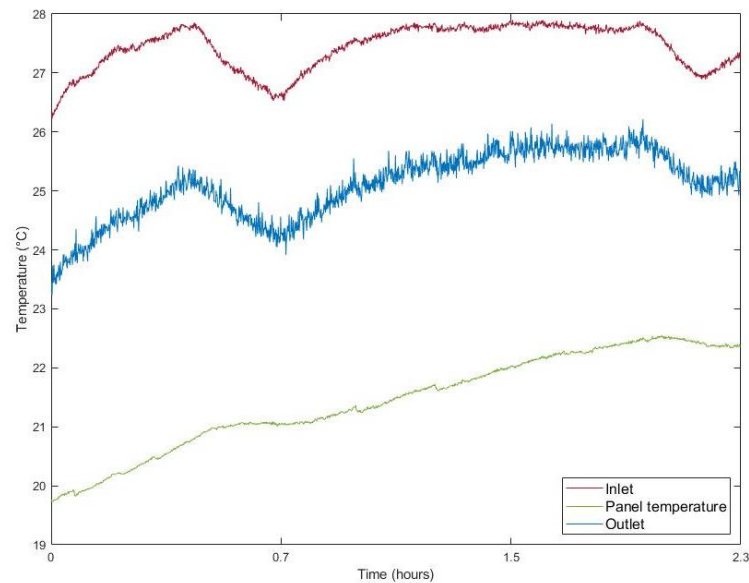


Figure 5.10 Metallic pot environmental chamber, test 1.

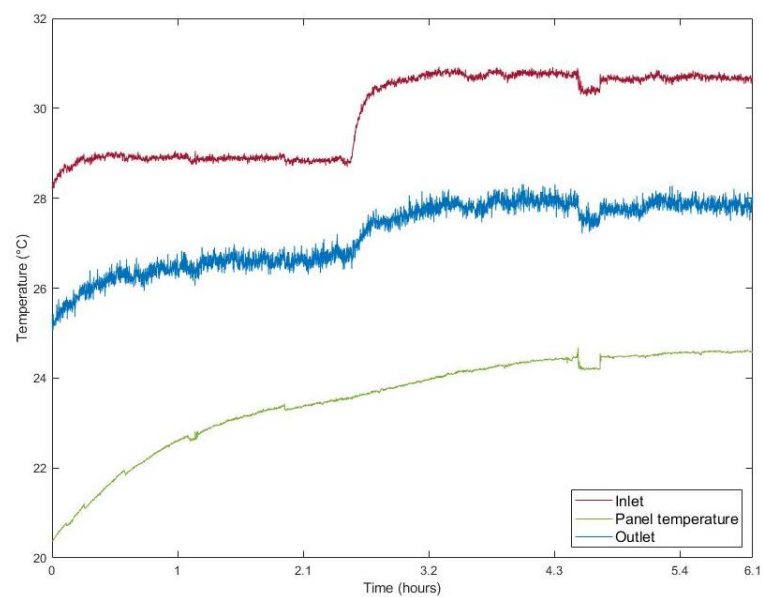


Figure 5.11 Metallic pot environmental chamber, test 2.

A second test is presented in Figure 5.11, the starting temperature was set at 32 °C and after three hours the temperature was increased to 35 °C. It can be observed that the panel temperature is considerably lower reaching a maximum of 24.6 °C.

#### **5.2.4.3 Aluminium bar pouch panel**

The aluminium pouch panel consisted of 6 pouches containing an aluminium metal bar inside. The PCM utilized is the INERTEK 23 and had an average weight of 0.369 kg each (the metal bar weights 0.146kg) using a Mylar bag as a container, the panel is displayed in Figure 5.12.



Figure 5.12 Aluminium pouch panel.

Figure 5.13 exposes the results from the aluminium pouch panel. The average temperature difference between inlet and outlet was 3.3 °C, the test was maintained for 6.2 hours, the average panel temperature was 23.22 °C.

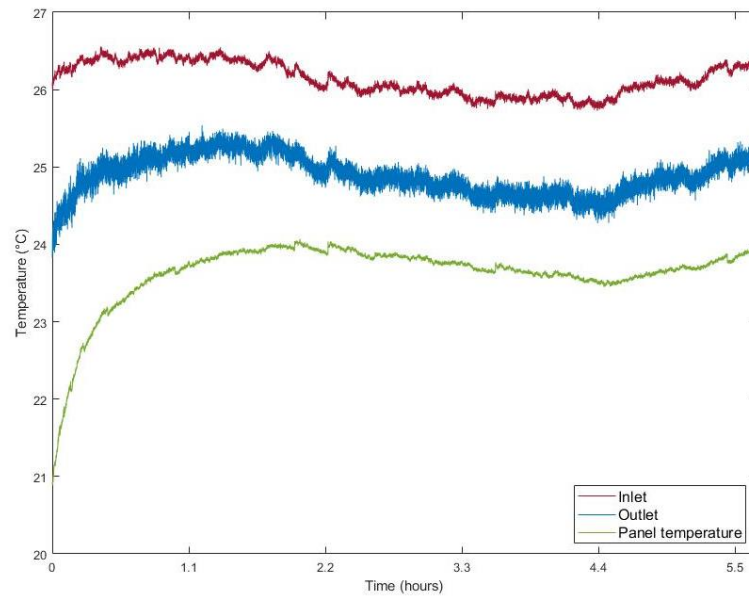


Figure 5.13 Aluminium pouch panel, test 1.

#### 5.2.4.4 Plastic Pouch Panel

The plastic pouch panel was developed by Phase Change Material Products Limited, containing S23 PCM with a weight of 1.41 kg per pouch and having around 4 pouches per panel, having a total weight of 11.27 kg as shown in Figure 5.14.



Figure 5.14 Plastic pouch with S27.

The testing has a duration was of 6.3 hours, the chamber temperature was set at 35 °C and is presented in Figure 5.15. In this case, the

temperature difference between the inlet and outlet was 3.35 °C. The panel temperature was stable at 23 °C, after the initial peak.

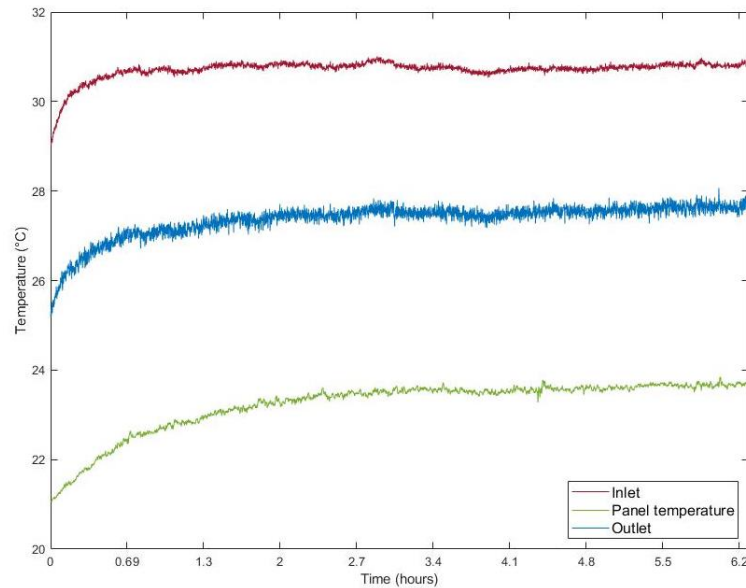


Figure 5.15 S27 plastic pouch, test 1.

Figure 5.16 presents an average temperature difference between inlet and outlet of 1.6 °C. In this case, the average panel temperature was 27.3 °C over 5.7 hours.

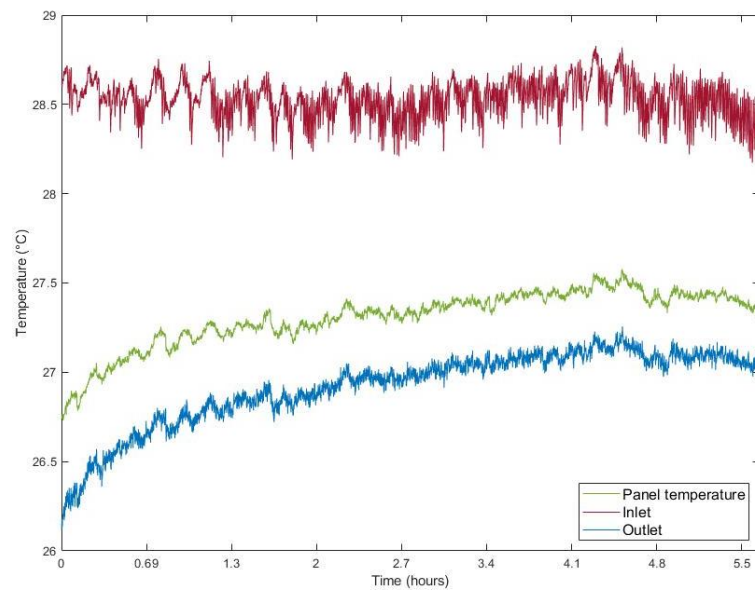


Figure 5.16 S27 plastic pouch, test 2.

#### 5.2.4.5 INTERKEK 23 Blister Panel

A blister panel consisting of 9 individual panels was tested. In this case, the panels contain INERTEK 23. The PCM material was placed inside the blister and after vibrating the panel it was sealed with thermal conductive tape. The panel is presented in Figure 5.17 having a total weight of 0.596 kg. The advantage of this panel design is that allows airflow through each blister cell, facilitating the PCM melting and freezing process. In this case, the panel was tested under different environmental conditions to prove the performance of this particular encapsulation method.



Figure 5.17 INERTEK 23 blister panel.

The first test presented in Figure 5.18 had a temperature of 28 °C and the experiment was carried out for 6.9 hours. It is observed that the panel temperature increases as it is absorbing heat from the environmental chamber stabilizing after 2.7 hours.

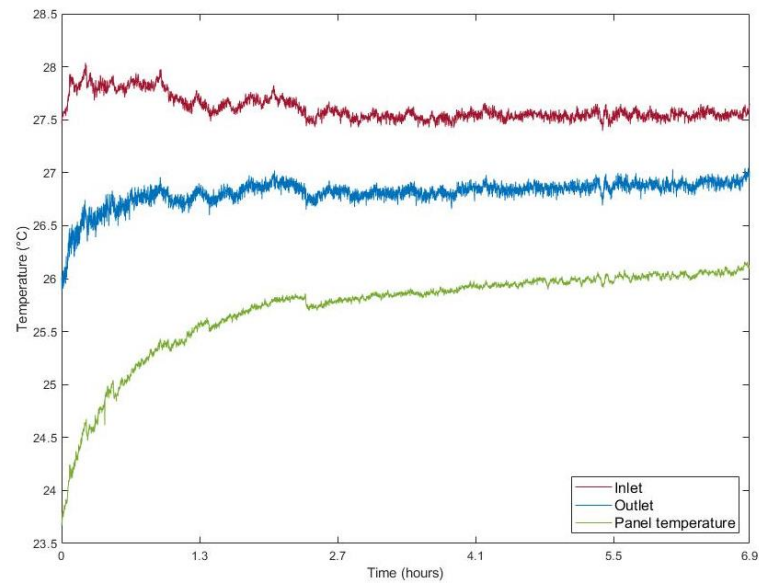


Figure 5.18 INERTEK 23 blister panel, test 1.

Similarly to the first test, Figure 5.19 shows the second testing in which the chamber temperature was set at 27 °C. The average temperature difference between inlet and outlet was 0.79, by reducing 1 °C the temperature difference between inlet and outlet was 0.61 °C.

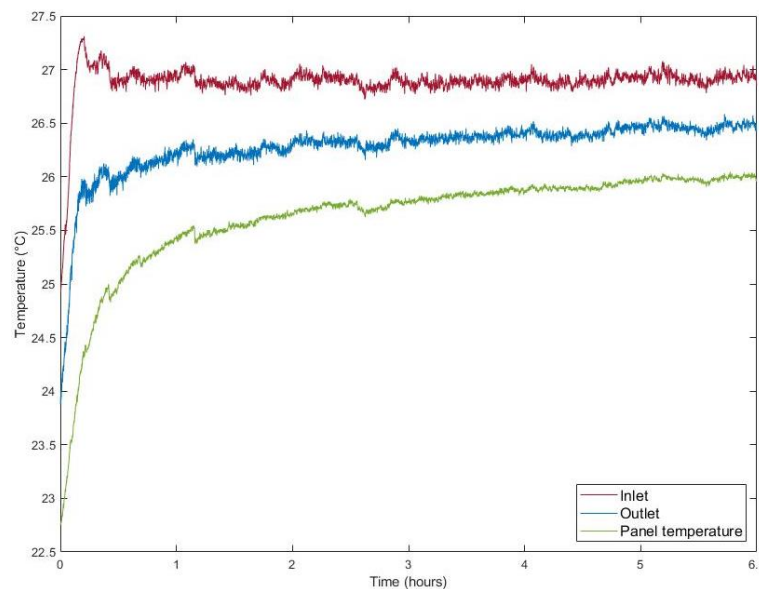


Figure 5.19 INERTEK 23 blister panel, test 2.

Having a higher ambient temperature ensures that the PCM is melting throughout the experimental procedure and in this case allows the PCM

panel to maintain a relatively stable temperature through the testing period.

Figure 5.20 presents the temperature analysis with two temperature increments throughout the testing period. The initial temperature was set at 23 °C and the final temperature at 27 °C, the testing duration was of six hours with 2 °C temperature increments every two hours.

Although the test does not have a constant temperature, it is predictable to see a higher temperature difference as the chamber temperature increases. This would be expected if the chamber temperature ranges between the PCM enthalpy phase and the panels are charging.

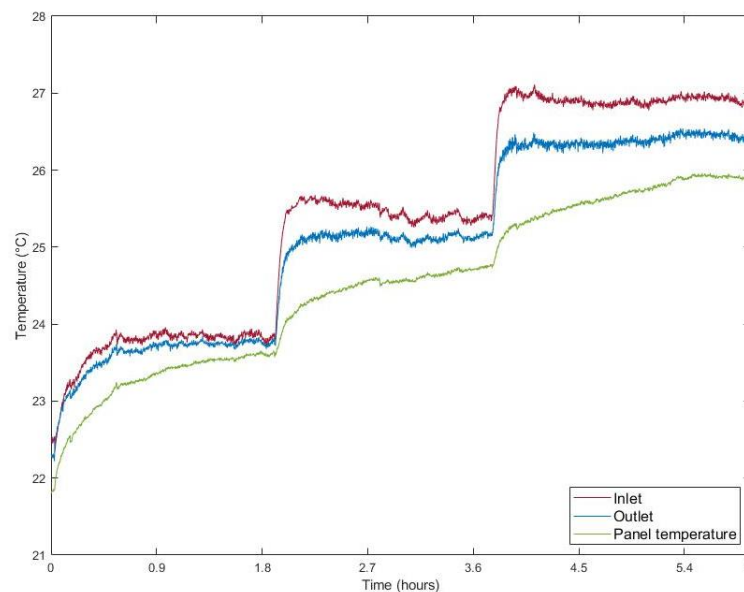


Figure 5.20 INERTEK 23 blister panel with 2 hours temperature increments.

#### 5.2.4.6 S23 Blister Panel

Using the same blister encapsulation method, S23 was selected for testing. This gives the advantage to contain the salt hydrate material without corrosion, conductive tape was used to seal the blister panel for experimental purposes. For building incorporation using a thermal



conductive material such as a thermal plastic bag is recommended. Figure 5.21 shows the PCM panel, the total weight of 2.1 kg, for the nine blisters.



Figure 5.21 S23 blister panel.

The first test is shown in Figure 5.22, presented a temperature difference between the inlet and outlet of 1 °C. The testing duration was of 3.8 hours and the average panel temperature was 28.98 °C. After the testing period, the PCM panels presented leakage, for this salt hydrates PCM this encapsulation method is not recommended, alternative sealing techniques are advisable.

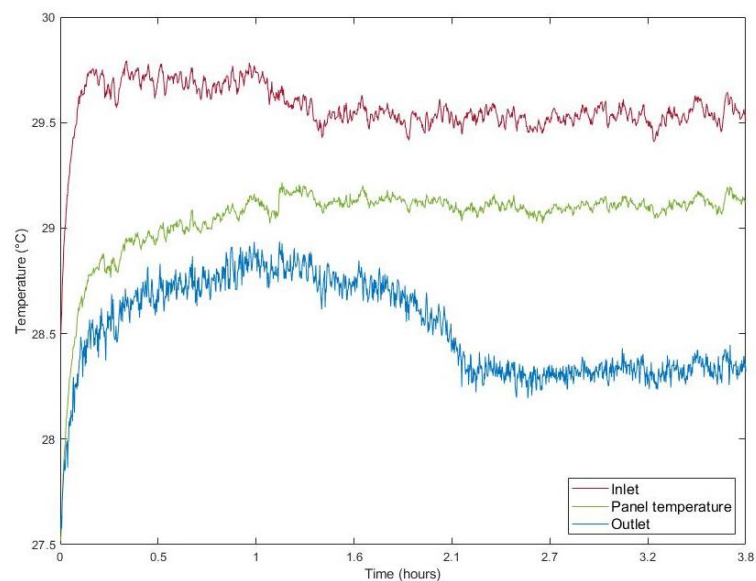




Figure 5.22 S23 blister panel, test 1.

#### 5.2.4.7 A28 Blister panel

Using the same encapsulation method, the blister panel was filled using A28; the total weight was 1.208kg. Figure 5.23 and Figure 5.24 present the panel view during the experimental procedure.

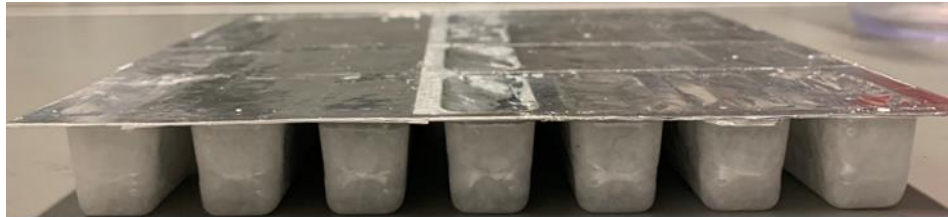


Figure 5.23 A28 blister panel.

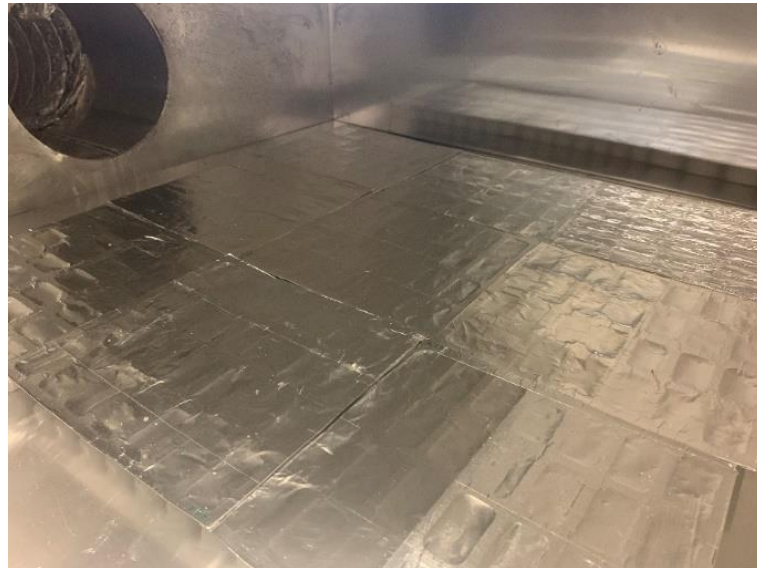


Figure 5.24 A28 blister panels in the testing box.

For the A28 shown in Figure 5.25, it is observed that the panel temperature is higher than the outlet temperature in comparison with previous results. The temperature between the inlet and outlet tends to decrease. The maximum temperature for the inlet is 28 °C; it is at this point that the values become steady. The temperature difference between the inlet and outlet was 4.3 °C.

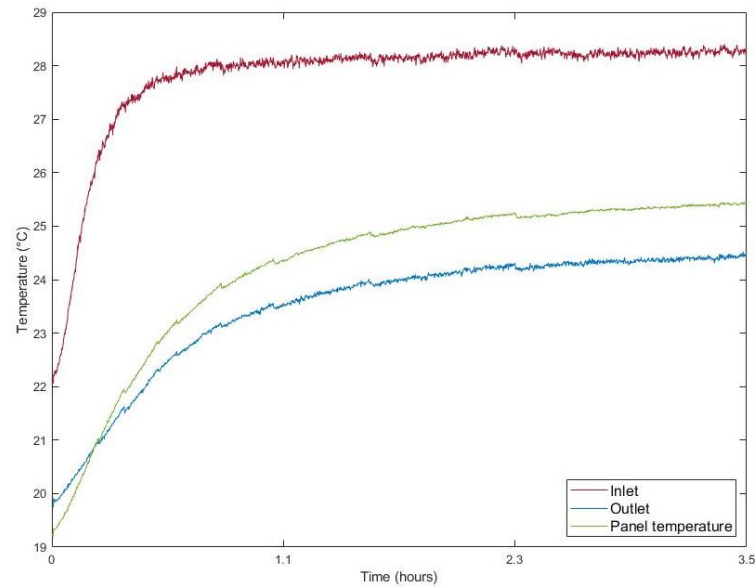


Figure 5.25 A28 blister panel, test 1.

#### 5.2.4.8 S27 capsule panel

A similar concept was utilized using S27 capsules as shown in Figure 5.26 for testing, in total 12 panels were used, carrying a total weight of 2.81 kg.

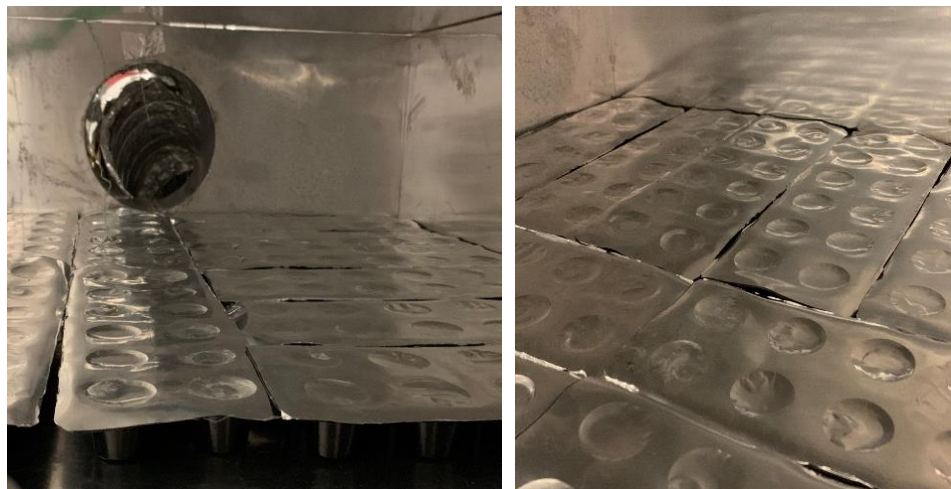


Figure 5.26 S27 capsule panel.

Figure 5.27 displays the temperature variation between the inlet and outlet of the S27 blister panel, the average temperature difference was around 2.3 °C.

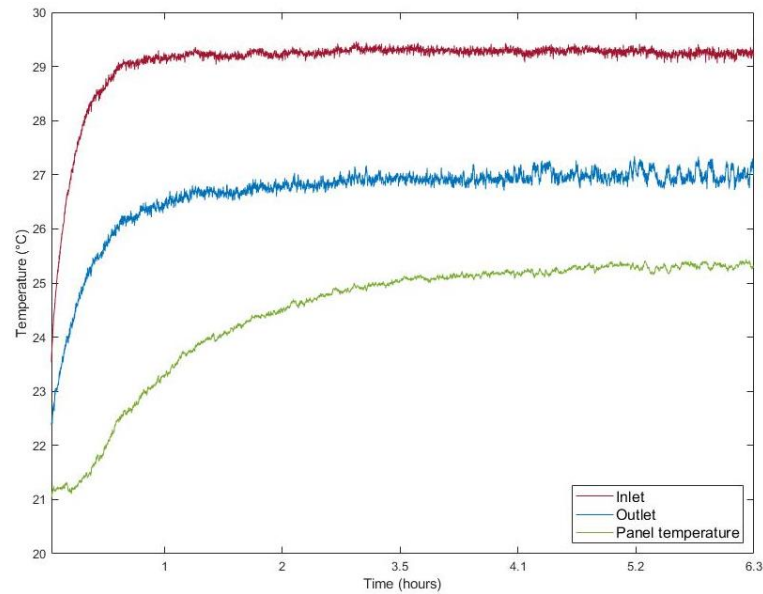


Figure 5.27 S27 capsule panel, test 1.

A second study contemplates presented in Figure 5.28 use an additional 28 panels and the weight characteristics can be found in Table 5.1. It is seen that 40 panels present higher temperatures during the first three hours. The 12 panels reach the highest temperature at the end of the testing period.

Table 5.3 Model comparison by PCM panels.

Panel name	Weight (kg)	Chamber temperature (°C)	Average temperature drop (°C)	$\Delta Q$ (kJ)
40 Panels	8.856	35	2.8	54.87195
12 Panels	2.657	35	2.4	13.84476

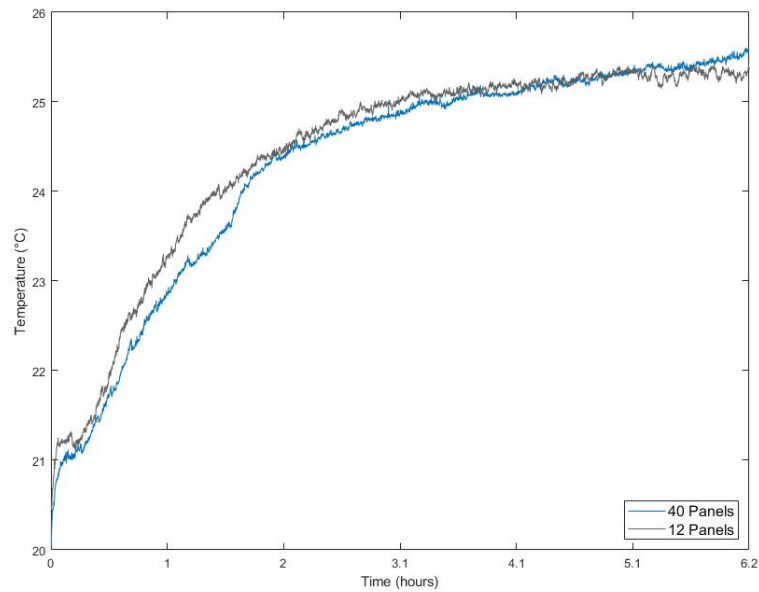


Figure 5.28 S27 capsule comparison by weight.

The temperature drop is compared in Figure 5.29, it is seen that the average temperature drop for the 40 panels was 2.8 °C, in contrast for the 12 panels the temperature drop was 2.4 °C.

Overall, the temperature drop presents similar trends. The 40 panels present's higher temperatures during both testing procedures.

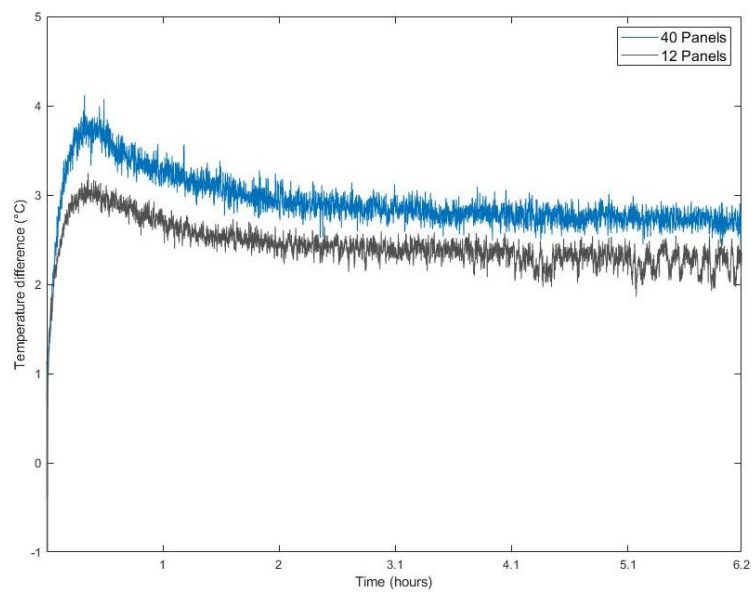


Figure 5.29 S27 capsule temperature drop comparison.

#### 5.2.4.9 Straws panel

A set of 29 straight straws filled with INERTEK 26 were prepared to test the performance in the environmental chamber. To prepare this samples the straws were filled with the microencapsulated material, ensuring vibration through this process to reduce the air gap. After this, the straws were left for 24 hours in a vertical position to further reduce the any gap and thermally sealed with the aid of a heat gun. Figure 5.30 shows the straws allocated in the testing box, having a total weight of 0.154 kg.

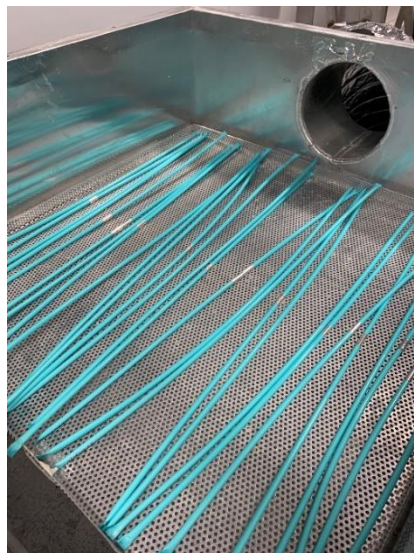


Figure 5.30 INERTEK 23 straw panel.

Figure 5.31 illustrate the testing results, the chamber temperature was increased every two hours, the starting temperature was set at 30 °C and the final temperature was 36 °C after six hours. The temperature difference between the inlet and outlet was 2.6 °C.

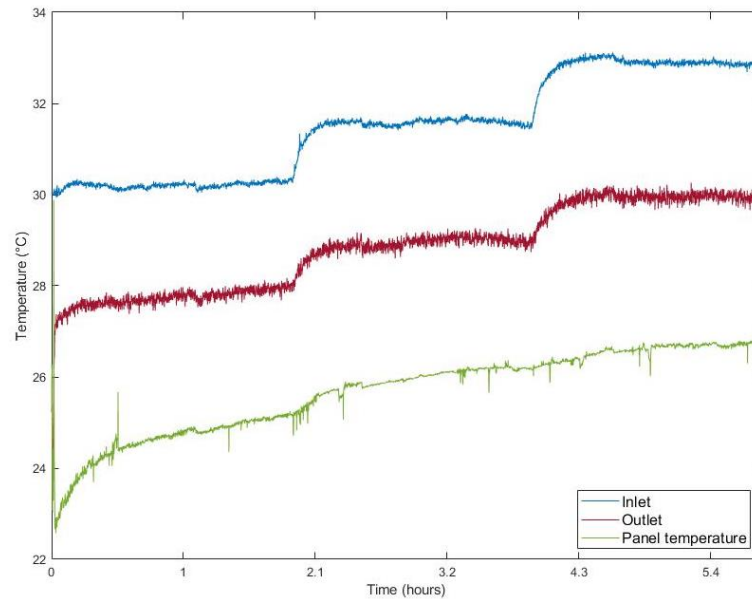


Figure 5.31 Straight straws, test 1.

### 5.2.5 Water tank testing

In addition to the environmental chamber, a water bath method was also adopted to investigate the thermal performance of PCM panels. A double insulated water bath was prepared, into which the PCM panels were placed and thus the water temperature loss was monitored.

#### 5.2.5.1 Aluminium bar pouch in the water tank

For the aluminium bar pouch is depicted in Figure 5.32, the water temperature was set at 32 °C, the panels had a weight of 2.214 kg and the temperature loss was monitored for 2.8 hours.



Figure 5.32 Aluminium pouch panel in water tank testing.

Figure 5.33 displays the experimental results, where the temperature loss is monitored. It is observed that the empty water tank temperature drop was 2.27 °C, while the aluminium pouch was 5 °C.

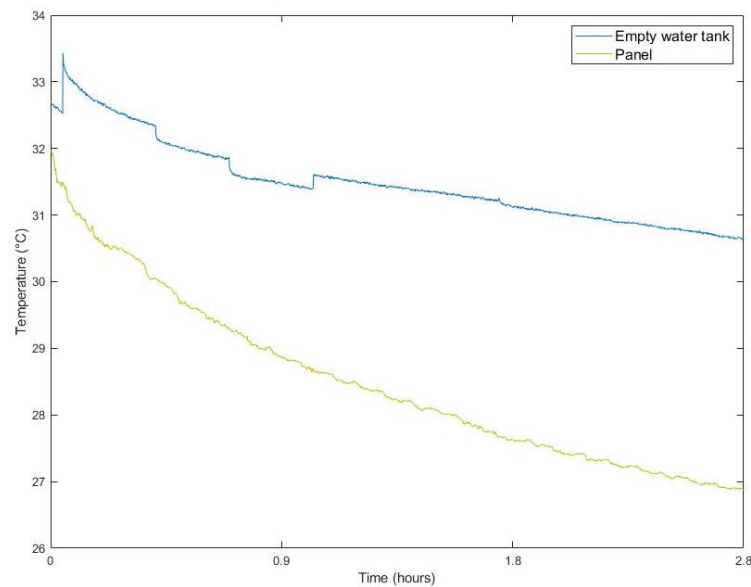


Figure 5.33 Aluminium pouch in water tank temperature, test 1.

#### 5.2.5.2 S27 pouch panel in the water tank

A set of four S27 plastic pouch panels were allocated in the water tank testing, as shown in Figure 5.34 and had a total panel weight was 7.7.

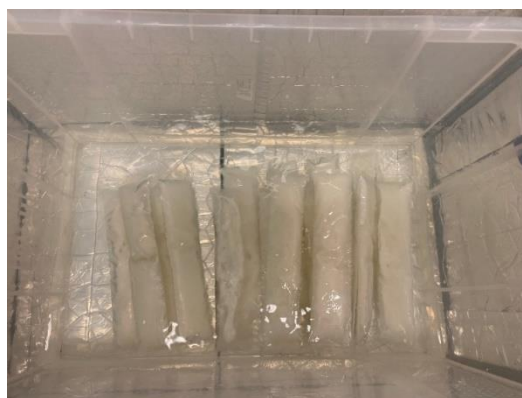


Figure 5.34 S27 pouch panel in the water tank.

Figure 5.35 presents the testing results, the temperature drop for the S27 panes was 5.19 °C over four hours. In contrast, the empty water tank



presented a temperature drop of 3.3 °C. It is important to mention that leakage was presented during the testing evaluation.

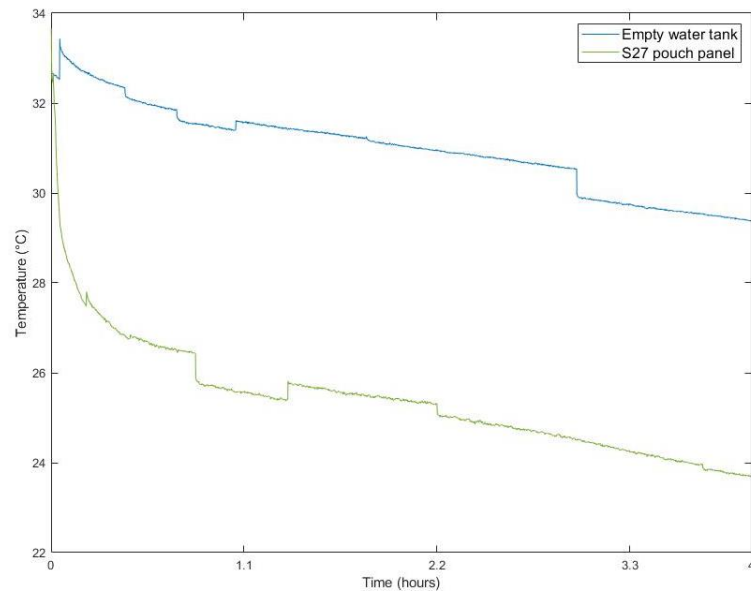


Figure 5.35 S27 pouch panel in the water tank, test 1.

### 5.2.5.3 A28 blister panel in the water tank

Figure 5.36 shows the A28 panel in the water tank, in this experiment the water temperature was set at 32 °C, the temperature loss was monitored for 2.7 hours. It was ensured that the PCM panels were fully submerged underwater.



Figure 5.36 A28 blister panel in the water tank.

It is seen in Figure 5.37 that the A28 absorbs the water heat in the first minutes of its submersion. The testing results for the A28 blister panel



present a temperature drop of 7.2 °C, while the empty water tank had a natural loss of 2 °C over the testing period.

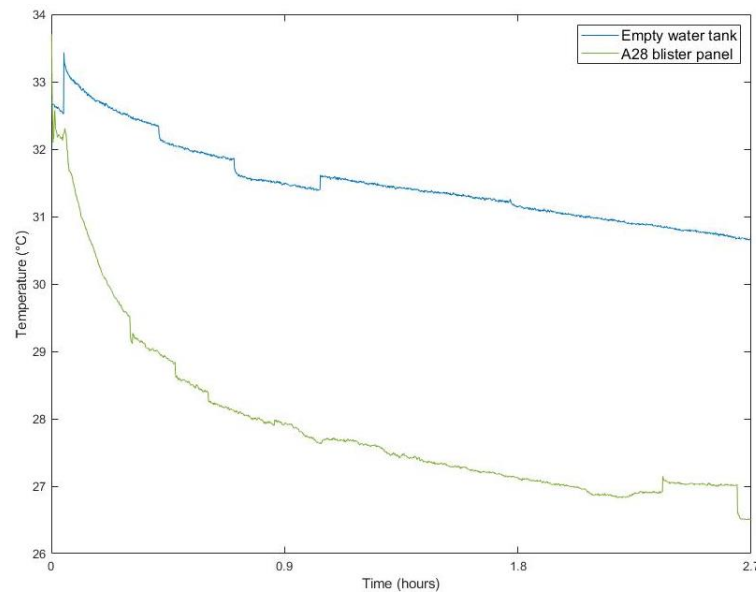


Figure 5.37 A28 blister panel in the water tank, test 1.

#### 5.2.5.4 S27 capsule in the water tank

Figure 5.38 presents the S27 capsule panel in the water tank testing, a set of 9 panels were used in this experimental evaluation with a total weight of 2 kg. This panel was thermally sealed by an external company and uses the idea of a capsule container. For the experimental process, the water initial temperature was set at 32 °C and the experiment lasted 7 hours.



Figure 5.38 S27 capsule panel in the water tank.

Figure 5.39 presents the water temperature variation with capsule panels. It can be noted that blister panels with S27 absorb heat from the water, which indicates the melting performance of the PCMs. The temperature difference was 4 °C and the experiment was maintained for 5.3 hours.

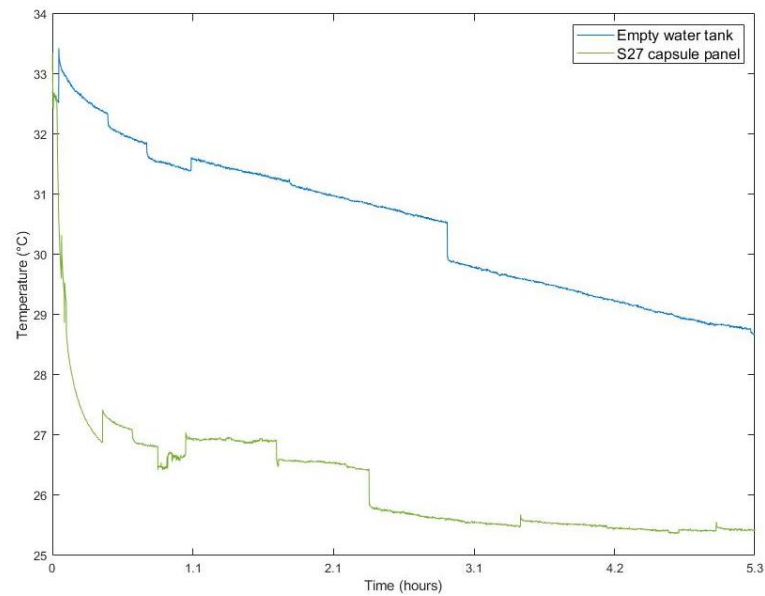


Figure 5.39 S27 capsule blister in the water tank, test 1.

#### 5.2.5.5 Corrugated straws in the water tank

A set of 10 corrugated straws were filled with INERTEK 26 for testing having a PCM total weight of 0.012 kg per straw with a total weight of 0.403 kg. Figure 5.40 presents the experimental setting, the initial water temperature was set at 30 °C,



Figure 5.40 Corrugated straws with INERTEK 26 the water tank.

Figure 5.41 displays the testing results. The temperature drops in both case scenarios present a considerable difference, the empty water temperature loss was 1.2 °C, while the corrugated straws had a temperature drop of 3 °C over three hours.

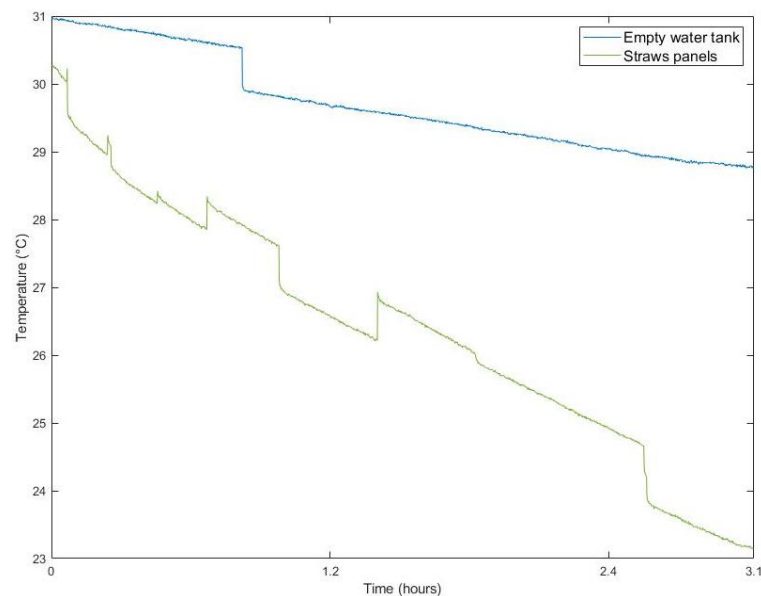


Figure 5.41 Corrugated straws, testing results in water tank.

#### 5.2.5.6 Straight straws in the water tank

The straight straws were tested in the water tank kg as shown in Figure 5.42. The experiment considered 29 straws equivalent to 0.0154 kg with a net amount of PCM of 0.125 kg.

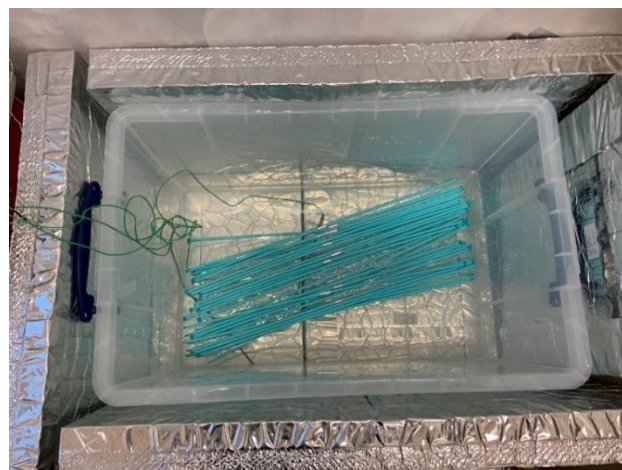


Figure 5.42 Straws in water tank.

Figure 5.43 presents the comparison between the straight straws and the corrugated straws. In this case, it is noticed that the straight straws are able to absorb more heat in the water tank; this could be due to the amount of PCM material (0.0154 kg), in comparison to the corrugated straws (0.012 kg). The straws provide a lightweight solution as an encapsulation method. However, to consider them as an effective encapsulation method the PCM quantity should increase as it would be reflected on the heat capacity absorption.

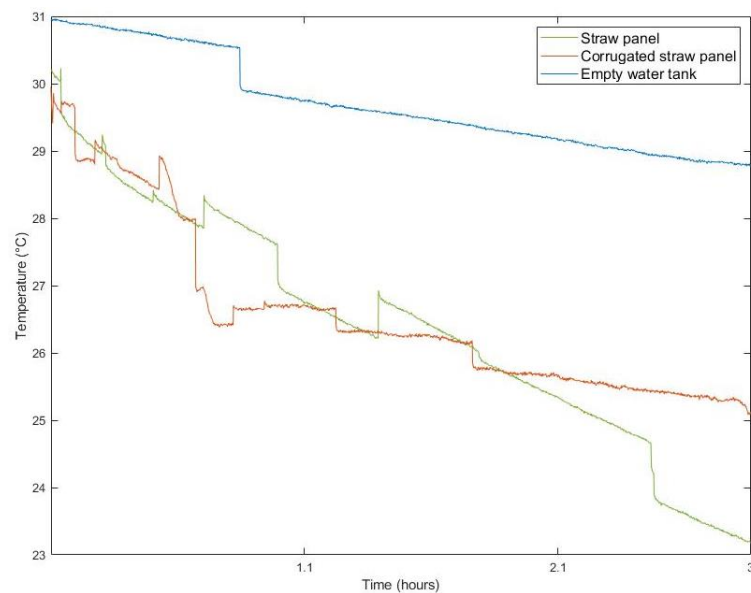


Figure 5.43 Straws comparison in water tank.

### 5.2.6 PCM panel performance comparison

All the preliminary testing for the different encapsulation methods is summarized in Table 5.4, including complementary results of some of the encapsulation methods, previously describe. To provide a better understanding on the performance of the encapsulation methods, some of the proposed containers have been tested with different PCMs, the weight may vary between each analysis, as additional panels may have been added. The environmental chamber temperature varies in each test,

the aim is to ensure the phase transition of the PCM, in some cases, the starting melting temperature has been chosen as a parameter, however through the experimental analysis it was seen a better response when the chamber temperature exceeded the melting temperature, hence the difference in the testing temperatures. The  $\Delta T$  presents the temperature variation between the inlet and outlet when the environmental chamber was used, similarly, it presents the temperature difference between the start and end temperature in the water tank testing.

Table 5.4 Testing record of encapsulation methods.

Panel	PCM	Weight (kg)	Testing method	Temperature (°C)	$\Delta T$ (°C)	Testing time (hr)
Honeycomb	INERTEK 23	1.178	E. Chamber	28	1.72	4
Honeycomb	INERTEK 23	5.672	E. Chamber	25	2.4	6.2
Honeycomb	INERTEK 23	1.178	E. Chamber	33	3.8	23.4
Honeycomb	INERTEK 23	1.178	E. Chamber	27	3.3	28.8
Honeycomb	A28	4.0	E. Chamber	30	4.75	2.4
Metallic panel	S23	4.0	E. Chamber	23	0.09	4.7
Metallic panel	S23	4.0	E. Chamber	23	0.13	22
Metallic pot	INERTEK 26	2.074	E. Chamber	30	2	5.4
Metallic pot	INERTEK 26	2.074	E. Chamber	32	2.3	2.3
Metallic pot	INERTEK 26	2.074	E. Chamber	32-35	2.6	6.1
Aluminium pouch	INERTEK 23	2.214	E. Chamber	27	1.25	23
Aluminium pouch	INERTEK 23	2.214	Water tank	32	5.89	2.8
Pouch panel	S27	11.27	E. Chamber	28.5	1.16 1	5.7
Pouch panel	S27	11.27	E. Chamber	33	3.7	6
Pouch panel	S27	11.27	E. Chamber	27	1.33	8.2
Pouch panel	S27	11.27	E. Chamber	30	3.35	6.3
Pouch panel	S27	11.27	E. Chamber	35	3.35	31

<b>Pouch panel</b>	S27	11.27	E. Chamber	27-30	6.1	4.6
<b>Pouch panel</b>	S27	11.27	E. Chamber	33	3.7	6
<b>Pouch panel</b>	S27	11.27	Water tank	32	5.1	4.1
<b>Blister</b>	INERTEK 23	0.597	E. Chamber	27	0.61	6.1
<b>Blister</b>	INERTEK 23	0.597	E. Chamber	28	0.79	6.9
<b>Blister</b>	INERTEK 23	0.597	E. Chamber	23-25-27	0.34	6.1
<b>Blister</b>	S23	2.1	E. Chamber	30	1.22	3.8
<b>Blister</b>	A28	1.208	E. Chamber	29	4.31	3.5
<b>Blister</b>	A28	1.208	Water tank	32	0.9	2.8
<b>Capsule</b>	S27	2.647	E. Chamber	32	2.4	6.3
<b>Capsule</b>	S27	8.8	E. Chamber	35	2.8	6.4
<b>Capsule</b>	S27	2	Water tank	32	6.8	5.8
<b>Corrugated straws</b>	INERTEK 26	0.613	Water tank	30	5.6	3
<b>Straws</b>	INERTEK 26	0.0154	E. Chamber	30-32-34-36	2.6	6
<b>Straws</b>	INERTEK 26	0.0154	Water tank	30	7.1	3

Figure 5.44 comprises the comparison relationship between the panel weight and the temperature difference of the inlet and outlet extracted from Table 5.5.

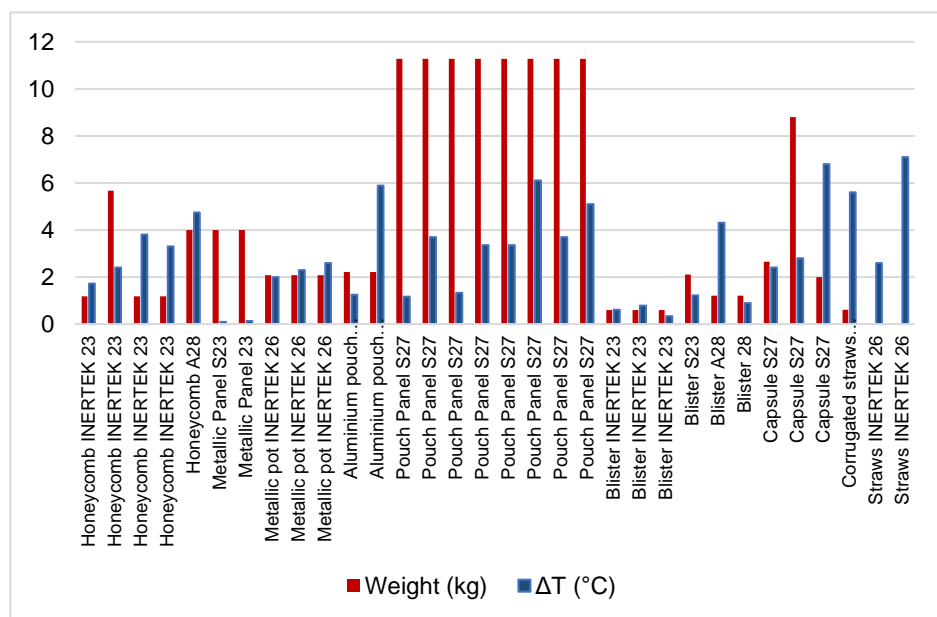


Figure 5.44 Results comparison by weight and temperature difference.

### 5.3 Solid desiccant selection

An ideal dehumidifier material would have high moisture absorption and at the same time lower regeneration temperature (Singh, Mishra and Das, 2018). Solid desiccants include a wide variety of materials such as silica gels, molecular sieves, metal-organic frameworks, polymers, among others.

The selection of the solid desiccant material would depend on the specific application. There are different parameters to consider, such as the thermo-physical properties, availability, and cost. The dehumidification and regeneration performance of a solid desiccant-based system is expected with high water adsorption capacity, good renewability at relatively low regeneration temperature, low desorption energy input, and high durability.

Represented in Figure 5.45, MOFs have higher adsorption in comparison to the rest of the desiccant materials. Nevertheless, the regeneration temperature can reach up to 90 °C which complicates their application for building incorporation. In contrast, clay-based composite solid desiccant materials have relatively lower regeneration temperatures (e.g., 35 °C to 55 °C), which indicates that low-grade heat sources can be utilised for regeneration.

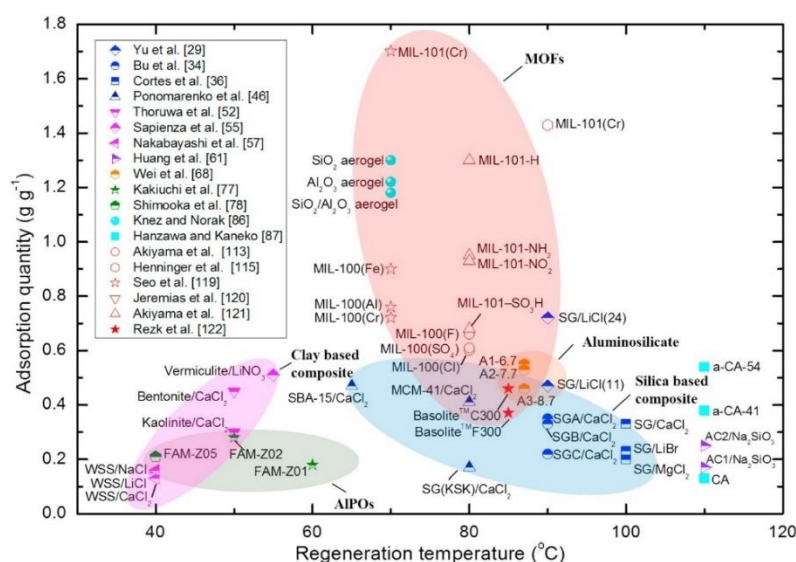


Figure 5.45 Water adsorption quantity and regeneration ability of desiccant materials (Zheng, Ge and Wang, 2014).

For the preliminary experimentation, silica gel has been selected for comparison analysis, due to its commercial availability, low cost and high humidity performance. The major drawback of this material is its regeneration temperature, this could complicate its suitability for building integration. The second material proposed for comparison purposes is vermiculite, which in contrast to silica gel presents lower regeneration temperatures. Moreover, vermiculites are low cost and highly available, environmentally stable and have a high affinity for pairing with salts, making them suitable for composite applications (Sapienza *et al.*, 2012; Casey *et al.*, 2014a; Shkatulov *et al.*, 2020).

### 5.3.1 Environmental chamber testing setup

To analyse the effect of the solid desiccant materials, the environmental chamber and test box described in section 5.2.3 were utilized. The experimental setup consisted of a control box of 70 x 67 x 73 cm, in which the composite materials were allocated over a metallic mesh, as shown in Figure 5.46. The measurements were made using a humidity sensor



(EK-H4 Sensirion) coupled with Digital Humidity Sensor SHT7x (RH/T), with a standard deviation of  $\pm 1.8\%$  RH and  $\pm 0.3$  °C. Sensors were placed in the inlet, outlet as shown in Figure 5.47. The inlet and outlet had openings of 18 cm diameter, with airflow coming from the Environmental Chamber blown through with the assistance of an electric fan.

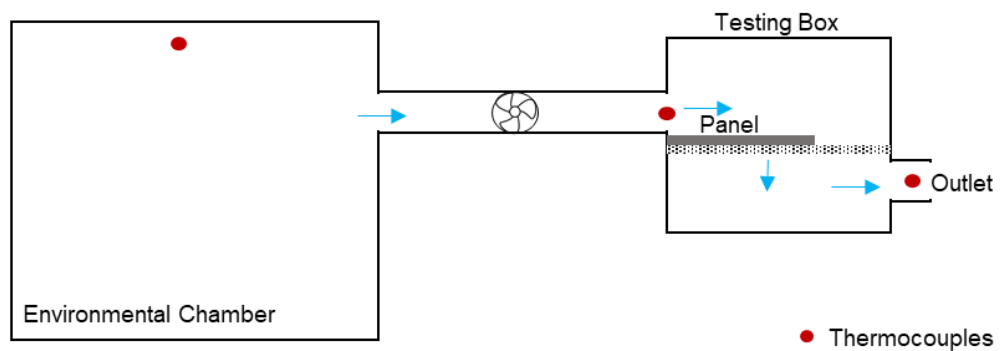


Figure 5.46 Schematic diagram of the experimental apparatus for solid desiccants.

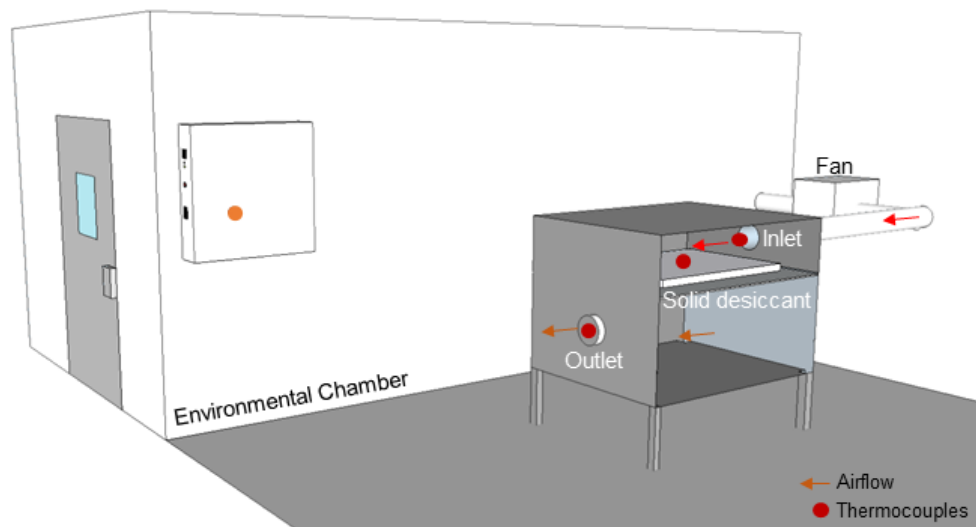


Figure 5.47 Experimental rig for solid desiccants.

The silica gel was placed in a fabric material that ensured proper contact with the air moisture. To ensure the maximum performance of the material, before testing the panel was placed in an oven for 24 hours at 85 °C to ensure the silica gel was dried.

Before testing, the panel was let to cool down, after this period it was placed on the top shelf of the control box ensuring the minimum exposure.

The absolute humidity, relative humidity and temperature were monitored. Additionally, the sample weight was compared before and after the test. Two panels of different weight measurements were created, the panel design is presented in Figure 5.48.



*Figure 5.48 Silica gel testing panel.*

Figure 5.49 presents the testing results of panel A; in this case, the test duration was set for 18 hours. The silica panel was placed in the testing box and the chamber temperature was set at 27 °C and the Relative Humidity at 80%. The initial panel weight was 3.442 kg and presented a weight gain of 0.69 kg equivalent 16% adsorption rate.

Figure 5.50 presents the testing results of panel B; in this case, the test duration was set for 4 hours. The silica panel was placed in the testing box and the chamber temperature was set at 20 °C and the Relative

Humidity at 75%. The initial panel weight was 2.62 kg and presented a weight gain of 0.20 kg equivalent 7% adsorption rate. Both panels present a difference in the absolute humidity between the inlet and outlet, suggesting the ability of the panels to continue the moisture adsorption. Understandably, the difference between the inlet and outlet tends to decrease as the time-span increases.

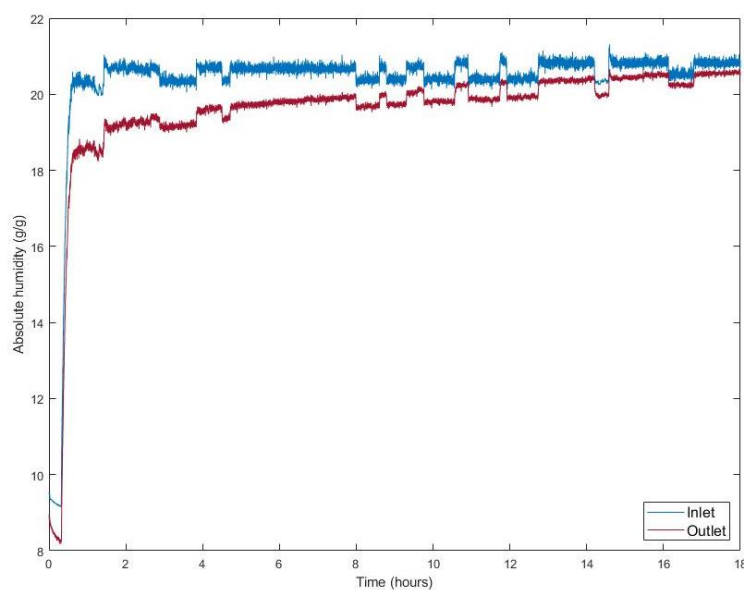


Figure 5.49 Silica gel humidity adsorption, panel A.

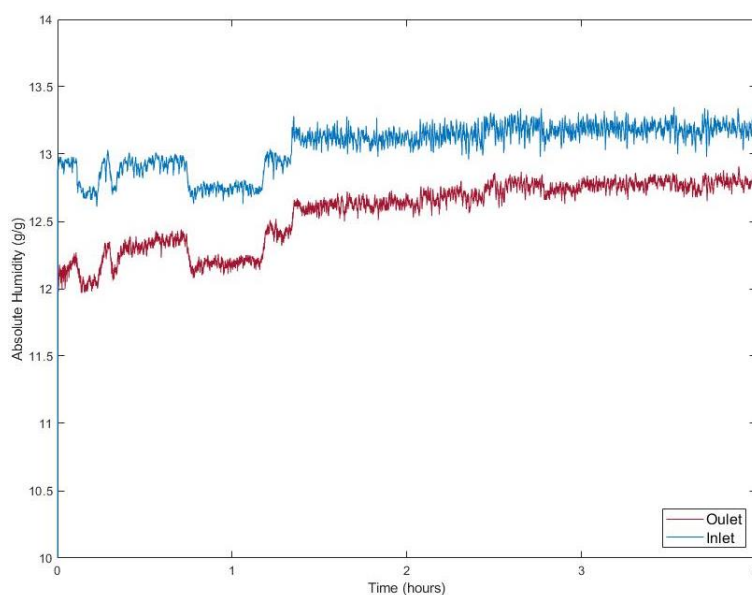


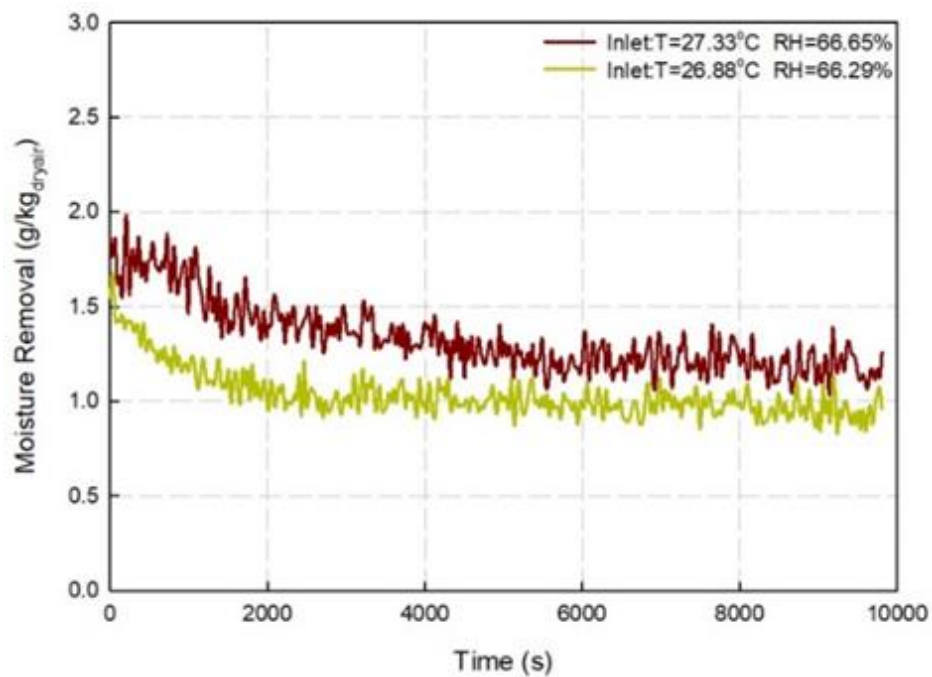
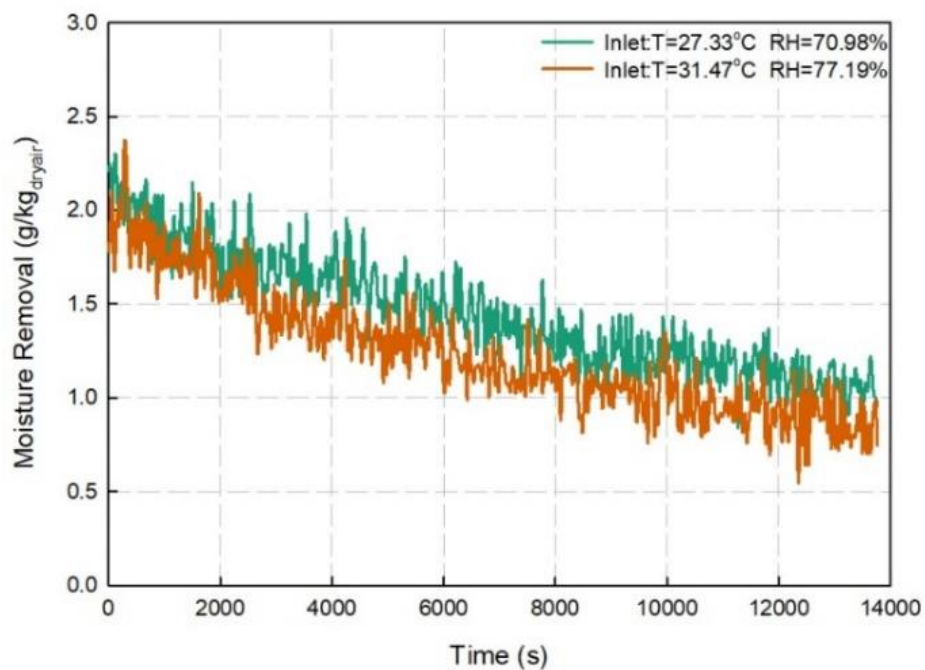
Figure 5.50 Silica gel panel humidity adsorption, panel B.

The suitability of a solid desiccant is based on two main conditionings, the first and most important one is the humidity adsorption performance and the second one is its ability to regenerate at low temperature. For building integration, the available sources of heat to suitable for the solid desiccant regeneration range between 55 °C to 70 °C. For this reason, the silica gel was placed in the oven at 60 °C to analyse the regeneration performance as shown in Table 5.5. From the results, it can be observed that the reduction percentage is not directly related to the oven temperature, for example when the oven temperature is set at 80 °C the percentage reduction is lower in comparison to 60 °C, even though the testing period is longer.

Table 5.5 Silica gel regeneration in the oven.

No.	Panel	Start weight (kg)	End weight (kg)	Weight reduction (kg)	Time (hrs)	Oven temperature (°C)	Reduction (%)
1	A	4.07	3.77	0.30	3	60	7.49
2	A	3.77	3.52	0.24	20	60	6.47
3	A	3.52	3.44	0.08	24	80	2.43
4	B	2.96	2.93	0.03	1	60	1.04
5	B	3.05	2.74	0.30	20	60	9.86
6	B	2.74	2.64	0.10	24	80	3.67

Chen et al. compared the humidification performance of the silica gel was and vermiculite. In this study, Vermiculite  $\text{CaCl}_2$  and vermiculite  $\text{MgSO}_4$  -  $\text{CaCl}_2$  were compared with silica gel and silica gel- $\text{CaCl}_2$  under the same environmental conditions and having the same experimental setup as described in Figure 5.46 and Figure 5.47 (Chen, Velasco-Carrasco and Riffat, 2019). The experimental results are presented in Figure 5.51 to Figure 5.54.

Figure 5.51 Moisture removal by Vermiculite CaCl<sub>2</sub>.Figure 5.52 Moisture removal by Vermiculite MgSO<sub>4</sub>-CaCl<sub>2</sub>.

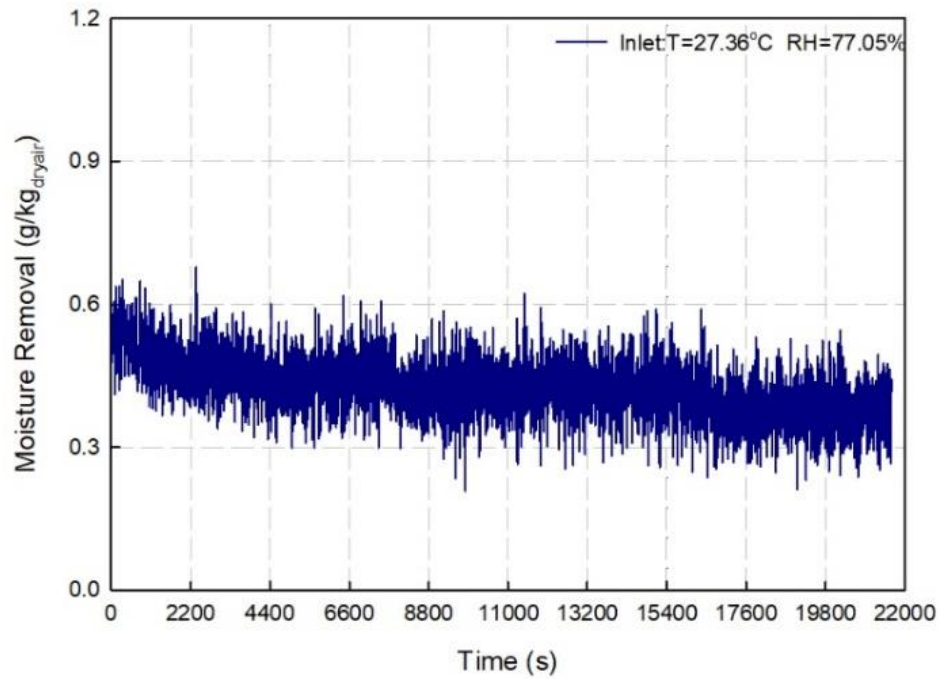


Figure 5.53 Moisture removal by silica gel.

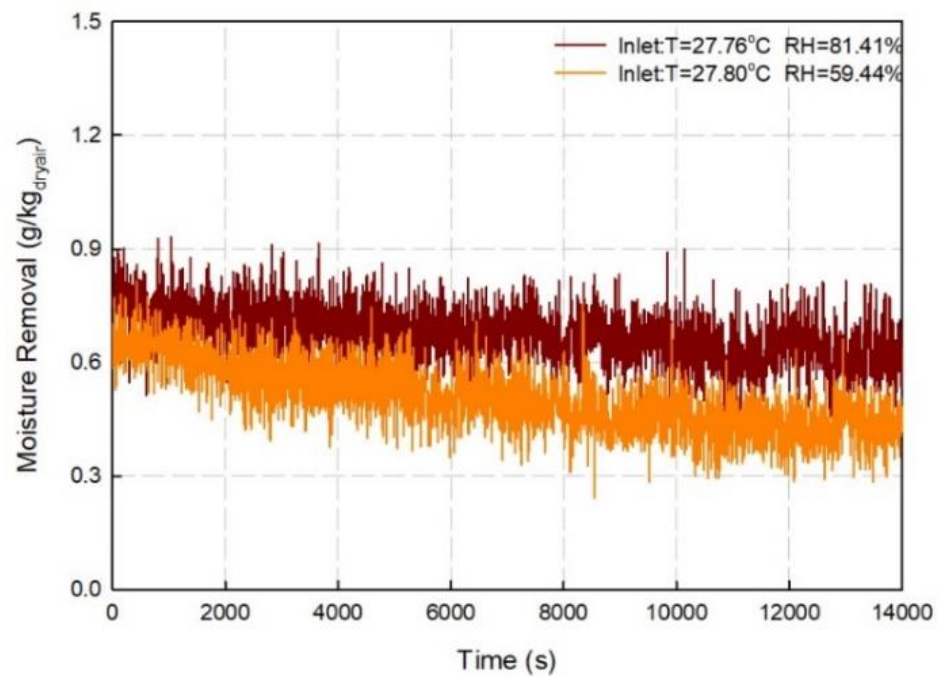


Figure 5.54 Moisture removal silica gel-CaCl<sub>2</sub>.

As mentioned in the literature silica gel is a widely used dehumidification material. Nevertheless, during the experimental evaluation the performance of the silica gel was outdone by the vermiculite composite material. The study revealed that higher dehumidification performance

was observed for both Vermiculite- $\text{CaCl}_2$  and Vermiculite- $\text{CaCl}_2\text{-MgSO}_4$  in comparison to both the silica gel and silica gel-  $\text{CaCl}_2$ . This

Further analysis on different composite materials is detailed in Chapter 6, where the adsorption performance of four different composite desiccants is evaluated and compared.

## 5.4 Summary

### 5.4.1 PCM panel testing

Several PCM panels have been developed and analysed, having a wide range of innovative solutions that include honeycomb structures, metallic panels and pots, pouches, blisters and straws containers. In addition, different types of PCMs have been tested, including paraffin A28, salt hydrates S23 and S27, microencapsulated INERTEK 23 and INERTEK 26. A testing rig has been constructed to test the thermal performance of PCM panels. The environmental chamber was adopted to simulate various operating conditions. In addition, the water bath testing method has been also considered for evaluating the performance of PCM panels. Based on the experimental data, the following findings have been obtained:

- The temperature drop is directly related to the PCM quantity.
- Depending on the quantity of the PCM, the phase change does not occur instantly. Typically, long periods are required for the phase change to occur.
- Pouched PCM panels provided a lightweight solution for encapsulating PCMs, with a favourable thermal performance.

However, the leakage problem has been noticed which affects the application in ceilings.

- The capsule panel containing S27 performance was satisfactory, however, the weight is considerably higher in comparison to the blister panel. The blister panel containing INERTEK 23 had the best performance of all the PCM tested, as a larger temperature drop is noted using less amount of PCMs.

For building integration, the manufacturing process must be considered, In this case, all the PCM panels were handcrafted, which in some cases represented having leakage problems.

#### 5.4.2 Solid desiccant testing

Based on the literature review in Chapter 2, vermiculite has been suggested as a suitable option for building dehumidification. To analyse the performance of the vermiculites, silica gel has been used as a reference material to analyse the performance. Silica gel is one of the more popular solid desiccant materials as they are widely used in adsorption processes because of their high mechanical and thermal stability and functional groups on the surface of the pores. In this case, the silica gel adsorption and regeneration performance, finding that the material struggles to regenerate in the oven with a temperature of 80 °C, difficulting its application for building incorporation. Furthermore, an experimental evaluation developed by Chen et al. has been used to compare the performance of both materials, proving the effectiveness of the vermiculite over the silica gel (Chen, Velasco-Carrasco and Riffat,



2019). The adsorption enhancement methods for the vermiculite will be further analysed in Chapter 6.

Based on the experimental data, the following findings have been obtained:

- The difference between the inlet and outlet measurements suggests the ability of the silica gel panel to absorb moisture, this is proven by the panel weight gain.
- Evidently, the difference between the inlet and outlet tends to decrease as the time-span increases, as the absorbances performance is reduced.
- The regeneration of the silica gel was not meet with the oven temperature at 80 °C, higher temperatures are recommended to dry the material. However, due to this factor, the application for the tri-modular system is not suitable.
- Higher dehumidification performance was observed for both Vermiculite  $\text{CaCl}_2$  and Vermiculite  $\text{MgSO}_4$  -  $\text{CaCl}_2$  in comparison to both the silica gel and silica gel-  $\text{CaCl}_2$ . Proving the adsorption capacity of vermiculites over silica gels.

# Chapter 6 Experimental results: heating, cooling, and humidity control in buildings

## 6.1 Introduction

The preliminary work presented in Chapter 5 establishes the benchmark for the work carried out in this chapter, specifically in terms of the selection of the materials and encapsulation methods. In terms of the PCM panels, the blister panel, capsule panel, and a new commercial panel are adopted for medium scale testing. Following the promising results of the blister panel in Chapter 5, an in-depth evaluation of the thermal properties and enhancement methods is presented in this chapter. The introduction of a commercial container is assessed using the S23 and S27 for the laboratory room testing, helping increase the PCM testing amount. Lastly, the capsule container is further investigated as a promising option.

For moisture control, this chapter focuses on the development of a composite desiccant, using different enhancement materials. Four

hygroscopic salts are added to the vermiculite host matrix and the adsorbance and regeneration performance were monitored.

In addition, this chapter presents the laboratory results for the solar-assisted heat pump, using a solar simulator to investigate the performance of the solar thermal collector. The operation of the fan coil unit is also assessed, showing the system's ability to provide indoor heating.

## **6.2 Experimental results on PCM materials**

This chapter introduces the evaluation of the thermal conductive analysis of the different capsule containers. In this case, the phase transition was monitored, using different mean temperatures. This shows the efficacy of each encapsulation method, using the thermal conductivity obtained, a simulation setting was set to measure the performance in the modelled house. Following the PCM selection and previous encapsulation methods, a selection of the some of highest performance PCMs and capsule containers is further investigated. In this case, a plastic encapsulation container and the capsule container are tested using S27. The experimental evaluation was set at medium scale, using the laboratory facilities to monitor the room temperature with the PCM ceiling panels.

### **6.2.1 Thermal conductive analysis**

The thermal properties of PCMs in relation to the latent heat capacity can be measured as follows:

- DSC (Differential Scanning Calorimetry): this study evaluates the material thermal response in a series of isothermal steps or a dynamic temperature ramp. For PCMs the measurement considered the heating and cooling mode. The major drawback of this technique is that the measurement can only be performed on homogeneous and small sized samples, which difficulties the ability to assess any enhancement methods. Moreover, some results may be influenced to a great extent by the test procedure.
- T-History: measures the temperature variation during the material phase change and compares the results with a reference material. Additionally, it can be used to measure the thermal conductivity of PCMs, this study has the ability to measure larger samples.
- DHFM (Dynamic Heat Flow Meter Apparatus): this method is used to evaluate large samples (buildings components). This apparatus uses a conventional Heat Flow Meter to measure the thermal conductivity, as shown in Figure 6.1. The temperature is changed in small steps (as in DSC), and the resulting heat flux that crosses the specimen is measured. The heat capacity is determined as the ratio between the heat flow released or adsorbed by the specimen (heat flux variation) and the relative temperature increment.
- Hot-box: this technique is used for full-scale samples. The main limitations are in relation to the material thickness as it can get complicated to observe the phase transition. Moreover, the measurements of some phenomena, such as convection heat transfer, could represent a non-negligible source of uncertainty.

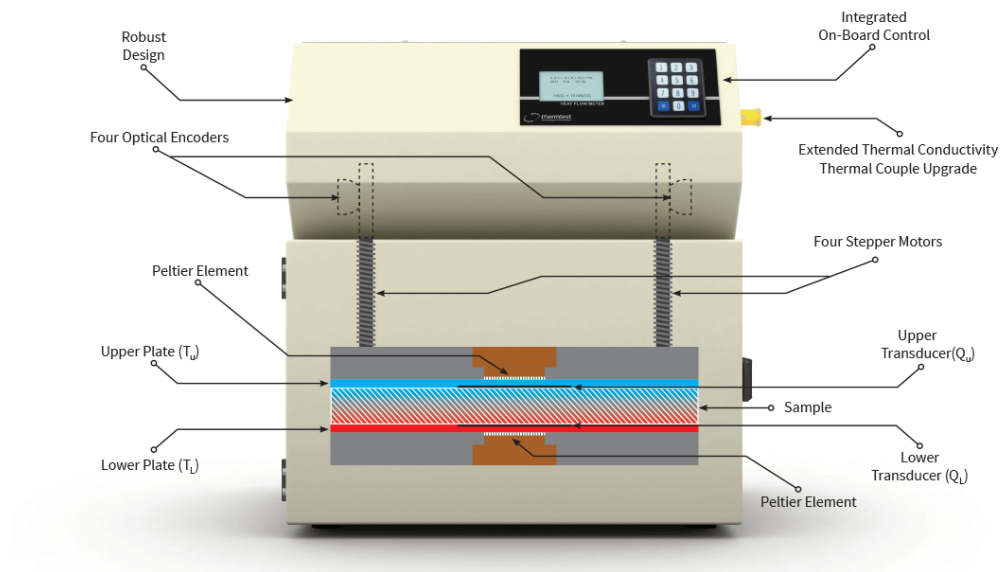


Figure 6.1 HFM-100 Heat Flow Meter.

To evaluate the thermal conductivity and enhancement performance of the PCM ceiling tiles the DHFM method has been selected, as the equipment is suitable to measure not only the PCM material but the encapsulation method as well. Providing a complete panorama of the ceiling panel performance.

The thermal response of the different encapsulation methods is presented in Table 6.1, comparing the panel phase transition and enhancement methods.




Table 6.1 Thermal conductivity analysis by panel.


Sample	Mean T. (°C)	Upper T. (°C)	Lower T. (°C)	$\lambda$ (W/Mk)	R (m <sup>2</sup> K/W)	Thickness (mm)	Weight (kg)
Corrugated Straws Inertek 23	0	-10	10	0.0762	0.2981	22.7	0.184
Corrugated Straws Inertek 23	20	10	30	0.0917	0.2945	22.7	0.184
Corrugated Straws Inertek 23	40	45	35	0.1059	0.2853	22.7	0.184
Honeycomb (plastic) A 23	0	-10	10	0.1026	0.1812	18.6	0.408
Honeycomb (plastic) A 23	20	10	30	0.1548	0.1195	18.5	0.408
Honeycomb (plastic) A 23	40	45	35	0.0964	0.1846	17.8	0.408

<b>Honeycomb (metal)</b>	0	-10	10	0.1902	0.1215	23.1	0.678
<b>Inertek 23</b>							
<b>Honeycomb (metal)</b>	20	10	30	0.166	0.1109	23.1	0.678
<b>Inertek 23</b>							
<b>Honeycomb (metal)</b>	40	45	35	0.1966	0.1211	23.1	0.678
<b>Inertek 23</b>							
<b>Honeycomb (metal)</b>	0	-10	10	0.1827	0.1286	23.7	0.306
<b>Inertek 26</b>							
<b>Honeycomb (metal)</b>	20	10	30	0.177	0.1339	23.7	0.306
<b>Inertek 26</b>							
<b>Honeycomb (metal)</b>	40	45	35	0.1489	0.1692	23.7	0.306
<b>Inertek 26</b>							
<b>PCM Idt 27</b>	-10	-20	0	0.214	0.143	30.9	0.744
<b>PCM Idt S27</b>	20	10	30	0.2261	0.1371	31	0.744
<b>PCM Idt S27</b>	40	30	50	0.3351	0.0922	30.9	0.744
<b>Blister S23</b>	-10	-20	0	0.1954	0.1576	30.8	0.388
<b>Blister S23</b>	20	10	30	0.232	0.1328	30.8	0.388
<b>Blister S23</b>	40	30	50	0.2445	0.1256	30.7	0.388

Following the results achieved by the thermal analysis, a simulation evaluation using the thermal conductivity of the PCM panels was input into the simulation software to analyse the effect of each type of ceiling panel. Table 6.2 presents the input parameters for each component.

Table 6.2 Simulation parameters based on thermal conductivity.

Capsule container	PCM	Melting Point (°C)	Heat storage capacity (J/g)	Thermal conductivity (W/Mk)	Image
<b>Corrugated Straws</b>	INERTEK 23	23-27	200	0.29	
<b>Honeycomb</b>	INERTEK 23	23-27	200	0.19	
<b>Honeycomb</b>	INERTEK 26	26-28	240	0.14	

<b>Blister</b>	S23	23	220	0.31	
<b>Plastic</b>	S27	27	220	0.31	

Following the simulation parameters established in Chapter 4 subsection 4.3.3 simulation settings, the PCM material properties were varied to measure the new thermal conductivity input found through the thermal conductive analysis and measuring how the encapsulation method affects the building thermal response. In this case, the PCM ceiling panel was considered on the ground floor as described in Figure 6.2.

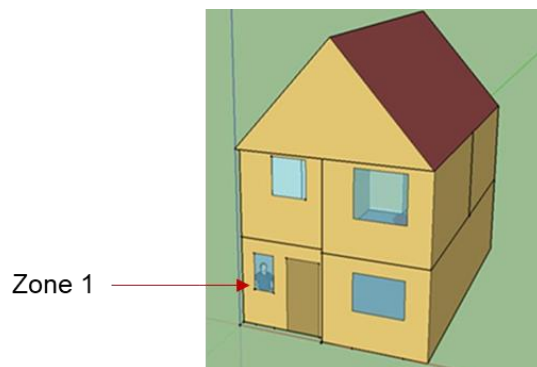


Figure 6.2 PCM ceiling tile simulation zone.

The annual indoor temperature comparison results are presented in Figure 6.6. Were after including the PCM ceiling encapsulations during the winter months a higher temperature is found and in the summer period a reduction in the peak temperatures is observed. The total amount of PCM used in the simulation corresponds to 20 kg for a 50 m<sup>2</sup>, which has created a temperature difference of +1.4 °C during winter and -1.7 °C in summer as presented in Figure 6.4 and using July as the reference month.

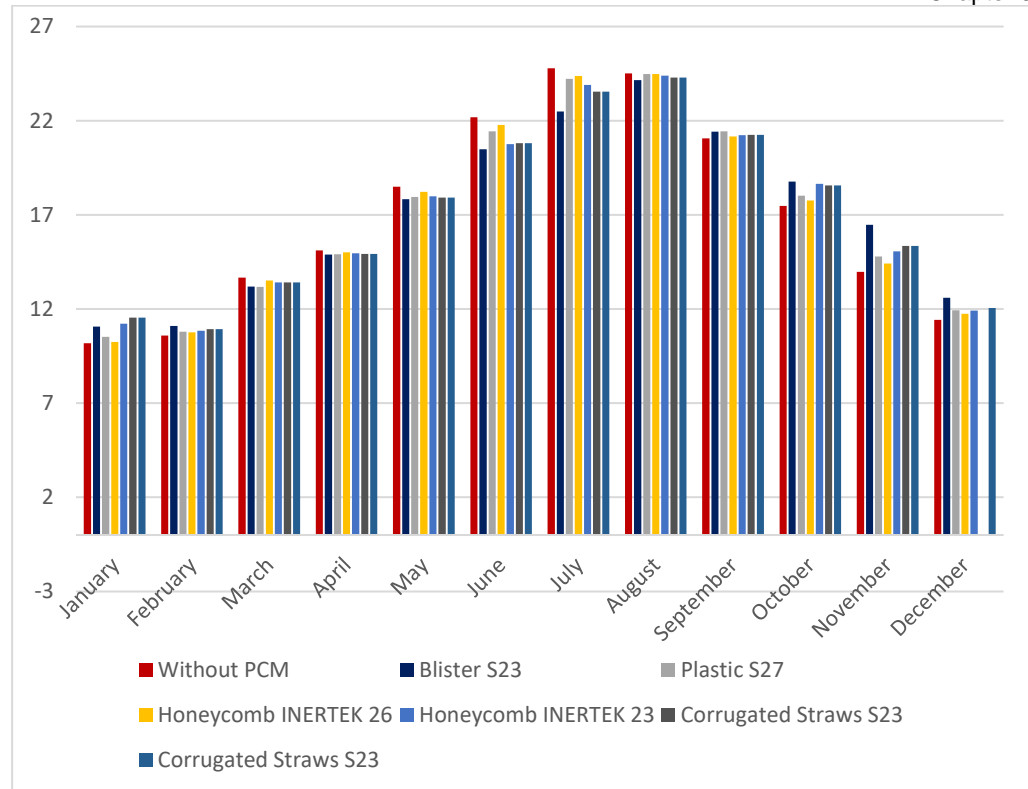


Figure 6.3 PCM ceiling annual indoor room temperature comparison.

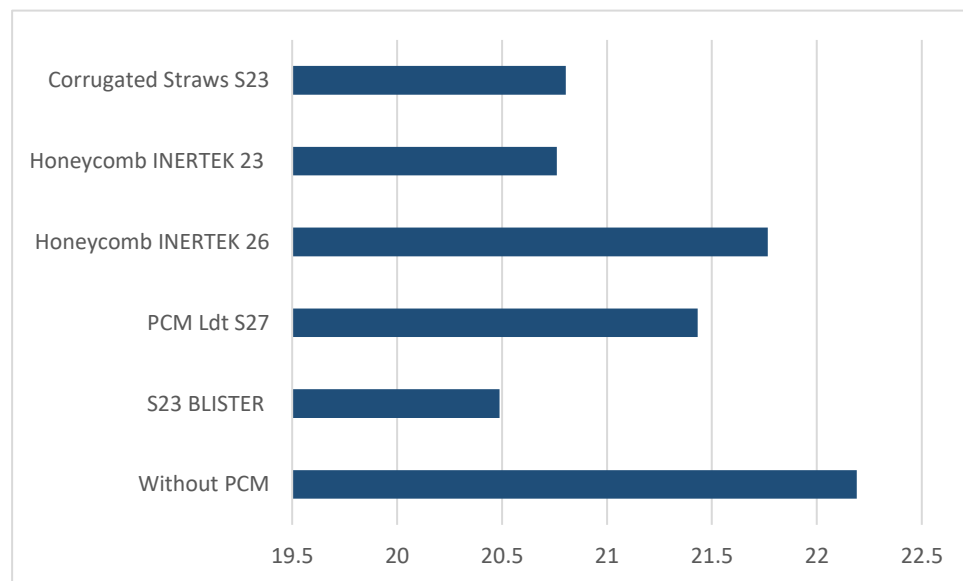


Figure 6.4 PCM ceiling indoor room temperature in July.

### 6.2.2 Blister panel INERTEK 23 and enhancement methods

The aim of this experiment was to experimentally investigate the feasibility of a novel blister PCM panel for ceiling tile applications. The thermal conductivity of steel and aluminium is further compared in Table



3, having different wt.% of the enhancement materials and the INERTEK 23. Experimental analysis of different encapsulation panels was carried out, favouring the blister encapsulation method. A set of three samples were tested, with INERTEK 23 as the base fluid: a base panel, containing only pure PCM; a second composite sample, integrating aluminium wool at 3.77wt.%; and a third composite, using steel wool at a concentration of 2.3wt.%.

Table 6.3 Blister panel enhancement method.

Sample	Mean T. (°C)	Upper T. (°C)	Lower T. (°C)	$\lambda$ (W/Mk)	R (m <sup>2</sup> K/W)	Thickness (mm)	Weight (kg)
<b>Inertek 23</b>	-10	-20	0	0.0704	0.2544	17.9	0.266
<b>Blister In 23</b>							
<b>4% Al</b>	-10	-20	0	0.0684	0.2617	17.9	0.216
<b>Blister In 23</b>							
<b>3% Steel</b>	-10	-20	0	0.0685	0.2568	17.6	0.198
<b>Inertek 23</b>	20	10	30	0.733	0.2443	17.9	0.266
<b>Blister In 23</b>							
<b>4% Al</b>	20	10	30	0.739	0.2423	17.9	0.216
<b>Blister In 23</b>							
<b>3% Steel</b>	20	10	30	0.0706	0.248	17.5	0.198
<b>Inertek 23</b>	40	30	50	0.0678	0.264	17.9	0.266
<b>Blister In 23</b>							
<b>4% Al</b>	40	30	50	0.0723	0.2516	18.2	0.216

#### 6.2.2.1 Experimental setup

Using the Environmental Climatic Chamber, the experimental setup was performed using the control box, the PCM panels were allocated over a metallic mesh. The temperature measurements were made using Type K thermocouples, and all readings were collected by the data logger (DT85), with a standard deviation of  $\pm 0.3^{\circ}\text{C}$ . Sensors were placed in the inlet, outlet, and inside the PCM blister panel, as shown in Figure 6.5.

The experiments consisted of creating an airflow through the control box at the desired temperature, in order to analyse the thermal performance

of the PCM blister panel. The aim of the methodology was to detect the panel temperature to analyse the energy storage capacity.

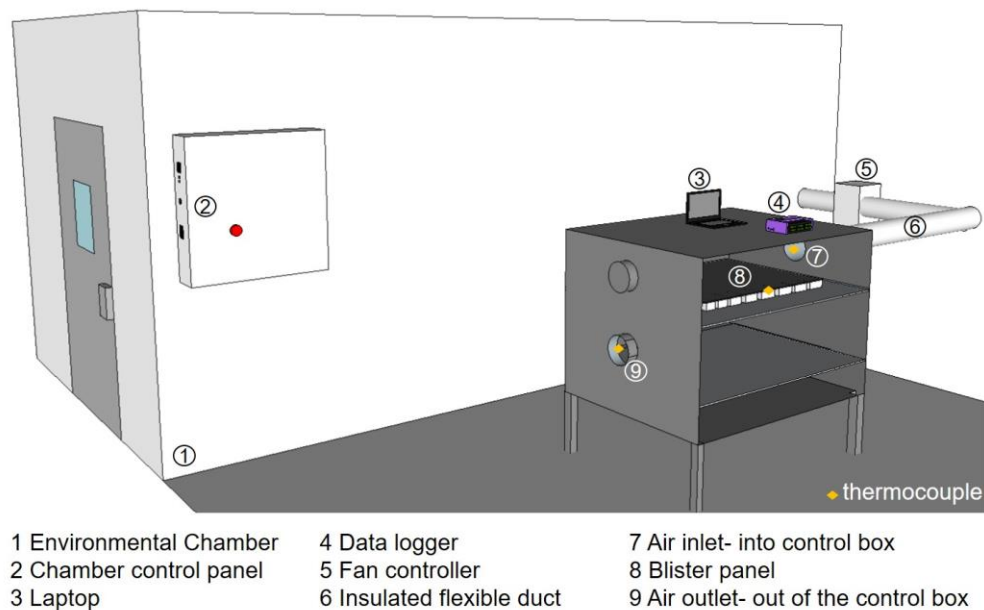


Figure 6.5 Schematic diagram of the experimental apparatus.

#### 6.2.2.2 Methodology

In the first experimental setup, the temperature was maintained constant at 28 °C to ensure the melting temperature of the PCM, whose enthalpy values range between 18 °C to 28 °C. The chamber temperature was stabilized for an hour before the testing period. After this interval, the panels were allocated over a metal mesh and the experiment began. The testing time was of 6 hours, and each test was repeated three times, during which the average temperature was noted.

In the second test, the chamber temperature was increased in two-hour intervals in order to analyse the response of the temperature over the panels. In this case, the starting temperature was considered at 23 °C and the finishing temperature was established at 27 °C. As in the first experiment, the chamber temperature was stabilized an hour before the

testing period. The testing time was 6 hours, and each test was repeated three times, during which the average temperature was noted.

The data extracted from the experiment was analysed in order to determine the thermal characteristics of the enhancement material over the PCM blister panels. The specific heat capacity of the PCM was calculated through the addition of the enhancement material to the blister panel using the following equation:

$$C_{composite} = C_{PCM} \cdot X_{PCM} + C_{matrix} \cdot (1 - X_{PCM})$$

where:

$C_{composite}$  = is the specific heat capacity of the composite, J/kgK.

$C_{PCM}$  = is the specific heat capacity of the PCM, J/kgK.

$X_{PCM}$  = is the weight ratio of the PCM to the composite.

$C_{matrix}$  = is the specific heat capacity of the matrix material, J/kgK.

### 6.2.2.3 Preparation of the composite-PCM

The sample PCM used in this research was a micro-encapsulated phase change material (MEPCMs) with granular particles ranging from 5 to 25  $\mu\text{m}$ ; the industrial reference is INERTEK 23 ©. The principle of microencapsulation is based on creating an envelope around the micro-particles in the phase change, improving the heat transfer to the surroundings while avoiding phase segregation. INERTEK 23 phase transition lies principally in the human comfort zone temperature; moreover, it has high latent heat, provides thermal stability, and avoids phase segregation. To enhance the thermal conductivity of the INERTEK

23, the addition of steel and aluminium wool particles was considered due to their low cost, light structure, and high thermal conductivity, ensuring an extended contact area with the base material.

The nano-enhanced PCM was integrated using a two-step method, in which both materials were created separately. Generally, a powder is mixed with nanoparticles with the help of magnetic force agitation (Yu & Xie, 2012). Due to the high surface area and surface activity, the powder particles tend to aggregate into the wool particles. The distribution of the materials was arbitrary as presented in Figure 6.6, and the particles fluctuated in size, geometry, and volume, as shown in Table 6.4.

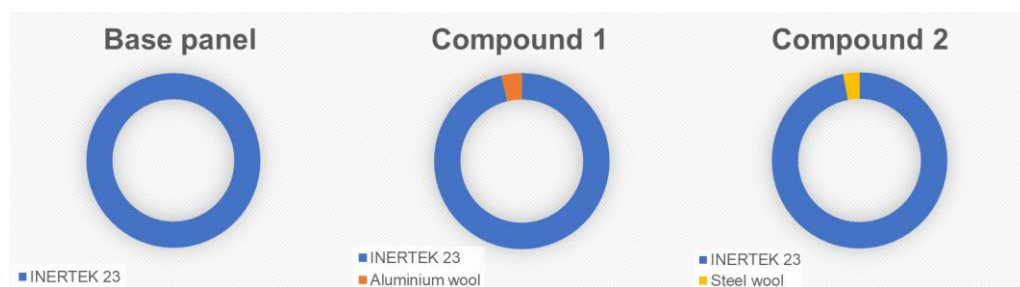


Figure 6.6 PCM blister panel schematic distribution.

Due to the manufacturing process, the proportion of the composite varies; these proportions were equivalent to weight percentages of 3.77wt.% for aluminium wool and 2.3 wt.% for steel wool.

Table 6.4 PCM blister panel composition.

Panel Name	PCM	Enhancement material	PCM mass (kg)	Enhancement mass (kg)	Total weight (kg)
Base Panel	INERTEK 23	N/A	0.538	N/A	0.538
Compound 1	INERTEK 23	Aluminium wool	0.371	0.014	0.385
Compound 2	INERTEK 23	Steel wool	0.385	0.009	0.399

#### 6.2.2.4 Panel design

The blister panel consists of an individual plastic blister measuring 15 x 15 x 2 cm. A schematic of the panel is shown in Figure 6.7. The PCM composite was allocated into the blister container and sealed with thermal conductive tape. The blister design promotes the airflow throughout the panel, facilitating the melting process of the PCM by increasing the contact area. To replicate a ceiling tile of 45 x 45 cm, an array of 3 x 3 blisters was added, having a total of 9 panels.

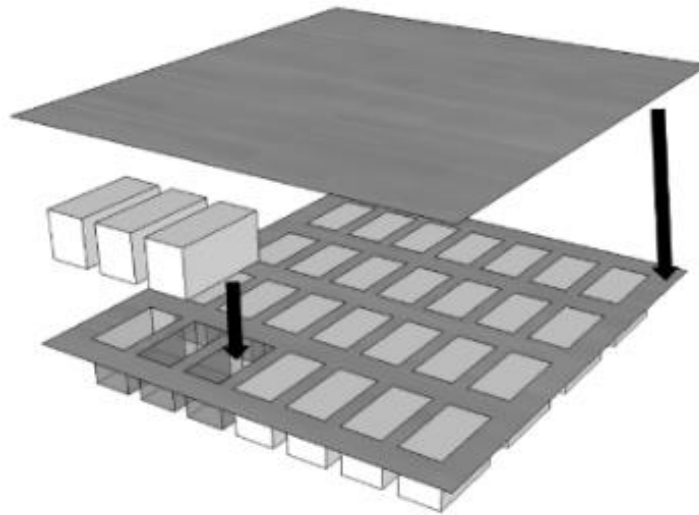


Figure 6.7 Schematic diagram of blister panel.

#### 6.2.2.5 Thermal conductive analysis

The thermal conductivity analysis is one of the main parameters considered for the application of a composite-PCM for TES buildings (Boussaba, et al., 2018). The thermal conductivity of the different samples was calculated using the HFM-100 Heat Flow Meter method, which is a popular technique for thermal conductivity and thermal resistance measurements and is presented in Figure 6.8. The equipment contains two flux sensors with a thermal conductive range between 0.005

to  $0.5 \text{ W/(m K)}$ . The temperature range varies from  $-20^\circ\text{C}$  to  $70^\circ\text{C}$ , with accuracy  $\pm 3\%$  (Thermtest, 2019). To ensure the accuracy of the measurement, an expanded polystyrene board was tested as a calibration material. The operational temperature was set at  $30^\circ\text{C}$  for the hot plate and  $10^\circ\text{C}$  for the cold plate.



Figure 6.8 Blister panel in HFM equipment.

#### 6.2.2.6 Effects of INERTEK 23 mixed with aluminium wool

The thermal performance of PCMs depends on the melting temperature, thermal conductivity, and energy storage density. According to Ji et al. and Wu et al. one commonly used technique is the dispersion of high thermal conductive nanometer-sized materials, such as nanoparticles, nanofibers, nanotubes, and nanosheets, in the PCM base fluid to significantly increase its thermal conductivity and enhance the capability of energy exchange is currently receiving increasing interest (Ji, et al., 2014; Wu, et al., 2013). This emerging mixture is called nano-enhanced phase change material and is used in both passive and active applications.

These nanoparticles enhance the properties of the PCM fluid, and the production is introduced as nanocomposite and nano-enhanced PCM.

The nano-enhance PCMs can be used in heating, cooling, ventilation, and air-conditioning systems to reduce the incompatibility between the energy supply and the demand by shifting and reduction of peak load and improving the energy performance of the buildings.

Some complications presented in the PCM application are the uncertainty of the speed of the moving solid-liquid interface, the interaction of nanometer-sized materials with PCM base fluids, and the highly nonlinear phase change characteristics make it extremely difficult to deal with the phase change problem and reliably estimate the flow and energy transport mechanisms when the materials undergo the phase transition in the melting and solidification cycles (Ma, et al., 2013).

Aluminium wool is a low-density permeable material. Thickness can range from 0.003" to approximately 2 mm for all metals. Some metals can also be rolled down as thin as 0.001" for use as an evaporation source in microelectronics, optics, magnetics, MEMS, and hard resistant coatings. The properties of the aluminium wool and the PCM thermal properties are presented in Table 6.5 and Table 6.6 respectively. As a reference, the enthalpy of the INERTEK 23 is presented in Figure 6.9.

Table 6.5 Aluminium wool composition.

<b>Molecular weight</b>	<b>Melting Point (°C)</b>	<b>Boiling Point (°C)</b>	<b><math>\rho</math> (kg/m<sup>3</sup>)</b>	<b><math>C_p</math> (Cal/g/ K @ 25 °C)</b>	<b><math>\lambda</math> (W/cm/ K @ 298.2 K)</b>
26.98	660.37	2467	2700	0.215	2.37

The PCM component is bio-based; INERTEK 23 microcapsules are made exclusively from vegetable waxes.

Table 6.6 PCM thermal characteristics.

Product		Melting area (°C)	Solidification area (°C)	Heat storage capacity (J/g (56Wh/kg))
INERTEK 23	Powder	23-27	23-18	200

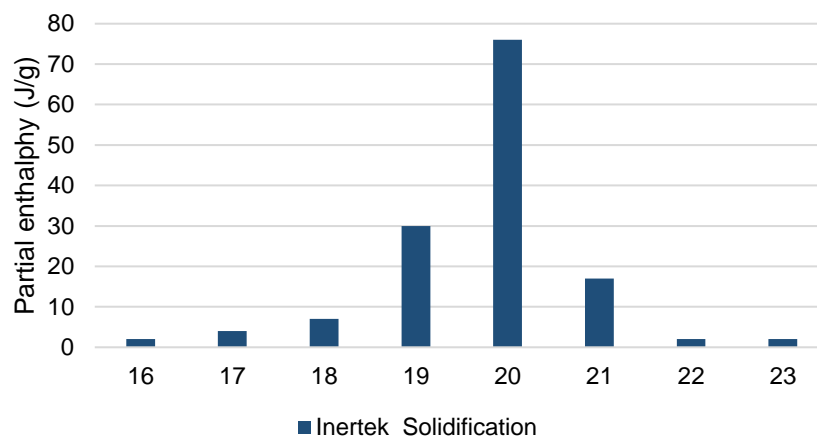


Figure 6.9 INERTEK 23 enthalpy values, (MCI Technologies).

Using a scanning electron microscope (SEM) three conditionings were analyzed, to see the effects of using aluminium wool as an enhancement material for the thermal conductivity of the INERTEK 23. The following samples were prepared:

1. Aluminium wool.
2. INERTEK 23.
3. Aluminium wool mixed with INERTEK 23.

SEM samples were prepared using the EDX detector on the 6490LV SEM machine as shown in Figure 6.10, prepared to withstand the vacuum conditions and the high-energy beam of electrons, and have to be small enough to fit on the specimen stage.





Figure 6.10 Scanning electron microscope 6490LV SEM (JEOL).

A carbon tape was utilized as a conductive adhesive to hold the samples, after a first attempt to capture the INERTEK 23 images it was determined that an ultrathin coating of gold was required to enhance the conductivity of the material. Coating with heavy metals may increase the signal/noise ratio for samples of low atomic number. The improvement arises because secondary electron emission for high-Z materials is enhanced. Figure 6.11 presents the image for the aluminium wool, it is seen the morphology of the material. The fiber is not smooth as appreciated on a larger scale.

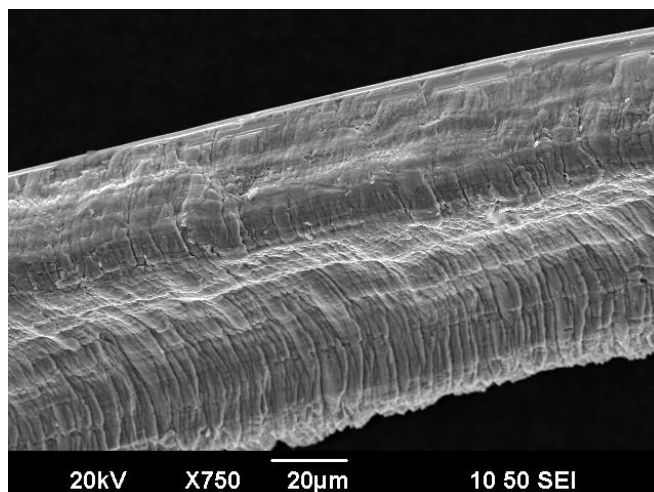


Figure 6.11 SEM Aluminium wool.

Figure 6.12 presents the image for INERTEK 23, in this image it is appreciated the particle distribution of the powder. It is seen that the

vegetable waxed is segregated among the sample, another important fact is the different particle sizes.

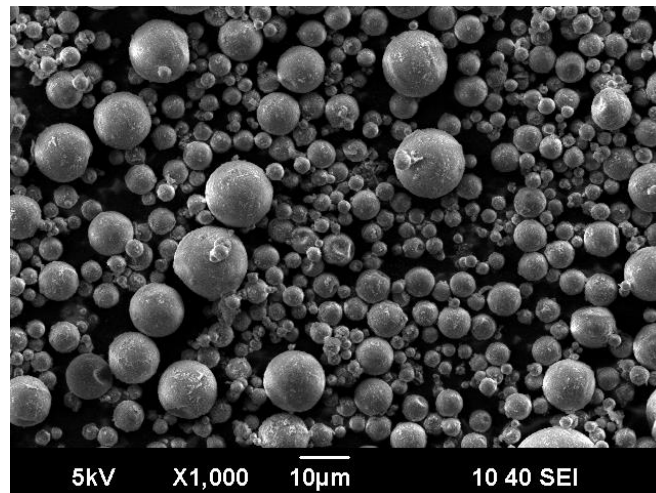


Figure 6.12 SEM INERTEK 23.

Figure 6.13 presents the mixture between the aluminium wool and the INERTEK 23.

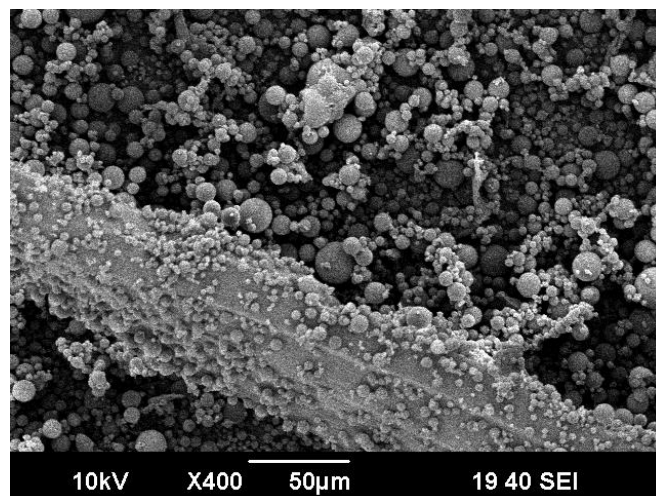


Figure 6.13 SEM Aluminium wool mixed with INERTEK 23.

Figure 6.14 presents a closer look into the aluminium wool fiber; in this case, it is further seen that the powder particles are attached to the fiber.

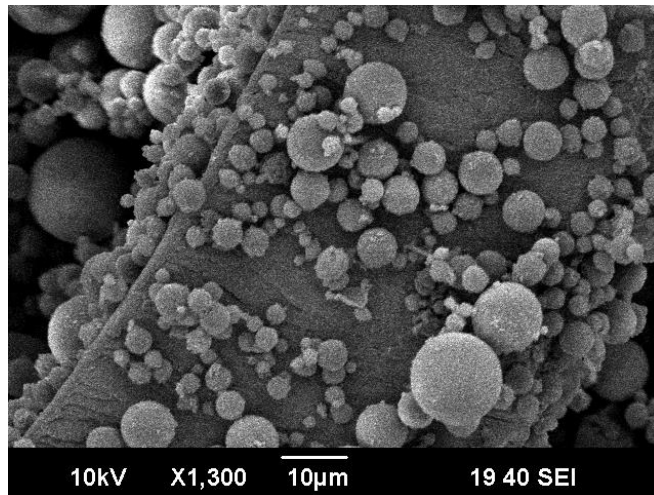


Figure 6.14 SEM Aluminium wool with INERTEK 23 close-up.

The most important fact is that it is observed that the powder particles are attached to the aluminum fiber, therefore facilitating the thermal conductivity enhancement. It is important to consider that aluminium possesses a higher melting temperature than INERTEK 23.

#### 6.2.2.7 Experimental Results

In the first experimental setup, the environmental chamber temperature was kept constant at 28 °C.

Figure 6.15 shows the panel temperature of the different samples. It can be observed that the temperature of the panels increased rapidly, as the chamber's initial temperature was higher than the PCM melting point. After the initial surge, compounds 1 and 2 stagnated after 14,005 seconds (4 hrs) of testing, while the base panel maintained temperature increments for most of the testing period. The base panel had the lowest values, reaching a maximum of 25.97 °C, with compound 1 and compound 2 presenting values of 26.17 °C and 26.34 °C, respectively.

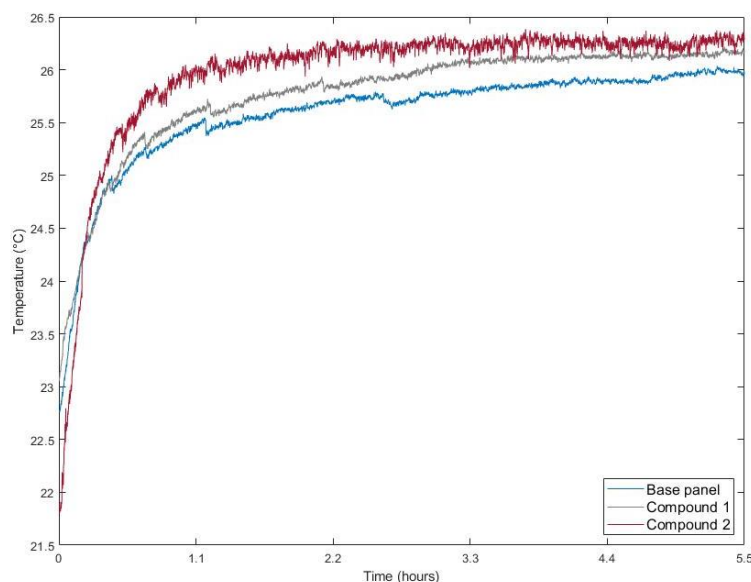


Figure 6.15 Blister panels comparison at 28 °C, test 1.

The second experimental setup compared the temperature variation of the three blister panels, as shown in Figure 6.16. The experiment was maintained for 21,600 s (6 hrs), with 2 °C increments every 2 hrs. The starting temperature was 23 °C and the finishing temperature was 27 °C. The base panel and compound 1 presented similar behaviour, with a slightly higher temperature range in the aluminium mixture, reaching 25.66 °C and 25.93 °C, respectively.

The compound 2 panel temperature levelled up once the second temperature increment was applied, and from this point onwards the temperature increased until it reached 27.11°C.

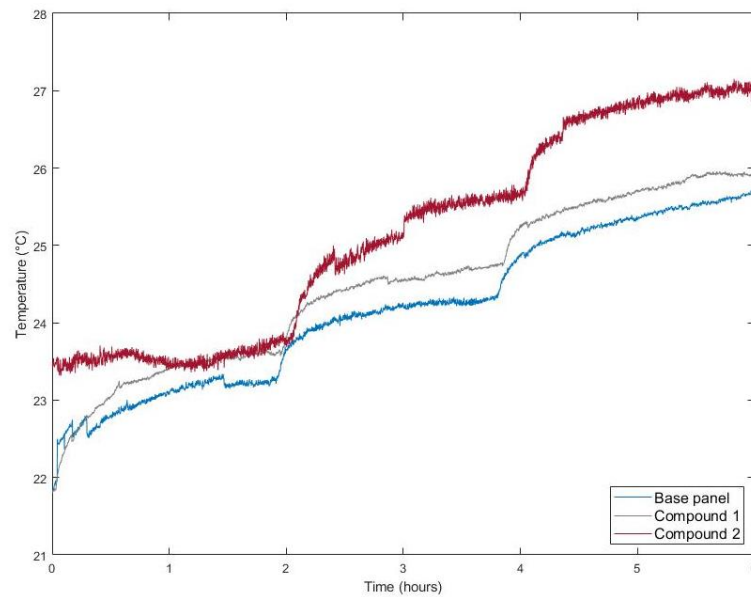


Figure 6.16 Blister panels comparison with 2 °C increments, test 2.

Based on the experimental results, the specific heat capacity was calculated to analyse the effect of the encapsulation method and enhancement material, as presented in Table 6.7. The specific heat capacity of the INERTEK 23 microcapsules was 66 (kJ/kg K), (Djamai, Si Larbi and Salvatore, 2019); that of the aluminium wool was 0.896 (kJ/kg K); and that of the steel wool was 0.502 (kJ/kg K), (Singh Rathore, Shukla, and Gupta, 2020). There are two main factors to consider when analysing heat capacity. First, the heat transfer performance is correlational to the PCM mass, thus the base panel presents higher mass in comparison to the composite panels. Second, the distribution of the particles in the PCM must be considered, as the heat transfer rate is determined by the percentage of the enhancement nanoparticles added (Abdelrahman *et al.*, 2019).

Results of the thermal conductive analysis found that the conductivity of the base panel was 0.733 W/(m K). The addition of the aluminium wool increased the thermal conductivity to 0.739 W/(m K); furthermore, the

steel particles provided thermal conductivity of 0.784 W/ W/(m K). From the experimental results, it is apparent that the addition of the enhancement material improved the thermal conductivity of the INERTEK 23.

Table 6.7 Thermal performance analysis.

Property	Base panel	Compound 1	Compound 2
Storage Heat Capacity (J/g)	200 (PCM)	200 (PCM)	200 (PCM)
Thermal Conductivity W/(m K)	0.733	0.739	0.784
Temperature Difference (°C)	2.29	3.12	3.4

From the experimental results, it is evident that the composite panels are able to adsorb more heat as the PCM melts, confirming that the aluminium and steel wool particles enhance heat transfer performance.

Blister encapsulation is a practical method to integrate the material into building elements, increasing thermal mass, reducing temperature fluctuations, and assisting in energy performance by regulating the indoor temperature. The thermal performance of three different PCM blister panels was evaluated in terms of heat adsorption capacity and thermal conductivity. INERTEK 23 was selected as the base PCM, having a phase transition range compatible with the human thermal comfort temperatures. In this study, aluminium and steel wool were selected as composite materials to enhance the thermal performance of the PCM blister panels.

The results suggest that the application of the PCM blister ceiling tiles can be considered as an innovative method for building incorporation. During the experimental procedure, the blister panels were able to absorb the heat from coming from the environmental chamber, proving that the encapsulation material was able to promote the heat exchange. Furthermore, the PCM enhancement indicates that both the aluminium

and steel wool particles improved blister panel thermal performance. This result was confirmed by thermal conductive analysis. The base panel presented a thermal at  $0.733 \text{ W/(m K)}$ ,  $0.739 \text{ W/(m K)}$  for compound 1, and  $0.784 \text{ W/(m K)}$  for compound 2. The latter, with steel enhancement, can be considered as the sample which has the highest thermal performance.

### 6.2.3 S23 and S27

The experiment was conducted in a testing room at the Sustainable Building Technology (SRB) laboratory at The University of Nottingham in the Architecture and Built Environment Department. The testing room is made of gypsum boards with an insulated roof and with a total area of  $5.49 \text{ m}^2$  as shown in Figure 6.17, for this experimental evaluation a set of 14 PCM panels were allocated in the ceiling room to evaluate the thermal performance, representing 25% of the surface area. The PCM panels can be appreciated in Figure 6.18, where each side has 7 panels.

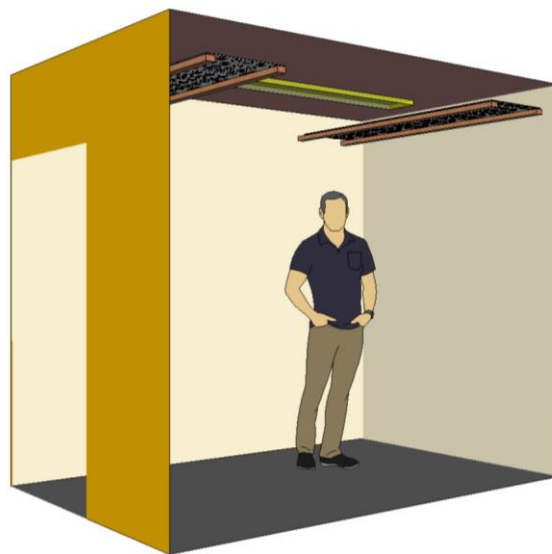


Figure 6.17 SRB laboratory test room.



Figure 6.18 Laboratory testing room.

### 6.2.3.1 Materials

The encapsulation material was filled with two different types of PCM, both salt hydrates from the PlusICE family developed by PCM Products Ltd ©. The first PCM is the S27 and has a melting point of 27 °C, the second PCM is the S23 and has a starting melting point of 23 °C and the specific heat capacity for both materials was 2.20 kJ/kg K. The capsule container consists of a rectangular container with a length of 24 cm x 49 cm, with a weight of 3.558 kg as shown in Figure 6.19.

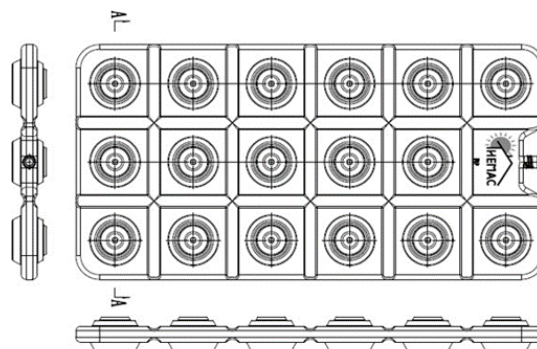


Figure 6.19 Encapsulation container.



### 6.2.3.2 Measurement equipment

The aim of the measurements is to determine the changing of the ambient temperature during the charging and discharging process, the PCM panels are displayed in Figure 6.20. The panels were charged using a radiator with a heat capacity of 2 kW and the room temperature loss was monitored after ensuring the complete charging of the PCM. The temperature measurements were made using Type K thermocouples, and all readings were collected by the data logger (DT80), with a standard deviation of  $\pm 0.3$  °C. In total 5 thermocouples were allocated in the testing room as depicted in Figure 6.21. A thermocouple was allocated at medium height in all the walls and an additional thermocouple was placed inside the PCM panel.



Figure 6.20 Panels mounted.

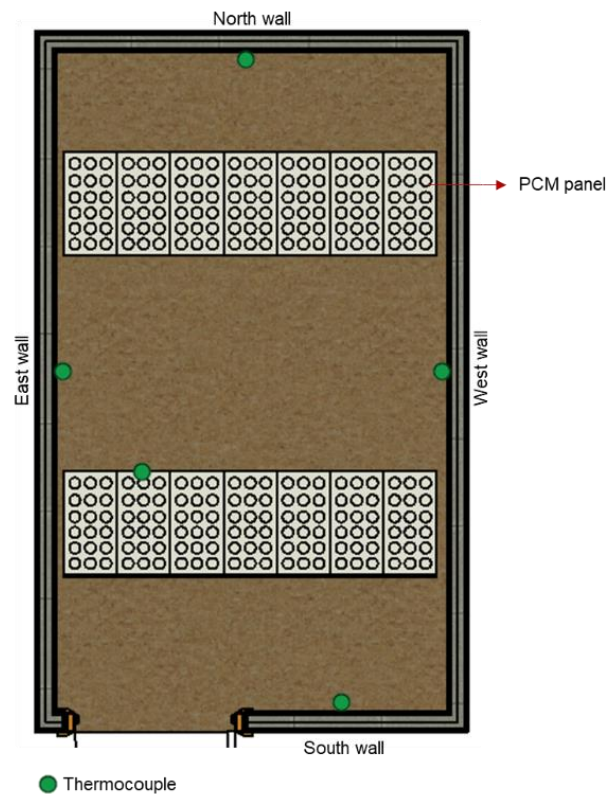


Figure 6.21 SRB testing room layout.

### 6.2.3.3 Measurement procedure

In order to analyse the effect of the PCM panel on the ambient temperature, the empty room temperatures were monitored as a benchmark. During the experimental procedure, the heating device was switched on until the melting point was achieved; thus, heating the room and consequently heating the PCM panels. To ensure the melting of the PCM panels the heating temperature reached up to 29.35 °C, furthermore, the PCM panels were visually inspected to verify the complete phase transition to a full liquid state. After the heating phase, the regeneration period took place ensuring the full freezing point, using the natural heat loss to the ambient.

6.2.3.4 Thermal images

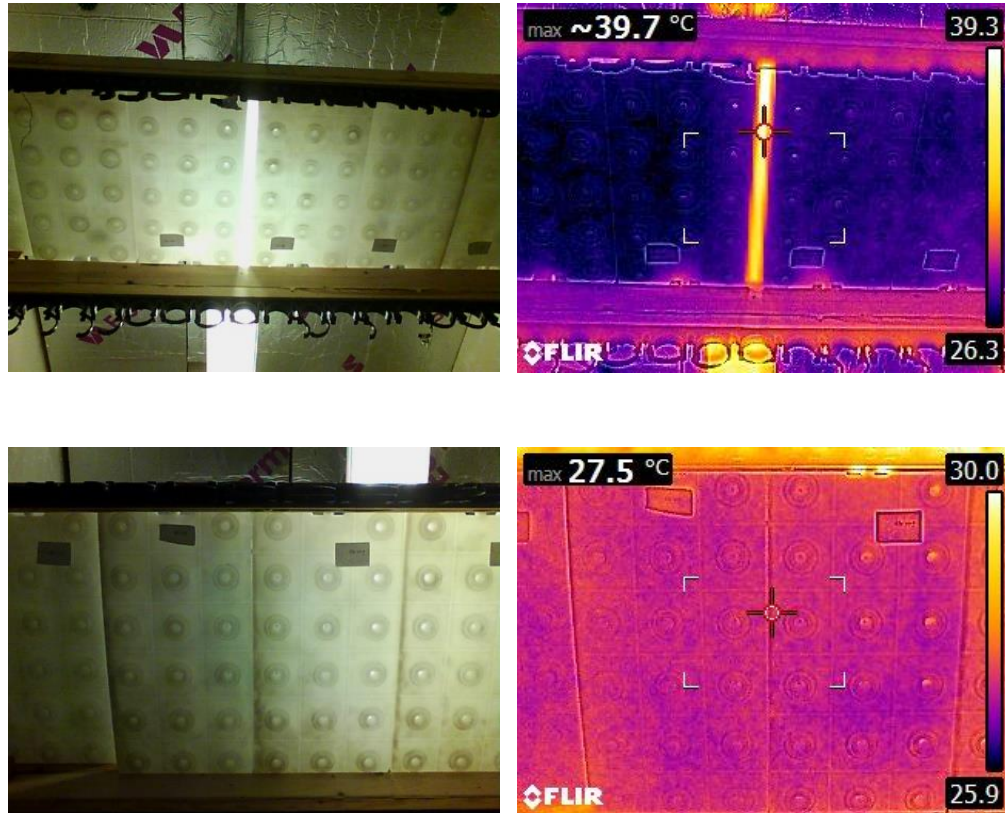
Pictures of the experimental setup were obtained using a thermal image camera (FLIR E5), with 19,200 pixels (160 x 120) and a temperature range of -20 °C up to +250 °C and accuracy of  $\pm 2\%$ , as shown in Figure 6.22. The thermal images presented in Table 6.8 and display the room temperatures, it is shown that the highest temperature is produced by the lamp with a maximum temperature of 39.5 °C while the PCM panel temperature was found between 25.9 to 26.5 °C.



Figure 6.22 Thermal camera.

Table 6.8 Thermal camera comparison analysis of S27.





#### 6.2.3.5 Heating results

Figure 6.23 presents the typical heating period without PCM in the testing room. In this case, the room temperature starts increasing after one hour of heating, reaching 23 °C; after 2.30 hours the temperature reaches 27 °C. The starting temperature was 17.03 °C and the final temperature was 29.35 °C, with a temperature difference of 12.32 °C.

The PCM effect over the room temperature can be observed in Figure 6.24. in which the heating temperature is compared. The heating mode shows the progress of the room heating, both with and without the 12 PCM panels. The graph presents the radiator temperatures at the top and room average temperature at the bottom. It is observed that the room temperature increases considerably when the PCM ceiling tiles are



placed, having an average temperature difference of 2.95 °C. It is also noticeable that the panels help maintain constant ambient temperatures.

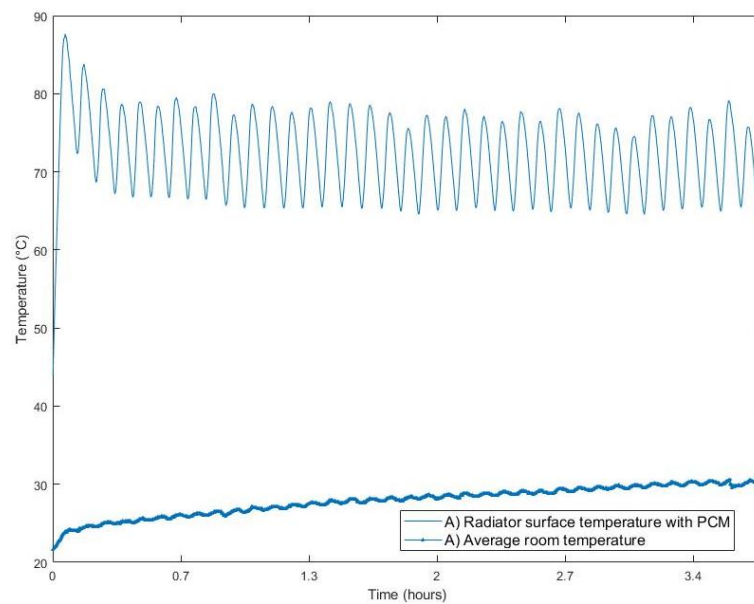


Figure 6.23 S27, heating without PCM.

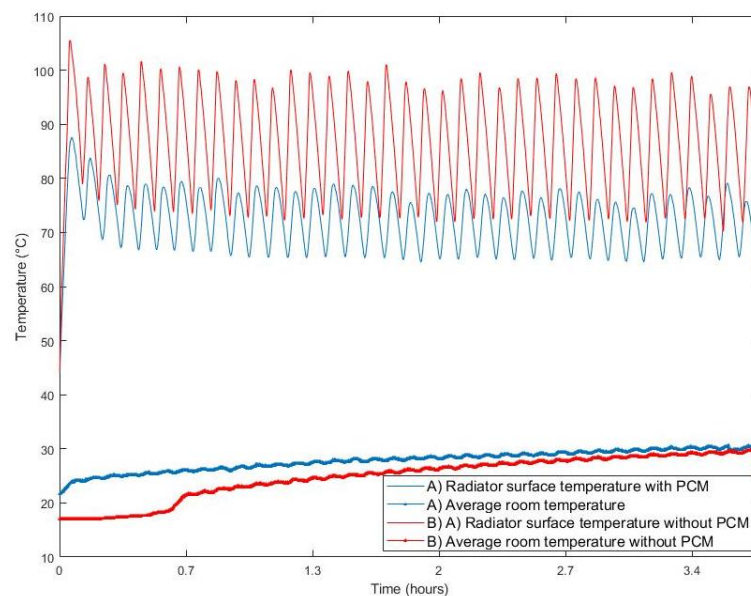


Figure 6.24 S27, heating temperature comparison.

### 6.2.3.6 Cooling results

Figure 6.25 exhibits a typical measurement for cooling purposes. In this case, the room was pre-heated for 7 hours and after this period the cooling interval started. It is seen that the highest room temperature is

presented when the PCM panels are placed. The average temperature of the room without PCM was 23.07 °C; in contrast, the room with the S27 was 23.97 °C.

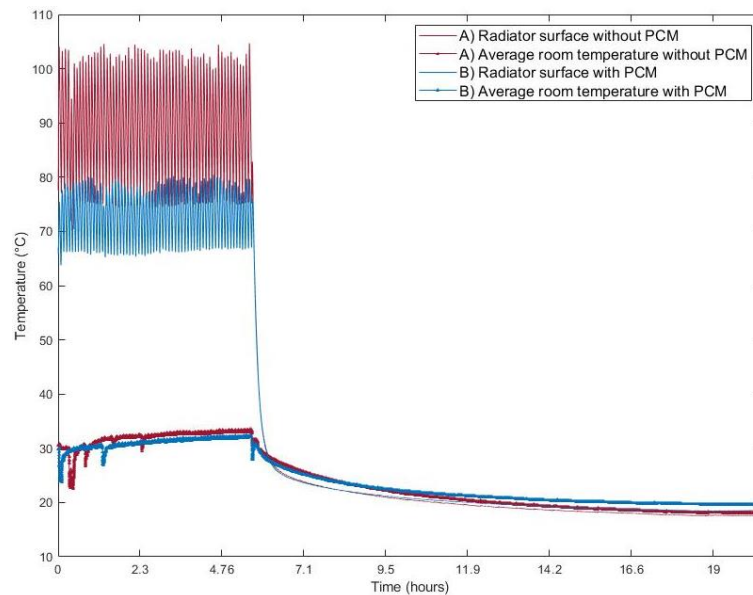


Figure 6.25 S27 representative cooling data.

The cooling properties are monitored as depicted in Figure 6.26 having 14 PCM panels corresponding to 49.81 kg. Initially, the room was heating for 24 hours after this time-lapse the radiator was turned off and the cooling period started. It is observed that the S27 was able to maintain higher temperatures, whereas the room without PCM presents a 1.7°C temperature decrement.

Increasing the PCM quantity creates a higher temperature difference as shown in Figure 6.27. In this case, the number of PCM panels was 30, corresponding to 106.74 kg. The room was heated for 24 hrs before the radiator was turned off and the cooling period started. It is observed a maximum temperature difference of 3.3°C after 11.2 hrs.

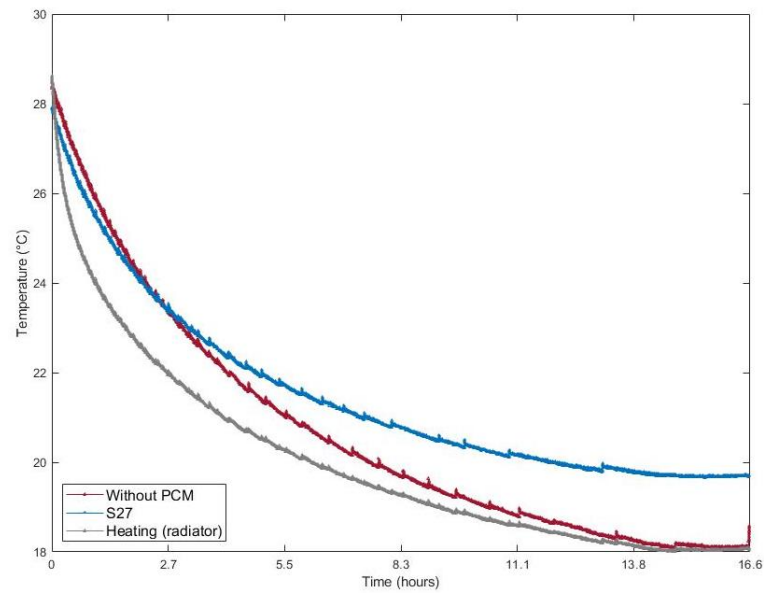


Figure 6.26 Cooling temperature comparison (14 panels).

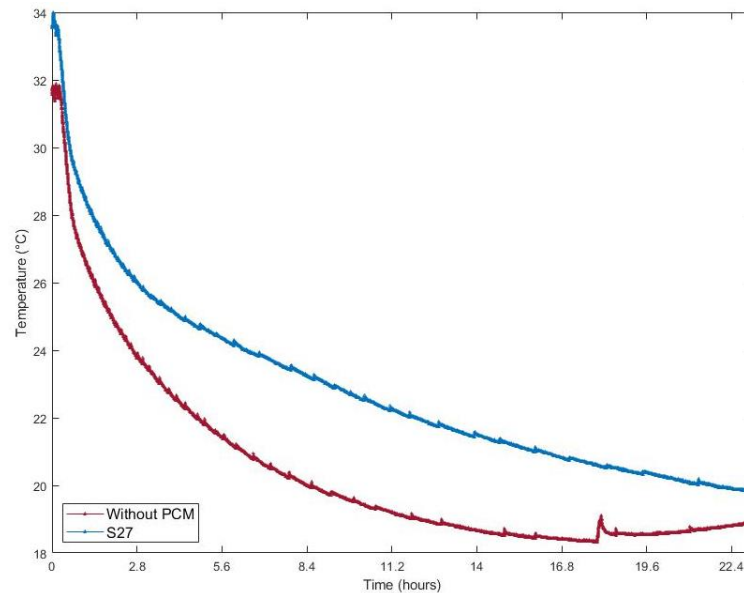


Figure 6.27 Cooling temperature comparison (30 panels).

The room ambient temperature was able to present higher temperatures with the addition of the PCM panels. In comparison, the room with PCM achieves 2.95 °C more than the room without PCM. The PCM quantity affects proportionally the temperature difference in the room. Having 14 panels of S27 created a maximum temperature difference of 1.7°C, while

30 panels generated 3.3°C. The PCM panels create a temperature difference of more than 22 hours.

#### 6.2.4 Capsule panel S27

Similarly, to the S27 experimental testing, the analysis of the capsule panel was performed using the S27 as shown in Figure 6.28. In this experimental evaluation, a set of 40 panels was allocated on the ceiling of the testing room as shown in Figure 6.29. The panels had a total weight of 8.640 kilos, with a PCM net amount of 5.148 kilos.



Figure 6.28 Capsule panel (10 panels).



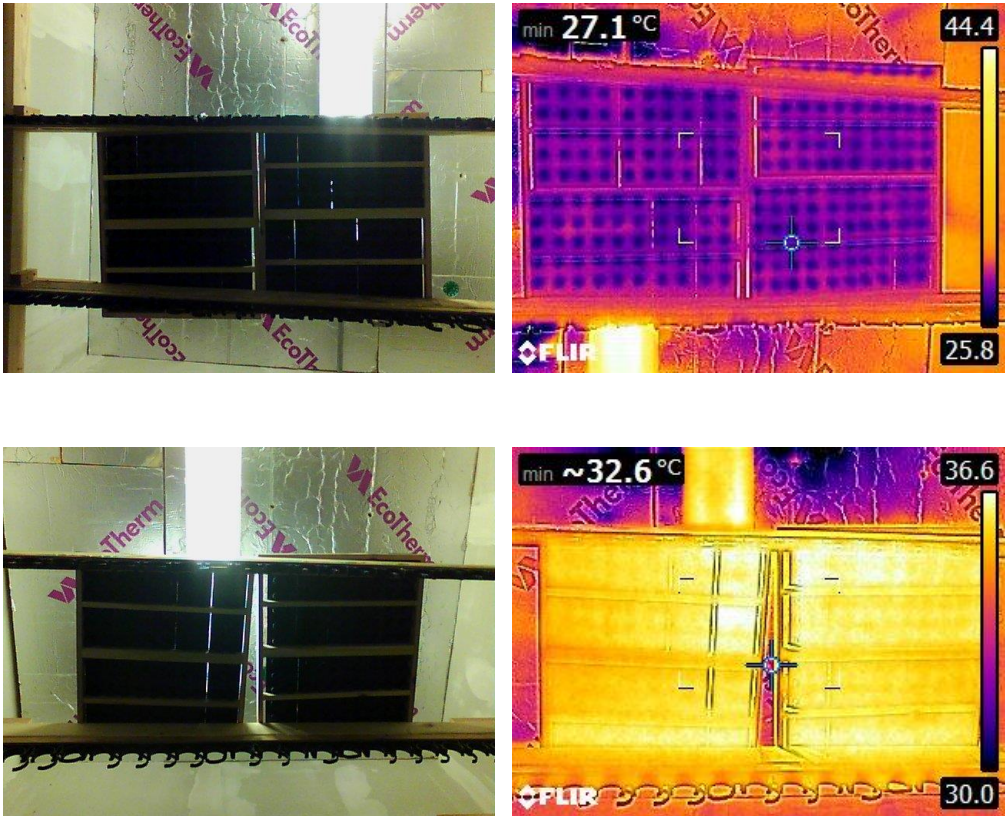
Figure 6.29 Capsule panels mounted on the testing room.

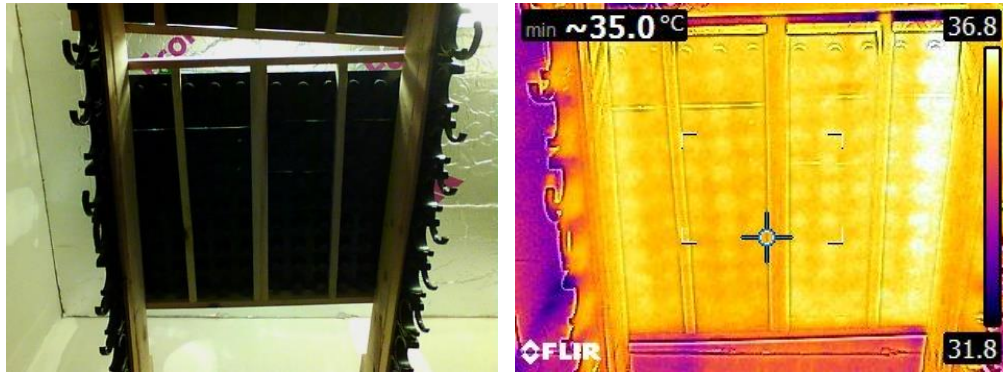


6.2.4.1 Materials

The encapsulation material was composed of a plastic container cover with an aluminium material that promotes thermal performance. In this case, the capsules are spread across the panel to promote the airflow of the S27 with a length of 24 cm x 49 cm and a weight of 0.216 kg. The thermal images are presented in Table 6.9 display the room temperatures. The images show that the PCM panels have the highest temperature, ranging between 25.8 °C to 30 °C.

Table 6.9 Capsule panel thermal images.





#### 6.2.4.2 Heating results

Figure 6.30 presents the capsule panel heating period and compares it with the empty room temperature. In general, the room temperatures without PCM are more stable, while the PCM room temperature increases constantly throughout the testing period. The maximum temperature for the S27 capsule is 29 °C, in contrast, the room without PCM has a temperature of 26.7 °C.

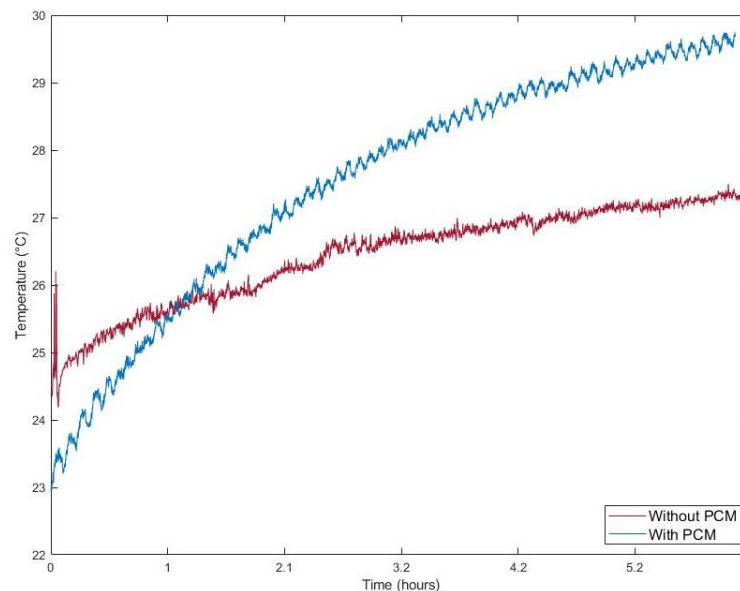


Figure 6.30 Capsule panel, heating temperature comparison.

Figure 6.31 presents the cooling period of the capsule panels. The testing duration was of 17 hours and it can be noticed that in this case, the room without PCM has lower temperatures, meaning that the S27 capsules

were able to sustain higher room temperatures, with an average of 24.8 °C.

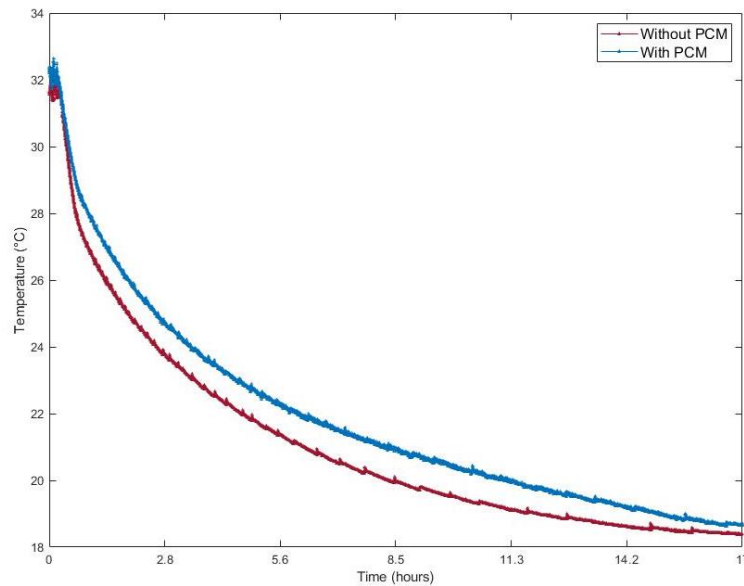


Figure 6.31 Capsule panel, cooling temperature comparison.

In general, the integration of the S27 capsules improves the testing room temperature performance for the heating and cooling periods. During the heating stage, the PCM panels were able to adsorb the room heat as demonstrated by the thermal images and graph description, showing the effectiveness of the encapsulation method. In the cooling period, the capsule panel was able to maintain higher room temperatures during the prolonged testing period, showing the effectiveness of the material to control the room peak temperatures. For building integration, a higher amount of PCM would be required in order to reach greater thermal performance.

### 6.3 Experimental results on vermiculites

To achieve thermal comfort the humidity should also be contemplated. For this reason, it is important to regulate the humidity levels, solid

desiccant materials can be installed in different rooms depending on the building requirements and zone distribution. The panel can easily adsorb and retain the moisture, the quantity should also be based on the room conditions. For example, the humidity levels in wet zones as the bathroom or kitchen area would be considerably higher than in other rooms such as the living space or bedrooms. Ideally, the solid desiccant would be easily incorporated in the building and its application would not be conditioned to an area, nevertheless, the connection to the heat pump system must be considered for regeneration purposes.

The selection of vermiculite as a suitable material for building incorporation has been based on the literature review and preliminary testing comparing its performance. The comparison of four different enhancement materials containing vermiculite as the base host matrix is analysed. Four hygroscopic inorganic salts have been selected  $\text{KHCO}_2$ ,  $\text{CaCl}_2$ ,  $\text{MgSO}_4\text{-CaCl}_2$ , and  $\text{LiCl}$ , to compare the effect as enhancement materials and raw vermiculite was selected as the base sample.

The humid air is a mixture of dry air and water vapor in which three variables are required, calculated by the dry bulb temperature, total pressure, and molar fraction of water. The total pressure is given by Dalton's Law as follows:

$$P_{tot} = P_{as} + P_{ve} \quad (6.1)$$

It is possible to characterize the water vapor quantity contained in kg dry air, as follow:

$$x = 0.622 \cdot \frac{P_{ve}}{P_{atm} - P_{ve}} \quad (6.2)$$

The relative humidity is defined as the ratio of the water vapor partial pressure at the saturated water vapor pressure.

$$\phi = \frac{100 \cdot P_{ve}}{P_{v,sat}} = \frac{100 \cdot x}{0.622 + x} \cdot \frac{P_{atm}}{P_{v,sat}} \quad (6.3)$$

Where the  $P_{v,sat}$  can be calculated in function of the temperature  $T > 0$ .

$$m_d = m - m_w \quad (6.4)$$

With a mass of water:  $m_w$  and a dry mass  $m_d$ .

The solution concentration  $C_s$  is defined as follow:

$$C_s = \frac{M_s}{M_{sol}} \text{ and } M_{sol} = M_s + M_w \quad (6.5)$$

### 6.3.1 Vermiculite preparation

The vermiculite contains a pore volume  $V_p$  of 2.84 ml/g (Jarimi *et al.*, 2018). Further composite materials are prepared based on the (Casey *et al.*, 2014), where the mass sample was calculated as follows:

$$m_{salt} = \frac{m_{SIM} - m_v}{m_{SIM}} \times 100(\%) \quad (6.6)$$

Where  $m_{SIM}$  indicates the mass of anhydrous SIM composite and  $m_v$  indicates the raw vermiculite. The relation between the vermiculite and the enhancement material is 1:3. Based on the selected enhancement material, the following steps have been applied to develop a composite material:

1. To procure the maximum adsorption, the raw vermiculite was dried in an oven for 24 hrs.

2. The enhancement component was prepared by saturating water with the selected salt material in a magnetic stirrer as shown in Figure 6.32 and Figure 6.33.

Add equal amounts of water and the salt solution.

Ensure the mixture is fully integrated.



Figure 6.32 Magnetic stirrer schematic function.

Depending on the component the saturation is done by adding small amounts at the time.



Figure 6.33 Magnetic stirrer.

3. Once the solution was saturated it was left to set down for 24 hrs. Note that the addition of the enhancement material can increase the sample temperature.
4. When the solution comprehends more than one element, the water saturation is done separately with equal volumes and combined after step 3. It is important to let them set for a minimum of 30 minutes before the next step.

5. The next step is to mix the dried vermiculite (host matrix) with the enhancement material. It is recommended to slowly add the saturated solution, as depending on the sample it can present high density and/or resistance. It is important to stir constantly, ensuring the matrix was in full impregnated by the solution. Afterward, the composite is left to set for 24 hrs, Figure 6.34 shows the example of the  $\text{MgSO}_4\text{-CaCl}_2$ .



Figure 6.34 Saturated  $\text{MgSO}_4\text{-CaCl}_2$ .

6. After this period, the composite is allocated in the oven, the temperature was selected depending on the specific enhancement material. The composite might change the colour appearance once dried.

Once the vermiculite is fully dried then is ready for testing. For testing purposes, the composite material should be at ambient temperature. It is advisable that the vermiculite composite is re-heated for 2 hrs before testing; to ensure it has not adsorbed ambient humidity, however, it is important to let it cool down before the test.

To store the material a hermetic container should be used. Table 6.10 presents a visual example of the preparation procedure for the



vermiculite with  $\text{CaCl}_2$  solution. The prepared samples are presented in Table 6.11, with solutions of raw vermiculite, potassium format ( $\text{KHCO}_2$ ), calcium chloride ( $\text{CaCl}_2$ ), magnesium chloride ( $\text{MgSO}_4\text{-CaCl}_2$ ), and lithium chloride ( $\text{LiCl}$ ).

Table 6.10 Example procedure of  $\text{CaCl}_2$ .



*Dried natural vermiculite (step 1).*



*Saturated  $\text{CaCl}_2$  (step 3).*



*Vermiculite +  $\text{CaCl}_2$  mixture (step 5).*



*Composite drying in the oven (step 6).*

Table 6.11 Vermiculite samples for testing.





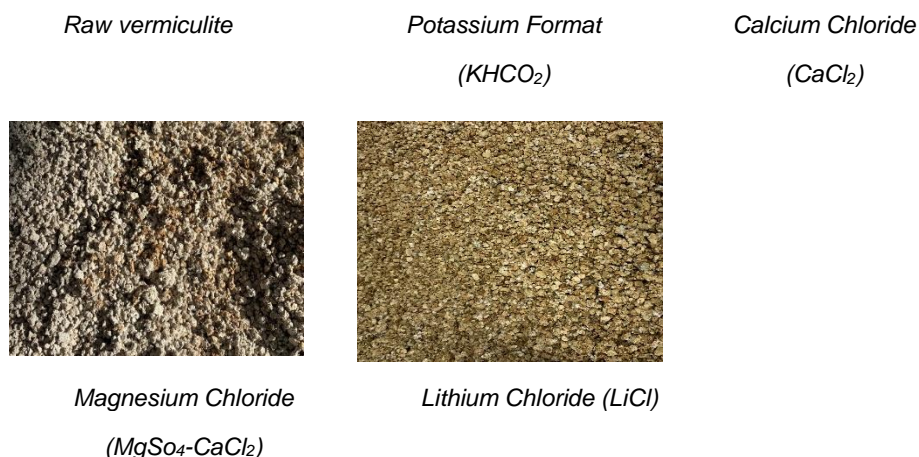


Table 6.12 presents the steps follow for the development of the composite materials. The numbers allude to the steps previously described.

Table 6.12 Vermiculite testing procedure.

Step	1	2	3	4	5	6
Raw Vermiculite	√	-	-	-	-	-
Vermiculite (KHCO <sub>2</sub> )	√	√	√	-	√	√
Vermiculite (CaCl <sub>2</sub> )	√	√	√	-	√	√
Vermiculite (MgSO <sub>4</sub> -CaCl <sub>2</sub> )	√	√	√	√	√	√
Vermiculite (LiCl)	√	√	√	-	√	√

### 6.3.2 Experimental setup: Method 1

This study describes the effect of the different composite materials. The experimental evaluation was performed with the assistance of the Environmental Climatic Chamber and control box, in which the composite materials were allocated over a metallic mesh. The measurements were made using a humidity sensor (EK-H4 Sensirion) coupled with Digital Humidity Sensor SHT7x (RH/T), with a standard deviation of  $\pm 1.8\%$  RH and  $\pm 0.3$  °C. Sensors were placed in the inlet, outlet as shown in Figure 6.35, both the inlet and outlet had openings of 18 cm diameter, with airflow coming from the Environmental Chamber blown through with the assistance of an electric fan.

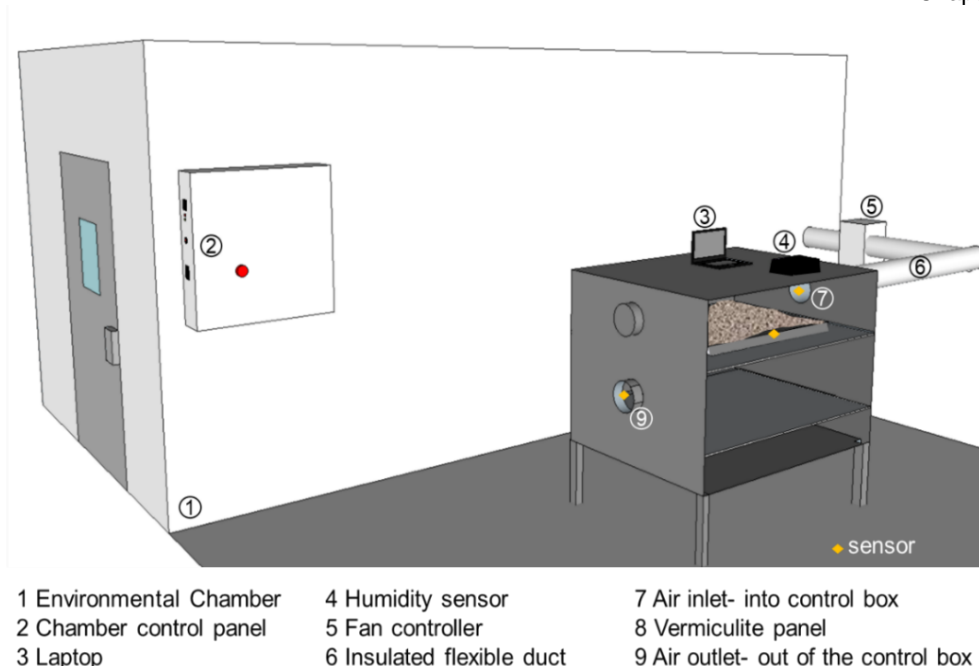


Figure 6.35 Vermiculite experimental rig in the environmental chamber.

The chamber temperature was set at 27 °C and the RH at 78%. The panels were placed on the top shelf of the control box ensuring minimum exposure to the ambient moisture. Once the lid was on, the experiment commences and was monitored for a minimum of 3 hours. The sample weight was compared before and after each test.

The experimental results aim to describe a set of four different experimental analyses. In the first set, Method 1 was applied, having two comparison analyses based on the adsorption rates. In Method 2 the samples are tested simultaneously, and the results are compared based on the testing hours and weight adsorption.

### 6.3.2.1 Method 1, experimental results test 1

In this experiment, the five different samples are compared based on the weight and contact area. All samples weigh between 2.2 to 2.3 kg. The individual analysis is described as follow:

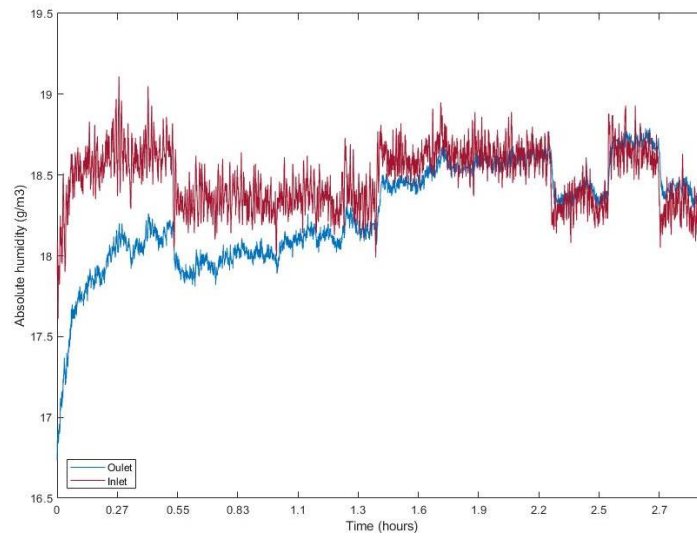


Figure 6.36 Raw vermiculite.

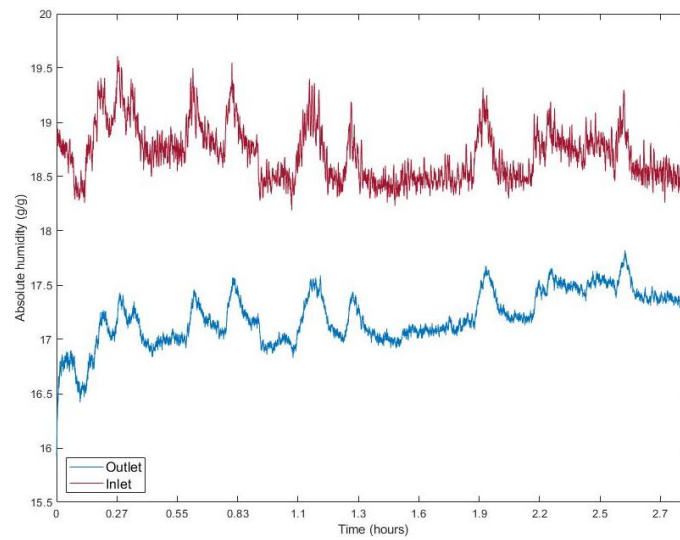


Figure 6.37 Vermiculite + Potassium Formate ( $\text{KHCO}_2$ ).

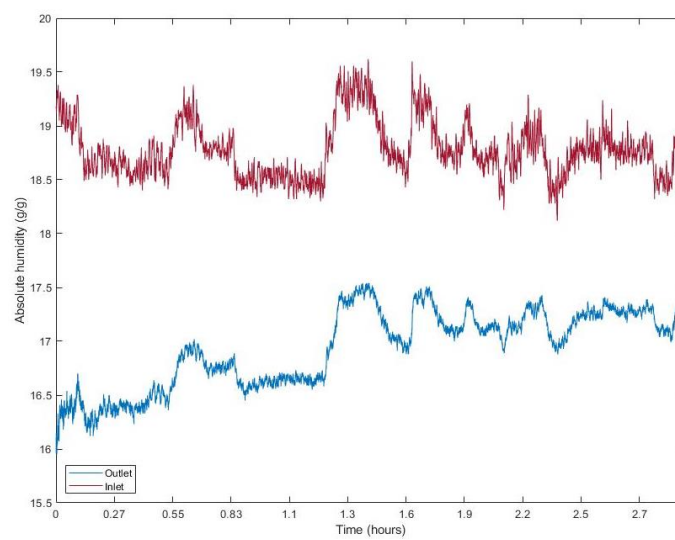


Figure 6.38 Calcium Chloride ( $\text{CaCl}_2$ ).

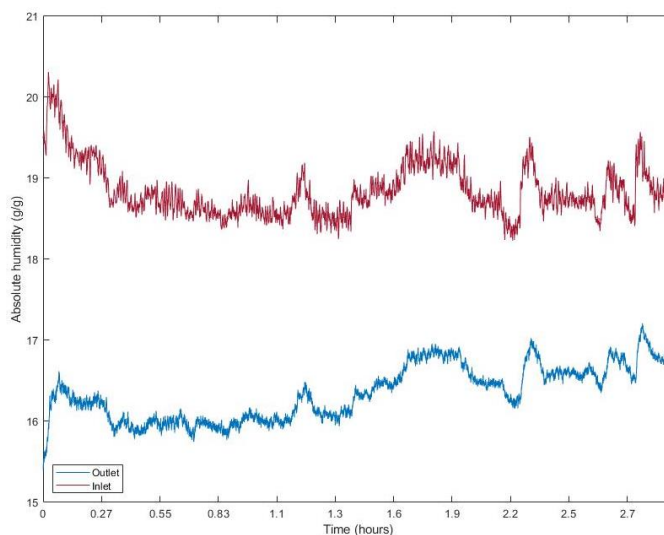
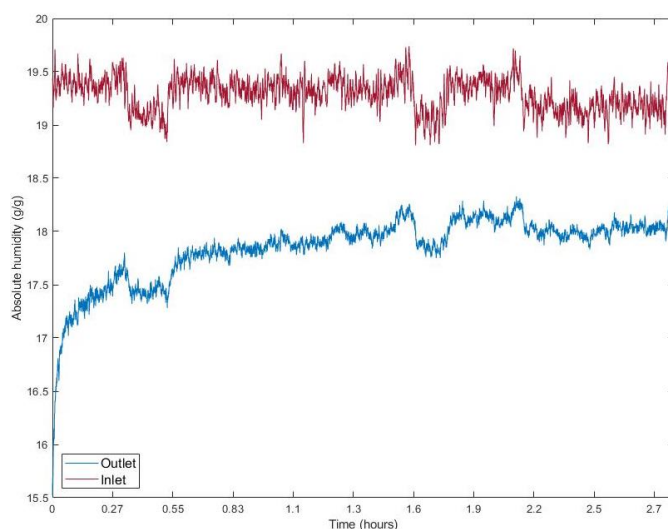
Figure 6.39 Vermiculite + Magnesium Chloride ( $\text{MgSO}_4\text{-CaCl}_2$ ).Figure 6.40 Vermiculite + Lithium Chloride ( $\text{LiCl}$ ).

Figure 6.41 presents the testing results, in which the composites present an improved performance of moisture adsorption in comparison to the raw vermiculite. The highest performance was obtained by the  $\text{LiCl}$ , followed by the  $\text{MgSO}_4 - \text{CaCl}_2$  and  $\text{CaCl}_2$ . Out of all the hygroscopic salts, the  $\text{KHCO}_2$  presented the lowest adsorption performance.

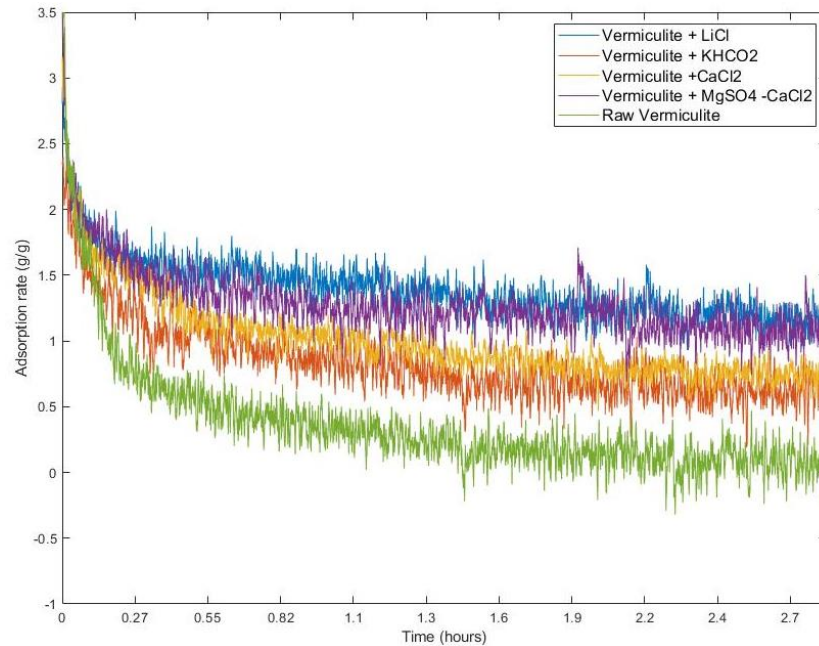


Figure 6.41 Vermiculite adsorption rate comparison. Method 1, test 1.

Measurements for the initial and final weight can be found in Table 6.13. In this case, the adsorption percentage is in relation to the weight. The raw vermiculite presents the highest weight gain, this is due to the area of contact inside the testing. Raw vermiculite is lighter in comparison to the composite desiccants, and in some cases represents almost double the volume area.

Table 6.13. Humidity adsorption capacity  $\pm 2$ kg. Method 1, test 1.

Material	Initial weight (kg)	Final Weight (kg)	Adsorption (kg)	Relative Humidity (%)	Adsorption (%)
Raw Vermiculite	2.323	2.582	0.259	65	11.15
Vermiculite LiCl	2.323	2.463	0.141	65	6.07
Vermiculite MgSO <sub>4</sub> -CaCl <sub>2</sub>	2.352	2.486	0.134	75	5.70
Vermiculite CaCl <sub>2</sub>	2.272	2.382	0.110	65	4.84
Vermiculite KHCO <sub>2</sub>	2.322	2.426	0.104	65	4.48

### 6.3.2.2 Method 1, experimental results test 2

To limit the margin error the experimental procedure was repeated using the weight as the only comparison element, therefore disregarding the

contact area. As a mean to compensate the contact area, the initial weight was reduced to 1.5 kg. The individual test results are shown as follow:

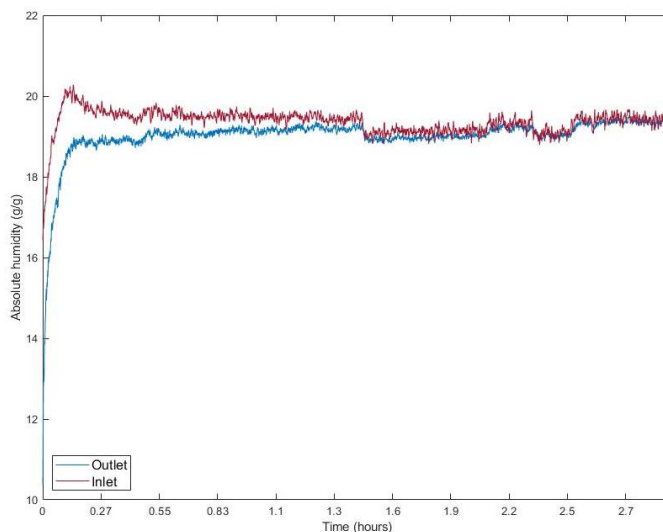


Figure 6.42 Raw Vermiculite at 1.5 kg.

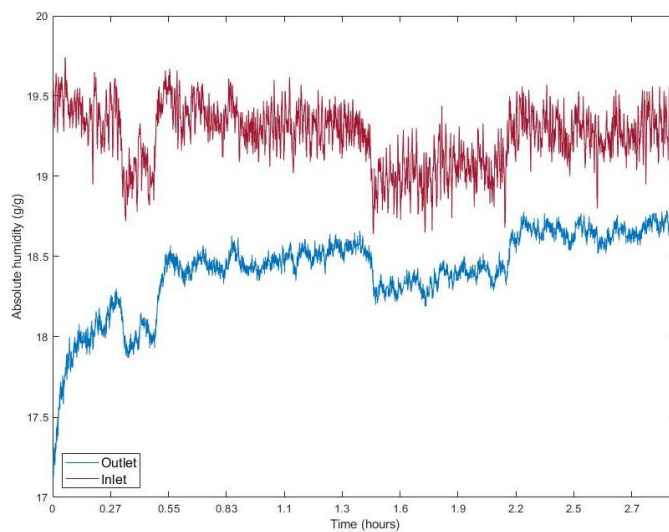


Figure 6.43 Vermiculite + Potassium Formate ( $\text{KHCO}_2$ ) at 1.5kg.

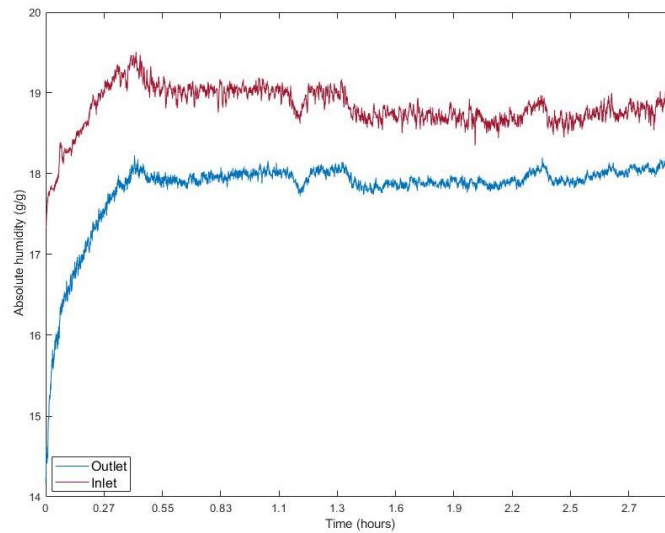


Figure 6.44 Calcium Chloride ( $\text{CaCl}_2$ ) at 1.5kg.

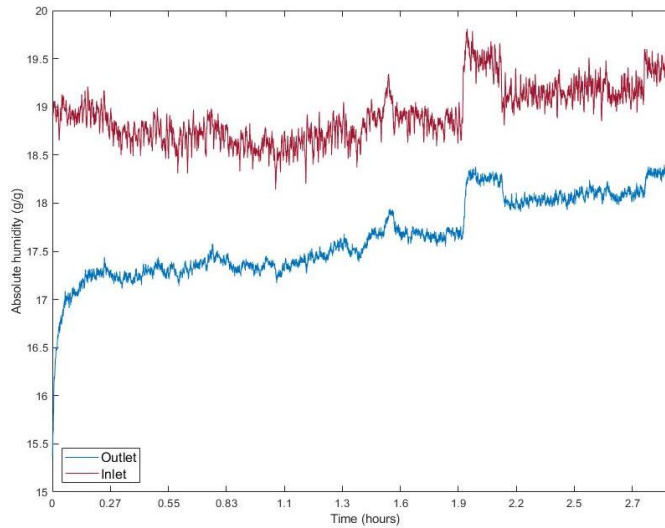


Figure 6.45 Vermiculite + Magnesium Chloride ( $\text{MgSO}_4\text{-CaCl}_2$ ) at 1.5 kg.

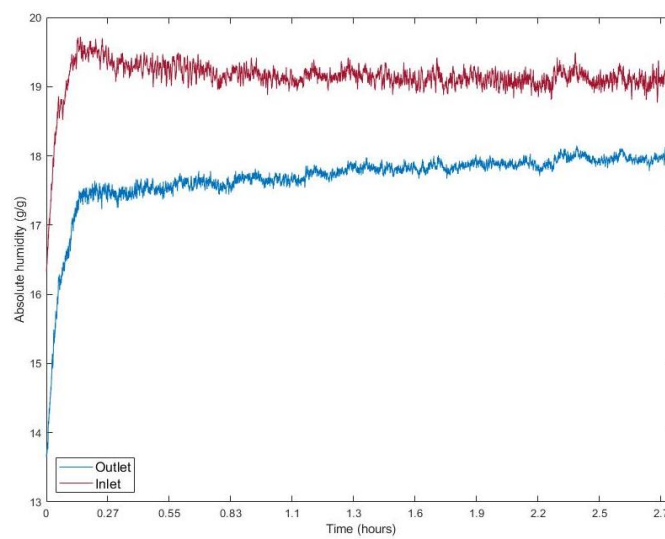


Figure 6.46 Vermiculite + Lithium Chloride ( $\text{LiCl}$ ) at 1.5 kg.



Figure 6.47 represents the adsorption rate comparison. In this case, the LiCl presents the highest adsorption capacity, followed by the  $\text{MgSO}_4\text{-CaCl}_2$  and the  $\text{CaCl}_2$ , the  $\text{KCHO}_2$  and raw vermiculite present the lowest adsorption rate as in the previous experiment. The adsorption percentage in relation to the weight is found in Table 6.14.

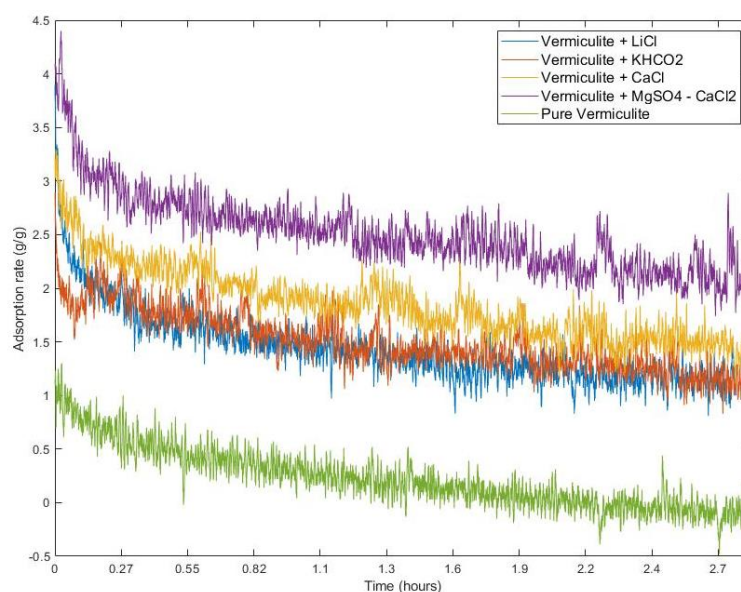


Figure 6.47 Humidity adsorption performance. Method 1, test 2.

As the contact area has been balanced in this experiment, the weight gain differs from the previous test where the highest weight adsorption was obtained by the  $\text{MgSO}_4\text{-CaCl}_2$ .

Table 6.14 Humidity adsorbed capacity 1.5 kg. Method 1, test 2.

Material	Initial weight (kg)	Final Weight (kg)	Adsorption (kg)	Relative Humidity (%)	Adsorption (%)
Vermiculite	1.5	1.634	0.134	78	8.93
$\text{MgSO}_4\text{-CaCl}_2$	1.5	1.624	0.124	78	8.27
Vermiculite LiCl	1.5	1.621	0.121	78	8.07
Vermiculite $\text{CaCl}_2$	1.5	1.612	0.112	78	7.47
Vermiculite $\text{KHCO}_2$	1.5	1.562	0.062	78	4.13
Raw Vermiculite	1.5	1.562	0.062	78	4.13

### 6.3.3 Experimental setup: Method 2

A second evaluation was conducted inside the Environmental Chamber.

The testing samples were placed simultaneously, using 2 kg of each. The



contact area was selected as a key parameter to consider as the raw vermiculite presented greater volume. The samples were allocated in a perforated metal tray and were evenly distributed, to maximize the moisture intake the trays were lifted 60 cm above the floor. The chamber temperature was set at 27 °C and the relative humidity at 80%. The weight was monitored every 2 hours using a scale and the testing duration was set for 6 hours.

### 6.3.3.1 Method 2, experimental results test 1

Four different samples were allocated inside the environmental chamber, the key parameter was to measure the weight gain presented by the samples under a controlled environment as shown in Figure 6.48.

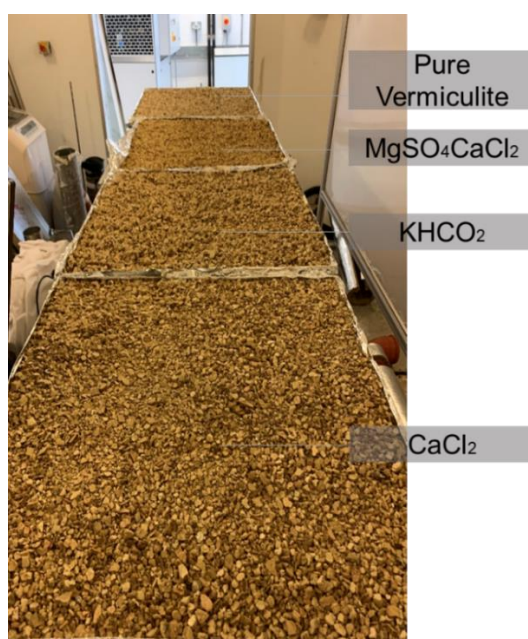


Figure 6.48 Vermiculite, experimental setup. Method 2, test 1.

Table 6.15 presents the adsorption percentage in relation to the testing time. In this case, the  $\text{MgSO}_4\text{-CaCl}_2$  presents the highest value, followed by the  $\text{CaCl}_2$  and the  $\text{KHCO}_2$ . The percentage distribution is compared in Figure 6.49.

Table 6.15 Vermiculite experimental results. Method 2, test 1.

Material (kg)	Time Lapse				Adsorption %		
	10:55	13:00	15:00	9:40 (+1)	2hrs	4hrs	20hrs
Vermiculite MgSO <sub>4</sub> -CaCl <sub>2</sub>	1.80	2.01	2.10	2.26	11.39	16.44	25.67
Vermiculite CaCl <sub>2</sub>	1.54	1.70	1.78	1.93	9.99	15.24	24.97
Vermiculite KHCO <sub>2</sub>	1.89	2.03	2.09	2.20	7.41	10.75	16.46
Raw Vermiculite	0.68	0.74	0.75	0.75	8.04	9.50	9.94

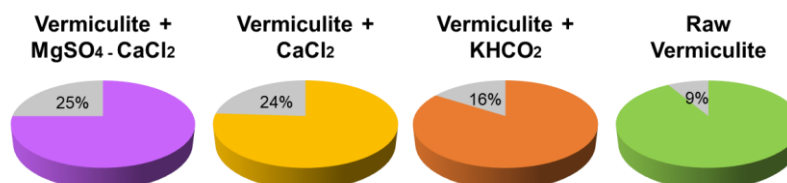


Figure 6.49 Humidity adsorption results by percentage. Method 2, test 1.

### 6.3.3.2 Method 2 – Experimental results test 2

The second test contemplates the addition of the lithium chloride (LiCl) and the previous vermiculite composites. Experimental studies have proved that the mass transfer potential of LiCl solution is better than that of CaCl<sub>2</sub> solution in the same desiccant mass (Bouzenada *et al.*, 2016). The testing conditions were repeated, placing the samples inside the environmental chamber and comparing the weight gain as shown in Figure 6.50.

Table 6.16 presents the adsorption percentage in relation to the testing time. In this case, the LiCl presents the greatest adsorption performance, followed by the MgSO<sub>4</sub>-CaCl<sub>2</sub> and the CaCl<sub>2</sub>. The percentage distribution is compared in Figure 6.51

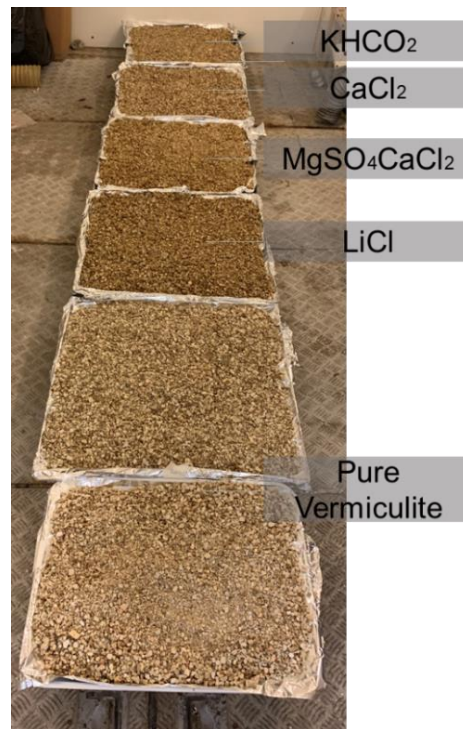


Figure 6.50 Vermiculite, experimental setup. Method 2, test 2.

Table 6.16 Vermiculite experimental results. Method 2, test 2.

Material (kg)	Time Lapse				Adsorption %		
	09:30	11:30	13:30	15:30	2hrs	4hrs	6hrs
Vermiculite LiCl	2.006	2.299	2.451	2.571	14.61	22.18	28.17
Vermiculite MgSO <sub>4</sub> -CaCl <sub>2</sub>	2.002	2.207	2.333	2.425	10.24	16.53	21.13
Vermiculite CaCl <sub>2</sub>	2.000	2.145	2.227	2.331	7.25	11.35	16.55
Vermiculite KHCO <sub>2</sub>	2.000	2.147	2.225	2.271	7.35	11.25	13.55
Raw Vermiculite	1.627	1.707	1.722	1.733	4.92	5.84	6.52

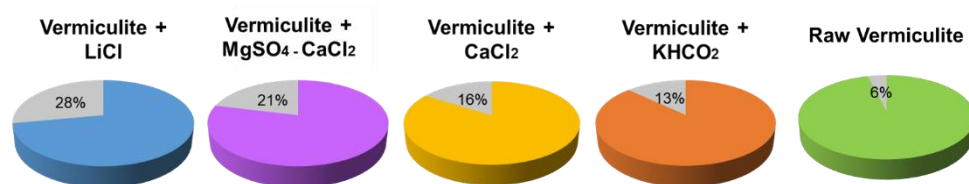


Figure 6.51 Humidity adsorption percentage. Method 2, test 2.

### 6.3.4 Vermiculite regeneration in oven

The vermiculite regeneration is an important part for the moisture adsorbent to perform effectively, the enhancement materials have been selected based on their suitability to regenerate in a temperature range compatible with the heat pump water temperature. For this reason, the vermiculite was dried at a temperature range between 60 °C to 68 °C.

Table 6.17 presents the comparison results of the composite materials at

0.6 kg, with a regeneration temperature of 60 °C. The LiCl presents the highest reduction percentage in relation to the initial weight, followed by the CaCl<sub>2</sub> and the MgSO<sub>4</sub>-CaCl<sub>2</sub>. The KHCO<sub>2</sub> and raw vermiculite present the lowest weight reductions.

Table 6.17 Vermiculite oven regeneration at 0.6 kg.

Material	Start weight (kg)	End weight (kg)	Weight reduction (kg)	Time (hrs)	Oven temperature (°C)	Reduction (%)
Vermiculite LiCl	0.6	0.542	0.58	3	60	9.66
Vermiculite CaCl <sub>2</sub>	0.6	0.546	0.54	3	60	9.00
Vermiculite MgSO <sub>4</sub> -CaCl <sub>2</sub>	0.6	0.551	0.49	3	60	8.17
Vermiculite KHCO <sub>2</sub>	0.6	0.568	0.32	3	60	5.33
Raw Vermiculite	0.6	0.584	0.16	3	60	2.67

The selection of the optimal solid desiccant for humidity control has been made after revising the literature review and some preliminary testing. Composite desiccant has been selected as a suitable solution to enhance the dehumidification performance, allowing to have a low regeneration material, including silica gel-based composite desiccants and vermiculite-based composite desiccants. The main findings from the experimental evaluation for the composite desiccants can be summarized as follows:

The composite desiccant Vermiculite-CaCl<sub>2</sub>, Vermiculite-LiCl, and Vermiculite-MgSO<sub>4</sub>-CaCl<sub>2</sub> presented the highest performance. The Vermiculite-MgSO<sub>4</sub>-CaCl<sub>2</sub> has been selected for large-scale testing due to the cost-benefit.

In terms of regeneration temperature, the regeneration temperature is below 65 °C. The solar-assisted heat pump provides temperatures of

$\leq 60$  °C, facilitating the regeneration of the material and reducing the timeframe in this process.

## **6.4 Experimental results on solar assisted heat pump**

The selection of the solar-assisted heat pump is a practical solution that not only covers the household requirements for hot water and space heating but also assists in the performance of the tri-modular system with the regeneration of the dehumidification system. The solar collector takes the role of the heat generator in the system and is the main source of thermal energy. The application of solar collectors coupled with heat pumps is widely used as a sustainable solution to reduce the CO<sub>2</sub> generated by the domestic heating demand.

A novel high-capacity heat storage system is introduced in this section. The proposed experiment model contemplates the application of a solar-assisted heat pump coupled with a fan coil unit and a solar collector system. The aim of the experiment is to evaluate the performance of the heat pump for space heating and to confirm its viability to regenerate the composite desiccant dehumidification system. The experimental procedure and operating parameters are also defined at the same time.

### **6.4.1 Experimental setup**

The solar-assisted heat pump is manufactured by Arkaya Ltd., combining two technologies, namely heat pump and solar thermal collector. The direct-expansion solar-assisted heat pump is a system combining both solar thermal collector and heat pump evaporator into one unit, where the

refrigerant evaporates by the effect of both incident solar energy and ambient as depicted in Figure 6.52. It has an operational range from -7 °C to 60 °C and consists of four main elements: a heat pump, a fan coil unit, two solar collectors, and a domestic hot water tank that is connected with one loop to the HP system and has a capacity of 150 litres.

Additionally, the system contemplates a compressor to help alleviate the pressure of the heat pump, a system of insulated pipes, and the data logger with a laptop to capture the data. The energy consumption was monitored using a conventional power meter. The solar-assisted heat pump had two primary cycles one being the water cycle and the other one being the refrigerant cycle.

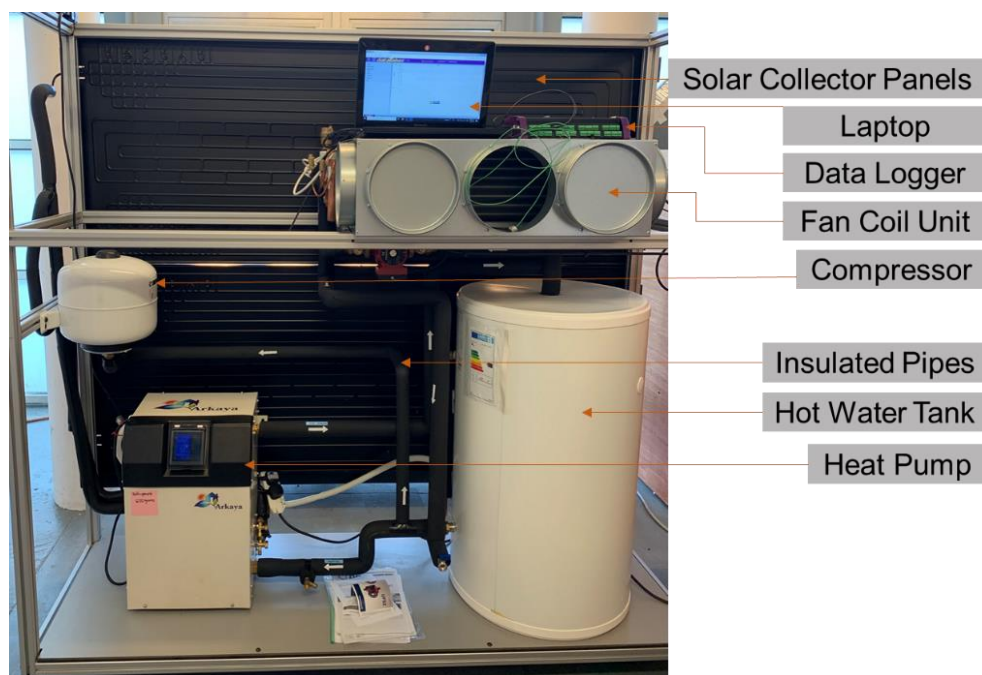


Figure 6.52 Solar-assisted heat pump experimental setup.

In order to evaluate the system performance, a solar simulator was implemented to heat the solar collector panels. This equipment is used to simulate the solar irradiance and spectrum.

The lamps shown in Figure 6.53 were let to reach a stable condition for a minimum period of 30 minutes before taking the readings. To reduce the impact of the natural and artificial lighting inside the laboratory, a black cover was used to protect cover the glazing units proximal to the solar simulation.

The indirect lighting of the laboratory lamps and translucent glazing units is negligible in this experimental procedure. The solar simulator was placed facing the solar collectors with a minimum distance of 0.75 m. It has a total of 30 halogen lamps with a capacity of 500W as depicted in Figure 6.54.





Figure 6.53 Solar simulator front view (left), solar thermal collector schematic array (right).



Figure 6.54 Solar simulator back view (left), solar thermal collector (right).

According to the British Standard BS EN 12975-2:2006 a pyranometer was used to measure the global short-wave radiation. This equipment measured the irradiance of the solar simulator and was strategically placed in such a way as to minimize the effects on the readings of the infrared radiation of wavelength above  $3\text{ }\mu\text{m}$  from the solar simulator light source. To measure the irradiance the RS Mini Pocket Solar Meter with a measuring range of  $1999\text{ W/m}^2$ ,  $634\text{ BTU} / (\text{ft}^2 * \text{h})$  was utilized. This sensor has an accuracy range of within  $\pm 10\text{ W/m}^2$  [ $\pm 3\text{ BTU}/(\text{ft}^2 * \text{h})$ ] or  $\pm 5\%$ . A set of nine points were used across the solar collectors to



measure the readings as shown in Figure 6.55. Different settings were used to compare the irradiance, however, for each testing, the lamp's array was maintained throughout the testing period.

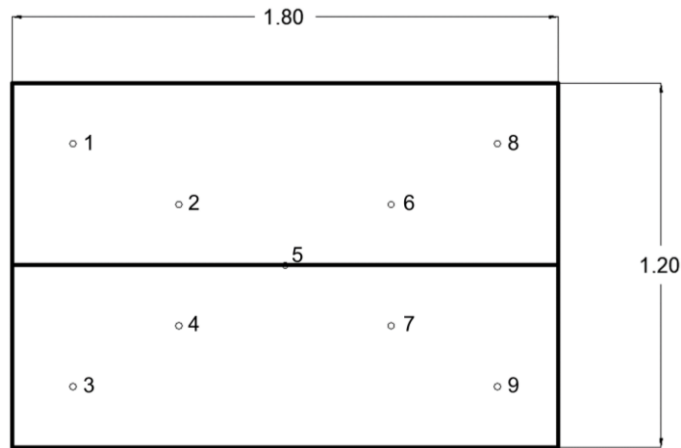


Figure 6.55 Distribution of the measurement reading points in the solar collector.

The temperature measurements were made using Type K thermocouples, and all readings were collected by the data logger (DT85), with a standard deviation of  $\pm 0.3$  °C. Sensors were placed in the refrigerant inlet ( $T_{w,i}$ ) and outlet ( $T_{w,o}$ ), water hot inlet ( $T_{w,h,i}$ ) and outlet ( $T_{w,h,o}$ ), water cold inlet ( $T_{w,c,i}$ ), and outlet ( $T_{w,c,o}$ ), fan pipe (inlet), thermal collector (centre), fan air (centre), and ambient temperature as presented in Figure 6.56.

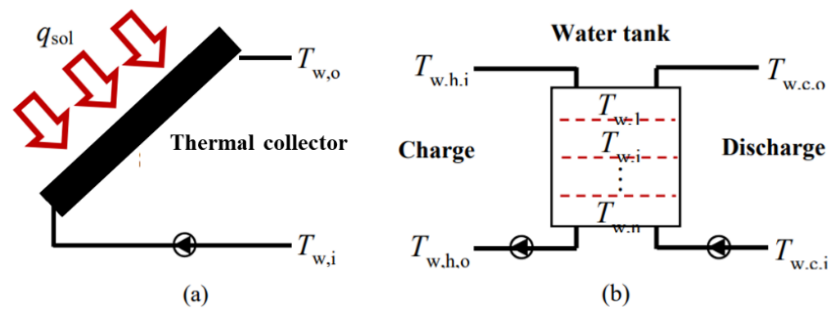


Figure 6.56 Schematic model of solar heating subsystem (a) solar thermal collector ; (b) water tank. Adapted from (Yin et al., 2017).

### 6.4.2 Solar simulator

The measurements of the solar radiation provided by the solar simulator were done under different setting conditionings. The radiation measurements were done across the nine points on the solar thermal panel as previously described, the average value was noted. The lamp's row was varied aiming to cover the totality of the solar simulator, however, the distribution of the solar radiation presented variations in the obtained solar radiation. Figure 6.57 shows three reference points with the average value. The lowest measurement recorded was  $93 \text{ W/m}^2$  and the highest was  $309 \text{ W/m}^2$ . As a reference, the radiation levels of Nottingham UK, have minimum radiation of  $83 \text{ Wh/m}^2$  and a maximum of  $632 \text{ Wh/m}^2$ . The data for each set is presented in Table 6.18. According to the climatic data is obtained from the surface meteorology and solar energy from Nasa the monthly average solar radiation is low from October (maximum  $152 \text{ Wh/m}^2$ ) to March (maximum  $563 \text{ Wh/m}^2$ ). From April (maximum  $590 \text{ Wh/m}^2$ ) to August (maximum  $601 \text{ Wh/m}^2$ ), the solar radiation fluctuates slightly between  $300 \text{ W/m}^2$  and  $330 \text{ W/m}^2$ .

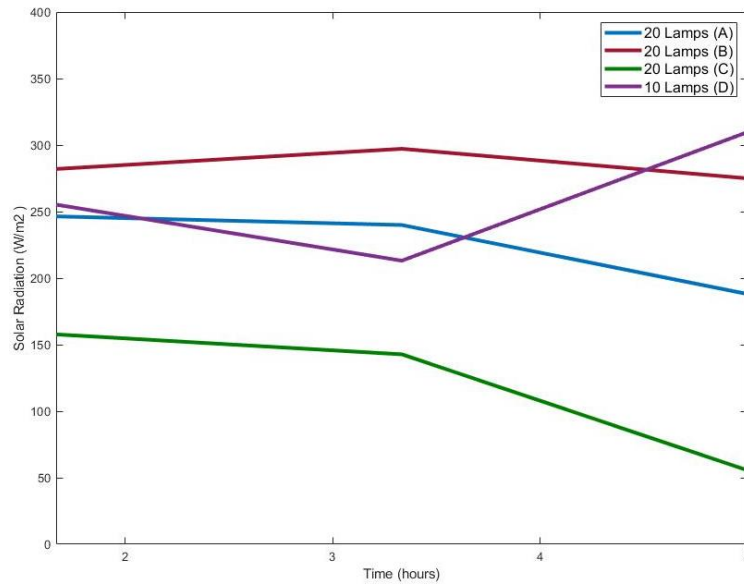


Figure 6.57 Solar radiation simulator.

Table 6.18 Solar radiation simulation data ( $\text{W/m}^2$ ).

No.	A			Average		B		Average
1	1070.22	1218.48	708.85	999.18	1199.95	1121.18	991.46	1104.20
2	3855.29	2714.99	2733.09	3101.13	3276.09	3384.69	3113.19	3257.99
3	367.42	241.40	188.15	265.65	996.09	1144.35	597.66	912.70
4	1547.42	1630.81	787.61	1321.95	3981.99	3855.29	4316.84	4051.37
5	3782.89	3619.99	2588.29	3330.39	5710.54	6443.59	6633.64	6262.59
6	3076.99	3882.44	3918.64	3626.03	5022.74	5167.54	4543.09	4911.12
7	3049.84	2859.79	1991.00	2633.54	1839.30	2145.08	1408.43	1797.60
8	1810.00	2135.80	1248.90	1731.56	417.12	528.94	289.32	411.79
9	1399.16	1130.45	1070.22	1199.95	401.14	282.22	379.84	354.40
No.	C			Average		D		Average
1	228.92	245.27	137.10	203.77	326.59	360.318	308.84	331.91
2	538.34	359.73	137.10	1097.33	1223.11	1616.91	1232.37	1357.46
3	249.05	344.64	93.08	228.92	362.09	314.16	521.84	399.36
4	2995.54	3104.14	1022.65	2374.11	1811.50	1528.88	1927.32	1755.90
5	2554.74	1981.23	875.91	1803.96	6805.58	5429.98	8289.78	6841.78
6	1860.68	1074.52	540.30	1158.50	4615.49	3918.64	6362.13	4965.42
7	2950.29	3140.34	1149.35	2413.33	4823.64	3176.54	5728.63	4576.27
8	303.99	232.53	69.03	201.85	367.41	555.56	358.54	427.17
9	1093.39	1079.49	477.20	883.36	337.24	362.09	360.31	353.21

### 6.4.3 Solar Assisted Heat Pump

The COP is a measure of system efficiency, and it depends on many factors, such as the evaporator temperature, the temperature of delivered useful heat, the working medium used, and the characteristics of

components. Among the above-mentioned, the temperature of the evaporator is the key factor. The COP is calculated as follows:

$$COP = \frac{Q_{out}}{W_{in}} \quad (6.7)$$

$$Q_{out} = mw C_p (T_{out} - T_{in}) \quad (6.8)$$

where:

$W_{in}$  = compressor power output

$mw$  = mass flow rate

$C_p$  = specific heat

$T_{out}$  = water temperature outlet

$T_{in}$  = water temperature inlet

The heat pump is commonly used as a water source heat pump which is a vapor compression system. It is integrated of four main components: compressor, condenser, expansion valve, and evaporator. As this heat pump is a water source heat pump, the evaporator is a heat exchanger which transfers the collected heat from the collector into the heat pump. This heat is used as the energy source for the heat pump. To determine the refrigerant mass flow rate can be determined as follow:

$$Q_{evaporator} = m_r \cdot (h_{e+SH} - h_e) \quad (6.9)$$

where:

$m_r$  = is the refrigerant mass flow rate.

$h_e$  = is the evaporator inlet specific enthalpy.

$h_{e+SH}$  = is the evaporator outlet specific enthalpy.

The refrigerant temperature difference between the inlet and outlet is shown in Figure 6.58. In general, the temperature fluctuates as the heat pump reaches a stable condition (close to 60 °C) and is fully dependant on the radiation received by the solar thermal panels. In this case, the readings reach a stable condition after 1 hour and the average temperature difference between the inlet and outlet was 3.3 °C.

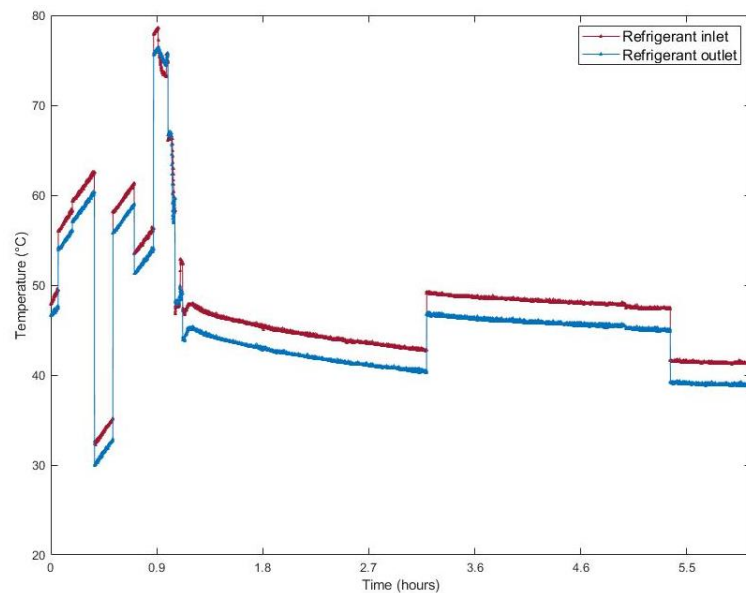


Figure 6.58 SAHP refrigerant temperature inlet/outlet.

The COP is monitored and compared using different radiation levels. An electric plug meter (Energie, ENER007) was used to measure the system energy consumption. The COP is calculated at three points, the first one is done one hour after the solar simulator is on, the second point is at midday of the testing period and the last point is one hour before turning off the system. During the experimental procedure, measurements were taken at 10:00 am, 12:00 pm and 15:00 pm. Model A presented in Figure 6.59 displays the first evaluation; were using 20 laps, the radiation levels

reached a peak at  $239 \text{ W/m}^2$  with a COP of 3.9. This value increased by the end of the experimental procedure reaching a total of 4.5.

Model B presented in Figure 6.60 has maximum average radiation of  $297 \text{ W/m}^2$  with a COP of 3. This model contemplates the usage of 20 laps, by the end of the experimental procedure the COP decrease to 2.8.

Model C presented in Figure 6.61 reached the maximum average radiation at  $143 \text{ W/m}^2$  with a COP of 3.06 and used 20 lamps. The COP reached a peak at 4.3 by the end of the experimental procedure.

Model D presented in Figure 6.62 reached the maximum average radiation at  $213 \text{ W/m}^2$  with a COP of 3.3 and using 10 lamps. There is a reduction in the COP to 2.8 by the end of the testing period.

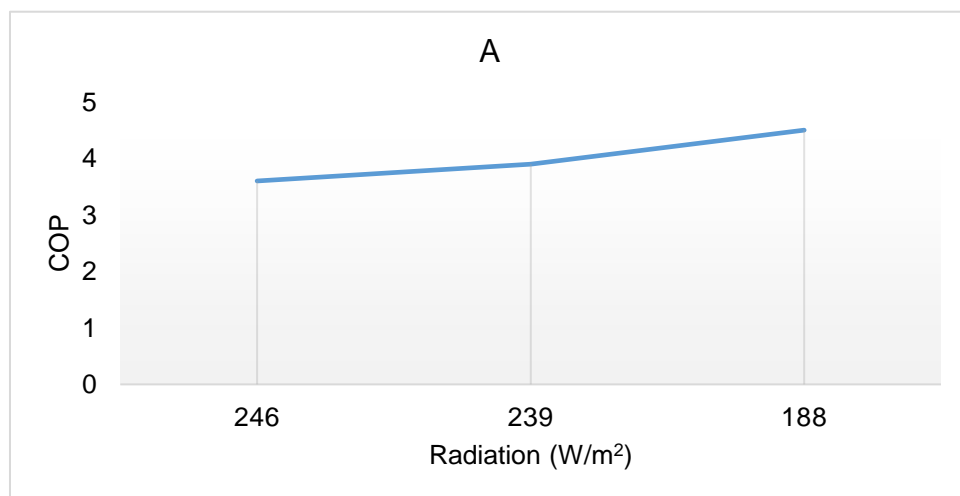


Figure 6.59 Model A: COP.

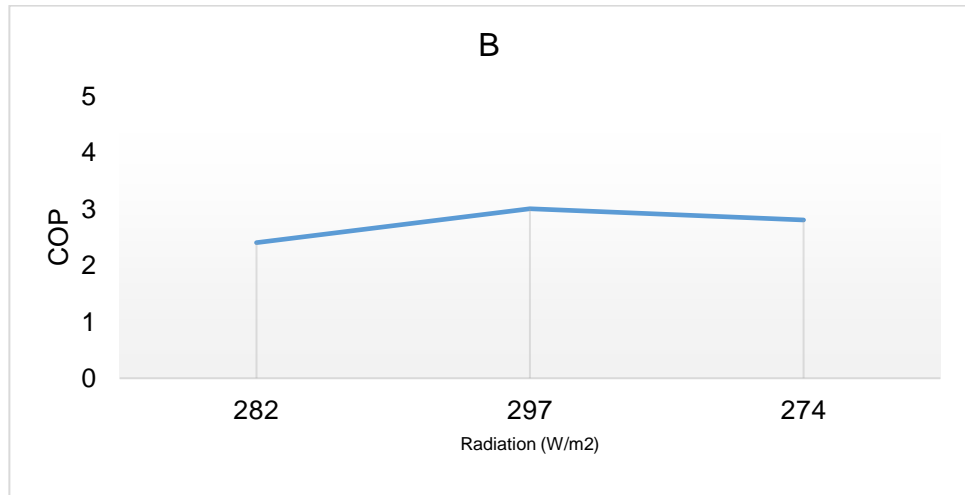


Figure 6.60 Model B: COP.

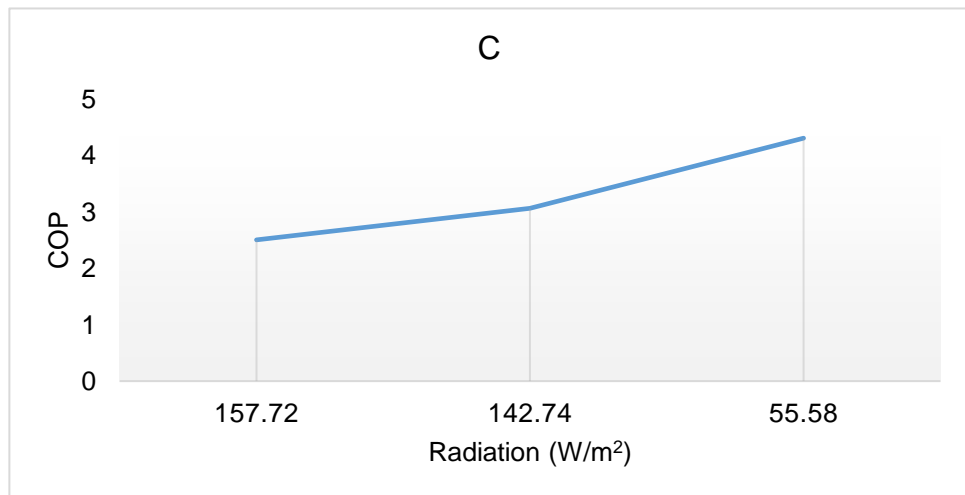


Figure 6.61 Model C: COP.

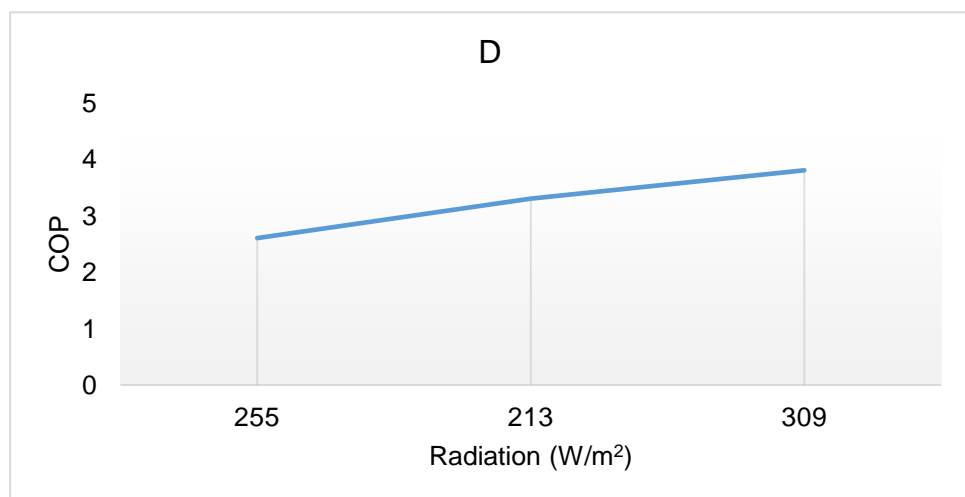


Figure 6.62 Model D: COP.

#### 6.4.4 Fan Coil Unit

The measurements of the air temperature and the hot water pipe were monitored for the regeneration of the solid desiccant material.

Figure 6.63 shows the fan air temperature and the hot water pipe coming from the SAHP. Once the fan is turned on the average air temperature was 35.2 °C and the hot water temperature was 51 °C. During the experimental procedure, the fan air temperature drops considerably at halftime of the testing procedure.

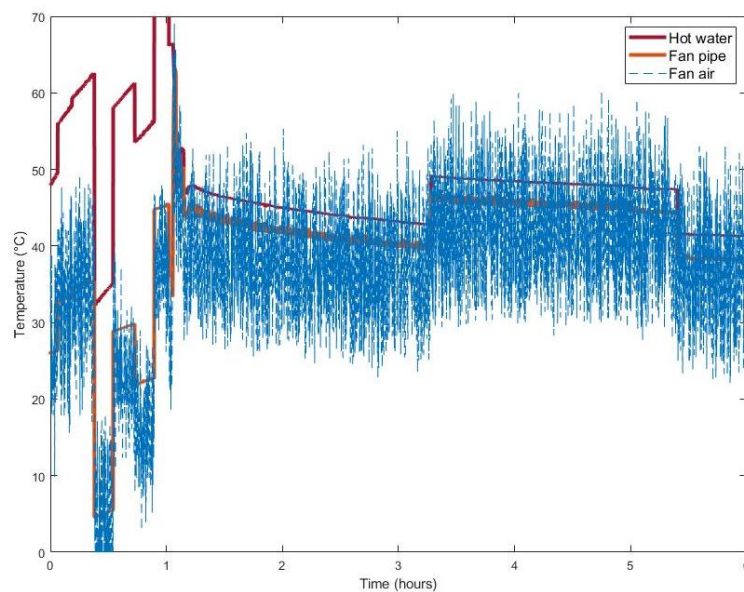


Figure 6.63 Model A: fan air.

Figure 6.64 has a hot water temperature average of 48 °C, with a maximum temperature of 63.3 °C, the air temperature average was 49 °C with a maximum temperature of 86.3 °C.

Figure 6.65 shows the fan air temperature and the hot water pipe coming from the SAHP. When the fan is turned on, the average air temperature was 56 °C and the hot water temperature was 60 °C. It is noticed that there is a direct correlation between both temperatures.



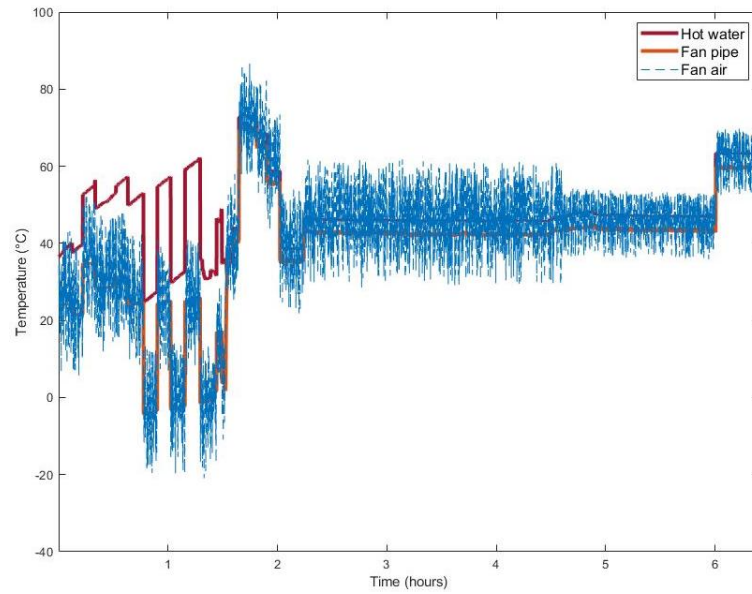


Figure 6.64 Model B: fan air

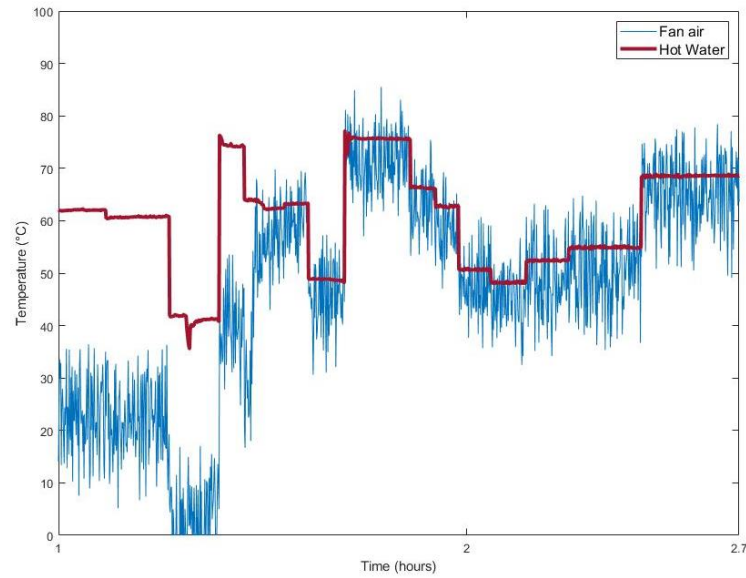


Figure 6.65 Model C: fan air.

Figure 6.66 shows the fan air temperature and the hot water pipe coming from the SAHP. In this case, the fan average air temperature was 38 °C and the hot water temperature was 45 °C. The maximum air temperature was 65 °C.

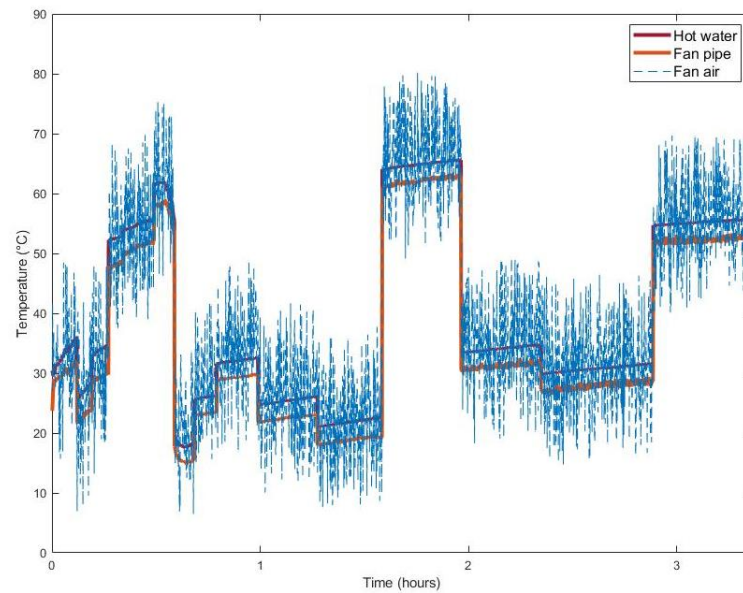


Figure 6.66 Model D: fan air

Figure 6.67 presents a fan air temperature average of 44 °C and the hot water temperature was 48 °C. During this experiment, the maximum hot water temperature was at 73 °C.

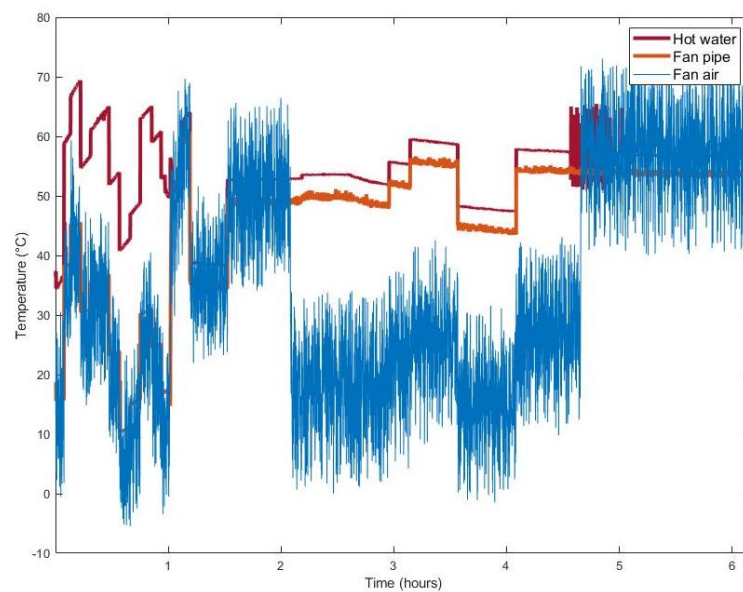


Figure 6.67 Model E: fan air.

The heat pump system can be mounted on roofs or walls. It adsorbs the thermal energy from the environment, even without direct solar irradiance. This gives the system a higher COP in comparison to traditional systems, reaching up to 73 °C. The system works at a higher pressure than

traditional systems, improving the COP and reducing heat losses in winter and overnight. The high temperatures allow the heat pump to supply energy for the solid desiccant regeneration via heated air or with a hot pipe system.

It can be observed that there is a constant temperature fluctuation through the SAHP performance, this is mainly dependant on the solar radiation.

During the experimental evaluation, a direct correlation between the hot water pipe the air temperature was noticed. It can be inferred that the hot water temperature is equal to the fan air temperature of the system.

For solid desiccant regeneration purposes, the fan air temperatures are unstable, difficulting the material regeneration. For this reason, investigating the regeneration performance through a hot water pipe system is recommended. This not only would provide a stable condition, but also remove any restrains for the placement of the desiccant panel as it would not have to be dependent on the accessibility to the fan unit.

## **6.5 Summary**

The experimental analysis of the ceiling PCM panels shows the efficacy to interact with the ambient temperature. The tested PCM panels were able to adsorb the ambient temperature and passively release it during the cooling period. In comparison to the ambient room without PCM, the room temperatures presented a reduction in the peak temperatures.

The composite desiccant materials testing showed the ability for this composite material to adsorb the air humidity, furthermore, proving the effectiveness of the enhancement method. The regeneration process proves the material's capacity to dry at relatively low temperatures (60 °C). The Vermiculite  $\text{CaCl}_2$ , Vermiculite  $\text{LiCl}$ , and Vermiculite  $\text{MgSO}_4\text{-CaCl}_2$  presented the highest performance.

In addition, this chapter presents the laboratory results for the solar-assisted heat pump, using a solar simulator to investigate the performance of the system. The COP average was found at 3.23. The experimental evaluation exhibited the direct relation between solar radiation and the COP.

The operation of the fan coil unit was also assessed, showing the system's ability to provide indoor heating. For the solid desiccant regeneration purposes, it was found that the heated air presented large temperature fluctuations, that could potentially difficult the material regeneration in consecutive cycles. For this reason, alternative regeneration methods are suggested, for example, the application of hot water piping.

# Chapter 7 House monitoring of the system

## 7.1 Introduction

This chapter presents the in-situ testing performance of the tri-modular system. The house monitoring provides the opportunity to test the system components on a large scale, with the required environmental conditions for the system application, which ultimately will be decisive for the commercial application of the system. Intensive testing standards have been set to validate the operational conditionings of the system. In this chapter, the simultaneous application of the heat pump and solid desiccant is presented, ensuring the viability of the heat pump for regeneration purposes. The outcomes of this chapter testify on how the system integration enhances the thermal performance in buildings, reducing energy consumption.

## 7.2 PCM house testing

Following the PCM selection and previous experimental evaluation, the house testing focuses on the integration of the plastic panel, with S23 and S27. This encapsulation method was selected for the house evaluation as it presents a strong structure and due to its commercial manufacturing is highly concealed, preventing any leakage that would represent a safety hazard.

### 7.2.1 S23 in Tarmac House

The experiment was conducted in a bedroom located in of the Creative Energy Houses at The University of Nottingham. The Tarmac Houses depicted in Figure 7.1 are a set of semidetached properties constructed based on the Code for Sustainable Homes (CfSH) Level 4. The testing house consists of a kitchen, living area, 1 1/2 toilets, and 3 bedrooms. The experiments were performed during the winter season, having an outside temperature range from 2 °C to 12 °C.

The test room was located on the first floor and had a total area of 6.34 m<sup>2</sup>, with a double glazed window in the southwest facade as shown in Figure 7.2. The room was used as a bedroom and for the testing procedure a heater was used to simulate the building occupancy, the windows had double glazing and the house ventilation system was sealed, to prevent external temperature interaction.



Figure 7.1 Tamarc Masonry Houses, front and back facades.

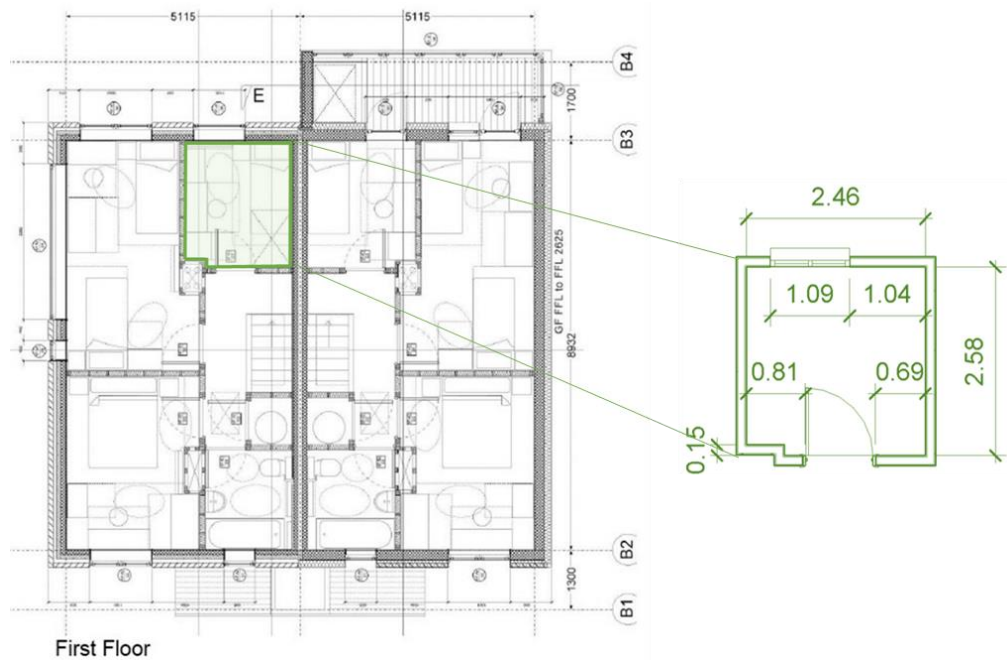


Figure 7.2 First floor layout measurements, (The University of Nottingham).

The PCM panels were placed in the testing bedroom, the room height was 2.45 m, and panels were placed in a shelving system set at 2.33 m, 2.12 m, 1.91 m, and 1.7 m. A set of four panels were placed per row to maximize the contact area in the room, Figure 7.3 and Figure 7.4 present

the shelving unit with the PCM panels, where the supporting structure was reduced to allow the airflow.

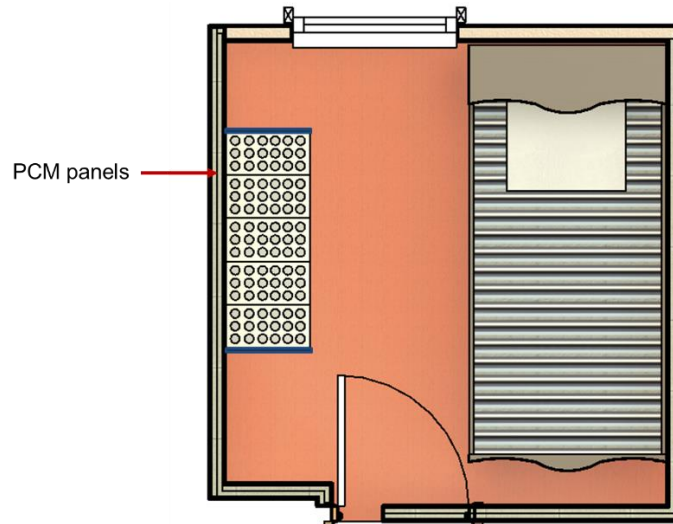


Figure 7.3 PCM panels on a shelving system.

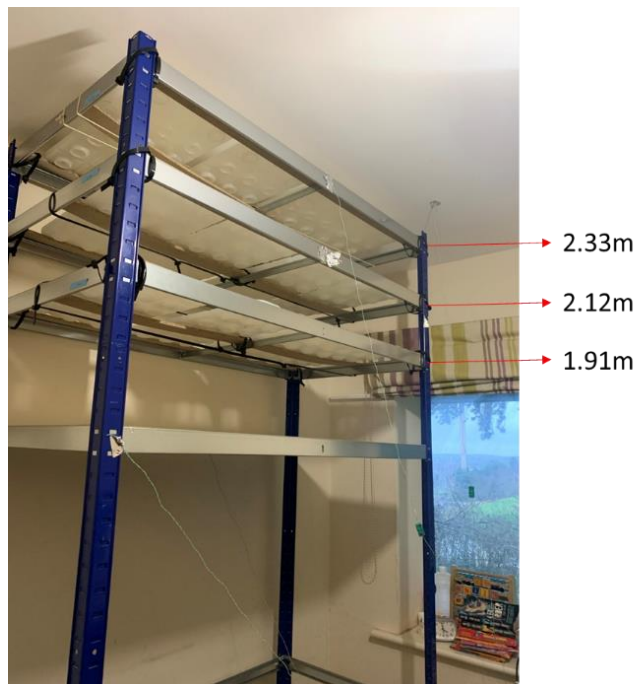


Figure 7.4 Shelving system in the testing room.



### 7.2.1.1 Measurement equipment

The aim of the measurements is to determine the changing of the ambient temperature during the charging and discharging process. The panels were charged using a radiator with a heat capacity of 2 kW, the room temperature loss was monitored after ensuring the complete charging of the PCM. The temperature measurements were made using Type K thermocouples, and all readings were collected by the data logger (DT85), with a standard deviation of  $\pm 0.3$  °C. A total of 14 sensors were placed in the room, aiming to be at the centre of the monitor element, the sensors were placed in the shelving system at different heights, walls, ceiling, floor, window, and radiator as depicted in Figure 7.5. An additional sensor was placed inside a PCM panel.

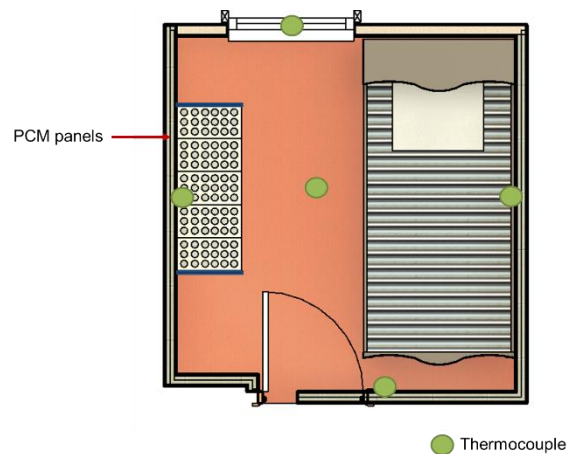


Figure 7.5 Room sensors location in Tarmac House.

### 7.2.1.2 Materials

S23 and S27 are salt hydrates developed by PCM Products Ltd ©. The panels melting point is 23 °C and 27 °C and have a specific heat capacity

of 2.20 kJ/kg K. The weight per panel for the S23 is 3.126 with a net amount of PMC of 2.626 kg, as for the S27 the weight per panel was of 3.128 kg with a net amount of PCM of 2.628 kg.

### 7.2.1.3 Experimental results

Figure 7.6 displays the room temperature performance, monitoring the temperature increase over 5.4 hours, the initial trend shows that the S27 absorbs the ambient temperature during the first 1 hour, after this period the temperature stabilizes. The final temperature for the empty room was 32.5 °C, while the S27 room temperature was 31 °C.

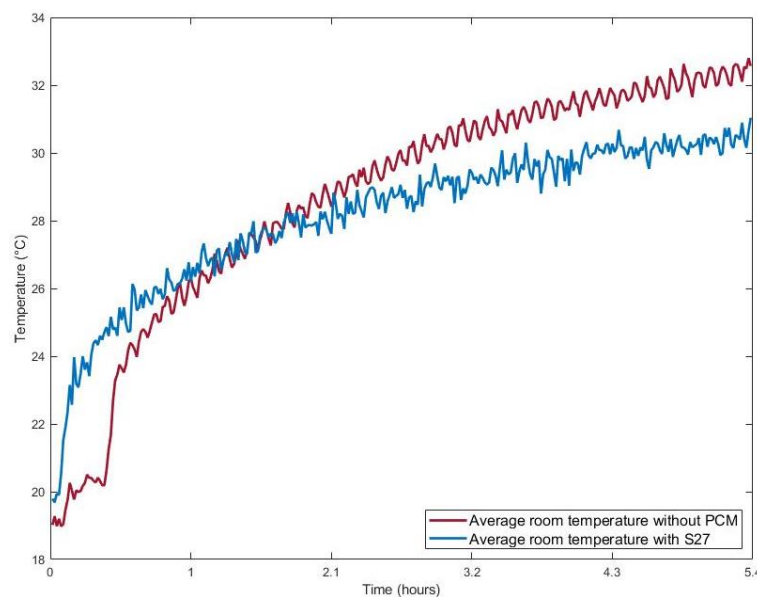


Figure 7.6 Average room temperature heating comparison with S27.

Figure 7.7 presents the experimental results of the S27, the experiment was maintained for 24.2 hours. The final temperature was 22 °C, in contrast, the room without PCM presented a temperature of 18.7 °C. It is

noticeable that the S27 presents a slight temperature increase at the end of the testing period, this is due to an increase in the house temperature.

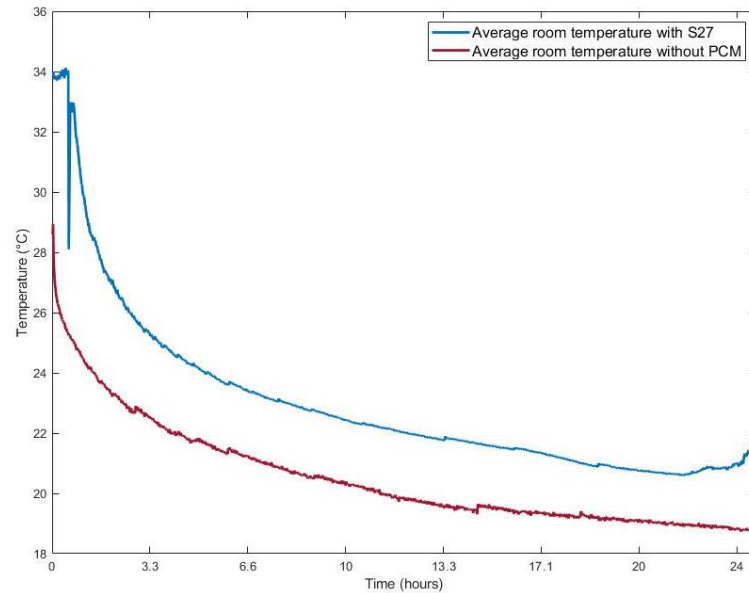


Figure 7.7 Average temperature loss comparison with S27.

The S23 was selected for testing as the S27 panels melting temperature is considered high for the UK climate and the performance of both panels is compared. Figure 7.8 shows the experimental results for the room temperature heating with and without the S23 panels. In this case, it can be noticed that the temperature increment during the first two hours is considerably higher for the room with S23, after 3.4 hours the room temperature without PCM increases.

Figure 7.9 presents the cooling period of the PCM panels. The room temperature was monitored for 21.3 hours. In this case, the temperature drop was reduced by having the S23 panels. The final room temperature was 20.6 °C for the S23 and 18.9 °C for the room without PCM.

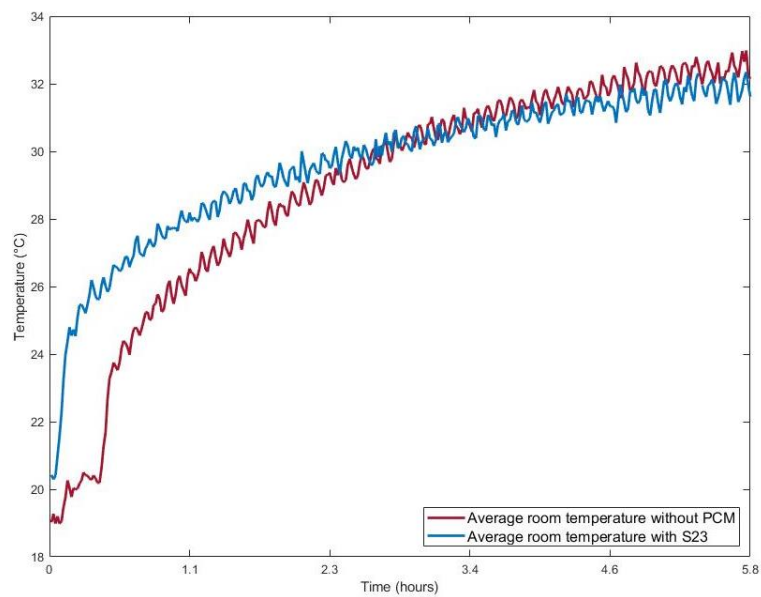


Figure 7.8 Average room temperature heating comparison with S23.

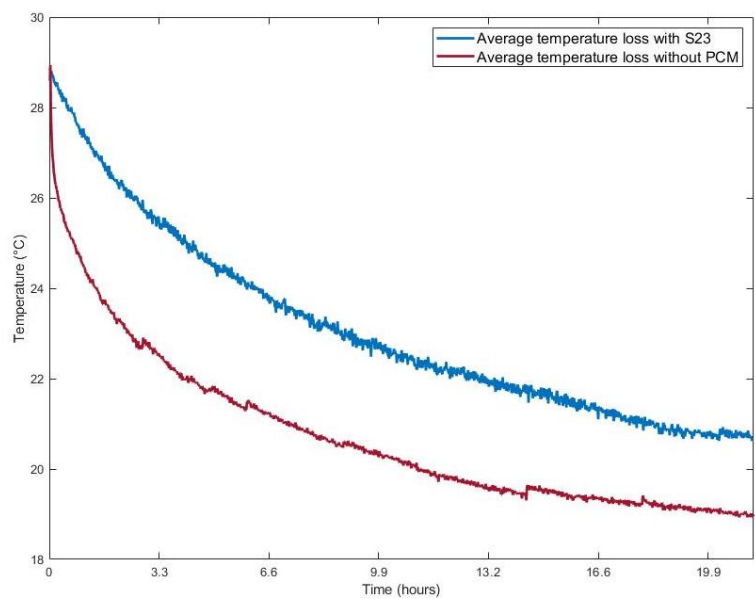


Figure 7.9 Average temperature loss comparison with S23.

7.2.1.4 Discussion

The temperature comparison for both heat gain and heat loss are presented in Table 7.1. It can be seen that both samples present similar patterns, as the heat gain is higher during the initial testing time and then

it tends to stabilize, in contrast, the empty room temperature keeps increasing throughout the testing period. After the experimental procedure, the S27 achieve a heat gain of 10.4 °C, while the S23 managed a temperature gain of 13 °C. This shows that having a lower melting temperature is beneficial to achieve the phase transition. As for the temperature loss, in both cases, the temperature drop for the PCM panels is lower in comparison to the empty room. This shows how the PCM helps stabilize the room temperature, reducing the temperature fluctuations, helping absorb and maintain the heat. Overall, the room temperature loss was 12.2 °C and 8.2 °C for the S27 and S23, respectively.

Table 7.1 Temperature comparison between S23 and S27.

PCM	PCM temperature gain (°C)	Empty room temperature loss (°C)	PCM temperature loss (°C)
S27	10.4	9.8	12.2
S23	13	9.6	8.2

## 7.2.2 S23 in Z blockhouse

### 7.2.2.1 Experimental setup

The experiment was conducted at The University of Nottingham. The test room is allocated in a Georgian period house part of the Architecture and Built Environment Department. The floor surface is 8.3 m<sup>2</sup>, the height is 3.31 m, the room contains two windows covering a surface area of 2.99 m<sup>2</sup> and is shown in Figure 7.10. The walls are constructed out of brick with gypsum plaster and paint finish with a thickness of 15 cm; the ceiling is made of concrete with a thickness of 15 cm and the windows are single

glazed. For experimental purposes, the panels were placed in the top section of a shelving system to represent the ceiling height as shown in Figure 7.11.



Figure 7.10 House layout with testing room in yellow (The University of Nottingham, 2020a).

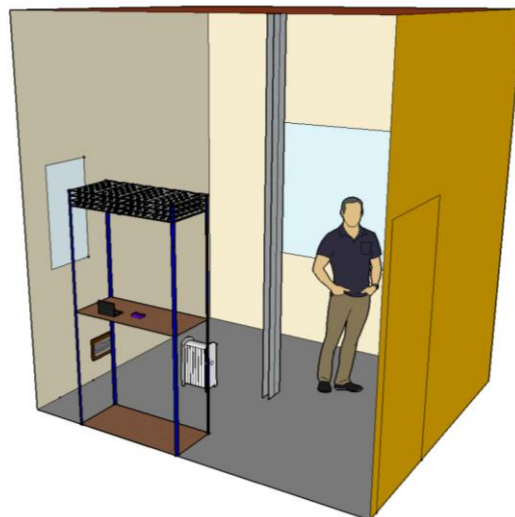


Figure 7.11 Testing room with PCM panels.

### 7.2.2.2 Materials

The PCM material was selected based on its thermal properties and melting point. The enthalpy range is key for the effective response of the material in regulating indoor ambient temperatures. Table 7.3 describes the thermal properties corresponding to the selected PCM material. The capsule material consists of a rectangular plastic container of 24 cm x 49 cm (Figure 7.12), the design contemplates circular rings on the top and bottom in order to facilitate the panel stacking when required. Each panel has a total weight of 3.558 kg and in this experimental evaluation, a set of 20 panels were used, having a net PCM weight of 52.06 kg and representing 28% of the ceiling area.

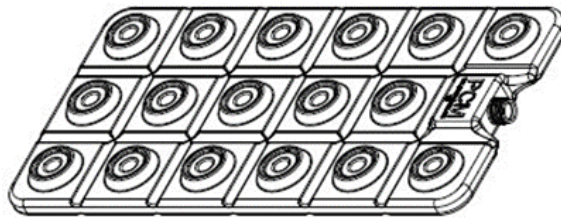


Figure 7.12 S23 panel (PCM Products Ltd, 2020).

Table 7.2 S23 panel (PCM Products Ltd, 2020).

Phase change temperature (°C)	Density (kg/m <sup>3</sup> )	Latent Heat Capacity (kJ/kg)	Specific Heat Capacity (kJ/kgK)	Thermal Conductivity (W/(m·K))
23	1,530	200	2.20	0.54

### 7.2.2.3 Differential Scanning Calorimetry

The testing was performed using the Mettler Toledo DSC, which has 56 thermocouples with a temperature range of -150 °C to 700 °C.

#### 7.2.2.4 Thermal conductivity analysis

The thermal conductivity was measured using the HFM-100 Heat Flow Meter method, in which two flux sensors were utilized to measure the thermal conductivity and thermal resistance. The equipment sensors have a thermal conductive range between 0.005 to 0.5 W/(m·K) and the temperature range of -20 °C to 70 °C, with accuracy  $\pm 3$  %. To validate the accuracy of the measurement an expanded polystyrene board was tested as a calibration material; furthermore, each test was repeated three times to corroborate the results. As the original panel exceeds the equipment dimensions a small-scale sample was provided by the same manufacturer as shown in Figure 7.13.

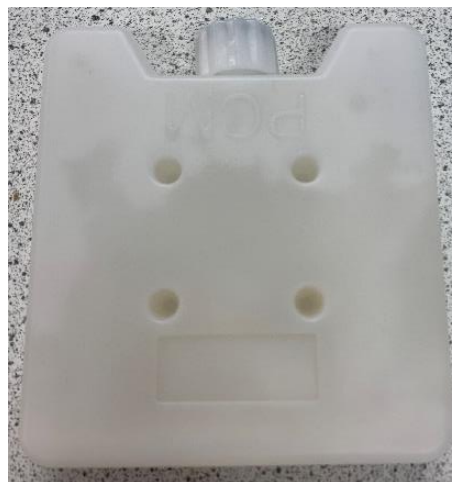


Figure 7.13 Thermal conductivity S23 sample panel.

#### 7.2.2.5 Room measurement equipment

The aim of the measurements is to determine the change in the ambient temperature during the charging and discharging process. The panels



were charged using radiators with a heat capacity of 2 kW and the room temperature loss was monitored after ensuring the complete charging of the PCM. The temperature measurements were made using Type K thermocouples and all readings were collected by the data logger (DT85), with a standard deviation of  $\pm 0.3$  °C. The sensors were placed in the four walls, ceiling, floor, windows, radiators, and inside the PCM panel as shown in Figure 7.14 a total of 16 thermocouples were placed inside the room and the average temperature was noted for the analysis of the results. In addition, 10 THD sensors (EL-USB-2), having a standard temperature deviation of  $\pm 0.55$  °C, 2.25 % for the relative humidity, and 1.7 °C for the dew point.

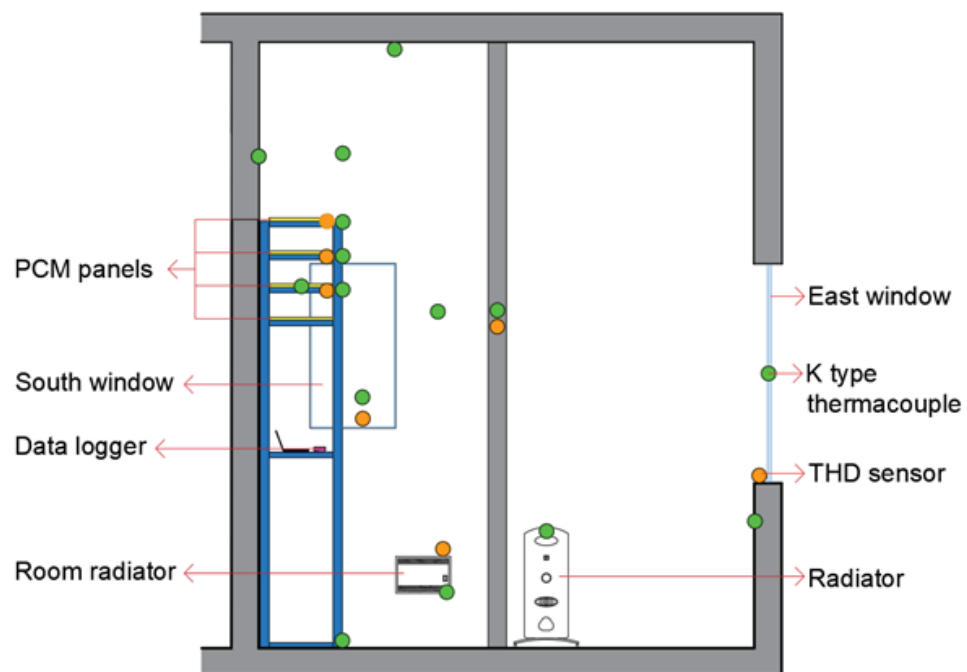


Figure 7.14 Testing room section with components.

### 7.2.2.6 Measurement procedure

Figure 7.15 displays the shelving system with the PCM panels in the testing room. The heating devices were switched on for a minimum duration of 6 hours, thus heating the room and consequently the PCM panels. The heating temperature exceeds the enthalpy phase of the PCM, additionally, the PCM panels were visually inspected to verify the complete phase transition to a full liquid state. After the heating phase, the regeneration took place for another 24 hrs, using the natural heat loss to the ambient. The average room temperature without PCM for the heating period was 27.6 °C.

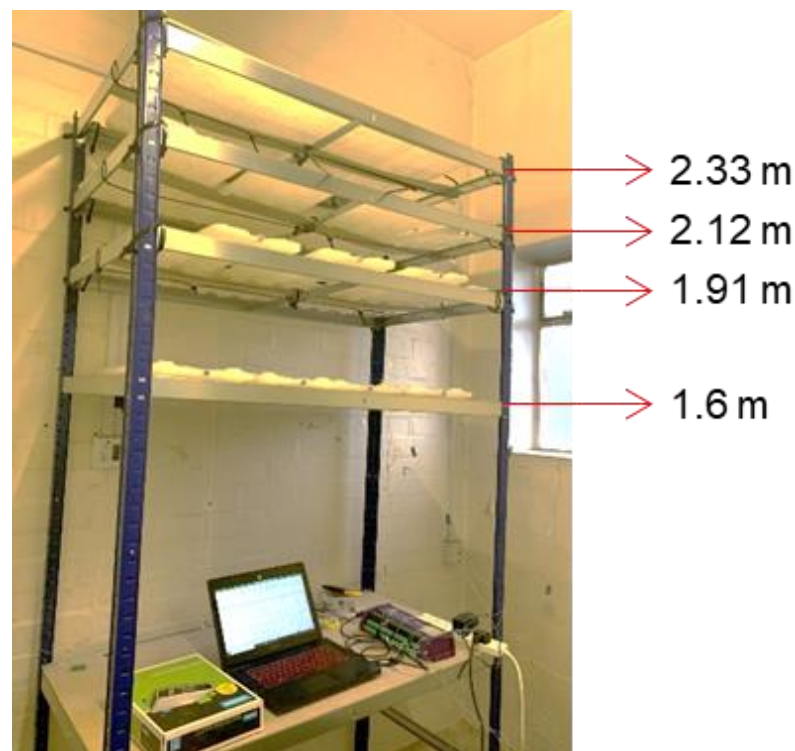


Figure 7.15 Panels in shelving system.

The average temperature varies between the two sensors having a  $\pm 0.11$  °C. The temperature comparison is shown in Figure 7.16. All the testing results present the average temperature using both sensors.

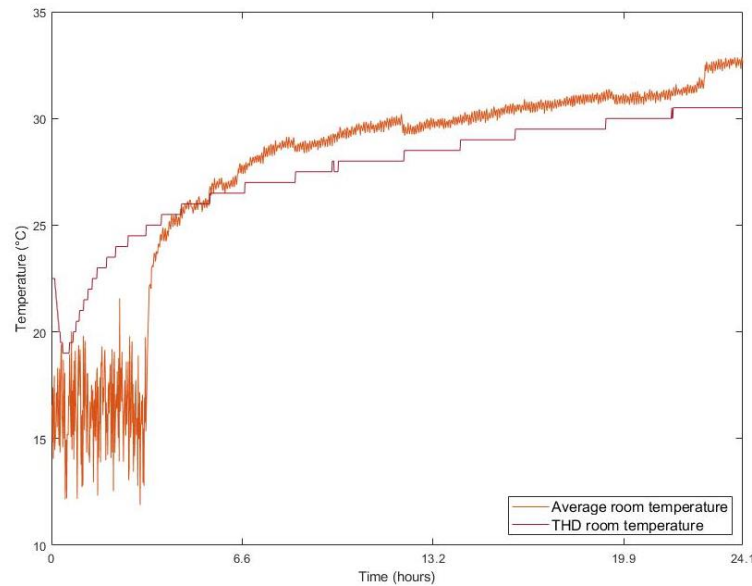


Figure 7.16 Sensors temperature comparison.

#### 7.2.2.7 DSC analysis

Figure 7.17 presents the DSC results of the S23, it can be observed that the PCM thermal response starts at 18 °C and ranges up to 41 °C, having a peak temperature of 27.28 °C.

In this case, the peak point at 23 °C is only found during one of the evaluations. These results provide additional information in terms of the performance and suggest that the material would react better to higher temperature conditionings.

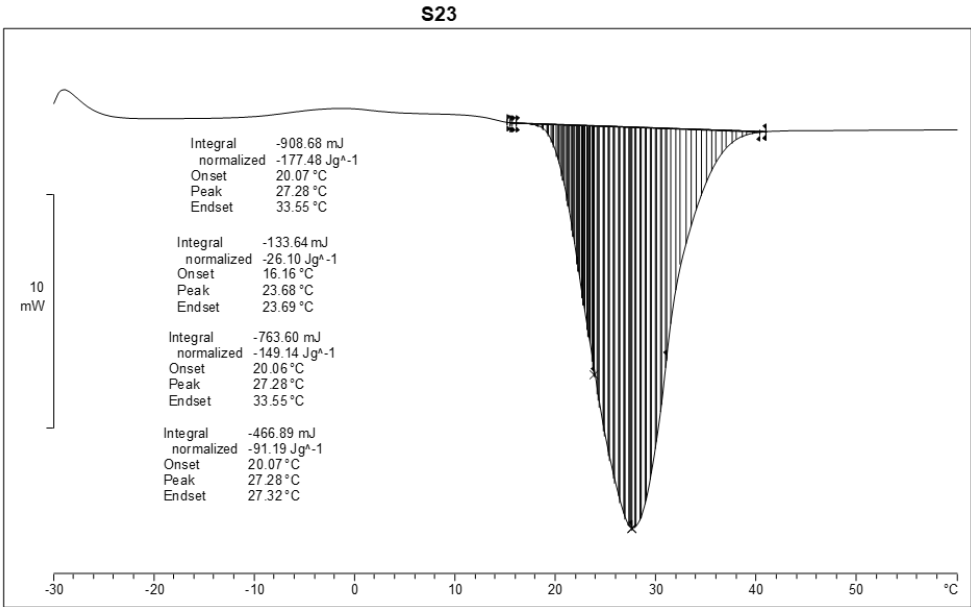


Figure 7.17 DSC analysis for the S23.

**7.2.2.8 Thermal conductive analysis**

The operational parameters of the thermal conductive analysis are described in Table 7.4 and correspond to three different mean temperatures, comparing the effect of the phase transition (solid, transitioning, liquid). When the test was performed at a solid state (mean temperature -10 °C) the thermal conductivity was found at 0.1954 W/(m·K), the lowest value recorded during the experiment. In the second evaluation, the mean temperature was considered at 20 °C, in this temperature range the panel had already started the phase transition; the thermal conductivity was found at 0.232 W/(m·K). The highest thermal performance was presented at a mean temperature of 40 °C, at this stage the panel fully transitioned to a liquid state, having a thermal conductivity of 0.2445 W/(m·K).

Table 7.3 S23 thermal conductive results.

PCM	Mean Temperature (°C)	Upper Temperature (°C)	Lower Temperature (°C)	$\lambda$ (W/(m·K))	Thickness (mm)	Weight (kg)
S23	-10	-20	0	0.1954	30.8	0.388
S23	20	10	30	0.232	30.8	0.388
S23	40	30	50	0.2445	30.8	0.388

According to the manufacturer data the thermal conductivity of the S23 is 0.54 W/(m·K), this value is higher than the obtained results and it is due to the encapsulation material. In the case of the salt hydrates, their corrosiveness reduces the encapsulation solutions, thus plastic materials are an appealing solution (Velasco-Carrasco *et al.*, 2020).

The importance of the container material is pivotal for the PCM to perform adequately in indoor environments and in this case, it is expected a slight reduction from the plastic capsule in comparison to the natural thermal conductivity of the PCM. Table 7.5 shows the thermal conductivity of PCMs with similar melting temperatures found in the literature for comparison purposes.

Table 7.4 PCM thermal conductivity comparison.

PCM	Melting Temperature (°C)	Liquid [W/(m·K)]	Solid [W/(m·K)]	Reference
Paraffin C13-C24	22-24	0.21	-	(Cabeza <i>et al.</i> , 2011)
RT22	22	0.2	0.2	(Rubitherm GmbH, 2020)
RT24	24	0.2	0.2	(Rubitherm GmbH, 2020)
RT 25	25	0.17 ± 0.01	0.19 ± 0.01	(Weinläder, Beck and Fricke, 2005)
S27	27	0.48 ± 0.04	0.79 ± 0.03	(Weinläder, Beck and Fricke, 2005)
L30	30	0.56 ± 0.03	1.02 ± 0.05	(Weinläder, Beck and Fricke, 2005)

The thermal conductivity observed across the six examples gave a good indication of the performance of the S23. In this case, the S23 panel presents a competitive performance in comparison to pure PCM samples; this confirms that using the plastic capsule container is an advantageous method for building integration.

#### 7.2.2.9 Room testing

Figure 7.18 represents a typical data recording during the heating and cooling period. The room was heated for 6.8 hours, while the cooling period had a duration of 17.25 hours. The average room temperature during the heating period was 26.3 °C and after the cooling period was 16.32 °C with a final temperature of 15.22 °C.

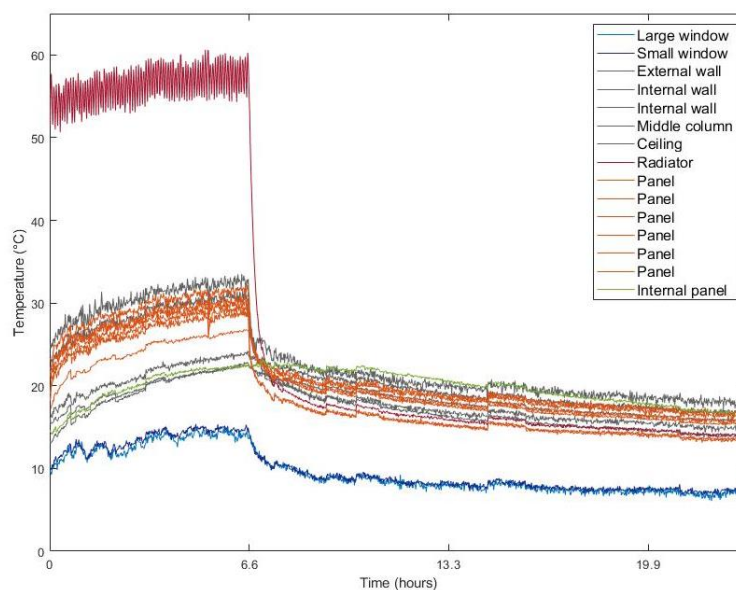


Figure 7.18 S23, room temperature monitoring.

Figure 7.19 shows the extended heating and cooling period, having an average temperature of 27.65 °C and 19.54 °C respectively. It is seen

that the room temperature increases constantly during the heating period reaching a maximum temperature of 30 °C, after the radiator is turned off the temperature starts to decrease and the PCM panels are not able to retain the room heat, reaching 16.6 °C after 35 hours. This can be attributed to the temperature difference between the indoor and outdoor environments during the test day, having an ambient temperature between 4 to 6 °C.

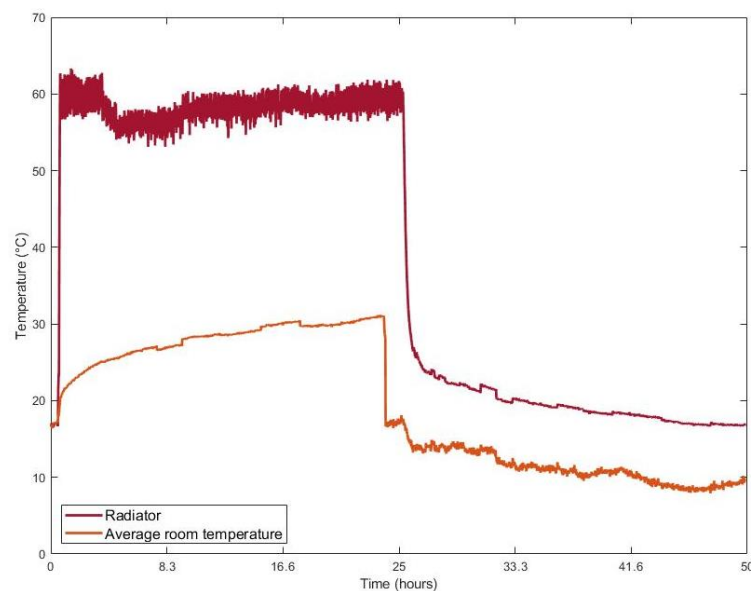


Figure 7.19 S23, room temperature monitoring heating and cooling.

#### 7.2.2.10 Melting process

The PCM effect over the room temperature can be observed in Figure 7.20. The heating mode displays the increasing room temperature, both with and without PCM panels. This graph represents four different testing days, one without PCM and the remnant having 20 S23 panels allocated in the room. The graph presents the radiator temperature and room

average temperature. It is possible to see that for the day without PCM the radiator temperature corresponding to the red line achieves higher temperatures in comparison to the PCM testing days, in contrast, the average room temperature presented the lowest ambient temperature. When the PCM panels are present, the radiator temperature tends to decrease after 2.5 hours, meaning that the panels are being charged and therefore reducing the heating temperature; this factor is proved by the average room temperature increment. The maximum room temperature of the testing room without PCM was 24.43 °C; in contrast, the room with the S23 reached 30.70 °C.

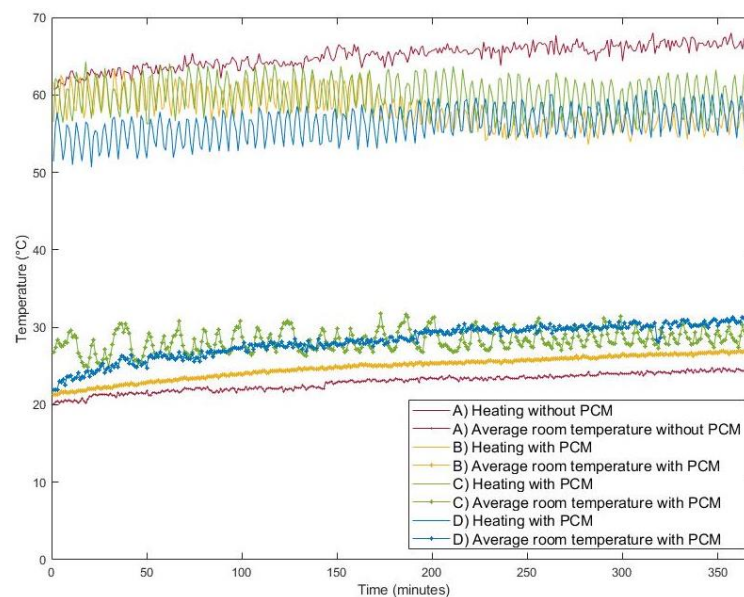


Figure 7.20 Heating performance comparison.

Table 7.5 presents the numerical results of the heating experiment, showing the average temperature. It was shown that the addition of the PCM decreases the heating temperature, creating a minimum



temperature difference of 4.81 °C. Consequently, the average room temperature with PCM has increased, having a minimum temperature difference of 1.98 °C. These results lead to the conclusion the 20 PCM ceiling tiles are able to store up to 5 °C.

Table 7.5 Average temperature comparison results.

A) Without PCM		B) With PCM		C) With PCM		D) With PCM	
Radiator (°C)	Room (°C)	Radiator (°C)	Room (°C)	Radiator (°C)	Room (°C)	Radiator (°C)	Room (°C)
65.01	22.92	58.02	24.88	60.20	28.28	56.30	28.30
$\Delta T$		- 6.98	+ 1.96	- 4.81	+ 5.36	- 8.71	+ 5.37

#### 7.2.2.11 Solidification process

The cooling mode measurements show the freezing progress of the PCM panels. It is possible to see the effect of the room temperature when compared to the empty room. The heating devices were turned on for 24 hours, thus heating the room. After this period the radiator was turned off and the monitoring period started for 24 hours as seen in Figure 7.21. The graph presents higher room temperatures when the PCM panels are allocated in the room, this factor is marked for the first 20 hours. After this period both temperatures appear to reach similar values, however, the room temperature with PCM remains higher throughout the testing period. The starting temperature for the room without PCM was 34.31°C and the final temperature 17.24 °C, in comparison the S23 room temperature started at 36.76 °C and the final temperature reached 17.41 °C.

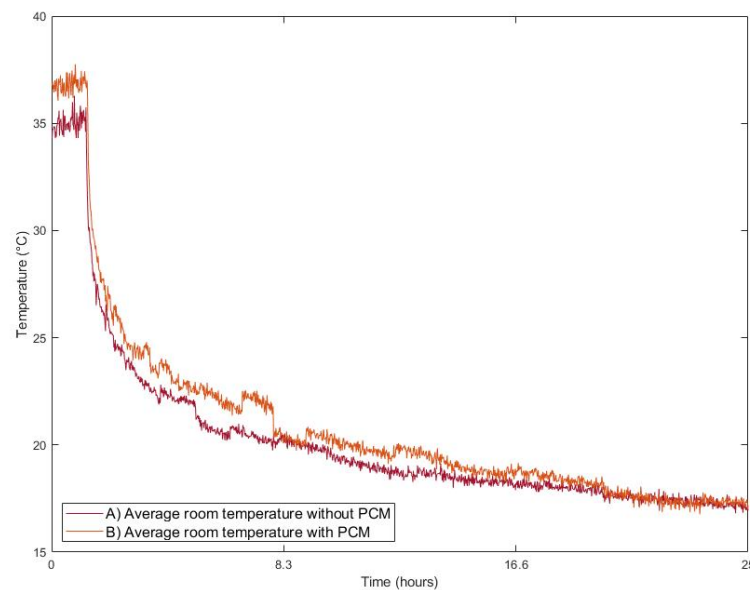


Figure 7.21 Cooling performance comparison.

The numerical results obtained from the analysis of the graph are displayed in Table 7.6. For the PCM room, it can be observed that the panels are able to drop 14.6 °C during the first 6.2 hours, reaching 22.1 °C which is below the melting point. These results show the ability of the PCM to start the regeneration after 6 hours, allowing the thermal cycle process to be completed in 24 hour period.

Table 7.6 Room temperature cooling comparison.

Time-lapse	Start	6. 2 (hr)	12.5 (hr)	18.7 (hr)	25 (hr)
A) Without PCM (°C)	34.31	20.52	18.51	17.90	16.94
B) With PCM (°C)	36.76	22.10	19.62	18.31	17.16
$\Delta T$	-2.45	-1.58	-1.11	-0.41	-0.22

#### 7.2.2.12 Summary of PCM house testing

This study aims to support the application of PCM technologies as a passive alternative to generate energy saving, hence improving the building energy performance. The experimentation has been used to

explore the effect of adding insulation to the building envelope, the operating principle is based on storing the available heat through the melting process of the PCM and discharging it to the inner environment. The tested system has demonstrated the potential to provide energy savings, by reducing the peak indoor temperatures and therefore reducing the energy operation requirements for heating and cooling.

In this case, the S23 panel performance presents favourable results for building incorporation, as the panel is able to securely contain the PCM and at the same time promote the heat exchange with the thermal environment. Due to the corrosive nature of the S23, plastic encapsulation was adopted as a feasible solution. The main findings of this investigation are as follows:

The DSC analysis found early signs of phase change at 16.1 °C, the peak temperature was found at 27 °C, this temperature range was found within the human thermal comfort.

The thermal conductive was found  $0.19 \pm 0.24 \text{ W/(m}\cdot\text{K)}$ , S23 panel presents a competitive performance in comparison to “pure” PCM materials, this confirms the application of the plastic capsule container as an advantageous method for building integration.

Adding the S23 panels decrease the heating temperature, as a result, the average ambient temperature increased. This result led to the conclusion

that having 20 PCM ceiling panels created an impact in the room temperature of 5 °C.

For cooling purposes, the S23 maintains higher room temperatures in comparison to the empty room. After 6 hours the PCM panels temperature decreased below their melting point; this indicates the ability of the panel to cool down fast enough to complete the thermal cycle in a 24 hour period.

Phase segregation was observed during the melting period, a reduction in the panel dimensions would be advisable to counteract this drawback.

It is pivotal to ensure that the correct climate conditions are provided for the specific PCM melting temperature, to ensure a complete thermal cycle.

From the above results, it can be concluded that the addition of the S23 ceiling panels can be considered as an innovative solution, having the potential for passive TES, leading to energy savings by reducing the energy demand through storing the available energy and releasing the heat to the environment at inaccessible periods.

### **7.3 Solid desiccant and heat pump site testing**

The test site for the vermiculite and heat pump unit was at a property in Southampton built by Taylor Wimpey in 2018, the view site is presented

in Figure 7.22. The building itself is a converted garage with single skin brickwork and a timber frame internally with an insulated cavity.

The converted garage was selected for the project as this was the easiest section of the property to install all of the system components, considering the heat pump. The room dimensions are 3.92 m x 3.89 m x 2.4 m (W x L x H). The solar thermal panels were mounted on the sidewall as described in Figure 7.23.



Figure 7.22 House testing site.



Figure 7.23 Installation of the thermal collector panels.

## 7.4 Vermiculite house testing

Figure 7.24 and Figure 7.25 present the experimental rig for the house testing, a box was created containing 4 panels and using 10 kilos of the Vermiculite- $\text{MgSO}_4\text{CaCl}_2$ . The box encloses the solid desiccant across 4 levels to maximize the air distribution.



Figure 7.24 Desiccant box in room testing.

The system contemplates the application of hot water pipes to dry and regenerate the material once it has fully absorbed the ambient humidity. The fan helps assist the moisture from the regeneration process. Humidity and temperature sensors have been placed inside and outside the desiccant box to monitor the performance.



Figure 7.25 Solid desiccant array inside testing box.

#### 7.4.1.1 Monitoring Results

The desiccant box was tested for both dehumidification and regeneration cycles. Figure 7.26 presents the relative humidity results, monitoring the vents and the outlet represents the exit of air aided by the fan. The test was carried out for 7 consecutive days, proving the performance of the desiccant material for the adsorption and regeneration process. It can be observed that the vermiculite-based composite material is adsorbing the ambient air throughout the week, as during the adsorption period the inlet presents higher relative humidity, which tends to slowly decrease through the day.

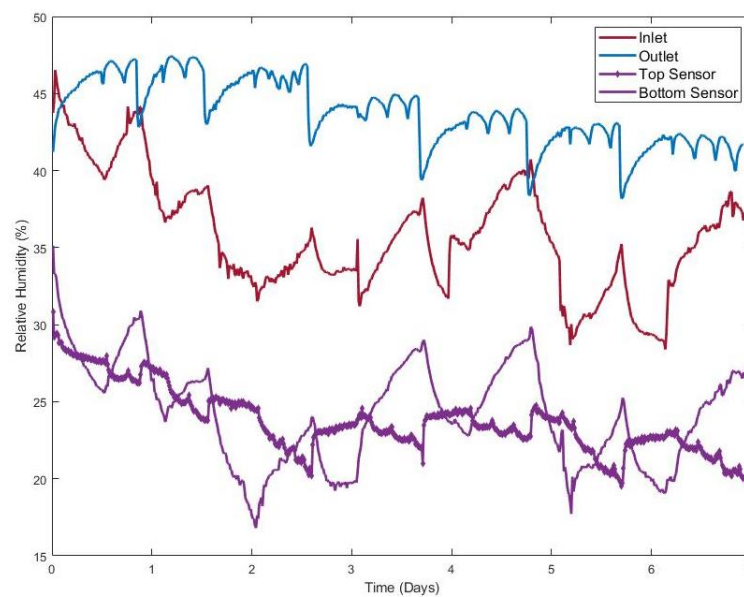


Figure 7.26 Desiccant box control temperature.

For the regeneration performance, it can be noticed that the inlet temperature drops drastically, demonstrating that the desiccant material is not adsorbing as much moisture during this time. The inlet and outlet present opposite tendencies as when the material is adsorbing the room humidity the outlet relative humidity drops. On the contrary, when the vermiculite is regenerating through the hot water pipe system the outlet relative humidity increases as the moisture is exiting the box with the fan assistance. The top and bottom lines present an insight into the adsorption distribution inside the box. In general, both measurements follow the inlet pattern as the variable in the experiment is the difference in the adsorption performance through the desiccant box levels.

Figure 7.27 presents the analysis of adsorption and regeneration cycles in detail. It can be observed a consistent performance through the testing period, nevertheless, certain testing days present a peak in the



adsorption performance that can be attributed to the humidity of the testing day. Another possible explanation could be the ability of the desiccant material to regenerate.

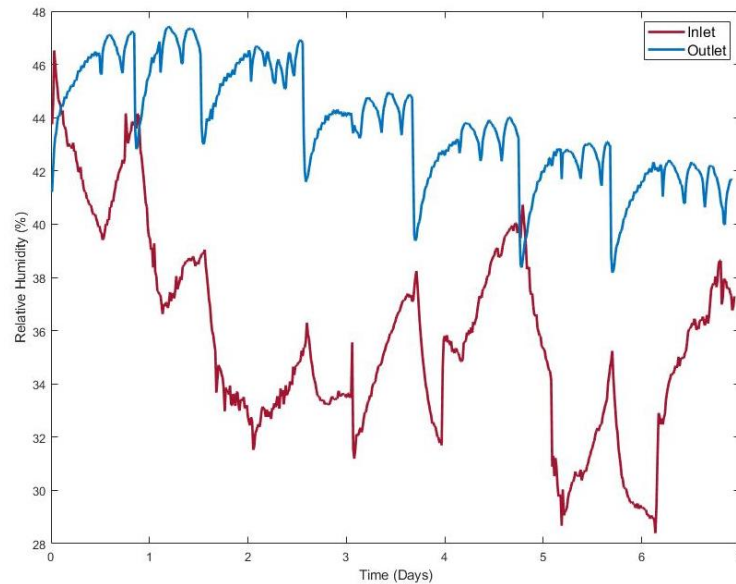


Figure 7.27 Desiccant adsorption and regeneration cycle.

The regeneration cycle is directly related to the moisture of the desiccant material and for this reason, the values increase when the vermiculite-based composite material has adsorbed more humidity.

Figure 7.28 presents the hot water pipe temperature. As the regeneration is pivotal for the vermiculite-based desiccant functioning, the system has a hot water pipe running through the desiccant box to reset the material through consecutive cycles. The hot water comes directly from the heat pump system and can reach more than 80 °C. The overall performance of the regeneration system is proved by the capacity of the material to adsorb moisture through consecutive days.

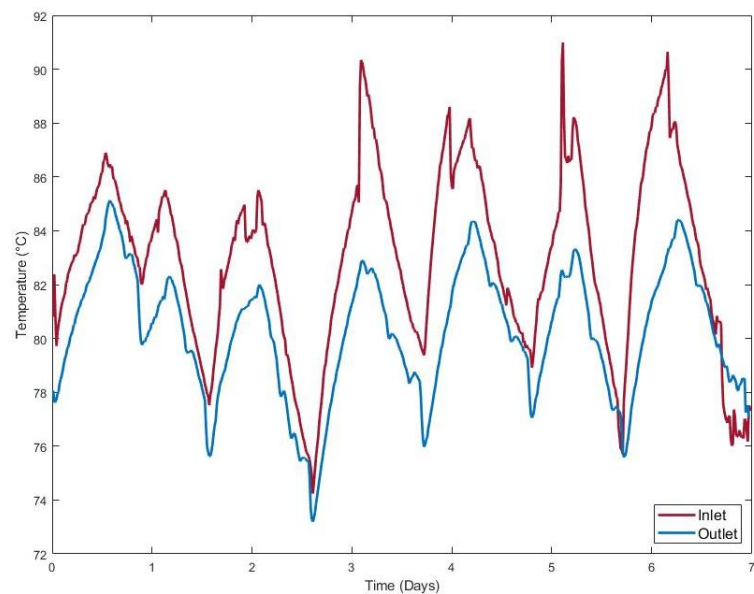


Figure 7.28 Regeneration process with hot water pipe.

Figure 7.29 presents a 24-hr cycle of desiccant material performance. In this case, the relative humidity starts at 43% and slowly decreases through the 12 hour testing period reaching 32% at the outlet vent, this reduction represents the ability of the material to capture the ambient humidity.

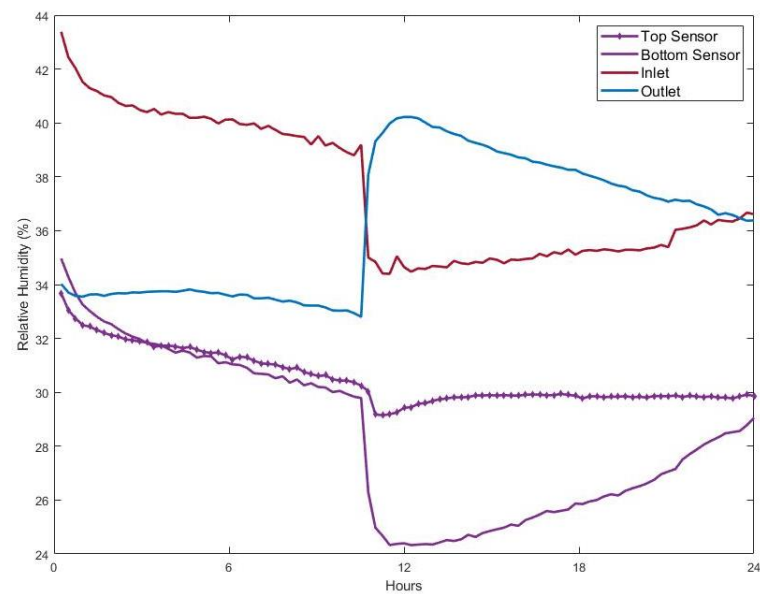


Figure 7.29 Adsorption and regeneration cycle.

During the regeneration process, the RH ranges between 39% to 36 % as the material is losing moisture with the assistance of the hot water pipe and fan.

#### **7.4.1.2 Summary of solid desiccant testing**

This experimental investigation supports the application of an innovative method to assist in the control of building humidity. The desiccant box provides a novel solution to adsorb the ambient moisture and help improve human thermal comfort. The testing results provided by the desiccant box support the application of the vermiculite composite as a humidity control mechanism. During the experimental phase, the desiccant was able to adsorb 12% of the humidity in the room. For the regeneration process, the hot water provided by the heat pump was able to dry the material during the 12 hour cycle. Furthermore, the composite desiccant proves the effectiveness to maintain the performance for consecutive days without maintenance.

### **7.5 Solar assisted heat pump house testing**

The solar-assisted heat pump is designed to heat domestic hot water cylinders and functions by transferring the heat from the ambient temperature to water enabling the heat pump to provide hot water up to 65 °C or higher. The heat pump system uses a traditional vapour compression cycle like Air source or Ground Source Heat Pump. The system achieves greater efficiency by achieving latent heat through all

three modes of heat transfer namely conductive, convective and radiant through solar radiation. The SAHP is able to operate efficiently at low temperatures down to  $-10\text{ }^{\circ}\text{C}$  ambient temperature with high output temperatures of up to  $70\text{ }^{\circ}\text{C}$ . The solar-assisted heat pump was installed and tested in the demo site. The heat pump was connected to the desiccant box, in order to provide hot water for the regeneration purpose. The thermal collectors were placed in the building wall to harvest the solar radiation and the COP of the was evaluated under different conditions.

#### **7.5.1.1 Testing results**

The purpose of the testing was to demonstrate that the SAHP system is able to achieve the temperatures required for desiccant recharging mainly  $60\text{ }^{\circ}\text{C}$  condensing temperature consistently. The system was set in cycles of 10 to 12 hours a day, from 9 am to 9 pm. Measurements were made using the HOBO Data Logger with an accuracy:  $\pm 0.2\text{ }^{\circ}\text{C}$  and  $\pm 2\%$  RH.

Daytime application: on an average day of testing mostly varying between  $2\text{ }^{\circ}\text{C}$  to  $7\text{ }^{\circ}\text{C}$  ambient temperature with a maximum heat index of approximately  $2\text{ }^{\circ}\text{C}$  higher than the average temperature. The system was consistently operated for 6 hours (during sun hours) and 6 hours during the evening hours (without sunlight).

Night-time application: during the night cycle (12 hours), the system was turned on for 30 minutes to cope with the indoor temperature of around 22 °C. This showcased how the system can effectively shift the load demand. The system has shown its capability of operating during daylight hours for 10 to 12 hours and then effectively storing that energy using the domestic hot water tank. Table 7.7 presents the experimental results, focusing on the COP performance, that presented a temperature range from 1.8 to 4.6.

Table 7.7 SAHP COP.

$t_{a.db}$	$t_{a.wb}$	$t_{w.i}$	$t_{w.o}$	kWh	$COP_h$	$t_{evp}$	$t_{cond}$
-7	-8	30	35	4.625	3.24	17.5	40
		40	45	4.043	2.75	17.5	50
		47	55	3.613	2.4	17.5	57
		57	65	3.198	2.05	17.5	65
2	1	30	35	6.537	3.82	-10	40
		40	45	5.816	3.29	-10	50
		47	55	5.261	2.9	-10	57
		57	65	4.718	2.54	-10	65
7	6	30	35	8.107	4.23	-5	40
		40	45	7.269	3.68	-5	50
		47	55	6.619	3.23	-5	57
		57	65	5.75	2.55	-5	68
12	11	30	35	9.93	4.65	0	40
		40	45	8.958	4	0	50
		47	55	8.2	3.56	0	57
		57	65	7.43	4.34	0	65
-10	-11	30	35	4.054	3.05	-20	40
		40	45	3.513	2.57	-20	50
		47	55	3.12	2.22	-20	57
		57	65	2.744	1.88	-20	65

#### 7.5.1.2 Summary of solar-assisted heat pump

The experimental results showed that the HP system is capable to recharge the desiccant and provide domestic hot water.

The system is able to cope with the heating demand at night-time, without solar radiation. The system can manage with a surge in demand requiring it to operate at night if the conditions are required. The system was able to maintain the condensing temperature of 60 °C at night for a period of 8 to 10 hours recharging the desiccant whilst coping with the space heating demand at night. This demonstrated the versatility of the system to work at night if needed through just convective heat transfer.

The heat pump reduced operating costs through the incorporation of solar thermal panels. The system has demonstrated the capability to operate with direct solar radiation at various ambient temperature conditions ranging from -0.5 °C to 15 °C. The condensing temperatures were achieved without compromising the reliability of the system.

## **7.6 System integration**

As the experimental results present, the system integration would depend on the dwelling and energy performance requirements. Nevertheless, there are some general parameters to size the system components. For a standard 3 bedroom house, the proposed solar-assisted heat pump is able to provide domestic hot water, and at the same time provide the hot water to regenerate the solid desiccant material. The PCM cooling performance will be directly related to the climate conditions and building envelope performance.

For the dehumidification performance, the required amount would depend on the building ventilation system, user occupancy, and climate conditions. An energy assessment is recommended to size the system components, for adequate system performance. The system integration is presented in the house model used for the modelling procedure. It can be seen in Figure 7.30 that PCM and the solid desiccant panel could potentially be integrated as a ceiling tile to achieve higher aesthetics.

The tri-modular system aims to attain thermal comfort in the residential environment. For the successful application of the system, energy saving, easy integration, low maintenance, and aesthetics should be considered. In this regard, energy simulation tools and the basic principles for the system sizing presented in Chapter 3, provide the reference for the optimal integration of the system components.

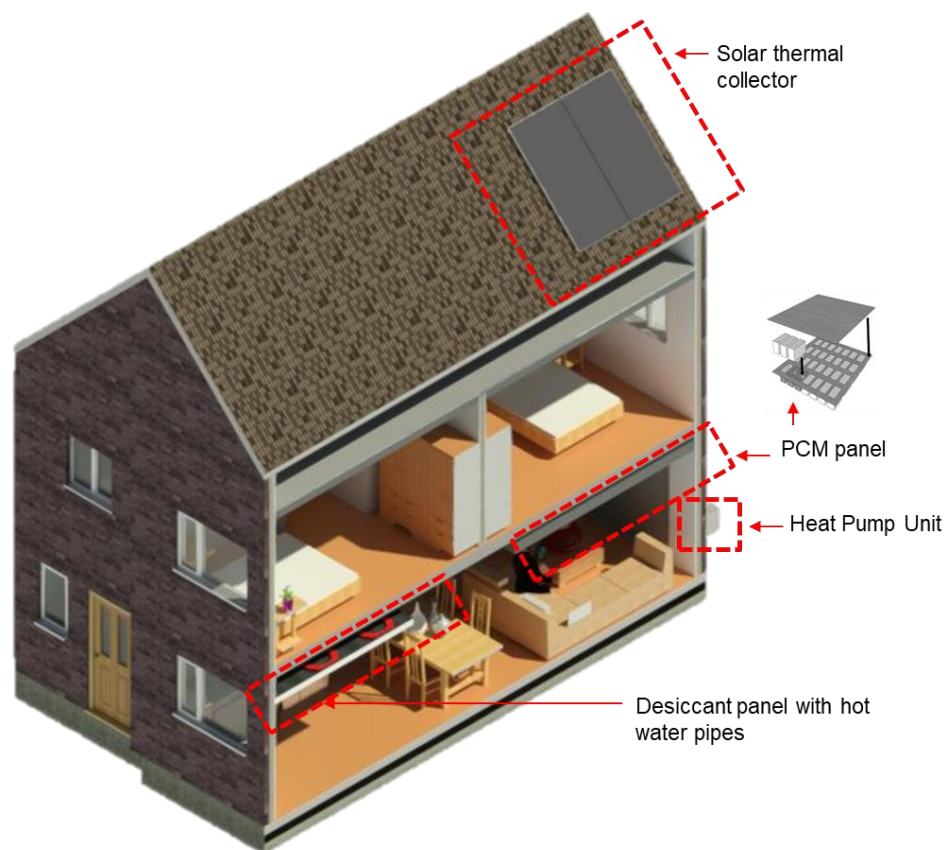


Figure 7.30 Tri-modular system integration in a residential dwelling.

## 7.7 Summary

This chapter evaluates the performance of the tri-modular system in residential buildings. For this research, testing the performance of the technologies in a large-scale scenario provides insight for its commercial application. In the case of the PCM, it was found that the ceiling panels could attain a 5 °C temperature difference. This could potentially eliminate the requirements for HVAC systems in the UK, as during the modelling evaluation the maximum indoor temperature was 30 °C.



The desiccant box provides an alternative solution for the system integration, as it is considering the use of hot water pipes for regeneration purposes. During the experimental evaluation, it was found that the system adsorbed 12% of the humidity in the room. Furthermore, the regeneration process could be completed in a 12 hour cycle. This showcases the ability to incorporate this material in residential dwellings, as both cycles could be attained during 24 hours.

The experimental results for the solar-assisted heat pump demonstrate the ability of the system to harvest the solar radiation, producing domestic hot water, a proportion of this hot water was used to recharge the desiccant panel. Moreover, the system showed the capacity to cope with the heating demand at night-time, without solar radiation.

It can be concluded that the tri-modular system can successfully be integrated for residential application, assisting with the heating and cooling loads and helping regulate the humidity levels.

# Chapter 8 Economic analysis and environmental impact

## 8.1 Introduction

In this chapter, the economic and environmental analysis of the system components is evaluated. Assessing the commercial viability of the energy saving technologies is complicated as there is no economic gain, and only focuses on the reduction of the economic loss. The integration of the tri-modular system is considered for the UK market and contemplates each technology individually. The estimated capital cost concentrates on the integration of the system as established during the experimentation evaluation, considering the installation cost. The systems are compared with commercially available solutions. In the case of the PCM application, the environmental assessment is investigated in Energy Plus, where it compares the CO<sub>2</sub> emission reduction by the integration of this material.

## 8.2 Economic evaluation

### 8.2.1 Market environment

Worldwide, the current energy panorama requires accelerated transitions towards sustainable measures. The UK government set policies to encourage efficient and sustainable new builds as part of the climate change mitigation strategies (Greenwood, Congreve and King, 2020); furthermore, some of the policies consider the retrofit for older homes. The green building sector is of key importance for sustainability and climate change, having a considerable impact in terms of materials, energy consumption, and greenhouse gas emissions (O'Neill and Gibbs, 2020). The UK Government has changed the legislation in order to reduce the carbon emissions from Green House Gases (GHG) to net-zero by 2050. The government roadmap to achieve the net carbon zero is shown in Figure 8.1.

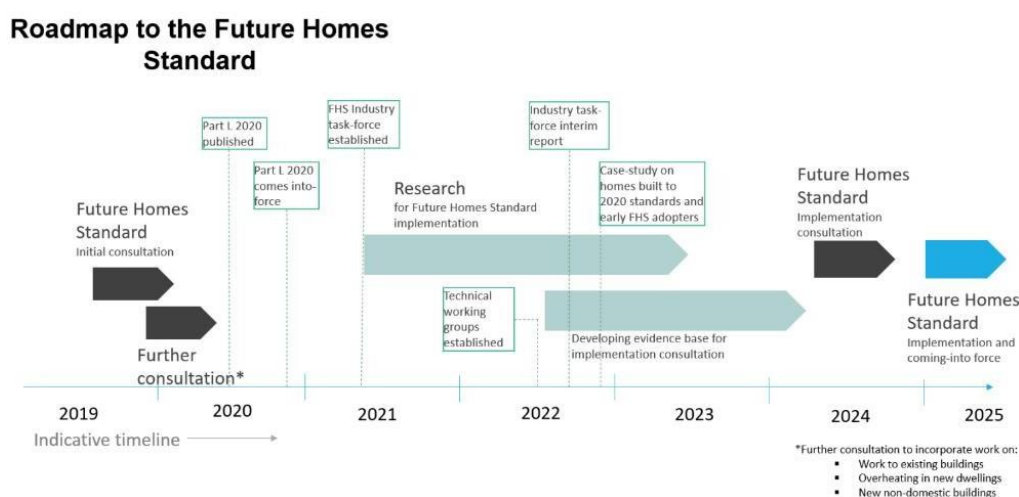


Figure 8.1 Roadmap to future homes standard.

This includes the electrification of the heating, transport and increasing the proportion of renewable electricity on the National Grid. The

Government is putting in place financial rewards for low carbon electricity generation, the new Future Homes Standard aims to improve the energy performance of new homes, making them 'zero carbon ready' by 2025.

#### **8.2.1.1 PCM- passive cooling**

Across the UK, local councils have introduced policies for new buildings encouraging passive and free cooling approaches to be considered first, with AC only to be used as a last resort. Costs, both capital and running, are one of the main things limiting the widespread use of AC in countries such as the UK. In the UK, an estimated 0.5% of homes have air conditioning, in contrast to USA where AC accounts for about 15% of the country's energy consumption. Although the use of AC in UK homes is expected to grow by 50% by 2030, its use will remain quite limited (*Residential Energy Consumption Survey (RECS) - Energy Information Administration, 2015*). The lack of widespread use of AC in UK homes can also be attributed to social factors. In the UK, AC is often considered more of a luxury than a necessity, limiting its widespread use (Mclachlan *et al.*, 2016). This is closely linked to the high costs of AC systems; therefore, one of the main drivers to change people's perception of the accessibility of home cooling would be to reduce costs. For this reason, PCM panels provide an environmentally friendly solution to address the cooling loads in the UK weather.

#### **8.2.1.2 Solid desiccants**

There has been a significant increase in the use of soft adsorbents and desiccants in emerging economies. The average prices of European and

the Americas suppliers have increased in the past three years, due to an increase in the costs of raw material, energy, and labor. The major end-user segments are oil and gas refineries, petrochemicals, process industries, construction, pharmaceutical, refractories, water treatment plants, and abrasives. The global market for desiccants and adsorbents is growing; the market in terms of volume during 2014 was estimated to be 3,016 thousand MT. Desiccants and adsorbents are ceramic mineral-based products, which are produced by specialized manufacturing units globally. Conventional porous desiccant materials such as silica gel, mesoporous silicate, active carbon, and natural rocks, have the advantages of stable characteristics and low cost; nonetheless, they tend to present low adsorption capacity.

#### **8.2.1.3 Heat pumps**

The technological challenges exist in the marketplace with an increased need for improvement in heat pump technology. Carbon dioxide emission savings from a heat pump system as compared with a gas boiler would depend on a country's electricity grid fuel mix. Greening et al. assessed UK domestic heat pumps and found that the lifetime cycle emissions of the GSHPs remain higher than a conventional gas boiler due to the electricity grid's fuel mix (Greening and Azapagic, 2012). For this reason, adding a PVT or SAHP would directly increase the benefits of the system as it would reduce or eliminate the energy consumption replace by the PV and thermal panels. Heat Pump technology is considered one of the best solutions for reducing both domestic and commercial carbon footprints.

### 8.2.2 Estimation cost

Performance evaluation every scenario was evaluated based on the cooling load reduction, energy reduction, and cost evaluation. Equations (1) to (2) were used to evaluate the cooling and energy performance.

The simple payback is calculated for the energy savings measures in aggregate by dividing the total incremental cost of the measures by the energy savings in pounds. The estimated cost is in relation to the UK market. The following equations were used to calculate the economic evaluation and payback period (Nazi *et al.*, 2017).

$$\text{Energy load reduction (kWh)} = \text{Initial energy load} - \text{Energy load with PCM} \quad (8.1)$$

$$\text{Energy load reduction (\%)} = \frac{\text{Energy load reduction (kWh)}}{\text{Initial energy load} \times 100\%} \quad (8.2)$$

$$\text{Energy reduction cost (£/kWh)} = \text{Initial cost} / \Sigma \text{Energy reduction} \quad (8.3)$$

$$\Sigma \text{Energy reduction (kWh)} = \text{Annual energy reduction} \times \text{lifetime} \quad (8.4)$$

$$\text{Payback period (year)} = \Sigma \text{Retrofit cost} / \Sigma \text{Saving on energy bills} \quad (8.5)$$

$$\Sigma \text{Saving on energy bills (£)} = \Sigma \text{Energy reduction} \times \text{Energy price per kWh} \quad (8.6)$$

$$\Sigma \text{Retrofit cost/ installation cost (£)} = [(\text{Material cost}) + (\text{reinforcement structure} \times \text{installation area})] \times 10\% \text{ installation cost} \quad (8.7)$$

#### 8.2.2.1 PCM – Cooling control

Concerning the economic return, both electricity tariff and capital cost of PCM are essential factors affecting the successful application of PCM integrated into the ceiling of buildings. Following the PCM calculations presented in Chapter 3 and considering S23 as the selected candidate.

$$S23 \ V_{PCM} = 50 / 1530 = 0.326 \text{ m}^3 \quad (8.8)$$

Considering the panel thickness at 0.018 m the required space is 18 m<sup>2</sup>, each panel has a dimension of 24 cm x 49 cm. The cost of the PCM panel

is £7.00 and was obtained from PCM Products Ltd ©, the estimated number of panels to cover the area is 72. Table 8.1, includes the reference parameters for the PCM cost, savings, and payback period, using the data from the simulation results and equations (1-7).

Table 8.1 Cooling control system cost.

Cooling load reduction (kWh)	572.50
Cooling load reduction (%)	50.89
Energy reduction cost (£/kWh)	1.24
ΣEnergy reduction (kWh)	17175.05
Payback period (year)	2.58
ΣSaving on energy bills (£)	8226.85
ΣRetrofit cost/ installation cost (£)	21240.00

According to the Energy Savings Trust, the average price of a kWh in the UK is around 14.37p (October 2021). The installation cost considers the metal reinforcement gross internal floor area Rate (£/m<sup>2</sup>) BCIS Index 100 having a range of 83 – 108 per m<sup>2</sup>. In this investigation the average price was utilized, having a cost for the structural reinforcement at 95.5 (£/m<sup>2</sup>), an addition of 10% of the retrofit/installation cost was added to cover the labour. The maintenance cost is negligible during the lifetime period and in this case, the lifetime duration of the PCM panel is 30 years.

An additional benefit to adding this thermal mass is a reduction in future variable time-based charges for energy use from electricity consumed for heating. As the temperature of the house remains more stable and requires less heating during peak tariff times of the day.

#### 8.2.2.2 Solid desiccant – Humidity control

The building insulation has developed additional drawbacks due to the airtightness. This has increased moisture concerns in buildings that sometimes have been compensated by the incorporation of air-

conditioning systems. The application of the solid desiccant absorbent provides an easy installation, with limited maintenance requirements reducing the cost of the system. Following system sizing presented in Chapter 3 and assuming a room temperature of 15 °C, humidity at 70% RH, and the desired humidity of the room at 50% RH.

The following calculations are estimated:

Absolute humidity corresponding to 70% RH is equal to 9 g/m<sup>3</sup>

Absolute humidity corresponding to 50% RH is equal to 6.4 g/m<sup>3</sup>

The cost-benefit analysis is calculated by calculating the payback period and considering the energy save for dehumidification through the desiccant system. Based on the model house used for the simulation analysis and allocating the desiccant composite in the kitchen, with a room size of 18.6 m<sup>3</sup>. The difference in the absolute humidity is 2.6 g/m<sup>3</sup>, multiplied by 18.6 m<sup>3</sup>= 48.36 g/m<sup>3</sup>. This is equal to 0.048 kilograms per hour or 0.048 litres per hour, multiplied for 24 hours is equal to 1.15 kg per day. The retail price of the raw vermiculite is £26.62 per 10 kg, the price of MgSO<sub>4</sub>-CaCl is £46.97 per kg (Fisher Scientific). The cost of the vermiculite - MgSO<sub>4</sub>-CaCl<sub>2</sub> is £78.95 per 1.15 kg. The prefabricated panel containing the hot water pipes as described in Figure 8.2 have a price range between £120 to £320. The average price for the extractor fan has a price range between £80 to £160. The average price of the system is presented in Table 8.2 and is in reference to the UK market.

Table 8.2 Humidity control system components.

Component	Cost (£)
Raw vermiculite	0.66



Salts ( $\text{MgSO}_4\text{-CaCl}_2$ )	78.29
Pump	91.00
Radiant panel	220
Fan	509.95
Installation cost 10%	50.99
Total	560.94

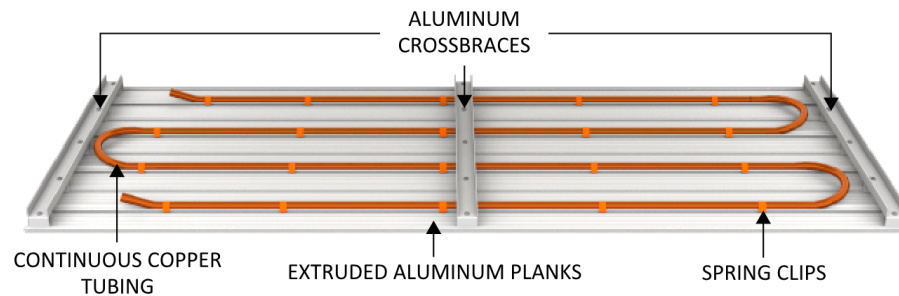


Figure 8.2 Prefabricated panel with copper pipes.

To calculate the payback period, the energy savings are compared to a commercial dehumidification system as shown in Table 8.3.

Table 8.3 Energy loads comparison of the desiccant composite vs a commercial dehumidification system.

Vermiculite - $\text{MgSO}_4\text{-CaCl}_2$			Ecor Pro DH800 dehumidification system	
	kWh/ day	Annual (£)	kWh/ day	Annual (£)
Regeneration heat (0.72 kW)	*	*	Compressor (0.5 kW)	6 314.70
Pump (0.12 kW)	1.44	75.52		
Fan (0.015 kW)	0.18	65.7	Fans (0.21kW)	2.52 132.17
Total annual running cost		141.22	Total annual running cost	446.87

\*Cover by the solar assisted heat pump.

Following equations (1-7) the payback period is presented in Table 8.4

Table 8.4 Humidity control system cost.

Energy load reduction (kWh)	2518.50
Energy load reduction (%)	80.98
Energy reduction cost (£/kWh)	0.02
ΣEnergy reduction (kWh)	25185.00
Payback period (year)	0.00
ΣSaving on energy bills (£)	355864.05
ΣRetrofit cost/ installation cost (£)	560.94

The vermiculite composite is accessible and affordable, reducing the cost, in comparison to the commercial dehumidifier (Ecor Pro DH800) the composite desiccant presents economic benefits due to the energy saving from the first year of installation. As presented by the experimental results, the application of the solid desiccant composite provides an environmentally friendly solution, based on natural components with a regeneration process that is powered by solar energy. In comparison to commercial solutions, the cost of the composite desiccant panel provides a competitive solution. Similar dehumidification methods are presented in Table 8.5.

Table 8.5 Commercial humidity control systems.			
Cost	Reference name	Cost	Reference name
£2,103.40	DH 95 S Industrial Dehumidifier	£825.00	Dri-Eaz The Cube Dehumidifier
			
£639.00	Ecor Pro DryBoat 12 DH1200 INOX	£549.99	Dehumidifier - CR70 230V
			
£428.95	Ecor Pro DH800 Commercial Dehumidifier		

### 8.2.2.3 Heat Pump System – Heating control

The integration of the solar-assisted heat pump system generates a sustainable alternative to standard air-source systems. The system is composed of two solar thermal collectors, the heat pump unit and the domestic hot water tank with a capacity of 150 litres. Following the system sizing presented in Chapter 3, the calculations for the solar assisted heat pump are as follows:

$$Q_s = (949) \times (1) \times (4) \times (0.9) \times (0.71) \times (0.45) \times (1) = 1091.53 \text{ kWh/year}$$

Collector Area is the total aperture area of the collectors, i.e. the area of the opening through which solar radiation is admitted, not the total collector area. Zero-loss Collector Efficiency ( $\eta^0$ ) In an ideal system all the sunlight that falls on the collector would be absorbed but this is not the case in reality. The value would depend on the collector type as described in Table 8.6.

The zero-loss collector efficiency measures the fraction of sunlight absorbed by a collector. It has a value between 0 and 1 with a higher value indicating more energy is absorbed.

Collector Heat Loss Coefficient ( $a_1$ ) As the collector absorbs sunlight it will heat up and become warmer than its surroundings, which inevitably leads to some loss of heat from the collector. The heat loss coefficient,  $a_1$ , accounts for this heat loss. A small value indicates that only a small amount of the heat absorbed is lost to the surroundings.

In this case the collector factor is equal to:

$$= 0.97 - 0.0367 \left( \frac{a^*}{\eta_0} \right) + 0.0006 \left( \frac{a^*}{\eta_0} \right)^2 \text{ if } \frac{a^*}{\eta_0} < 20 \quad (8.9)$$

$$= 0.693 - 0.0108 \times \left( \frac{a^*}{\eta_0} \right) \text{ if } \frac{a^*}{\eta_0} \geq 20 \quad (8.10)$$

Table 8.6 Default collector parameters (BRE, 2014).

Collector type	$\eta_0$	$a^*$	Ratio of aperture area to gross area
Evacuated tube	0.6	3	0.72
Flat plate glazed	0.75	6	0.9
Unglazed	0.9	20	1

Overshading is the amount of shading of the collector by adjacent structures, e.g. buildings, trees, etc, and is described in Table 8.7.

Table 8.7 Overshading factor (BRE, 2014).

Overshading	% of sky blocked by obstacles	Overshading factor
Heavy	>80%	0.5
Significant	>60% - 80%	0.65
Modest	20% - 60%	0.8
None or very little	<20	1.0

The commercial cost of the fitted system is £6500 (Arkaya Energy Ltd., 2016), and includes two solar thermal collectors, the heat pump unit, fan, a 300 litres hot water tank, and the installation cost with the additional components (pipes, insulation material, pumps, etc.); compared to the Mitsubishi Electric Ecodan system which consists of an air source heat pump and the pre-plumbed cylinder is £8500 excluding installation costs. This provides an initial cost saving of £2000 plus the labour cost of installation of the alternative system.

In addition to the energy saving provided, the solar-assisted heat pump reduces the required amount of refrigerant used which has a positive environmental impact and due to the limited number of components, there is less maintenance required.

## 8.3 Environmental analysis

Assessing the economic viability of energy saving technologies focuses on the reduction of the economic loss, rather than a direct economic gain, for this reason, it is important to evaluate the environmental impact of the system application. Evidence shows that the global environment could lose its qualities for sustainability, due to human activities, causing irreversible damage to the environment. In the built environment the focus has been towards energy and resources, driving sustainable designs and operations.

### 8.3.1 Life Cycle Assessment

The life cycle assessment (LCA) comprises a systematic evaluation of the environmental impacts arising from the provision of a product or a service and is described in Figure 8.3.

Life cycle assessment has developed rapidly over recent decades, identifying the resource flows and environmental impacts associated with building construction and services. The life cycle assessment functions as an environmental assessment tool. The interest in LCA has accelerated alongside the growing demand to assess and reduce greenhouse gas emissions across different manufacturing and service sectors (Horne, 2009).

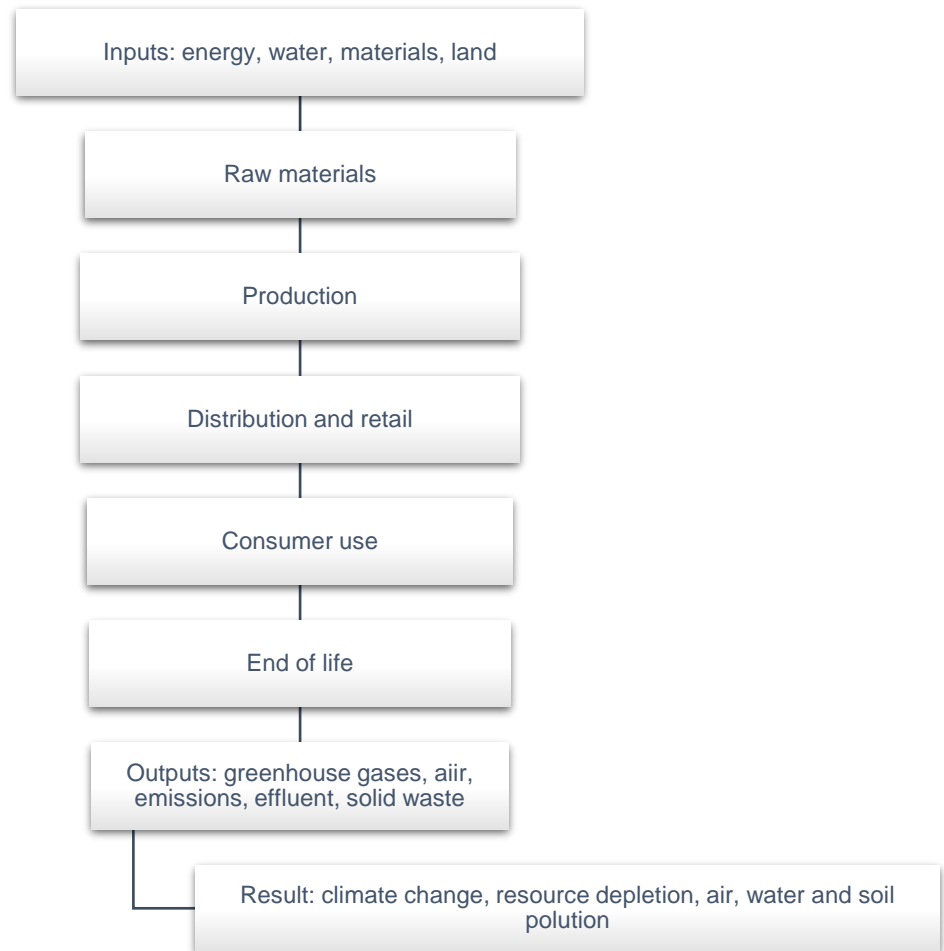


Figure 8.3 LCA chain.

### 8.3.2 Modelling method

To assess the LCA performance of the house model the parameters applied in the Chapter 4 modelling method are maintained. The environmental evaluation was performed using Energy-Plus v8.4. In this case, S23 was used as the PCM in all the simulations.

### 8.3.3 Environmental impact

Typically, when a new building technology is evaluated the energy performance of a baseline building is compared to the energy and life-cycle costs of alternatives to determine cost-effectiveness. The energy performance calculated by Energy Plus has converted into a mass or volume of pollutants emitted. To calculate the mass or volume of each

pollutant, consumption is multiplied by an emissions factor for each fuel (natural gas, electricity, fuel oil, diesel, or coal). Figure 8.4 presents the total CO<sub>2</sub> emissions carbon equivalent mass in kg per month, showing a 3% reduction in the emissions with the application of the PCM ceiling panels.

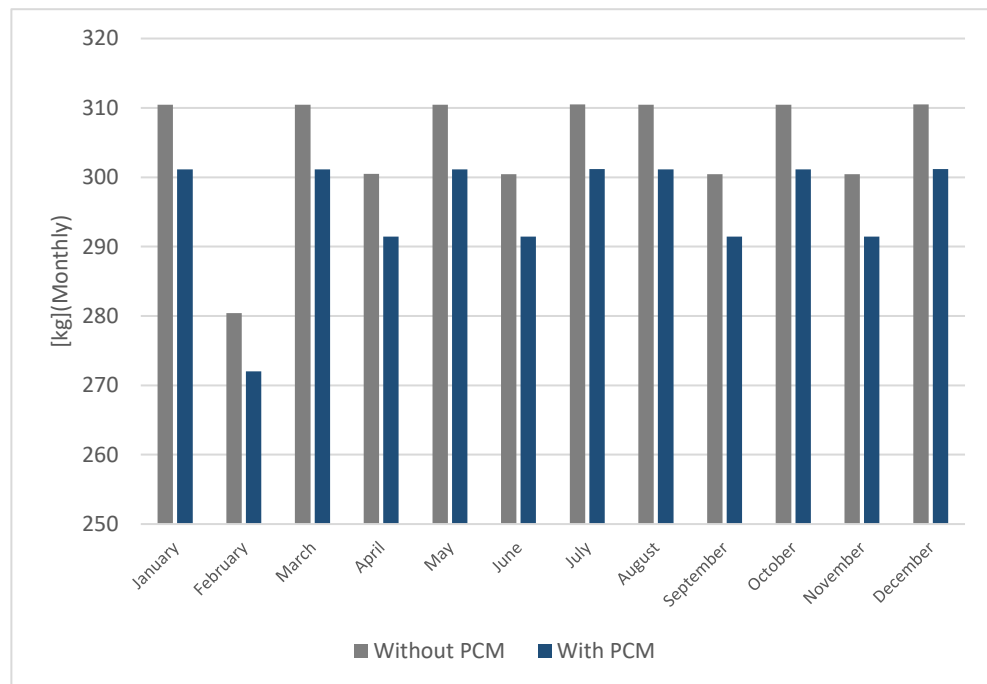


Figure 8.4 Environmental impact (total CO<sub>2</sub>).

### 8.3.3.1 Electricity consumption

The building energy demand can have a critical influence on building carbon emissions. The software simulates the equipment in the zone which consumes electricity, such as computers, televisions, and cooking equipment, also known as “plug loads.” All of the energy consumed by the equipment becomes a heat gain in the zone or is lost (exhausted). The electrical input to the equipment ultimately appears as heat that contributes to zone loads. Figure 8.5 presents the electricity

reduction of 6% due to the energy savings generated in the heating and cooling demand.

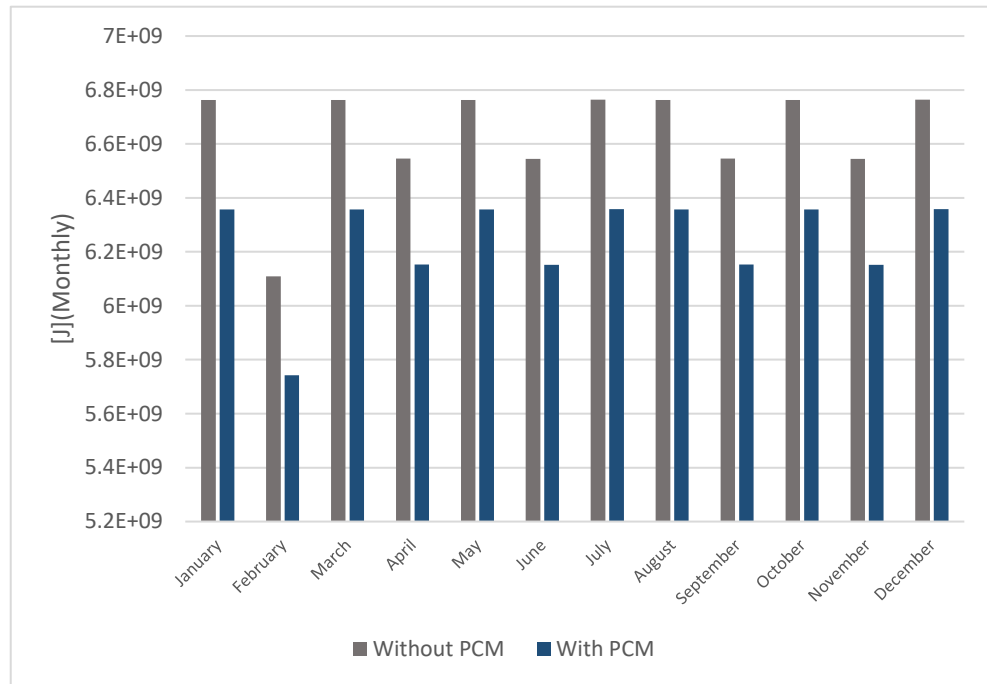


Figure 8.5 Electricity consumption comparison with and without PCM.

### 8.3.3.2 Carbon dioxide (CO<sub>2</sub>)

The units are grams per Megajoule. Carbon dioxide gas is naturally produced by animals during respiration and through the decay of biomass and used by plants during photosynthesis. Although it only constitutes 0.04 percent of the atmosphere, it is one of the most important greenhouse gases. The combustion of fossil fuels is increasing carbon dioxide concentrations in the atmosphere, which is believed to be contributing to global warming. Figure 8.6 presents the CO<sub>2</sub> reduction in kg per month, having a consistent reduction through the year and generating a 10% decrease.



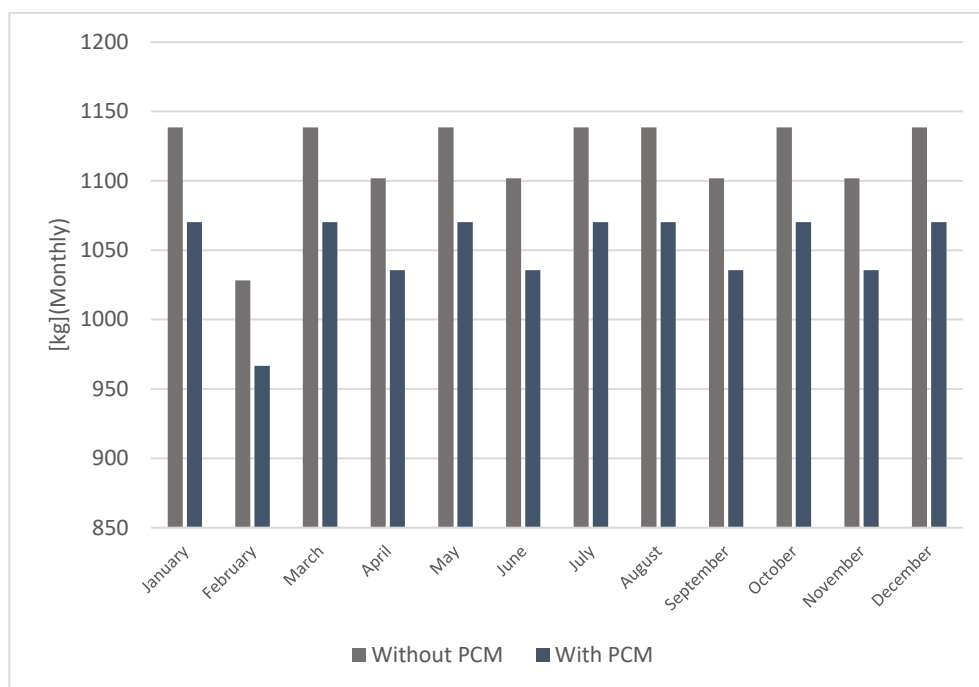


Figure 8.6 Carbon emissions.

### 8.3.3.3 Carbon Equivalent

This equivalent is based on a factor of 1.0 for carbon. This group of gases includes carbon dioxide (CO<sub>2</sub>), carbon monoxide, nitrous oxide, methane, halocarbon emission, hydrofluorocarbons (HFC), perfluorocarbons (PFC), and chlorofluorocarbons (CFC). Figure 8.7 presents the carbon equivalent reduction of the greenhouse gases, having an overall average reduction of 3%.

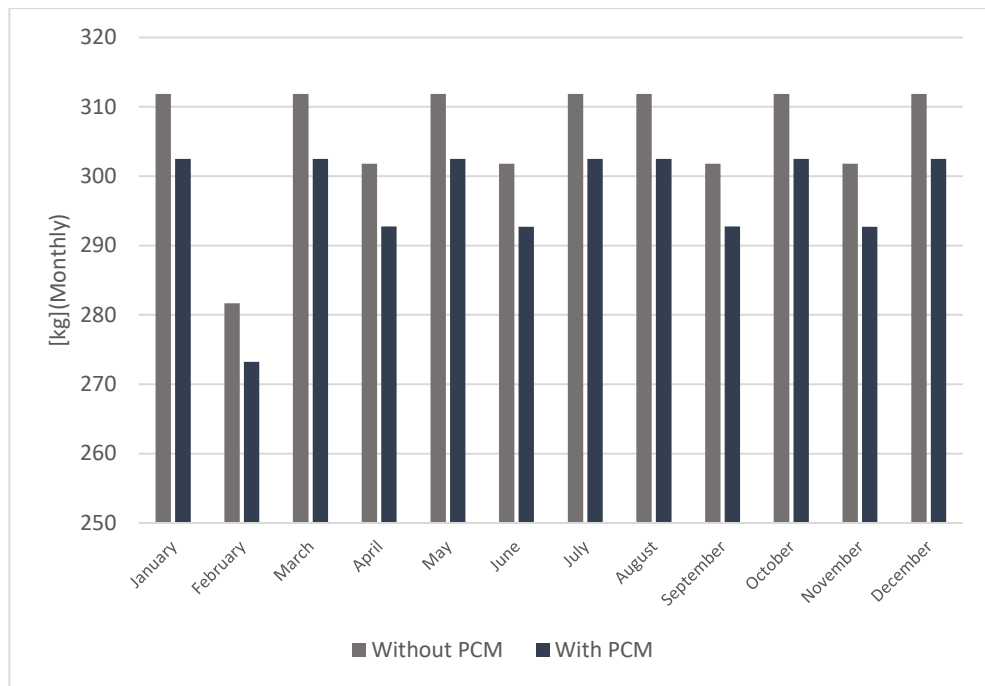


Figure 8.7 Carbon Equivalent CE.

Table 8.8 presents the monthly heating and cooling loads in watts. It can be noticeable the reduction in the energy demand with the application of the PCM ceiling tiles.

Table 8.8 Heating and cooling calculations per month.

Date	Average heating Without PCM (W)	Average cooling Without PCM (W)	Average heating With PCM (W)	Average cooling With PCM (W)
January	1491.79	0	1099.41	0
February	1435.13	0	1057.65	0
March	947.44	3.46	698.24	2.55
April	764.32	9.27	563.28	6.83
May	344.98	52.13	254.24	38.41
June	71.36	167.73	52.59	123.61
July	1.37	317.54	1.01	234.02
August	21.06	274.90	15.52	202.59
September	155.26	49.42	114.42	36.42
October	549.95	3.55	405.30	2.62
November	1011.61	0	745.53	0
December	1380.63	0	1017.49	0

Assuming an expected life cycle of 20 years, the total energy savings and CO<sub>2</sub> reductions can be calculated by multiplying the energy savings and CO<sub>2</sub> reductions per annum by life cycle. The results shown in Table 8.5 present the economic benefits of incorporating PCM ceiling panels in buildings.

Table 8.9 CO<sub>2</sub> emissions over a 20 year period.

<b><math>COST_e</math></b>	<b>Energy Cost (£)</b>	<b>CO<sub>2</sub> Reduction (kg)</b>	<b>CO<sub>2</sub> Reduction (tons)</b>
Without PCM		6200	6.8
With PCM	3810.629	6020	6

In general, the environmental assessment supports the conclusion that the addition of the PCM ceiling panels generates energy savings throughout the year. The electricity, CO<sub>2</sub> emissions, carbon equivalent, and the overall environmental impact total CO<sub>2</sub> emissions carbon equivalent mass have been positively affected by the addition of the S23 PCM panels. The numerical results presented in this study highlight the potential of energy consumption reduction due to the implementation of PCM ceiling panels all year round. With the assistance of computational software now it is possible to evaluate novel materials using their thermal properties and have a better understanding of the thermal performance, providing evidence about the economic and environmental improvements.

## 8.4 Summary

The work conducted in this chapter focuses on the commercial application of the system. The estimated capital cost focuses on the integration of the system as previously tested, taking into account the installation cost. For the solid desiccant and heat pump system, the commercial value is easier to identify as the market provides similar systems as reference. The application of PCM panels in residential buildings is very limited and for this reason, assessing the cost and determining the environmental impact is important to promote the application of this technology in the current construction sector. To determine the environmental impact, a simulation model using S23

panels has been developed focusing on the previously presented house design described in Chapter 4.

The findings from the model-based economic assessment offered promising energy and financial savings, electricity tariffs play an additional role in the system's economic impact. As the electricity tariffs tend to increase over time installing the tri-modular system is a cost-effective solution despite the initial investment cost.

Besides the clear advantages in the environmental and technical aspects, the investment cost is significant for achieving a widespread diffusion in the market. To promote and increase the system implementation, manufacturers should work on lowering market prices in a relatively short period. In addition to the system cost, governmental entities should support the inclusion of energy saving technologies in residential and commercial buildings.

# Chapter 9 Conclusions and future work

## 9.1 Summary of the work

This investigation aims to design, develop and evaluate a cost-effective and environmentally friendly system that focuses on heating, cooling, and humidity control in buildings. The project focuses on the development of a new class of smart materials for building interiors to reduce energy consumption and CO<sub>2</sub> emissions. The system objective focuses on obtaining a “total comfort” solution by controlling both temperature and humidity.

The individual objectives have been discussed throughout this investigation. First of all, a comprehensive literature review has provided the grounds for the experimental procedure, each element of the system has been analysed. An extensive literature review of PCMs and solid desiccants have been included, with a high emphasis on enhancement methods. The state-of-the-art heat pump systems have been incorporated, with special attention to the SAHP systems.

Simulation and preliminary testing have set the grounds for the experimental evaluation. The tri-modular system has been designed and tested in the laboratory, furthermore, each component has been integrated into a residential testing site for experimental analysis, proving a satisfactory performance.

This research addresses the system components design, aiming to create an aesthetically pleasing solution for commercial applications. For this reason, the evaluation of different PCMs and composite desiccants has been assessed. The experimental results of the tri-modular system have shown its effectiveness to control the heating, cooling, and humidity under UK weather.

To promote the application of the proposed system the economic cost has been assessed. The cost analysis provided an insight into the commercial application of the system as the current economical trends endorse the application of energy saving technologies. The tri-modular system provides an environmentally friendly solution for heating and cooling, eliminating the need for alternative systems. In terms of humidity control, solid desiccant materials were adopted as a viable method for moisture control in the UK climate, which is characterized to present high humidity levels.

## **9.2 Major findings**

This research has demonstrated energy, environmental and economic benefits obtained by the tri-modular system that controls the heating,

cooling, and humidity in buildings. Novel materials have been developed for building applications, where the performance has been experimentally tested.

The system is able to control the heating, cooling, and humidity aspects involved in residential buildings.

The work undertaken offer further knowledge of the performance of PCMs for building integration. With the evaluation of several materials and enhancement methods.

Novel PCM encapsulation methods have been proposed for ceiling applications, proving their efficacy with experimental evaluation.

The selection of low-cost, environmentally stable, and abundant solid desiccant material has been selected for moisture control. The development of new composite material has been experimentally evaluated, proving its suitability for building integration.

The solar-assisted heat pump system has been evaluated under different environmental conditions, demonstrating its effectiveness to cope with the heating requirements limited radiation periods. The SAHP was able to meet the requirements for space heating and to regenerate the solid desiccant absorbent.

### **9.3 Limitations and recommendations**

The research has investigated the performance of a tri-modular system aiming to control heating, cooling, and humidity to achieve thermal comfort in buildings. This has been focusing on the development of novel

materials and is supported by the integration of a solar-assisted heat pump.

During the PCMs laboratory evaluation, special interest was given to the encapsulation methods as an enhancement device. Several panels presented high performance, however, the manufacturing process limited large-scale testing, as in some cases the panels presented leakage. Improving the manufacturing process would not only alleviate some safety concerns but also provide the opportunity for a comprehensive evaluation.

### 9.3.1 Recommendations and future work

The work conducted has unveiled novel findings in the application of both enhanced PCM materials and composite solid desiccants based on vermiculite as the host matrix. These investigations act as the base ground for further investigations.

In this regard, future work is advised to investigate PCMs ceiling panels for different climate conditions. The experimental work has set the ground for the application of the ceiling panels as a TES system.

Forthcoming research on optimizing the design of the proposed encapsulation methods and continuing evaluating the performance for building applications will help accelerate the commercial integration of the PCMs panels. Furthermore, the consideration of additional highly conductive materials should be assessed to improve the current performance.



As suggested by the literature review, the application of PCMs has shown beneficial performance under different climate conditions. Later work contemplates the application of PCM ceiling tiles for hot climates, following the same principles established in this investigation. The cooling system is considered and expanded with the integration of a novel system design, where the PCM is coupled with a PV system and a DC-vapor compressor to address the cooling requirements under extremely hot weather. Alternative applications consider using lower melting temperatures to address the energy requirements. Moreover, considering different envelope materials and their impact on PCMs is desirable.

Analysing the construction trends, and considering the PCM ceiling load into the building structure could expand the amount of PCM incorporated and potentially exponentiate its application.

Similarly, in the case of the solid desiccant panels, the climate conditions would give the baseline in terms of alternative applications. Nevertheless, the evaluation of different building envelope materials could have a significant impact on the performance of this moisture control method. In addition, considering the loads into the building structure could increase the applications solutions.

The preliminary testing in Chapter 5, showed the prominent results of some encapsulation methods. Subsequent investigation contemplates modifying the manufacturing process to allow a larger-scale production. Particularly in the case of the blister panel and the honeycomb panel, that

due to the manufacturing process it could only be tested on a small scale using the environmental chamber. For the desiccant panel, new encapsulation methods could be implemented, as the popularity of the material grows, providing new solutions for encapsulation.

## **9.4 Concluding remarks**

The proposed tri-modular system addresses some of the key factors involved in thermal comfort, providing a solution in terms of heating, cooling, and humidity control. The experimental evaluation has shown the potential application for UK house dwellings, which could easily be adapted to different climatic conditions.

Each component has been individually tested, showing its feasibility to control the heating in the case of the solar-assisted heat pump unit, cooling attributed to the PCMs, and humidity in the case of the solid desiccants. The system shows endless possibilities, as each technology can work as a stand-alone system. The versatility of the solutions can be easily adapted to different climate conditions and can address the key elements involved in the human perception of thermal comfort.

The system potential for building incorporation has been assessed, demonstrating the effectiveness of the system to generate energy savings. To support the application of the system, the functionality must be accompanied by the user's satisfaction. In this regard, the aesthetic of the ceiling panels should be considered to increase the attractiveness of the system from a commercial point of view.

The UK has set itself the ambitious goal of reducing greenhouse gas emissions. Technological innovation and declining costs have accelerated energy saving solutions, revolutionizing the possibilities for a low-carbon future. The tri-modular system provides an integral approach, contributing with an environmentally friendly alternative for the building's highest energy requirements. Undoubtedly, the energy benefits produced by the system are a step forward in the transition to a net-zero future.

# Appendix

## Journal publications

Velasco-Carrasco, M. *et al.* (2020a) 'Experimental Evaluation of Thermal Energy Storage (TES) with Phase Change Materials (PCM) for Ceiling Tile Applications', *Future Cities and Environment*. Ubiquity Press, 6(1). doi: 10.5334/fce.101.

Velasco-Carrasco, M. *et al.* (2020b) 'Experimental evaluation of phase change material blister panels for building application', *Future Cities and Environment*, 6(1), pp. 1–7. doi: 10.5334/fce.84.

Aguilar-Santana, J. L. *et al.* (2020) 'Thermal Transmittance ( U-value ) Evaluation of Innovative Window Technologies', 6(1), pp. 1–13. doi: 10.5334/fce.99.

Aguilar-Santana, J. L. *et al.* (2019) 'Review on window-glazing technologies and future prospects', *International Journal of Low-Carbon Technologies*, 15(1), pp. 112–120. doi: 10.1093/ijlct/ctz032.

### 9.1.1 Conference participation

Chen, Z. *et al.* (2019) 'Experimental Study on Dehumidification Performance of Vermiculite-based Desiccants'. *Proceedings of the 18th International Conference on Sustainable Energy Technologies* vol. 2 pp. 9-17.

Velasco-Carrasco, M. *et al.* (2018) 'A Review in PCMs Application to Enhance Building Performance'. *Proceedings of the International Academic Conference for Graduates, NUAA*. vol. A2, pp.13-19.

Chen, Z. et al. (2018) 'Review on solid desiccant materials for humidity control in buildings'. *Proceedings of the 17th International Conference on Sustainable Energy Technologies*, vol. 2 pp. 245-255.

# References

- Abdelrahman, H. E. *et al.* (2019) 'Performance enhancement of photovoltaic cells by changing configuration and using PCM (RT35HC) with nanoparticles Al<sub>2</sub>O<sub>3</sub>', *Solar Energy*. Elsevier, 177(November 2018), pp. 665–671. doi: 10.1016/j.solener.2018.11.022.
- Abdelsalam, M. Y. *et al.* (2017) 'Heat transfer characteristics of a hybrid thermal energy storage tank with Phase Change Materials (PCMs) during indirect charging using isothermal coil heat exchanger', *Solar Energy*. Elsevier, 157(September), pp. 462–476. doi: 10.1016/j.solener.2017.08.043.
- Adams, S. *et al.* (2020) 'Energy consumption, economic policy uncertainty and carbon emissions; causality evidence from resource rich economies', *Economic Analysis and Policy*. Elsevier B.V., 68, pp. 179–190. doi: 10.1016/j.eap.2020.09.012.
- Adedoyin, F. F. and Zakari, A. (2020) 'Energy consumption, economic expansion, and CO<sub>2</sub> emission in the UK: The role of economic policy uncertainty', *Science of the Total Environment*. Elsevier B.V., 738, p. 140014. doi: 10.1016/j.scitotenv.2020.140014.
- Ahmad, K. *et al.* (2020) 'Engineering of Zirconium based metal-organic frameworks (Zr-MOFs) as efficient adsorbents', *Materials Science and Engineering B: Solid-State Materials for Advanced Technology*. Elsevier Ltd, p. 114766. doi: 10.1016/j.mseb.2020.114766.
- Ahmad, M. W. *et al.* (2016) 'Building energy metering and environmental monitoring - A state-of-the-art review and directions for future research', *Energy and Buildings*. Elsevier Ltd, pp. 85–102. doi: 10.1016/j.enbuild.2016.03.059.
- Ai, F. *et al.* (2021) 'Research into the super-absorbent polymers on agricultural water', *Agricultural Water Management*. Elsevier B.V., 245, p. 106513. doi: 10.1016/j.agwat.2020.106513.
- Amani, M. and Bahrami, M. (2021) 'Greenhouse dehumidification by zeolite-based desiccant coated heat exchanger', *Applied Thermal Engineering*. Elsevier Ltd, 183, p. 116178. doi: 10.1016/j.applthermaleng.2020.116178.
- Anandarajah, G. and Strachan, N. (2010) 'Interactions and implications of renewable and climate change policy on UK energy scenarios', *Energy Policy*. Elsevier, 38(11), pp. 6724–6735. doi: 10.1016/j.enpol.2010.06.042.
- Ansuini, R. *et al.* (2011) 'Radiant floors integrated with PCM for indoor temperature control', *Energy and Buildings*. Elsevier B.V., 43(11), pp. 3019–3026. doi: 10.1016/j.enbuild.2011.07.018.
- Arkaya Energy Ltd. (2016) *Thermodynamic System Solar assisted heat pump*. Available at: <http://www.arkaya.co.uk/> (Accessed: 24 July 2021).

- Azari, A. *et al.* (2020) 'Comprehensive systematic review and meta-analysis of dyes adsorption by carbon-based adsorbent materials: Classification and analysis of last decade studies', *Chemosphere*. Elsevier Ltd, p. 126238. doi: 10.1016/j.chemosphere.2020.126238.
- Barreneche, C. *et al.* (2016) 'In situ thermal and acoustic performance and environmental impact of the introduction of a shape-stabilized PCM layer for building applications', *Renewable Energy*, 85, pp. 281–286. doi: 10.1016/j.renene.2015.06.054.
- Barthelmes, V. M. *et al.* (2017) 'Occupant behaviour lifestyles and effects on building energy use: Investigation on high and low performing building features', in *Energy Procedia*. Elsevier Ltd, pp. 93–101. doi: 10.1016/j.egypro.2017.11.126.
- Biswas, K. *et al.* (2014) 'Combined experimental and numerical evaluation of a prototype nano-PCM enhanced wallboard', *Applied Energy*. Elsevier Ltd, 131, pp. 517–529. doi: 10.1016/j.apenergy.2014.02.047.
- Borderon, J., Virgone, J. and Cantin, R. (2015) 'Modeling and simulation of a phase change material system for improving summer comfort in domestic residence', *Applied Energy*. Elsevier Ltd, 140, pp. 288–296. doi: 10.1016/j.apenergy.2014.11.062.
- Bouzenada, S. *et al.* (2016) 'Experimental Comparative Study on Lithium Chloride and Calcium Chloride Desiccants', in *Procedia Computer Science*. Elsevier, pp. 718–725. doi: 10.1016/j.procs.2016.04.159.
- BRE (2014) *The Governments Standard Assessment Procedure for Energy Rating of Dwellings 2012 edition*. Available at: [www.bre.co.uk/sap2012](http://www.bre.co.uk/sap2012) (Accessed: 4 August 2021).
- Broad, O., Hawker, G. and Dodds, P. E. (2020) 'Decarbonising the UK residential sector: The dependence of national abatement on flexible and local views of the future', *Energy Policy*. Elsevier Ltd, 140, p. 111321. doi: 10.1016/j.enpol.2020.111321.
- Cabeza, L. F. *et al.* (2011) 'Materials used as PCM in thermal energy storage in buildings: A review', *Renewable and Sustainable Energy Reviews*. Elsevier Ltd, 15(3), pp. 1675–1695. doi: 10.1016/j.rser.2010.11.018.
- Cai, Y. *et al.* (2011) 'Effects of nano-SiO<sub>2</sub> on morphology, thermal energy storage, thermal stability, and combustion properties of electrospun lauric acid/PET ultrafine composite fibers as form-stable phase change materials', *Applied Energy*. Elsevier Ltd, 88(6), pp. 2106–2112. doi: 10.1016/j.apenergy.2010.12.071.
- Cascione, V. *et al.* (2019) 'A review of moisture buffering capacity: From laboratory testing to full-scale measurement', *Construction and Building Materials*. Elsevier Ltd, pp. 333–343. doi: 10.1016/j.conbuildmat.2018.12.094.
- Casey, S. P. *et al.* (2014a) 'Salt impregnated desiccant matrices for “open”

thermochemical energy storage—Selection, synthesis and characterisation of candidate materials', *Energy and Buildings*. Elsevier, 84, pp. 412–425. doi: 10.1016/J.ENBUILD.2014.08.028.

Casey, S. P. *et al.* (2014b) 'Salt impregnated desiccant matrices for "open" thermochemical energy storage - Selection, synthesis and characterisation of candidate materials', *Energy and Buildings*. Elsevier B.V., 84, pp. 412–425. doi: 10.1016/j.enbuild.2014.08.028.

Castrillo, N., Mercado, A. and Volzone, C. (2018) 'Solid desiccants from natural and modified bentonites', *Ceramica*. Associacao Brasileira de Ceramica, 64(372), pp. 526–537. doi: 10.1590/0366-69132018643722447.

CEN (2007) 'EN 15251 – Indoor environmental input parameters for design and assessment of energy performance of buildings-addressing indoor air quality, thermal environment, lighting and acoustics.'

Çengel, Y. A. (1998) *Heat transfer : a practical approach*. 15th ed. Boston: Mass: WBC McGraw-Hill.

Cevallos, O. R. F. (2012) 'Adsorption Characteristics of Water and Silica Gel System for Desalination Cycle', p. 72. Available at: [http://repository.kaust.edu.sa/kaust/bitstream/10754/273097/1/OscarFonseca113292\\_Thesis\\_final.pdf](http://repository.kaust.edu.sa/kaust/bitstream/10754/273097/1/OscarFonseca113292_Thesis_final.pdf).

Chata, F. B. G., Chaturvedi, S. K. and Almogbel, A. (2005) 'Analysis of a direct expansion solar assisted heat pump using different refrigerants', *Energy Conversion and Management*. Pergamon, 46(15–16), pp. 2614–2624. doi: 10.1016/j.enconman.2004.12.001.

Chen, Y. (2017) 'Packaging selection for solid oral dosage forms', in *Developing Solid Oral Dosage Forms: Pharmaceutical Theory and Practice: Second Edition*. Elsevier Inc., pp. 637–651. doi: 10.1016/B978-0-12-802447-8.00023-6.

Chen, Z. *et al.* (2018) 'Review on solid desiccant materials for humidity control in buildings', in. SET, pp. 245–255.

Chen, Z., Velasco-Carrasco, M. and Riffat, S. (2019) 'Experimental Study on Dehumidification Performance of Vermiculite-based Desiccant', in. SET, pp. 9–17.

Chua, K. J. and Chou, S. K. (2003) 'Low-cost drying methods for developing countries', *Trends in Food Science and Technology*. Elsevier Ltd, pp. 519–528. doi: 10.1016/j.tifs.2003.07.003.

Chua, K. J., Chou, S. K. and Yang, W. M. (2010) 'Advances in heat pump systems: A review', *Applied Energy*. Elsevier Ltd, 87(12), pp. 3611–3624. doi: 10.1016/j.apenergy.2010.06.014.

Chwieduk, D. A. (2017) 'Towards modern options of energy conservation in buildings', *Renewable Energy*. Elsevier Ltd, 101, pp. 1194–1202. doi: 10.1016/j.renene.2016.09.061.



- Colella, F., Sciacovelli, A. and Verda, V. (2012) 'Numerical analysis of a medium scale latent energy storage unit for district heating systems', *Energy*. Elsevier, 45(1), pp. 397–406. doi: 10.1016/j.energy.2012.03.043.
- Colla, L. *et al.* (2017) 'Nano-PCMs for enhanced energy storage and passive cooling applications', *Applied Thermal Engineering*. Elsevier Ltd, 110, pp. 584–589. doi: 10.1016/j.applthermaleng.2016.03.161.
- Contreras, G. and Platania, F. (2019) 'Economic and policy uncertainty in climate change mitigation: The London Smart City case scenario', *Technological Forecasting and Social Change*. Elsevier Inc., 142, pp. 384–393. doi: 10.1016/j.techfore.2018.07.018.
- Crawley, D. B. *et al.* (2000) 'EnergyPlus: Energy Simulation Program', *ASHRAE Journal*, pp. 49–56.
- Cui, Y. *et al.* (2011) 'The experimental exploration of carbon nanofiber and carbon nanotube additives on thermal behavior of phase change materials', *Solar Energy Materials and Solar Cells*. Elsevier, 95(4), pp. 1208–1212. doi: 10.1016/j.solmat.2011.01.021.
- Dannemand, M., Perers, B. and Furbo, S. (2019) 'Performance of a demonstration solar PVT assisted heat pump system with cold buffer storage and domestic hot water storage tanks', *Energy and Buildings*. Elsevier B.V., 188–189, pp. 46–57. doi: 10.1016/j.enbuild.2018.12.042.
- Department for Business, E. & I. S. (2020a) *Enabling a High Renewable, Net Zero Electricity System: Call for Evidence*. Available at: <https://www.elexonportal.co.uk/article/view/7324?cachebust=0hmjty3qx>, (Accessed: 9 March 2021).
- Department for Business, E. & I. S. (2020b) *Energy Consumption in the UK (ECUK) 1970 to 2019*. Available at: <https://www.gov.uk/government/collections/digest-of-uk-energy-statistics-dukes> (Accessed: 11 March 2021).
- Department for Business, E. & I. S. (2021a) *ECUK 2021: End uses data tables*. Available at: <https://www.gov.uk/government/statistics/energy-consumption-in-the-uk-2021>.
- Department for Business, E. & I. S. (2021b) 'UK Energy Trends: Section 1 - Total Energy', (December).
- Department of Energy and Climate Change (DECC) and National Statistics (2021) 'UK Energy in Brief 2021', *Energy*, p. 48. Available at: [https://www.gov.uk/government/uploads/system/uploads/attachment\\_data/file/350941/UK\\_Energy\\_in\\_Brief\\_2014\\_revised.pdf](https://www.gov.uk/government/uploads/system/uploads/attachment_data/file/350941/UK_Energy_in_Brief_2014_revised.pdf).
- Djamai, Z., Si Larbi, A. and Salvatore, F. (2019) 'A Non-paraffinic PCM Modified Textile Reinforced Concrete Sand-Wich Panel', in, pp. 453–458. doi: 10.1007/978-981-15-0802-8\_70.
- Dott, R., Genkinger, A. and Afjei, T. (2012) 'System evaluation of combined solar & heat pump systems', in *Energy Procedia*. Elsevier Ltd, pp. 562–570. doi: 10.1016/j.egypro.2012.11.066.

- Doughty, M. R. C. and Hammond, G. P. (2004) 'Sustainability and the built environment at and beyond the city scale', *Building and Environment*. Pergamon, 39(10), pp. 1223–1233. doi: 10.1016/j.buildenv.2004.03.008.
- Dowds, M. and You, S. (2019) 'Economic analysis of the routes for fulfilment of net-zero energy buildings (NZEBs) in the UK', in *Energy Procedia*. Elsevier Ltd, pp. 3541–3546. doi: 10.1016/j.egypro.2019.01.914.
- Druckman, A. and Jackson, T. (2008) 'Household energy consumption in the UK: A highly geographically and socio-economically disaggregated model', *Energy Policy*. Elsevier BV, 36(8), pp. 3177–3192. doi: 10.1016/j.enpol.2008.03.021.
- Duan, C. *et al.* (2020) 'Removal of heavy metals from aqueous solution using carbon-based adsorbents: A review', *Journal of Water Process Engineering*. Elsevier Ltd, p. 101339. doi: 10.1016/j.jwpe.2020.101339.
- Duarte, C., Raftery, P. and Schiavon, S. (2018) 'Development of Whole-Building Energy Models for Detailed Energy Insights of a Large Office Building with Green Certification Rating in Singapore', *Energy Technology*. Wiley-VCH Verlag, 6(1), pp. 84–93. doi: 10.1002/ente.201700564.
- Elarem, R. *et al.* (2020) 'A comprehensive review of heat transfer intensification methods for latent heat storage units', *Energy Storage*. Wiley. doi: 10.1002/est2.127.
- Elgafy, A. and Lafdi, K. (2005) 'Effect of carbon nanofiber additives on thermal behavior of phase change materials', *Carbon*. Pergamon, 43(15), pp. 3067–3074. doi: 10.1016/j.carbon.2005.06.042.
- Energy Information Administration, U. S. (2013) *World energy demand and economic outlook M*. Available at: [www.eia.gov](http://www.eia.gov) (Accessed: 16 March 2021).
- Energy, U. S. D. of (2020) *EnergyPlus*. Available at: <https://energyplus.net/> (Accessed: 14 December 2020).
- Enteria, N., Awbi, H. and Yoshino, H. (2017) *Desiccant Heating, Ventilating, and Air-Conditioning Systems*. Singapore: Springer Singapore Pte. Limited. doi: 10.1007/978-981-10-3047-5.
- Evangelisti, L., De Lieto Vollaro, R. and Asdrubali, F. (2019) 'Latest advances on solar thermal collectors: A comprehensive review', *Renewable and Sustainable Energy Reviews*. Elsevier Ltd, p. 109318. doi: 10.1016/j.rser.2019.109318.
- Evola, G., Marletta, L. and Sicurella, F. (2013) 'A methodology for investigating the effectiveness of PCM wallboards for summer thermal comfort in buildings', *Building and Environment*. Elsevier Ltd, 59, pp. 517–527. doi: 10.1016/j.buildenv.2012.09.021.
- Faghihian, H., Ghannadi Marageh, M. and Kazemian, H. (1999) 'The use

of clinoptilolite and its sodium form for removal of radioactive cesium, and strontium from nuclear wastewater and  $Pb^{2+}$   $Ni^{2+}$   $Cd^{2+}$   $Ba^{2+}$  from municipal wastewater', *Applied Radiation and Isotopes*. Elsevier Sci Ltd, 50(4), pp. 655–660. doi: 10.1016/S0969-8043(98)00134-1.

Fan, L. W. *et al.* (2013) 'Effects of various carbon nanofillers on the thermal conductivity and energy storage properties of paraffin-based nanocomposite phase change materials', *Applied Energy*, 110, pp. 163–172. doi: 10.1016/j.apenergy.2013.04.043.

Garg, H. *et al.* (2018) 'Design and analysis of PCM based radiant heat exchanger for thermal management of buildings', *Energy and Buildings*. Elsevier B.V., 169, pp. 84–96. doi: 10.1016/j.enbuild.2018.03.058.

Gauthier, B. M. *et al.* (2004) 'A fast supercritical extraction technique for aerogel fabrication', in *Journal of Non-Crystalline Solids*. North-Holland, pp. 238–243. doi: 10.1016/j.jnoncrysol.2004.06.044.

Ge, T. S. *et al.* (2018) 'Experimental testing on contaminant and moisture removal performance of silica gel desiccant wheel', *Energy and Buildings*. Elsevier Ltd, 176, pp. 71–77. doi: 10.1016/j.enbuild.2018.07.033.

Gordeeva, L. G. *et al.* (2009) 'Adsorption properties of composite materials (LiCl + LiBr)/silica', *Microporous and Mesoporous Materials*. Elsevier, 126(3), pp. 262–267. doi: 10.1016/j.micromeso.2009.06.015.

Greening, B. and Azapagic, A. (2012) 'Domestic heat pumps: Life cycle environmental impacts and potential implications for the UK', *Energy*. Pergamon, 39(1), pp. 205–217. doi: 10.1016/J.ENERGY.2012.01.028.

Greenwood, D., Congreve, A. and King, M. (2020) *Streamlining or watering down? Assessing the 'smartness' of policy and standards for the promotion of low and zero carbon homes in England 2010–15* | Elsevier Enhanced Reader. Available at: <https://reader.elsevier.com/reader/sd/pii/S0301421517305372?token=66937D32312D244433BF2D53963DCCEFA83734211048EA6C1EC12D91E16F339A00BD33777D6703F5DA6634412F07F0F2&originRegion=eu-west-1&originCreation=20210618100454> (Accessed: 18 June 2021).

Grekova, A. *et al.* (2019) "LiCl/vermiculite - Methanol" as working pair for adsorption heat storage: Adsorption equilibrium and dynamics', *Energy*. Elsevier Ltd, 186, p. 115775. doi: 10.1016/j.energy.2019.07.105.

Hadorn, J.-C. (2015) *Solar and Heat Pump Systems for Residential Buildings*. Berlin: Wiley (Solar heating & cooling programme).

Hamdan, M. A. and Elwerr, F. A. (1996) 'Thermal energy storage using a phase change material', *Solar Energy*. Pergamon Press Inc, 56(2), pp. 183–189. doi: 10.1016/0038-092X(95)00090-E.

Hawladar, M. N. A., Uddin, M. S. and Khin, M. M. (2003) 'Microencapsulated PCM thermal-energy storage system', *Applied Energy*, 74(1–2), pp. 195–202. doi: 10.1016/S0306-2619(02)00146-0.

He, Q. *et al.* (2012) 'Experimental study on thermophysical properties of

nanofluids as phase-change material (PCM) in low temperature cool storage', *Energy Conversion and Management*. Elsevier Ltd, 64, pp. 199–205. doi: 10.1016/j.enconman.2012.04.010.

Ho, C. J. and Gao, J. Y. (2009) 'Preparation and thermophysical properties of nanoparticle-in-paraffin emulsion as phase change material', *International Communications in Heat and Mass Transfer*. Elsevier Ltd, 36(5), pp. 467–470. doi: 10.1016/j.icheatmasstransfer.2009.01.015.

Horne, R. (2009) *Life cycle assessment principles, practice and prospects*. Edited by T. (Timothy F. Grant, K. Verghese, and ProQuest (Firm). Collingwood, Vic.: CSIRO Pub.

Huang, S. M. and Zhang, L. Z. (2013) 'Researches and trends in membrane-based liquid desiccant air dehumidification', *Renewable and Sustainable Energy Reviews*. Pergamon, pp. 425–440. doi: 10.1016/j.rser.2013.08.005.

Ianoş, R., Păcurariu, C. and Mihoc, G. (2014) 'Magnetite/carbon nanocomposites prepared by an innovative combustion synthesis technique - Excellent adsorbent materials', *Ceramics International*. Elsevier Ltd, 40(8 PART B), pp. 13649–13657. doi: 10.1016/j.ceramint.2014.05.092.

Ibáñez, M. *et al.* (2005) 'An approach to the simulation of PCMs in building applications using TRNSYS', *Applied Thermal Engineering*, 25(11–12), pp. 1796–1807. doi: 10.1016/j.applthermaleng.2004.11.001.

ISO, 2005. ISO 7730 – (2005) *Ergonomics of the thermal environment - analytical determination and interpretation of thermal comfort using calculation of the PMV and PPD indices and local thermal comfort criteria*. Geneva.

Jaguemont, J. *et al.* (2018) 'Phase-change materials (PCM) for automotive applications: A review', *Applied Thermal Engineering*. Elsevier Ltd, pp. 308–320. doi: 10.1016/j.applthermaleng.2017.12.097.

Jarimi, H. *et al.* (2018) 'Materials characterization of innovative composite materials for solar-driven thermochemical heat storage (THS) suitable for building application', *International Journal of Low-Carbon Technologies*, 13(1), pp. 30–42. doi: 10.1093/ijlct/ctx017.

Jelle, B. P. and Kalnæs, S. E. (2017) *Phase Change Materials for Application in Energy-Efficient Buildings, Cost-Effective Energy Efficient Building Retrofitting: Materials, Technologies, Optimization and Case Studies*. Elsevier Ltd. doi: 10.1016/B978-0-08-101128-7.00003-4.

Ji, H. *et al.* (2014) 'Enhanced thermal conductivity of phase change materials with ultrathin-graphite foams for thermal energy storage', *Energy & Environmental Science*, 7, p. 1185. doi: 10.1039/c3ee42573h.

Ji, P. *et al.* (2012) 'Improvement of the thermal conductivity of a phase change material by the functionalized carbon nanotubes', *Chemical Engineering Science*. Elsevier, 81, pp. 140–145. doi: 10.1016/j.ces.2012.07.002.

Jiang, J. *et al.* (2012) 'Preparation and performances of bulk porous Al foams impregnated with phase-change-materials for thermal storage', *Progress in Natural Science: Materials International*. Elsevier, 22(5), pp. 440–444. doi: 10.1016/j.pnsc.2012.05.004.

Johnson, C. D. and Worrall, F. (2007a) 'Novel granular materials with microcrystalline active surfaces-Waste water treatment applications of zeolite/vermiculite composites', *Water Research*. Elsevier Ltd, 41(10), pp. 2229–2235. doi: 10.1016/j.watres.2007.01.047.

Johnson, C. D. and Worrall, F. (2007b) 'Novel low density granular adsorbents - Properties of a composite matrix from zeolitisation of vermiculite', *Chemosphere*. Elsevier Ltd, 68(6), pp. 1153–1162. doi: 10.1016/j.chemosphere.2007.01.049.

Kalaiselvam, S., Parameshwaran, R. and Harikrishnan, S. (2012) 'Analytical and experimental investigations of nanoparticles embedded phase change materials for cooling application in modern buildings', *Renewable Energy*. Elsevier Ltd, 39(1), pp. 375–387. doi: 10.1016/j.renene.2011.08.034.

Kalnæs, S. E. and Jelle, B. P. (2015) 'Phase change materials and products for building applications: A state-of-the-art review and future research opportunities', *Energy and Buildings*. Elsevier B.V., 94(7491), pp. 150–176. doi: 10.1016/j.enbuild.2015.02.023.

Kasaeian, A. *et al.* (2017) 'Experimental studies on the applications of PCMs and nano-PCMs in buildings: A critical review', *Energy and Buildings*. Elsevier B.V., 154, pp. 96–112. doi: 10.1016/j.enbuild.2017.08.037.

Khodadadi, J. M., Fan, L. and Babaei, H. (2013) 'Thermal conductivity enhancement of nanostructure-based colloidal suspensions utilized as phase change materials for thermal energy storage: A review', *Renewable and Sustainable Energy Reviews*. Elsevier Ltd, pp. 418–444. doi: 10.1016/j.rser.2013.03.031.

Khudhair, A. M. and Farid, M. M. (2004) 'A review on energy conservation in building applications with thermal storage by latent heat using phase change materials', *Energy Conversion and Management*, 45(2), pp. 263–275. doi: 10.1016/S0196-8904(03)00131-6.

Kipp, J. A. ., Wever, G. . and Kreji, C. (2000) 'International Substrate Manual Elsevier International Business Information Doetinchem', *International Substrate Manual Elsevier International Business Information Doetinchem, the Netherlands*.

Kong, D. *et al.* (2019) 'Effects of indoor humidity on building occupants' thermal comfort and evidence in terms of climate adaptation', *Building and Environment*. Elsevier Ltd, 155, pp. 298–307. doi: 10.1016/j.buildenv.2019.02.039.

Krishna, J., Kishore, P. S. and Solomon, A. B. (2017) 'Heat pipe with nano enhanced-PCM for electronic cooling application', *Experimental*

*Thermal and Fluid Science*. Elsevier Inc., 81, pp. 84–92. doi: 10.1016/j.expthermflusci.2016.10.014.

Kumaresan, V. *et al.* (2013) 'Role of PCM based nanofluids for energy efficient cool thermal storage system', *International Journal of Refrigeration*. Elsevier Ltd and IIR, 36(6), pp. 1641–1647. doi: 10.1016/j.ijrefrig.2013.04.010.

Kuznik, F. and Virgone, J. (2009) 'Experimental assessment of a phase change material for wall building use', *Applied Energy*. Elsevier Ltd, 86(10), pp. 2038–2046. doi: 10.1016/j.apenergy.2009.01.004.

La, D. *et al.* (2010) 'Technical development of rotary desiccant dehumidification and air conditioning: A review', *Renewable and Sustainable Energy Reviews*. Pergamon, pp. 130–147. doi: 10.1016/j.rser.2009.07.016.

Labandeira, X. *et al.* (2020) 'The impacts of energy efficiency policies: Meta-analysis', *Energy Policy*. Elsevier Ltd, 147, p. 111790. doi: 10.1016/j.enpol.2020.111790.

Labat, M. *et al.* (2014) 'Experimental assessment of a PCM to air heat exchanger storage system for building ventilation application', *Applied Thermal Engineering*. Elsevier Ltd, 66(1–2), pp. 375–382. doi: 10.1016/j.applthermaleng.2014.02.025.

Liu, X. *et al.* (2019) 'Optimal design and operation of PV-battery systems considering the interdependency of heat pumps Optimal design and operation of PV-battery systems considering the interdependency of heat pumps', (May 2019). doi: 10.1016/j.est.2019.04.026.

Liu, Y. and Wang, R. (2003) 'Pore structure of new composite adsorbent  $\text{SiO}_2 \cdot x\text{H}_2\text{O} \cdot y\text{CaCl}_2$  with high uptake of water from air', *Science in China, Series E: Technological Sciences*, 46(5). doi: 10.1360/02ye0480.

Loiseau, T. *et al.* (2015) 'Crystal chemistry of aluminium carboxylates: From molecular species towards porous infinite three-dimensional networks', *Comptes Rendus Chimie*. Elsevier Masson SAS, pp. 1350–1369. doi: 10.1016/j.crci.2015.08.006.

Longo, G. A. and Gasparella, A. (2016) 'Experimental measurement of thermophysical properties of  $\text{H}_2\text{O}/\text{KCOOH}$  (potassium formate) desiccant', *International Journal of Refrigeration*. Elsevier Ltd, 62, pp. 106–113. doi: 10.1016/j.ijrefrig.2015.10.004.

Lu, H. C., Kuok, C. H. and Liu, S. H. (2020) 'High-performance humidity control coatings prepared from inorganic wastes', *Construction and Building Materials*. Elsevier Ltd, 263, p. 120169. doi: 10.1016/j.conbuildmat.2020.120169.

Lu, M. and Lai, J. H. K. (2019) 'Building energy: A review on consumptions, policies, rating schemes and standards', in *Energy Procedia*. Elsevier Ltd, pp. 3633–3638. doi: 10.1016/j.egypro.2019.01.899.

Lu, S. *et al.* (2016) 'Experimental research on a novel energy efficiency roof coupled with PCM and cool materials', *Energy and Buildings*. Elsevier B.V., 127, pp. 159–169. doi: 10.1016/j.enbuild.2016.05.080.

Luo, Y., Yang, H. and Lu, L. (2014) 'Dynamic and microscopic simulation of the counter-current flow in a liquid desiccant dehumidifier', *Applied Energy*. Elsevier Ltd, 136, pp. 1018–1025. doi: 10.1016/j.apenergy.2014.06.023.

Ma, Z., Lin, W. and Sohel, M. I. (2016) 'Nano-enhanced phase change materials for improved building performance', *Renewable and Sustainable Energy Reviews*. Elsevier, 58, pp. 1256–1268. doi: 10.1016/j.rser.2015.12.234.

Machado, L. C. R. *et al.* (2006) 'Polymer coated vermiculite-iron composites: Novel floatable magnetic adsorbents for water spilled contaminants', *Applied Clay Science*. Elsevier, 31(3–4), pp. 207–215. doi: 10.1016/j.clay.2005.07.004.

Maleki, B. *et al.* (2020) 'Development and thermal performance of nanoencapsulated PCM/ plaster wallboard for thermal energy storage in buildings', *Journal of Building Engineering*. Elsevier Ltd, 32, p. 101727. doi: 10.1016/j.jobbe.2020.101727.

Marino, C. *et al.* (2018) 'A generalized model of human body radiative heat exchanges for optimal design of indoor thermal comfort conditions', *Solar Energy*. Elsevier, 176(July), pp. 556–571. doi: 10.1016/j.solener.2018.10.052.

Mauree, D. *et al.* (2019) 'A review of assessment methods for the urban environment and its energy sustainability to guarantee climate adaptation of future cities', *Renewable and Sustainable Energy Reviews*. Elsevier Ltd, 112, pp. 733–746. doi: 10.1016/j.rser.2019.06.005.

Maurer, C., Cappel, C. and Kuhn, T. E. (2017) 'Progress in building-integrated solar thermal systems', *Solar Energy*. Elsevier Ltd, 154, pp. 158–186. doi: 10.1016/j.solener.2017.05.065.

Mazzeo, D., Oliveti, G. and Arcuri, N. (2017) 'Data demonstrating the influence of the latent storage efficiency on the dynamic thermal characteristics of a PCM layer', *Data in Brief*. Elsevier Inc., 12, pp. 274–276. doi: 10.1016/j.dib.2017.04.005.

MCI Technologies (no date) *MCI Technologies*. Available at: [www.winco-tech.com/wordpress/wp-content/uploads/2016/09/MCI-Technologies-MCP-english-20160620.pdf](http://www.winco-tech.com/wordpress/wp-content/uploads/2016/09/MCI-Technologies-MCP-english-20160620.pdf) (Accessed: 6 April 2020).

Mclachlan, C. *et al.* (2016) 'Prepared for Electricity North West by: Air conditioning demand assessment'.

Mehling, H. (2008) *Heat and cold storage with PCM an up to date introduction into basics and applications*. Edited by L. F. Cabeza. Berlin ; London: Springer (Heat and mass transfer).

Memon, S. A. (2014) 'Phase change materials integrated in building walls:

A state of the art review', *Renewable and Sustainable Energy Reviews*. Elsevier, 31, pp. 870–906. doi: 10.1016/j.rser.2013.12.042.

Memon, S. A. *et al.* (2015) 'Utilization of macro encapsulated phase change materials for the development of thermal energy storage and structural lightweight aggregate concrete', *Applied Energy*. Elsevier Ltd, 139, pp. 43–55. doi: 10.1016/j.apenergy.2014.11.022.

Mirzania, P. *et al.* (2019) 'The impact of policy changes: The opportunities of Community Renewable Energy projects in the UK and the barriers they face', *Energy Policy*. Elsevier Ltd, 129, pp. 1282–1296. doi: 10.1016/j.enpol.2019.02.066.

Mohammad, N. K., Ghaemi, A. and Tahvildari, K. (2019) 'Hydroxide modified activated alumina as an adsorbent for CO<sub>2</sub> adsorption: Experimental and modeling', *International Journal of Greenhouse Gas Control*. Elsevier Ltd, 88, pp. 24–37. doi: 10.1016/j.ijggc.2019.05.029.

Moreno-Rodríguez, A. *et al.* (2012) 'Theoretical model and experimental validation of a direct-expansion solar assisted heat pump for domestic hot water applications', *Energy*. Elsevier, 45(1), pp. 704–715. doi: 10.1016/j.energy.2012.07.021.

Munoz, M. *et al.* (2021) 'Carbon-encapsulated iron nanoparticles as reusable adsorbents for micropollutants removal from water', *Separation and Purification Technology*. Elsevier B.V., 257, p. 117974. doi: 10.1016/j.seppur.2020.117974.

Naeimi, S. and Faghihian, H. (2017) 'Performance of novel adsorbent prepared by magnetic metal-organic framework (MOF) modified by potassium nickel hexacyanoferrate for removal of Cs<sup>+</sup> from aqueous solution', *Separation and Purification Technology*. Elsevier B.V., 175, pp. 255–265. doi: 10.1016/j.seppur.2016.11.028.

Nazi, W. I. W. M. *et al.* (2017) 'Passive Cooling Using Phase Change Material and Insulation for High-rise Office Building in Tropical Climate', *Energy Procedia*. Elsevier B.V., 142, pp. 2295–2302. doi: 10.1016/j.egypro.2017.12.632.

Norouzi, N. and Soori, M. (2020) 'Energy, environment, water, and land-use nexus based evaluation of the global green building standards', *Water-Energy Nexus*. Elsevier BV, 3, pp. 209–224. doi: 10.1016/j.wen.2020.10.001.

O'Brien, W. *et al.* (2020) 'An international review of occupant-related aspects of building energy codes and standards', *Building and Environment*. Elsevier Ltd, 179, p. 106906. doi: 10.1016/j.buildenv.2020.106906.

O'Hegarty, R., Kinnane, O. and McCormack, S. (2014) 'A Simplified Procedure for Sizing Solar Thermal Systems; Based on National Assessment Methods in the UK and Ireland', *Energy Procedia*. Elsevier, 62, pp. 647–655. doi: 10.1016/J.EGYPRO.2014.12.428.

O'Neill, K. and Gibbs, D. (2020) 'Sustainability transitions and policy



dismantling: Zero carbon housing in the UK', *Geoforum*. Elsevier Ltd, 108, pp. 119–129. doi: 10.1016/j.geoforum.2019.11.011.

Oya, T. *et al.* (2013) 'Thermal conductivity enhancement of erythritol as PCM by using graphite and nickel particles', *Applied Thermal Engineering*. Elsevier Ltd, 61(2), pp. 825–828. doi: 10.1016/j.applthermaleng.2012.05.033.

Paksoy, H. and Sahan, N. (2012) 'Thermally enhanced paraffin for solar applications', *Energy Procedia*. The Authors, 30, pp. 350–352. doi: 10.1016/j.egypro.2012.11.041.

Papadopoulos, A. P. *et al.* (2008) 'Inorganic and synthetic organic components of soilless culture and potting mixes', in *Soilless Culture: Theory and Practice*. Elsevier, pp. 505–543. doi: 10.1016/B978-044452975-6.50014-9.

Papineau, M. (2017) 'Setting the standard? A framework for evaluating the cost-effectiveness of building energy standards', *Energy Economics*. Elsevier B.V., 64, pp. 63–76. doi: 10.1016/j.eneco.2017.02.011.

Parameshwaran, R. *et al.* (2014) 'Preparation, thermal and rheological properties of hybrid nanocomposite phase change material for thermal energy storage', *Applied Energy*. Elsevier Ltd, 115, pp. 320–330. doi: 10.1016/j.apenergy.2013.11.029.

Parameshwaran, R., Jayavel, R. and Kalaiselvam, S. (2013) 'Study on thermal properties of organic ester phase-change material embedded with silver nanoparticles', *Journal of Thermal Analysis and Calorimetry*, 114(2), pp. 845–858. doi: 10.1007/s10973-013-3064-9.

Parsons, K. (2014) *Human thermal environments: The effects of hot, moderate, and cold environments on human health, comfort, and performance, third edition, Human Thermal Environments: The Effects of Hot, Moderate, and Cold Environments on Human Health, Comfort, and Performance, Third Edition*. doi: 10.1201/b16750.

Parsons, K. C. (2000) *Environmental ergonomics: a review of principles, methods and models*.

Pasupathy, A. and Velraj, R. (2008) 'Effect of double layer phase change material in building roof for year round thermal management', *Energy and Buildings*, 40(3), pp. 193–203. doi: 10.1016/j.enbuild.2007.02.016.

Pei, C., Ou, Q. and Pui, D. Y. H. (2021) 'Effects of temperature and relative humidity on laboratory air filter loading test by hygroscopic salts', *Separation and Purification Technology*. Elsevier B.V., 255, p. 117679. doi: 10.1016/j.seppur.2020.117679.

Peippo, K., Kauranen, P. and Lund, P. D. (1991) 'A multicomponent PCM wall optimized for passive solar heating', *Energy and Buildings*. Elsevier, 17(4), pp. 259–270. doi: 10.1016/0378-7788(91)90009-R.

Pérez de Arce, M., Sauma, E. and Contreras, J. (2016) 'Renewable energy policy performance in reducing CO<sub>2</sub> emissions', *Energy*

*Economics*. Elsevier, 54, pp. 272–280. doi: 10.1016/j.eneco.2015.11.024.

Piselli, C. *et al.* (2020) 'Optimal control of natural ventilation as passive cooling strategy for improving the energy performance of building envelope with PCM integration', *Renewable Energy*. Elsevier Ltd, 162, pp. 171–181. doi: 10.1016/j.renene.2020.07.043.

Pistocchini, L., Garone, S. and Motta, M. (2016) 'Air dehumidification by cooled adsorption in silica gel grains. Part I: Experimental development of a prototype', *Applied Thermal Engineering*. Elsevier Ltd, 107, pp. 888–897. doi: 10.1016/j.applthermaleng.2016.06.103.

Qunli, Z. *et al.* (2017) 'Simulation Research on the Thermal Performance of the Cooling Ceiling Embedded with Phase Change Material for Energy Storage', *Energy Procedia*, 105, pp. 2575–2582. doi: 10.1016/j.egypro.2017.03.740.

Raish, J. (2019) *Thermal Comfort: Designing for People*. Available at: [https://soa.utexas.edu/sites/default/disk/urban\\_ecosystems/urban\\_ecosystems/09\\_03\\_fa\\_ferguson\\_raish\\_ml.pdf](https://soa.utexas.edu/sites/default/disk/urban_ecosystems/urban_ecosystems/09_03_fa_ferguson_raish_ml.pdf) (Accessed: 8 July 2020).

Ren, H. *et al.* (2021) 'Improving energy flexibility of a net-zero energy house using a solar-assisted air conditioning system with thermal energy storage and demand-side management', *Applied Energy*. Elsevier Ltd, 285, p. 116433. doi: 10.1016/j.apenergy.2021.116433.

*Residential Energy Consumption Survey (RECS) - Energy Information Administration* (2015). Available at: <https://www.eia.gov/consumption/residential/> (Accessed: 13 July 2021).

Royon, L., Karim, L. and Bontemps, A. (2013) 'Thermal energy storage and release of a new component with PCM for integration in floors for thermal management of buildings', *Energy and Buildings*. Elsevier B.V., 63, pp. 29–35. doi: 10.1016/j.enbuild.2013.03.042.

*Rubitherm GmbH* (2020). Available at: <https://www.rubitherm.eu/en/index.php/productcategory/organische-pcm-rt> (Accessed: 28 July 2020).

Rupp, R. F., Giraldo Vásquez, N. and Lamberts, R. (2015) 'A review of human thermal comfort in the built environment', *Energy and Buildings*, 105, pp. 178–205. doi: 10.1016/j.enbuild.2015.07.047.

Sadeghalvad, B. *et al.* (2021) 'Sorption, mechanism, and behavior of sulfate on various adsorbents: A critical review', *Chemosphere*. Elsevier Ltd, p. 128064. doi: 10.1016/j.chemosphere.2020.128064.

Saffari, M. *et al.* (2016) 'Economic impact of integrating PCM as passive system in buildings using Fanger comfort model', *Energy and Buildings*. Elsevier B.V., 112, pp. 159–172. doi: 10.1016/j.enbuild.2015.12.006.

Saffari, M. *et al.* (2017) 'Simulation-based optimization of PCM melting temperature to improve the energy performance in buildings', *Applied Energy*. Elsevier Ltd, 202, pp. 420–434. doi: 10.1016/j.apenergy.2017.05.107.

Salunkhe, P. B. and Shembekar, P. S. (2012) 'A review on effect of phase change material encapsulation on the thermal performance of a system', *Renewable and Sustainable Energy Reviews*. Elsevier, 16(8), pp. 5603–5616. doi: 10.1016/j.rser.2012.05.037.

Sapienza, A. *et al.* (2012) 'Adsorption chilling driven by low temperature heat: New adsorbent and cycle optimization', *Applied Thermal Engineering*. Pergamon, 32(1), pp. 141–146. doi: 10.1016/j.applthermaleng.2011.09.014.

Sayyar, M. *et al.* (2014) 'Experimental and numerical study of shape-stable phase-change nanocomposite toward energy-efficient building constructions', *Energy and Buildings*. Elsevier B.V., 75, pp. 249–255. doi: 10.1016/j.enbuild.2014.02.018.

Shehadi, M. (2018) 'Review of humidity control technologies in buildings', *Journal of Building Engineering*. Elsevier Ltd, pp. 539–551. doi: 10.1016/j.jobbe.2018.06.009.

Shilei, L. *et al.* (2007) 'Experimental study and evaluation of latent heat storage in phase change materials wallboards', *Energy and Buildings*, 39(10), pp. 1088–1091. doi: 10.1016/j.enbuild.2006.11.012.

Shkatulov, A. I. *et al.* (2020) *Stabilization of K<sub>2</sub>CO<sub>3</sub> in vermiculite for thermochemical energy storage* | Elsevier Enhanced Reader. Available at:

<https://reader.elsevier.com/reader/sd/pii/S0960148119318130?token=0E65A40AAE9B9F8BFA523CD0212A0B6F1DD28044CF78811C0604D68530D4F1FBD58593D8951390A004838B9525038AB8> (Accessed: 29 October 2020).

Singh, R., Mishra, V. and Das, R. (2018) 'Desiccant materials for air conditioning applications - A review', *IOP Conference Series: Materials Science and Engineering*, 404, p. 12005. doi: 10.1088/1757-899X/404/1/012005.

Singh Rathore, P. K., Shukla, S. K. and Gupta, N. K. (2020) 'Potential of microencapsulated PCM for energy savings in buildings: A critical review', *Sustainable Cities and Society*. Elsevier, 53(August 2019), p. 101884. doi: 10.1016/j.scs.2019.101884.

Stawiński, W. *et al.* (2017) 'Acid-base treated vermiculite as high performance adsorbent: Insights into the mechanism of cationic dyes adsorption, regeneration, recyclability and stability studies', *Chemosphere*. Elsevier Ltd, 173, pp. 107–115. doi: 10.1016/j.chemosphere.2017.01.039.

Stolarski, M. J. *et al.* (2020) 'Energy consumption and heating costs for a detached house over a 12-year period – Renewable fuels versus fossil fuels', *Energy*. Elsevier Ltd, 204, p. 117952. doi: 10.1016/j.energy.2020.117952.

Stopps, H. and Touchie, M. F. (2020) 'Managing thermal comfort in contemporary high-rise residential buildings: Using smart thermostats

and surveys to identify energy efficiency and comfort opportunities', *Building and Environment*. Elsevier Ltd, 173, p. 106748. doi: 10.1016/j.buildenv.2020.106748.

Streltsov, A. *et al.* (2020) 'Estimating residential building energy consumption using overhead imagery', *Applied Energy*. Elsevier Ltd, 280, p. 116018. doi: 10.1016/j.apenergy.2020.116018.

Sultan, M. *et al.* (2015) 'An overview of solid desiccant dehumidification and air conditioning systems', *Renewable and Sustainable Energy Reviews*. Elsevier Ltd, pp. 16–29. doi: 10.1016/j.rser.2015.02.038.

Tabares-Velasco, P. C., Christensen, C. and Bianchi, M. (2012) 'Verification and validation of EnergyPlus phase change material model for opaque wall assemblies', *Building and Environment*. Elsevier Ltd, 54, pp. 186–196. doi: 10.1016/j.buildenv.2012.02.019.

Takeda, S. *et al.* (2004) 'Development of a ventilation system utilizing thermal energy storage for granules containing phase change material', *Solar Energy*, 77(3), pp. 329–338. doi: 10.1016/j.solener.2004.04.014.

Teng, T. P. (2013) 'Thermal conductivity and phase-change properties of aqueous alumina nanofluid', *Energy Conversion and Management*, 67, pp. 369–375. doi: 10.1016/j.enconman.2012.12.004.

Teng, T. P. and Yu, C. C. (2012) 'Characteristics of phase-change materials containing oxide nano-additives for thermal storage', *Nanoscale Research Letters*, 7, pp. 1–10. doi: 10.1186/1556-276X-7-611.

Tran, L. N., Gao, W. and Ge, J. (2021) 'Sensitivity analysis of household factors and energy consumption in residential houses: A multi-dimensional hybrid approach using energy monitoring and modeling', *Energy and Buildings*. Elsevier, p. 110864. doi: 10.1016/j.enbuild.2021.110864.

Vaishak, S. and Bhale, P. V. (2019) 'Photovoltaic/thermal-solar assisted heat pump system: Current status and future prospects', *Solar Energy*. Elsevier Ltd, pp. 268–284. doi: 10.1016/j.solener.2019.07.051.

Velasco-Carrasco, M. *et al.* (2020) 'Experimental evaluation of phase change material blister panels for building application', *Future Cities and Environment*, 6(1), pp. 1–7. doi: 10.5334/fce.84.

Villa, C. C. *et al.* (2020) 'Molecular sieves for food applications: A review', *Trends in Food Science and Technology*. Elsevier Ltd, pp. 102–122. doi: 10.1016/j.tifs.2020.05.027.

Voelker, C., Kornadt, O. and Ostry, M. (2008) 'Temperature reduction due to the application of phase change materials', *Energy and Buildings*, 40(5), pp. 937–944. doi: 10.1016/j.enbuild.2007.07.008.

Wang, L., Bu, X. and Ma, W. (2012) 'Preparation and performance testing of silica gel/ calcium chloride composite adsorbents for waste heat adsorption refrigeration', *World Automation Congress Proceedings*.

- Wang, W. *et al.* (2013) 'Sulfuric acid modified bentonite as the support of tetraethylenepentamine for CO<sub>2</sub> capture', *Energy and Fuels*. American Chemical Society, 27(3), pp. 1538–1546. doi: 10.1021/ef3021816.
- Wang, X. and Niu, J. (2009) 'Performance of cooled-ceiling operating with MPCM slurry', *Energy Conversion and Management*. Elsevier Ltd, 50(3), pp. 583–591. doi: 10.1016/j.enconman.2008.10.021.
- Warwicker, B. (2010) '15 - Desiccant materials for moisture control in buildings', in *Materials for energy efficiency and thermal comfort in buildings*. Elsevier Ltd, pp. 365–383. doi: 10.1533/9781845699277.2.365.
- Wei, J. *et al.* (2005) 'Study on a PCM heat storage system for rapid heat supply', *Applied Thermal Engineering*, 25(17–18), pp. 2903–2920. doi: 10.1016/j.applthermaleng.2005.02.014.
- Weinläder, H., Beck, A. and Fricke, J. (2005) 'PCM-facade-panel for daylighting and room heating', in *Solar Energy*. Pergamon, pp. 177–186. doi: 10.1016/j.solener.2004.04.013.
- Wen, T. *et al.* (2018) 'Investigation on the regeneration performance of liquid desiccant by adding surfactant PVP-K30', *International Journal of Heat and Mass Transfer*. Elsevier Ltd, 123, pp. 445–454. doi: 10.1016/j.ijheatmasstransfer.2018.03.005.
- Whiffen, T. R. and Riffat, S. B. (2013) 'A review of PCM technology for thermal energy storage in the built environment: Part I', *International Journal of Low-Carbon Technologies*. Oxford Academic, 8(3), pp. 147–158. doi: 10.1093/ijlct/cts021.
- White, S. D. *et al.* (2011) 'Characterization of desiccant wheels with alternative materials at low regeneration temperatures', in *International Journal of Refrigeration*. Elsevier, pp. 1786–1791. doi: 10.1016/j.ijrefrig.2011.06.012.
- Wu, Q., Wang, J. and Meng, X. (2021) 'NC-ND license Influence of wall thermal performance on the contribution efficiency of the Phase-Change Material (PCM) layer'. doi: 10.1016/j.csite.2021.101398.
- Wu, S. *et al.* (2009) 'Thermal energy storage behavior of Al<sub>2</sub>O<sub>3</sub>-H<sub>2</sub>O nanofluids', *Thermochimica Acta*, 483(1–2), pp. 73–77. doi: 10.1016/j.tca.2008.11.006.
- Wu, S. *et al.* (2011) 'An investigation of melting/freezing characteristics of nanoparticle-enhanced phase change materials', *Journal of Thermal Analysis and Calorimetry*, 110. doi: 10.1007/s10973-011-2080-x.
- Wu, T., Prasetya, N. and Li, K. (2020) 'Recent advances in aluminium-based metal-organic frameworks (MOF) and its membrane applications', *Journal of Membrane Science*. Elsevier B.V., p. 118493. doi: 10.1016/j.memsci.2020.118493.
- Xie, Y. *et al.* (2017) 'A review on house design with energy saving system in the UK', *Renewable and Sustainable Energy Reviews*. Elsevier Ltd, pp. 29–52. doi: 10.1016/j.rser.2017.01.004.

- Yahaya, N. A. and Ahmad, H. (2011) 'Numerical investigation of indoor air temperature with the application of PCM Gypsum board as ceiling panels in buildings', *Procedia Engineering*, 20, pp. 238–248. doi: 10.1016/j.proeng.2011.11.161.
- Yang, L., Huang, J. nan and Zhou, F. (2020) 'Thermophysical properties and applications of nano-enhanced PCMs: An update review', *Energy Conversion and Management*. Elsevier Ltd, p. 112876. doi: 10.1016/j.enconman.2020.112876.
- Yang, Y., Rana, D. and Lan, C. (2015) 'Development of solid super desiccants based on a polymeric superabsorbent hydrogel composite', *RSC Adv.*, 5. doi: 10.1039/C5RA04346H.
- Yu, N., Wang, R. Z. and Wang, L. W. (2013) 'Sorption thermal storage for solar energy', *Progress in Energy and Combustion Science*, 39, pp. 489–514. doi: 10.1016/j.pecs.2013.05.004.
- Yu, S. *et al.* (2014) 'Bio-based PCM/carbon nanomaterials composites with enhanced thermal conductivity', *Solar Energy Materials and Solar Cells*. Elsevier, 120(PART B), pp. 549–554. doi: 10.1016/j.solmat.2013.09.037.
- Yu, S., Cui, Y. and Feng, G. (2016) 'Research on Performance of Humidity-controlling Materials Based on E+', in *Procedia Engineering*. Elsevier Ltd, pp. 318–326. doi: 10.1016/j.proeng.2016.06.399.
- Zeng, J. L. *et al.* (2007) 'Study of a PCM based energy storage system containing Ag nanoparticles', *Journal of Thermal Analysis and Calorimetry*, 87(2), pp. 371–375. doi: 10.1007/s10973-006-7783-z.
- Zhang, Q. N. *et al.* (2021) 'Hygroscopic property of inorganic salts in atmospheric aerosols measured with physisorption analyzer', *Atmospheric Environment*. Elsevier Ltd, 247, p. 118171. doi: 10.1016/j.atmosenv.2020.118171.
- Zheng, X., Ge, T. S. and Wang, R. Z. (2014) 'Recent progress on desiccant materials for solid desiccant cooling systems', *Energy*. Elsevier Ltd, pp. 280–294. doi: 10.1016/j.energy.2014.07.027.
- Zhong, K. *et al.* (2015) 'Simulation study on dynamic heat transfer performance of PCM-filled glass window with different thermophysical parameters of phase change material', *Energy and Buildings*. Elsevier B.V., 106, pp. 87–95. doi: 10.1016/j.enbuild.2015.05.014.
- Zhong, Y. *et al.* (2010) 'Heat transfer enhancement of paraffin wax using graphite foam for thermal energy storage', *Solar Energy Materials and Solar Cells*. Elsevier, 94(6), pp. 1011–1014. doi: 10.1016/j.solmat.2010.02.004.
- Zhou, B., Shi, J. and Chen, Z. qian (2018) 'Experimental study on moisture migration process of zeolite-based composite humidity control material', *Applied Thermal Engineering*. Elsevier Ltd, 128, pp. 604–613. doi: 10.1016/j.applthermaleng.2017.08.138.

Zhou, D., Zhao, C. Y. and Tian, Y. (2012) 'Review on thermal energy storage with phase change materials (PCMs) in building applications', *Applied Energy*. Elsevier Ltd, pp. 593–605. doi: 10.1016/j.apenergy.2011.08.025.